LIGHT INTENSITY ATTENUATION-BASED FIBRE-OPTIC CHEMICAL SENSORS: THEORETICAL ANALYSES AND DESIGN STUDIES

Thesis submitted for the degree of

Doctor of Philosophy

at the University of Leicester

by

Xu, Yu B. Eng. (Zhejiang, China) M. Eng. (Zhejiang, China)

Department of Engineering

University of Leicester

June 2000

行万里路

读万卷书

----------中国古代谚语

LIGHT INTENSITY ATTENUATION-BASED FIBRE-OPTIC CHEMICAL SENSORS: THEORETICAL ANALYSES AND DESIGN STUDIES

by

Xu, Yu

Declaration of originality

This thesis is submitted in fulfilment of the requirements for the degree of Doctor of Philosophy in the Department of Engineering, University of Leicester, UK. All work recorded in this thesis is original unless otherwise acknowledged in the text or by reference. No part of it has been submitted for any other degree, either to the University of Leicester or to any other University.

Xu, Yu

June 2000

I dedicate this Ph.D. to my family. Without their love this would never have been possible.

Contents

Chapter 4 An Approximate Theoretical Model of Surface Plasmon Resonance Optical Waveguide and Fibre-Optic Sensors

Chapter 5 Numerical Error and Limitation Analysis of Two-Wavelength Light Intensity Attenuation-Based Fibre-Optic Chemical Sensors

Part 2: Design Studies

Chapter 6 Design of "Propofol" Fibre-Optic Sensor

Chapter 7 Surface Plasmon Resonance Chemical Fibre-Optic Sensors

Chapter 8 Conclusions and Further Work

Appendices

Acknowledgements

Firstly I would especially like to thank Professor N. Barrie Jones who has given me the opportunity to work on my PhD project in University of Leicester. Ever since our contact, Barrie has given me a great deal of encouragement and support. During the course of study Barrie has spent lots of time on supervision, provided guidance and motivation, given constant trust to my research work. His guidance and support are unsurpassed, particularly for me, an overseas and mature student. It is absolutely no doubt that without Barrie's great support and kindness, it would be difficult for me to finish my PhD work within two years, and many things would have been very much different for me. I am very lucky to be supervised by such a nice professor.

I would like also to thank Dr. John C. Fothergill and Dr. Chris D. Hanning for their guidance and help. They have always been able to find time from their busy routine to attend the regular meetings about my research project. They gave me the help to find the invaluable support from Leicester Royal Infirmary and Biochemical Department for my experiments. Chris has made a great effort in finding industrial sponsor, and also given me the advice in clinical issues.

I have enjoyed the constructive discussions with Barrie, John and Chris, and enjoyed their thougthful comments. The experience of the past two years has been very memorable to me.

Thanks to Mr. Jim Strupish in Leicester Royal Infirmary and Dr. Clive Bagshaw in Biochemical Department for their help and support in experiments, both of them exceeded their duties to contribute their ideas to the sensor design of my project. Thanks also to Ms. Jo Denning, Mr. Alan Wale, Mr. Dave Dryden, Mr. Peter Clarke and Dr. Tim Pearce in Engineering Department.

CVCP Overseas Scholarship Scheme and Astra-Zaneca Ltd. have partly supported this research, I would like to express my appreciation to them.

Finally, I would like to thank my wife Yewei Zhou and lovely daughter Tianyan Xu for their constant love and support whenever I need. Without their love life would have been very much different. Their love provides me a great incentive in my work.

Light Intensity Attenuation-Based Fibre-Optic Chemical Sensors: Theoretical Analyses and Design Studies

Abstract

In the thesis light intensity attenuation-based fibre-optic chemical sensors are investigated. The investigation proceeds along two lines: theoretical analyses and design studies. Both intrinsic and extrinsic types of sensors are discussed from both aspects.

The theoretical analyses are concentrated on the construction of theoretical models and numerical calculations, which were previously not well developed but have been attracting a great deal of attention of researchers for some time. Under this topic, fibre-optic evanescent wave absorption sensors and fibre-optic surface plasmon resonance (SPR) sensors are studied as examples of the intrinsic type of sensors, and two-wavelength Beer-Lambert law based fibre-optic sensors as the extrinsic example.

The design studies are concentrated on the design of novel types of sensors which have potentially valuable applications. As the intrinsic type of sensors, novel types of fibre-optic surface plasmon resonance (SPR) chemical sensors are proposed and studied in both point and distributed systems. A fibre-optic sensor for concentration determination of the infusible anaesthetic ***Propofol*** is studied in detail as an example of an extrinsic type of sensor.

Chapter 1

Light Intensity Attenuation-Based Fibre-optic Chemical Sensors

1.1 Introduction

This research is focused on the investigation of light intensity attenuation-based fibre-optic chemical sensors. The investigation proceeds along two lines: theoretical analyses and design studies. The theoretical analyses are concentrated on theoretical models and numerical calculations of light intensity attenuation-based fibre-optic chemical sensors, which are not well developed but have been attracting a great deal of attention of researchers. The design studies are concentrated on the design of novel types of light intensity attenuation-based fibre-optic chemical sensors which have potentially valuable applications. In order to give this research a comprehensive extensive range, both intrinsic and extrinsic types of fibre-optic chemical sensors have been considered here from both aspects.

As an important branch of optical fibre technology, optical fibre sensing has been intensively studied and developed for a few decades. Fibre-optic sensors have been successfully used in many areas and have exhibited highly competitive features compared with conventional sensors. Since first proposed in 1962 [Polanyi 1962 and Enson 1962], fibre-optic sensors have demonstrated significant superiority in chemical measurements in many aspects, such as flexibility, sensitivity and economy etc.

Although there are a variety of designs, optical techniques applied in fibre-optic chemical sensors can be generally summarised as: light intensity modulation, light wavelength modulation, light phase modulation, light polarisation modulation and time modulation. Among these optical techniques, light intensity modulation is possibly the simplest in principle and the widest in use. Hence much R&D effort has been expended on fibre-optic chemical sensors using the optical technique of light intensity modulation.

Light intensity attenuation-based fibre-optic chemical sensors, as a typical application of light intensity modulation technique, is the topic of the research in this thesis.

This chapter presents a brief introduction to chemical sensors, fibre-optic sensors and fibre-optic chemical sensors. In addition, the light intensity attenuation-based fibre-optic chemical sensors are also generally reviewed. During the review the research orientations and directions of fibre-optic chemical sensors by light intensity modulation techniques are discussed in terms of both theory and design, which lead to the motivation of this research. Finally an overview of the thesis is given at the end of this chapter.

1.2 The concept of chemical sensors

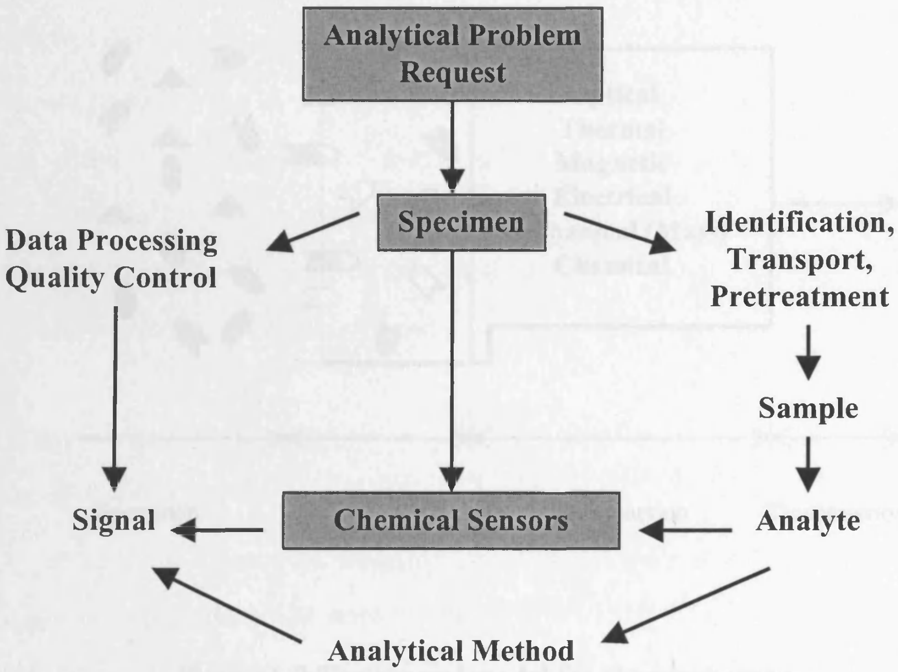

Figure 1-1 The analytical procedure and data evaluation process in a general analytical system

Chemical sensors provide the user with information about the chemical nature of their environments. One definition supported by IUPAC commission in a draft is [Hulanicki 1991]:

A chemical sensor is a device that transforms chemical information, ranging from the concentration of a specific sample component to total composition analysis, into an analytically useful signal.

In analytical chemistry today it appears that the most important decision is to select an appropriate, highly capable instrument to adapt the chemical procedure recommended by the standardisation authorities [Ursula 1998]. The chemical sensor is the instrument itself or the central element of this instrument. Figure 1-1 shows the analytical procedure and data evaluation process in a general analytical system, and the role of chemical sensors.

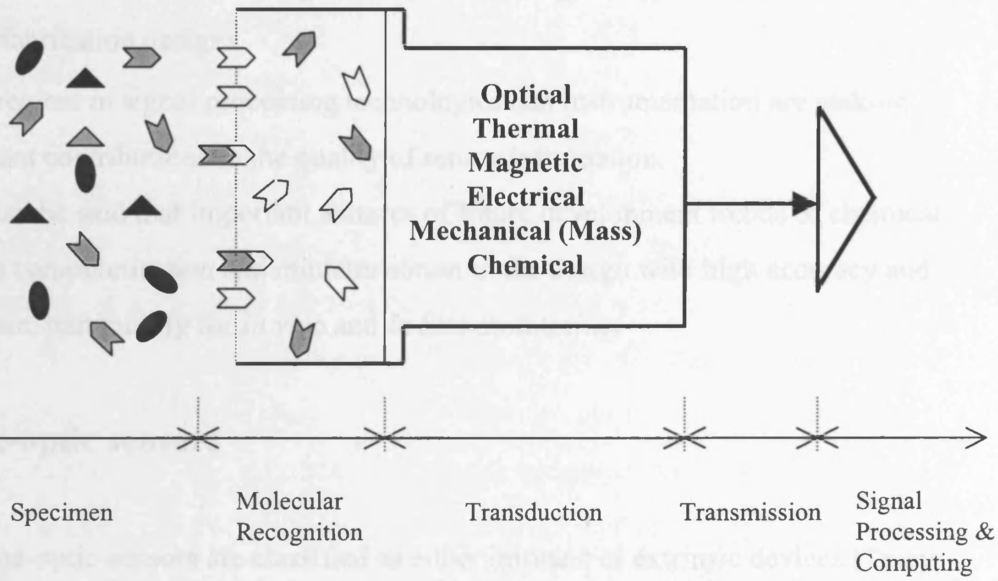

Figure 1-2 The general model for chemical sensors

Since the first really significant event from the commercial point of view occurred around 1932, when Arnold Beckman developed the modern glass electrode [Frant 1994], the development of chemical sensors has made great progress. In the present commercial market many modern chemical sensors are no longer purely electric devices. More and more mature techniques and principles which are successfully used in physical sensors, such as optics, magnetism and acoustics, have already been introduced in the design of chemical sensors as well.

Figure 1-2 shows a general model for chemical sensors, in which procedures are differentiated as specimen, molecular recognition, transduction, transmission and signal processing and computing.

Progress in chemical sensor development increasingly requires a multi-disciplinary effort and access to more complex fabrication technologies, meanwhile, it also brings many challenges in chemical sensor research, such as:

- Improving the recognition mechanism – this is of fundamental importance as it is the basis of the signal that will be obtained from the sensor.
- New materials are being investigated for use as a matrix in which to immobilise the receptor molecule.
- New sensor substrates are being investigated, arising mainly from a need for new planar fabrication designs.
- Improvement in signal processing technologies and instrumentation are making important contributions to the quality of sensor information.

It can be said that important features of future development trends of chemical sensors are computerisation and miniaturisation in the design with high accuracy and fast response, particularly for *In vivo* and *In Situ* monitoring.

1.3 Fibre-optic sensors

Fibre-optic sensors are classified as either intrinsic or extrinsic devices [Tracy 1991 and Jackson 1986]. The intrinsic fibre-optic sensor usually uses inherent properties of optical fibres to implement the light signal modulation in intensity, phase, polarisation, *etc.*. The extrinsic sensor involves the light leaving the confinement of the optical fibre core temporarily, it is then modified by a sensing element before being intercepted again by the optical system. The sensing element may be either physical, chemical or biological and normally requires that a multimode optical fibre be used. The light intensity modulation technique is also usually more appropriate for the design of extrinsic type of sensors.

There are various types of fibre-optic sensors for different measurement applications. The techniques by which the measurements are achieved can be broadly grouped in three categories depending on (a) how the sensing is accomplished, (b) the physical extent of the sensing, and (c) the role of the optical fibre in the sensing process.

Means of sensing

In this category, optical techniques are generally classified in terms of measuring light intensity change in one or more light beams or monitoring light wave phase change in the light beams by causing them to interact or interfere with one another. Thus sensors in this category are termed either light intensity or interferometric fibre-optic sensors. Techniques used in light intensity fibre-optic sensors include light intensity modulation, light wavelength modulation, light polarisation modulation and time modulation. These principles of modulations can realise the measurements via such processes as light absorption, light scattering, spectral transmission changes, microbending loss and reflectance changes, etc. Techniques used in light interferometric fibre-optic sensors are usually those physical effects which can induce the change of one of the optical paths, such as the magneto-optic effect, the laser Doppler effect, or the Sagnac effect.

Extent of sensing

This issue is concerned with whether fibre-optic sensors operate only at a single point or over a distribution of points. Thus, sensors can be categorised as either point or distributed fibre-optic sensors. For a point fibre-optic sensor, the probe may be either at the end of an optical fibre using a reflector to reflect the light beam from the probe to realise a reflection type of sensor or at the middle of an optical fibre, the light source and the receiver being connected to the two ends of the optical fibre to realise a transmission type of sensor. For a distributed fibre-optic sensor, as the name implies, sensing is performed all along the optical fibre length.

Role of optical fibre

The role of optical fibres in fibre-optic sensors is associated with different class of sensors, extrinsic or intrinsic, and whether measurands act externally or internally to the optical fibre. The optical fibre functions as a transmitter of light power and/or part of sensing element.

Advantages and disadvantages of fibre-optic sensors

The advantages of fibre-optic sensors come from both optical principles themselves and the features of the optical fibre, these advantages include small size, flexibility, good insulation, high bandwidth, high sensitivity, wide dynamic range, electromagnetic field immunity, opportunities for both point and distributed configurations, multiplexing capabilities and convenience for remote monitoring.

As with advantages, the disadvantages of fibre-optic sensors derive from the physics of the optical fibre. These disadvantages include the difficulty of projecting the radiation from the fibre deep into opaque objects and the "wire" based measurement of fibre-optic sensors (compared with "wireless" measurements).

Another difficulty with fibre-optic sensors (as with most kinds of sensors), is interference from multiple effects, for example: a sensor intended to measure strain or pressure may be very temperature-sensitive and a sensor, based on fluorescent excitation, intended to measure chemical concentration may be influenced by both concentration and temperature.

1.4 Fibre-optic chemical sensors

The use of optical fibres in chemical and biochemical analysis began in the 1960s [Polanyi 1962, Enson 1962 and Kapany 1964], particularly for oximetry, the measurement of oxygen in the blood. Since that time, many optical techniques, such as light bulk-absorption, optical fluorescence, internal reflection spectroscopy, Raman spectroscopy and surface plasmon resonance (SPR), have been studied and developed in the design of fibre-optic chemical sensors.

In fibre-optic chemical sensors, the typical transduction steps are:

electrical* ⟶ *light source* ⟶ *optical fibre

⟶ probe&chemical ⟶

optical fibre ⟶ detector ⟶ electrical

The first step of electrical to light source corresponds to the generation of light power from electrical power. Then light power is coupled into the optical fibre. Next step is to transmit light power by the optical fibre to the probe which is in contact with the chemical sample (possibly the optical fibre itself is the probe or a part of the probe). The probe&chemical to optical fibre step includes the chemical reactions, molecular recognition, and the transfer of the chemical signal into an optical signal using chemical approaches, for example, indicators immobilised on a support. Then this light signal related to chemical information is received by the detector in the step of optical fibre to detector. The final step is to convert the light signal into an electrical signal for recording and displaying to be analysed.

In fibre-optic chemical sensors, an important issue is the transduction of "chemical to optical". The main types of the transduction of information from the analyte into an optical signal are:

1. The spectral properties of the analyte are analysed directly,
2. Chemiluminescence or bioluminescence is used for sensing,
3. Typical transduction is performed with an indicator, label, or potential-sensitive dye (PSD),
4. The intrinsic properties of optical fibres are used in the transduction process (intrinsic fibre-optic chemical sensors),
5. The physicochemical properties of the analyte (e.g., refractive index) are measured by an optical fibre,
6. The analyte can be a tracer.

Advantage of fibre-optic chemical sensors

Besides, the common advantages of fibre-optic sensors mentioned above, fibre-optic chemical sensors have also some other distinguishing features:

- *Chemically stable*: The basic material from which optical fibres are made is amorphous silica. This is chemically inert, *i.e.*, it can be used in strongly acidic or moderately alkaline environments.

- *Thermally stable*: Pure silica softens a little above 1000°C, with other glasses softening above 500°C, and therefore the glasses are also thermally stable. Although, the upper working temperature of the majority of optical fibres is limited by their surrounding polymer, and is still often around 125°C. With polyimide, amorphous carbon and metallic coatings, optical fibres are capable of withstanding higher temperature (≥400°C).

- *Adaptable*: Optical fibres are easy to combine into currently used optical techniques and instruments in analytical chemistry, such as absorption, fluorescent and scattering spectrophotometry and chromatography.
- *Intrinsic*: Inherent properties of optical fibres, such as internal total reflection, can be used in the design of fibre-optic chemical sensors.

Limitations of fibre-optic chemical sensors

The limitations of fibre-optic chemical sensors are caused by both the weakness of optical principles, optical fibres and chemistry, such as:

1. The influence of parasitic optical signals due to light scattering and background fluorescence,
2. The interaction of the light and the chemical process,
3. The limited lifetime of the immobilised reagent,
4. Photodegradation, such as by bleaching of an indicator dye.

1.5 Light intensity attenuation-based fibre-optic chemical sensors

Light intensity attenuation measurement is most important and popular in fibre-optic chemical sensors. Typical principles are optical bulk-absorption and optical reflectance measurements. Both intrinsic and extrinsic principles are involved in the design of this type of sensor.

Optical bulk-absorption:

Light passing through a material can be absorbed by interaction with the molecules and atoms of the host material, or by impurities and defects. At any given wavelength λ, the intensity of the light passing through the material is attenuated as an exponential function of its path length (x). The absorption coefficient (α_λ) is defined relative to the concentration [M] and the cross section (s) of the absorbing molecules, expressed as the Beer-Lambert law:

$$I_\lambda(x) = I_\lambda(0)\exp(-\alpha_\lambda \cdot x) \tag{1.1}$$

$$I_\lambda(x) = I_\lambda(0)\exp(-s_\lambda \cdot [M] \cdot x / N) \qquad (1.2)$$

where $I_\lambda(x)$ is the light intensity at a distance *x*, $I_\lambda(0)$ is the incident light intensity at *x=0,* and *N* is Avogadro's number ($6.022 \times 10^{23}\ mol^{-1}$).

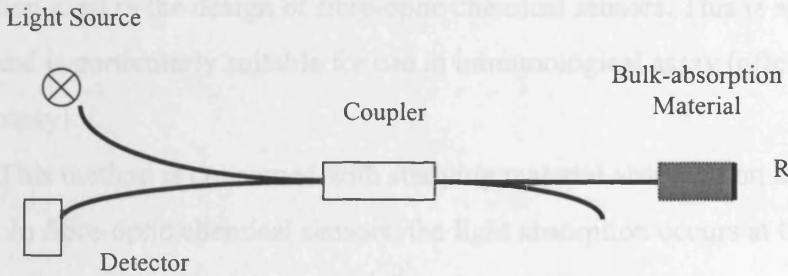

Figure 1-3 The arrangement of reflection type of bulk-absorption sensor

This is so-called light intensity attenuation by bulk-absorption. The basic arrangement is shown in Figure 1-3. Disturbances in the environment with chemical samples to be measured can change the light absorption, and light intensity attenuation relies on these disturbances.

The application of the principle of light bulk-absorption measurement has a long history. For example, optical spectrometry is widely and successfully used in conventional chemical analysis employing light bulk-absorption. By combining the basic principle of optical bulk absorption with the optical fibre technology, fibre-optic spectrometry further enhances its capabilities.

Light intensity attenuation-based fibre-optic chemical sensors using light bulk-absorption is designed as extrinsic fibre-optic sensors. A probe or a chamber has to be included, which is to contact the chemical sample and to sense the information of the chemical sample to be measured, or sometimes, even which contains the chemical sample itself. Light bulk-absorption happens inside the probe or chamber. By monitoring the light intensity attenuation, the information of the chemical sample, such as concentration, can be determined. Optical fibres are linked to the probe or chamber as transmitters (or carriers) to carry light power from the light source to the chemical sample and then from the chemical sample back to the detector.

Because of the simplicity of the principle, ease of manufacture and compatibility with bulk-optics, fibre-optic chemical sensors based on bulk-absorption have become the widest used extrinsic devices.

Optical reflectance measurement is another typical principle of light intensity attenuation used in the design of fibre-optic chemical sensors. This is an intrinsic design and is particularly suitable for use in immunological assay (often shortened to immunoassy).

This method is concerned with studying material absorbed on an optical surface. In fibre-optic chemical sensors, the light absorption occurs at the interface of a surrounding medium and the optical fibre (usually the exposed core of the fibre). That is so-called attenuated total internal reflection (ATIR). The medium is either the chemical sample itself or a layer in contact with the chemical sample.

There are two principle variations in attenuated total internal reflection(ATIR):

- Optical Evanescent Wave (EW) Absorption, and
- Optical Surface Plasmon Resonance (SPR).

Optical evanescent wave absorption:

In a multimode optical fibre, a ray of light is guided within the optical fibre if the angle of incident at the interface of optical fibre core and the transducing medium is greater than the critical angle θ_c, given by:

$$\theta_c = \sin^{-1}(\frac{n_2}{n_1}) \qquad (1.3)$$

where n_1 and n_2 are the refractive indexes of the optical fibre core and the transducing medium, respectively. Due to the evanescent wave absorption, the electric field amplitude of transmitted light E decays exponentially with the distance z into the medium:

$$E = E_0 \cdot \exp(-z / d_p) \tag{1.4}$$

where E_0 is the electric field at the interface of the core and the transducing medium. The depth of penetration, d_p, is defined as the distance for the electric field amplitude to fall to *1/e* of this value at the interface:

$$d_p = \frac{\lambda}{2\pi n[\sin^2\theta - (n_2/n_1)^2]^{1/2}} \tag{1.5}$$

Figure 1-4 shows a configuration of evanescent wave absorption in the optical fibre.

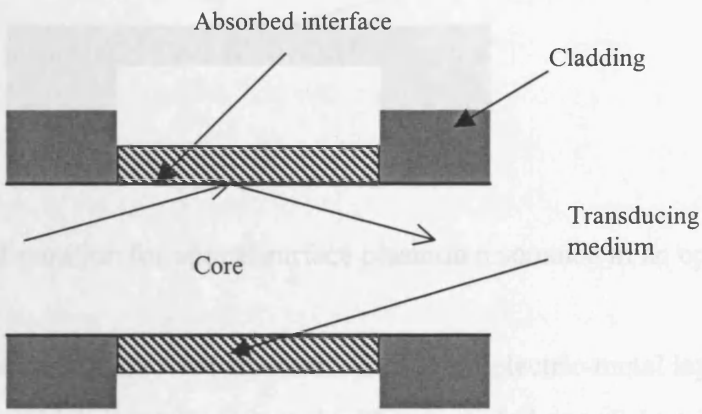

Figure 1-4 The configuration of evanescent wave absorption in an optical fibre

The depth determined by parameters in Equation (1.5) gives the degree of the interaction with the surrounding medium. The light intensity attenuation in optical fibres is determined by the optical reflectance in the interface of the optical core exposed and the surrounding medium. The change of the refractive index of the surrounding medium, for example induced by a concentration change of the chemical sample, will change the optical reflectance. Of course, there are also other factors determining the optical reflectance, such as the polarisation of the electric field and the size of the interaction area.

Optical surface plasmon resonance (SPR)

Optical surface plasmon resonance (SPR) is an extension of optical evanescent wave technique. The difference is that the exposed core of the optical fibre is covered with a thin metal film in SPR systems. The configuration is shown in Figure 1-5.

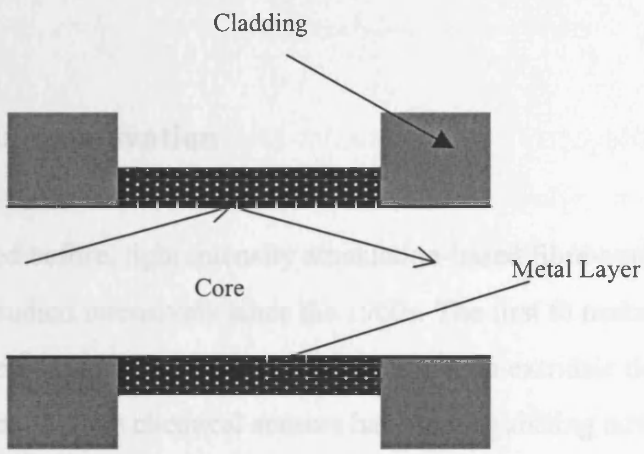

Figure 1-5 The configuration for optical surface plasmon resonance in an optical fibre

Optical surface plasmon resonance can occur at a dielectric-metal layer interface when light, which is totally reflected within an underlying dielectric, induces a collective oscillation in the free-electron plasma at the metal film boundary. The conditions for this to occur are that the momentum of the photons (K_x) in the plane of the film should match that of the surface plasmons (K_{sp}) on the opposite surface of the metal film [Liedberg 1983]. This occurs at a defined critical incident angle of light, θ_{sp}. The momentum, K_{sp}, of the surface plasmons, is a function of the dielectric constant, ε_m and ε_2, of the metal and sample layers, respectively:

$$K_{sp} = \frac{\omega}{c}\left(\frac{1}{\varepsilon_m} + \frac{1}{\varepsilon_2}\right)^{-½} \tag{1.6}$$

The resulting effect is to produce a large change in the reflection coefficient at this resonant angle. In optical fibres the reflection angle is selected by the numerical aperture which is determined by the refractive indexes of the optical fibre core and cladding. Hence the resonance condition changes with the light wavelength, the optical power spectrum of reflection is monitored to sense the properties of the chemical sample.

1.6 Discussion and motivation

As mentioned before, light intensity attenuation-based fibre-optic chemical sensors have been studied intensively since the 1960s. The first to make an appearance was a device using optical bulk-absorption in an extrinsic design. Although extrinsic optic-fibre chemical sensors have distinguishing advantages, they are not suitable for the monitoring of chemical reactions on surfaces, such as in immunoassays. In this situation, intrinsic devices are particularly useful and powerful. Therefore, most of research on modern light intensity attenuation-based fibre-optic chemical sensors could be principally divided into two main directions:

(1) Optical bulk-absorption measurement,

(2) Optical reflectance measurement — attenuated total internal reflection (ATIR) measurement, which includes the following two sub-divisions:

----------evanescent wave (EW) absorption measurement,

----------optical surface plasmon resonance (SPR)excitation, as an extension of evanescent wave (EW) absorption measurement.

The design and research on fibre-optic chemical sensors using optical bulk-absorption is mainly focused on the probe or chamber design and system optimisation, because the optical fibre here is simply functioning as a transmitter or carrier of light power.

The consideration of the probe or chamber design is to meet different requirements of applications in terms of space, environment, structure, and materials, etc.

The consideration of system optimisation is to achieve the best performance in terms of sensitivity, response time, cost and flexibility, etc.

The design and research on fibre-optic chemical sensors using optical reflectance (evanescent wave (**EW**) absorption and optical surface plasmon resonance (**SPR**) excitation) mainly focus on novel designs and theoretical analyses.

Research into novel designs is to explore applications where conventional sensors cannot be used, or where conventional sensors cannot achieve good performance, etc.

Research into theoretical analyses is to construct new theoretical models which can describe the characteristics, explain the experimental results and predict the performance of sensors. The theoretical models are also used to analyse the accuracy and to estimate the limitation of the sensor.

Aims of this research

Although optical fibre sensing technology has already had many successful applications in chemical measurements, there exist still many more potential applications which need to be explored.

Basically, the objective of this research is to have a better understanding of light intensity attenuation-based fibre-optic sensors in chemical measurements. Aims of this research include:

(1) Theoretical investigations of fibre-optic chemical sensors which do not yet have a well established and satisfactory theoretical basis,

(2) Design studies of fibre-optic chemical sensors which can be potentially useful in industrial and clinic applications.

Scope of this research

The investigation of this research involves both theoretical analyses and design studies.

In the theoretical analyses, mathematical and systematic derivations are given to establish new theoretical formulations which model fibre-optic chemical sensors more effectively. Numerical calculations are presented to explain experimental results, to describe characteristics and to predict performance.

In the design studies, an extrinsic type fibre-optic sensor is designed to measure the concentration of the anaesthetic “propofol” by using the optical bulk-absorption principle, and SPR fibre-optic sensors are designed for concentration measurements in both point and distributed systems as an design application of the intrinsic class of sensors.

1.7 Thesis overview

There are eight chapters in the thesis. Chapter 1 has introduced the rationale for the research, and some of optical principles and technologies exploited in light intensity attenuation-based fibre-optic chemical sensors. It has been proposed that both intrinsic and extrinsic devices be analysed to obtain a better understanding, and research has involved both theoretical analyses and design studies.

The main body of the thesis contains two parts — part 1: theoretical analyses, from Chapter 2 to Chapter 5, part 2: design studies, including Chapter 6 and Chapter 7.

Chapter 2 developes a theoretical model to evaluate the absorption coefficient of leaky skew rays in evanescent wave (EW) fibre-optic sensors. The model helps to construct a more comprehensive expression to depict evanescent wave absorption in optical fibre sensors, which is more accurate than previous results. Numerical calculations are presented to obtain the quantitative concept of the absorption of leaky skew rays.

Chapter 3 and Chapter 4 studies the characteristics of surface plasmon resonance (SPR) fibre-optic chemical sensors using both numerical and analytical approaches. These researches are based on the approximation of meridional rays, thus they are satisfied for optical waveguide SPR system. Chapter 3 is focused on the numerical analyses of the characteristics related to light reflectance. Chapter 4 is focused on the construction of approximate mathematical models.

Chapter 5 deals with a popular technique in intensity modulation fibre-optic sensors — two-wavelehgth compensation. A reference wavelength is introducted to monitor and compensate for noise and fluctuations of sensors. This chapter discusses the error in a two-wavelength system induced by microbending of optical fibre and the temperature instability of light source.

Chapter 6 develops an extrinsic fibre-optic chemical sensor to measure the concentration of the anaesthesic " propofol". From the design point of view, the overall system is studied. Materials are tested for the probe design. In order to meet the design targets, optics and electronics are considered, key components are evaluated.

Chapter 7 demonstrates the design of surface plasmon resonance (SPR) fibre-optic sensors. In the design the swellable transducing layer is an important element, which can help the sensor achieve high performance in terms of sensitivity and response time. On the other hand, the resonance wavelength in SPR fibre-optic sensors is considered as a distinguished feature to realise distributed system design.

Chapter 8 draws summary lessons. Conclusions for each element of the work have been set down. Further work leading from the research is given in terms of both theory and design.

Part 1: Theoretical Analyses

Chapter 2

Theoretical Analysis of the Evanescent Wave Absorption Coefficient for Multimode Fibre-Optic Evanescent Wave Absorption Spectroscopy and Sensors

2.1 Introduction

This chapter discusses the theoretical analysis of evanescent wave absorption for multimode fibre-optic evanescent wave absorption sensors and spectroscopy, paying particular attention to leaky skew rays which transmit light power in a different way from trapped and meridional rays. A brief introduction to fibre-optic evanescent wave techniques is presented as background for this chapter. A mathematical model of the absorption coefficient of leaky skew rays using geometric optics is developed. Further, a comprehensive expression for the effective evanescent wave coefficient is obtained. Some numerical results are given to illustrate the theoretical analysis.

2.2 Fibre-optic evanescent wave techniques in chemistry

Optical evanescent wave technology is a rapidly developing approach for optical sensing induced by molecules on the surface of the optical fibre or other waveguides (e.g., for measurement of a chemical reactions and concentrations). Fibre-optic chemical sensors and biosensors[1] using the evanescent wave are analytical devices that measure the interactions between biomolecules in real time without the need for any labels.

[1] IUPAC defines biosensor as a subgroup of chemical sensors in which a biologically based mechanism is used for analyte detection.

The motivation for adopting the optical evanescent wave technique derives from a number of advantages offered by the technique in particular applications [Diamond 1998]:

1. Because the interrogating light remains guided, no coupling optics are required in the sensing region and an all-fibre approach is feasible. Furthermore, considerable miniaturisation is possible and this is particularly relevant to integrated optic devices for which evanescent wave interactions are the predominant sensing mechanism.
2. By controlling the launch optics it is possible to confine the evanescent field to a short distance from the guiding interface and thereby discriminate to a large extent between surface and bulk effects. This is particularly important in some applications that involve surface interactions, such as fluoroimmunoassay [Walczak 1992].
3. The technique can provide enhanced sensitivity over conventional bulk-optic approaches. For example, optical fibre-based evanescent wave absorption devices are more sensitive than bulk-optic attenuated total internal reflection (ATIR) [Harrick 1967] crystals by virtue of the greater number of reflections per unit length (or equivalently, the greater power in the evanescent field).
4. It is often difficult or inconvenient to perform accurate absorption measurements on highly absorbing or highly scattering media. Fibre-optic evanescent wave spectroscopy is suitable for such samples because the effective path length is so small and the technique is much less sensitive to scattering.
5. If an optical fibre is configured to be sensitive to evanescent wave interactions all along its length or at discrete zones, then fully – or quasi-distributed sensing is possible. This would enable monitoring of the spatial profile of an analyte concentration over substantial distances.
6. In contrast with conventional distal-face optrodes, the evanescent wave approach affords the sensor designer greater control over interaction parameters such as interaction length, sensing volume and response time.

Fibre-optic evanescent wave sensors and spectroscopy are not without difficulties. One of chiefs among these is that the absorption coefficient is too small compared with bulk-absorption if the incident light angle is not near to the critical angle, which will reduce the sensitivity and require the use of a long interacting area. Another is the problem of surface fouling, which can reduce sensitivity and necessitate frequent recalibration until the sensor is no longer viable. A number of compensation techniques have been proposed, but these have not been implemented experimentally [Stewart 1990]. If suitable techniques are not found, then commercial evanescent wave devices will be restricted, in some appliations, to short-term or disposable use.

Fibre-optic evanescent wave absorption sensors and spectroscopy have been successfully employed in a variety of applications for studies of solid-liquid interfaces [Iwamoto 1984], chemical reaction rates [Margalit 1989], complex material curing [Wright 1989], organometallic thin films [Feinstein 1991], liquid [Paul 1987, and Simhony 1988] and gas [Giuliani 1983 and Messica 1994] detection and monitoring, concentration measurements [Mendelson 1988 and Krska 1992] and biological applications [Vo-Dinh 1987 and Schwotzer 1997]. The light wavelength employed has extended from infrared [Jakusch 1997 and Regan 1997], visible [DeGrandpre 1988 and Deboux 1995] to near-ultraviolet [Potyrailo 1998 and Merschman 1998]. Tuneable lasers have been incorporated into systems [Schnitzer 1990 and Messica 1992] instead of conventional blackbody light sources, which have improved the wavelength resolution, sensitivity and detection limit.

Theoretical evaluations of evanescent wave absorption has been attempted since the appearance of the sensor. Both electromagnetic field theory [Pitaud 1992 and Qing 1996] and geometric optics [Ruddy 1990, Schnitzer 1990 and Gupta 1994a] have been used to construct theoretical models for the explanation of experimental results. Because of its simplicity and effectiveness, geometric optics is playing an important role in the development of theoretical models. In the derivation of these models using geometric optics, Fresnel's law [Synder 1974a and 1974b] is applied, and only meridional or trapped rays have been considered so far. There is a class of weakly attenuated rays, so called leaky rays, in respect to optical fibres of circular cross section. The behaviour of these leaky rays is incorrectly predicted by Fresnel's law. Many skew rays or tunnelling rays within a circular optical fibre which geometric optics predicts are trapped by total internal reflection are in fact leaky. These leaky skew rays, which carry a significant proportion of the power, have different transmission characteristics. When there is absorbing cladding, leaky skew rays contribute to evanescent wave absorption in a different way to that of other rays. In order to construct an accurate theoretical model for evanescent wave absorption in fibre-optic sensors, it is necessary to analyse the transmission of these leaky skew rays in the optical fibre. In the following sections of this chapter, a theoretical analysis of evanescent wave absorption of leaky skew rays is proposed under the weakly guided approximation.

2.3 The evanescent wave absorption coefficient

2.3.1 The evanescent wave absorption coefficient for meridional rays

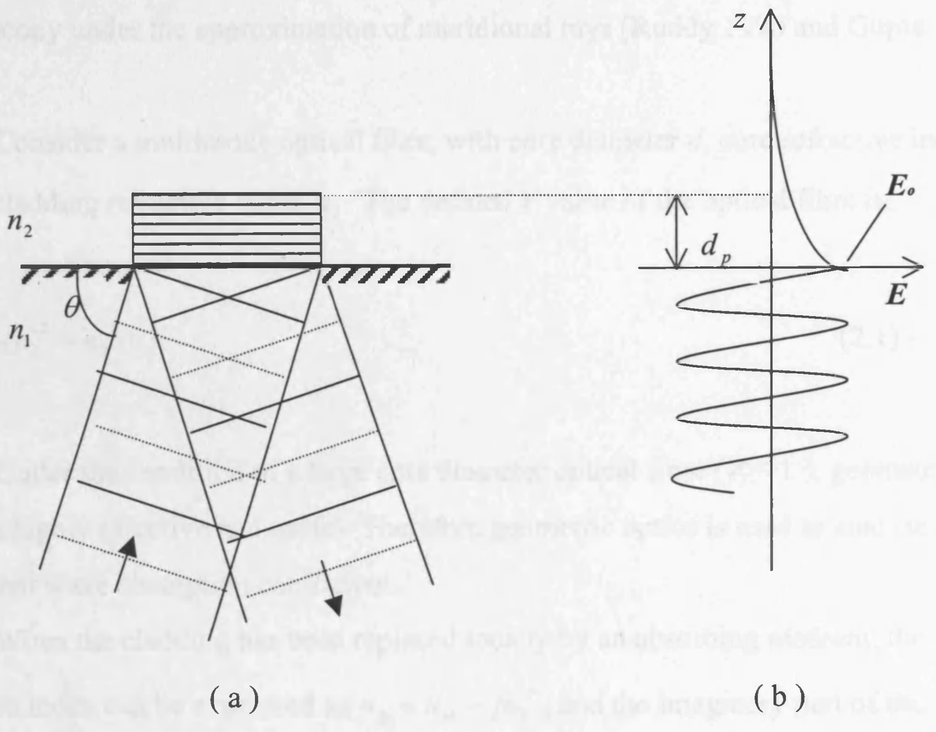

Figure 2-1 Optical evanescent wave principle: (a) a ray of light reflected at the interface of two media with $n_1 > n_2$ penetrates a small distance into the lower refractive index medium; (b) the electric field of the evanescent wave falls off exponentially into the lower refractive index medium.

With a light wave striking the interface between two media of refractive indices n_1 and n_2 ($n_1 > n_2$), total internal reflection occurs when the angle of reflection θ is less than the critical angle θ_c, there is an evanescent wave refracted through the interface in the *z* direction which penetrates the lower refractive medium a distance d_p, which is of the order of a wavelength (Note the redefinition of θ, Figure 2-1). It can be shown that the electric field of this wave (*E*) is largest at the interface (E_o) and decays exponentially with distance (*z*) as shown in Figure 2-1 (a) and (b). All values are given by equations of (1.3) to (1.5).

This model is derived for planar waveguides in bulk-optics, the interface is the boundary of two planar media. The bulk-optic model is suitable to apply to meridional rays of optical fibres. The following part of this section presents a brief review of the evaluation of the evanescent wave absorption coefficient of fibre-optic sensors and spectroscopy under the approximation of meridional rays [Ruddy 1990 and Gupta 1994a].

Consider a multimode optical fibre, with core diameter *d*, core refractive index n_1 and cladding refractive index n_2. The defined *V* value of the optical fibre is:

$$V = \frac{\pi d}{\lambda}(n_1^{\,2} - n_2^{\,2})^{1/2} \tag{2.1}$$

Under the condition of a large core diameter optical fibre ($V \gg 1$), geometric optics is highly effective and useful. Therefore geometric optics is used to analyse the evanescent wave absorption coefficient.

When the cladding has been replaced locally by an absorbing medium, the refractive index can be expressed as $n_2 = n_{cl} - jn_2^{\,*}$, and the imaginary part of the refractive index at the employed wavelength is:

$$n_2^* = \frac{\alpha\lambda}{4\pi} \tag{2.2}$$

where α is the bulk absorption coefficient of the medium.

If P_0 is the power transmitted by the optical fibre in the absence of an absorbing cladding, then the transmitted power in the presence of an absorbing medium is given by:

$$P(z) = P_0 \exp(NTz) \tag{2.3}$$

where z is the length of the cladding absorbing medium N is the number of ray reflections per unit length of optical fibre and T is the transmission coefficient of the light on penetrating the absorbing cladding.

Thus, the light intensity attenuation coefficient of evanescent wave absorption γ can be written:

$$\gamma = NT \tag{2.4}$$

And the number of ray reflections per unit length of optical fibre of N is:

$$N = \frac{\tan\theta}{d} \tag{2.5}$$

where θ and θ_T are the angles at which the light strikes the interface and the refractive angle, respectively, with respect to the longitudinal axis of optical fibre.

The transmission coefficient can be derived from the Fresnel equations using a complex refractive index for the cladding [Lorrain 1988],

$$T = \frac{4n_1 n_2 \sin\theta \sin\theta_T}{\left|n_1 \sin\theta + n_2 \sin\theta_T\right|^2} \tag{2.6}$$

Using $\sin\theta_T = -j[(n_1^2 / n_2^2)^2 \cos^2\theta - 1]^{½}$, equation (2.6) can be seen that for an absorbing cladding, T is real and given by:

$$T = \frac{4n_1^2 \sin\theta \,\mathrm{Im}[\cos^2\theta - (n_2/n_1)^2]^{1/2}}{n_1^2 - n_2^2} \tag{2.7}$$

The complex cladding index, $n_{cl} - jn_2^*$, and the imaginary part of $[\cos^2\theta - (n_2/n_1)^2]^{1/2}$ is expressed as:

$$\frac{n_2 n_2^*}{n_1^2[\cos^2\theta - (n_2/n_1)^2]^{1/2}} \tag{2.8}$$

Therefore, the transmission coefficient is:

$$T = \frac{\alpha\lambda n_2 \sin\theta}{\pi(n_1^2 - n_2^2)[\cos^2\theta - (n_2/n_1)^2]^{1/2}} \tag{2.9}$$

The light intensity attenuation coefficient of evanescent wave, $\gamma_m(\theta)$, for meridional rays of optical fibre is expressed as:

$$\gamma_m(\theta_z) = \frac{\alpha\lambda n_2 \sin^2\theta}{\pi d \cos\theta\sqrt{\cos^2\theta - (n_2/n_1)^2}\,(n_1^2 - n_2^2)} \tag{2.10}$$

The derivation above considers only one ray of light (with angle θ). In a multimode optical fibre with many thousands of guided modes (thousands of transmitted rays at different angles), an effective evanescent wave absorption coefficient for meridional rays has to be used. This includes the contributions from all guided modes, expressed as equation (2.11):

$$\gamma_m^{eff} = \frac{\int_{meridional-ray} s(\theta)\gamma_m(\theta)d\theta}{\int_{meridional-ray} s(\theta)d\theta} \tag{2.11}$$

where $s(\theta)$ is the light intensity distribution.

2.3.2 The evanescent wave absorption coefficient for leaky skew rays

A random ray of wavelength λ incident at P on the interface of a multimode step-profile fibre of core diameter d, with n_1 and n_2 the refractive indices of the core and the cladding, respectively, is shown in Figure 2-2. Relative to the normal PO, the angle of incidence or reflection is α. Both incident and reflected rays make angles θ_z with the axial direction PZ, and θ_ϕ in the cross-section between the tangent PQ and the path projection, *i.e.* PR for the reflected ray.

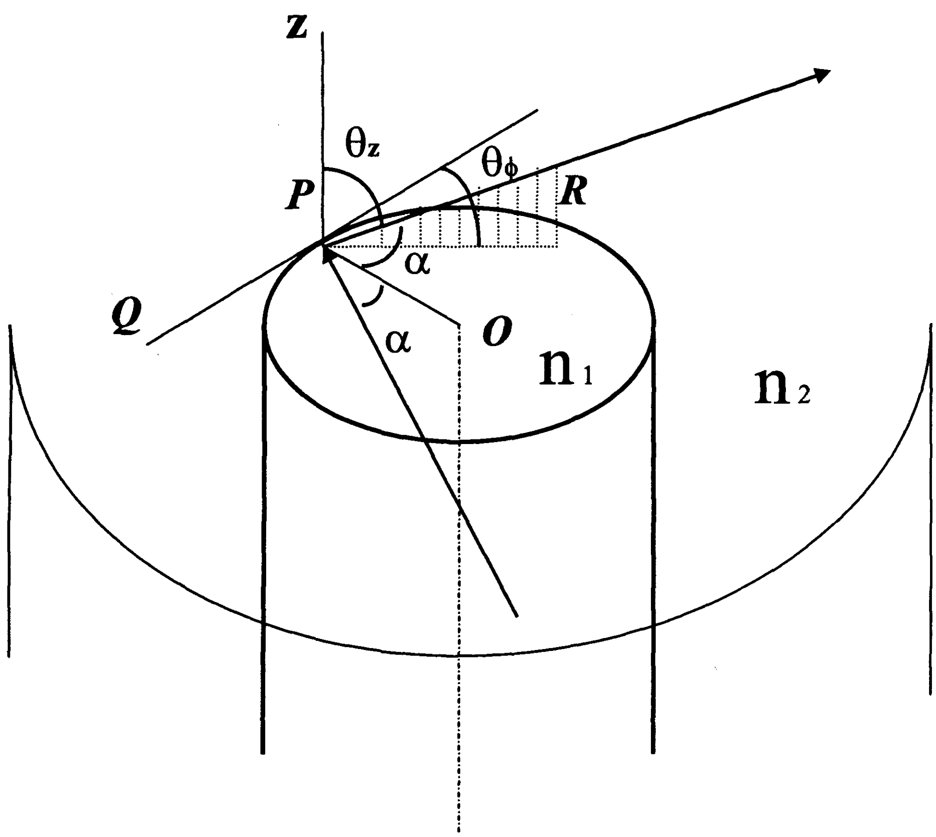

Figure 2-2 Definition of angles of the ray inside the optical fibre

Due to the curvature of the fibre surface, there are three classes of rays which transmit light power in totally different ways, and are differentiated by the critical angle, θ_c ($\cos\theta_c = n_2 / n_1$) [Synder 1974a and 1974b]:

(i) trapped rays: $0 \le \theta_z < \theta_c$,
(ii) refracted rays: $\alpha < (\pi/2 - \theta_c)$,
(iii) leaky skew rays: $\pi/2 \ge \theta_z > \theta_c$ and $\pi/2 \ge \alpha > (\pi/2 - \theta_c)$.

Under the weakly guided approximation, Synder gave a brief analysis of the importance of leaky skew rays to determine the power contribution of leaky skew rays to the total power of rays predicted to be transmitted by geometric optics [Synder 1974a and 1974b].

The power initially contained in the leaky skew rays depends on the source of illumination. Under the supposition that all rays are launched with equal power, as is the case for incoherent or diffuse illumination [Kapany 1967], the power predicted by geometric optics to be transmitted within the cylinder optical fibre is a sum of the power of trapped rays P_T plus the initial power of the leaky skew rays P_S.

The amount of power P_T transmitted by trapped rays is proportional to the square of the numerical aperture of the optical fibre. Thus

$$P_T = \sin^2\theta_c = 1 - (\frac{n_2}{n_1})^2 \tag{2.12}$$

Assuming a unit power source, ignoring the refracted rays, the summed power P_{TOT} transmitted by the leaky skew rays and trapped rays:

$$\begin{aligned} P_{TOT} &= P_T + P_S \\ &= 1 - \frac{2}{\pi}[(\delta - \delta^2)^{1/2} + (1 - 2\delta)\cos^{-1}\sqrt{\delta}] \end{aligned} \tag{2.13}$$

where $\delta = 1 - (n_2 / n_1)^2$

The percentage of leaky skew rays power p contribution to the total power prediced to be transmitted by geometric optics is:

$$p = \frac{P_S}{P_S + P_T}$$

$$= 1 - \frac{\sin^2 \theta_c}{1 - \frac{2}{\pi}\left[(\delta - \delta^2)^{1/2} + (1 - 2\delta)\cos^{-1}\sqrt{\delta}\right]} \quad (2.14)$$

Figure 2-3 shows the normalised total power P_{TOT} and the percentage of leaky skew rays power p against $\sin^2 \theta_c$.

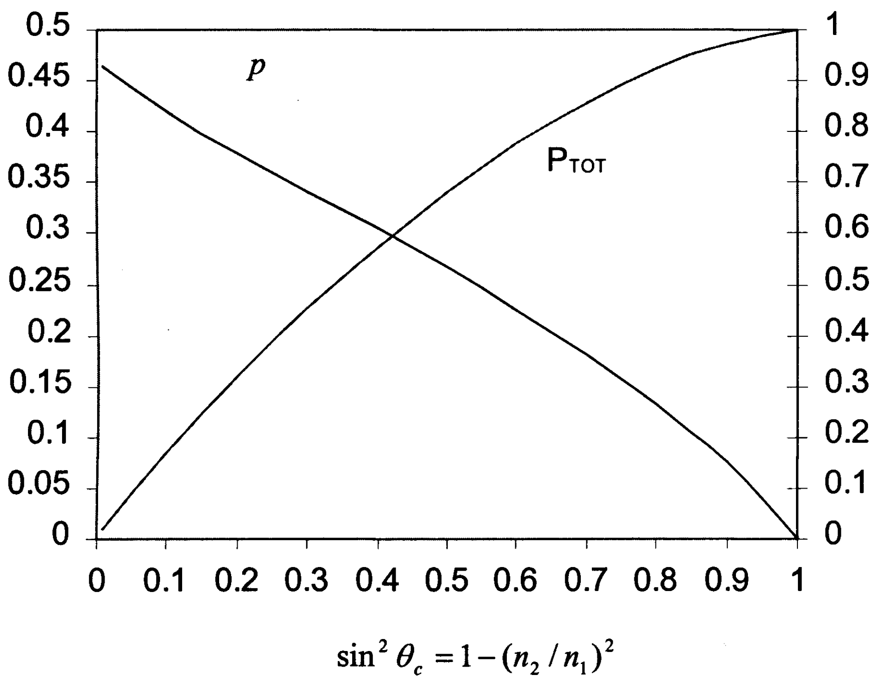

Figure 2-3 The normalised total power P_{TOT} and the percentage of leaky skew rays power p against $\sin^2 \theta_c$

Assuming a diffuse or incoherent illumination, the contribution of leaky skew rays to the total light-transmitting power of the optical fibre can be determined from the figure. When $n_1 \cong n_2$, as it is for optical communication fibres, nearly $50\,\%$ of the power is initially launched into the leaky skew rays. The P_{TOT} curve shows that, as the difference between n_1 and n_2 increases, the total power-transmission capability of the optical fibre increases.

On the other hand, it is easy to construct illumination conditions for which only leaky skew rays are launched. Two examples are presented below:

(1) The bright bands across the exit end of an optical fibre observed at steep angles are due to leaky skew rays [Kapany 1967 and Potter 1961].

(2) The so-called whispering-gallery modes in large-diameter optical fibres launched by highly skew illumination, are formed by leaky rays [Reick 1965].

It can be seen that leaky skew rays are important in many physical problems. Next, the absorption characteristics of leaky skew rays are discussed.

In evanescent wave absorption fibre-optic sensors or spectroscopy, the light intensity absorption is induced by the absorption of both trapped and leaky skew rays in the cladding medium. Evanescent wave absorption of trapped rays can be explained by the attenuated total internal reflection described by the Fresnel's law. However, it is known by theories and experiements that the transmission behaviour of leaky skew rays is quite different from that of trapped rays. Fresnel's law cannot predict the transmission of leaky skew rays correctly.

For a weakly guided, large diameter optical fibre ($V>>1$), the light intensity of leaky skew rays is expressed by equation (2.15) [Synder 1974a and 1974b].

$$\bar{\gamma}_s(\theta_z) = \frac{4\theta_c}{d}\left(\frac{\theta_z}{\theta_c}\right)^2\left[1-\left(\frac{\theta_z}{\theta_c}\right)^2\sin^2\theta_\phi\right]^{1/2} \times \exp\left[\left(-\frac{2}{3}V\right)\frac{\left(1-(\theta_z/\theta_c)^2\sin^2\theta_\phi\right)^{3/2}}{(\theta_z/\theta_c)^2-1}\right] \tag{2.15}$$

where $\theta_c \cong \sin\theta_c = [1-(\frac{n_2}{n_1})^2]^{1/2}$

Substitute $n_2 = n_{cl} - jn_2^*$ into θ_c obtain:

$$\theta_c = \frac{n_1^2 - n_{cl}^2 + n_2^{*2}}{n_1(n_1^2 - n_2^2)^{1/2}} + j\frac{2n_{cl}n_2^*}{n_1(n_1^2 - n_2^2)^{1/2}} \tag{2.16}$$

Thus,

$$\bar{\gamma}_s(\theta_z) = \left(\frac{n_1^2 - n_{cl}^2 + n^*{}_2^2}{n_1\left(n_1^2 - n_2^2\right)^{1/2}} + j\frac{2n_{cl}n^*{}_2}{n_1\left(n_1^2 - n_2^2\right)^{1/2}} \right) \times \frac{4}{d}\left(\frac{\theta_z}{\theta_c}\right)^2 \left[1 - \left(\frac{\theta_z}{\theta_c}\right)^2 \sin^2\theta_\phi\right]^{1/2}$$

$$\times \exp\left[\left(-\frac{2}{3}V\right)\frac{\left(1-(\theta_z/\theta_c)^2\sin^2\theta_\phi\right)^{3/2}}{(\theta_z/\theta_c)^2 - 1}\right] \tag{2.17}$$

where the definition of variables follows the above sections.

In most applications of optical fibre sensors, where the transmission distance is short, this attenuation can be neglected. However in the application of evansecent wave absorption sensors, when the cladding has become an absorbing medium, mostly, this attenuation can not be regarded as negligible. Such phenomena have been found and mentioned by many researchers [Deboux 1995, Gupta 1994b and Messica 1996].

Under the condition of weak absorption, from equation (2.17), the evanescent wave absorption coefficient, for leaky skew rays, induced by the absorbing cladding is obtained as:

$$\gamma_s(\theta_z) = \left(\frac{n^*{}_2^2}{n_1\left(n_1^2 - n_2^2\right)^{1/2}} \right) \times \frac{4}{d}\left(\frac{\theta_z}{\theta_c}\right)^2 \left[1 - \left(\frac{\theta_z}{\theta_c}\right)^2 \sin^2\theta_\phi\right]^{1/2}$$

$$\times \exp\left[\left(-\frac{2}{3}V\right)\frac{\left(1-(\theta_z/\theta_c)^2\sin^2\theta_\phi\right)^{3/2}}{(\theta_z/\theta_c)^2 - 1}\right] \tag{2.18}$$

Substitute $n_2^* = \alpha\lambda / 4\pi$ into equation (2.18), the evanescent wave absorption coefficient of leaky skew rays is expressed as:

$$\gamma_s(\theta_z) = \left(\frac{\alpha^2 \lambda^2}{4\pi^2 d n_1 \left(n_1^2 - n_2^2\right)^{1/2}} \right) \times \left(\frac{\theta_z}{\theta_c}\right)^2 \left[1 - \left(\frac{\theta_z}{\theta_c}\right)^2 \sin^2\theta_\phi \right]^{1/2}$$

$$\times \exp\left[\left(-\frac{2}{3}V\right) \frac{\left(1-(\theta_z/\theta_c)^2 \sin^2\theta_\phi\right)^{3/2}}{(\theta_z/\theta_c)^2 - 1} \right] \qquad (2.19)$$

2.4 The effective evanescent wave absorption coefficient

2.4.1 The effective evanescent wave absorption coefficient for uniform sensing regions of multimode optical fibres

In order to construct a comprehensive theoretical model of evanescent wave absorption in optic-fibre sensors, both trapped and leaky skew rays have to be considered carefully.

Under such considerations, the effective evansecent wave absorption coefficient for uniform sensing regions $\gamma_{eff}^{uniform}$ is given by:

$$\gamma_{eff}^{uniform} = \frac{\int_{leakily\_skew\_ray} s(\theta_z)\gamma_s(\theta_z)d\theta_z + \int_{trapped\_ray} s(\theta_z)\gamma_m(\theta_z)d\theta_z}{\int_{trapped+leakily\_skew\_ray} s(\theta_z)d\theta_z} \qquad (2.20)$$

where $s(\theta_z)$ represents the power distribution of the rays and integrations are performed according to different classes of rays.

Equation (2.20) is an accurate expression for the effective evanescent wave absorption coefficient for uniform sensing regions of multimode optical fibres, and using this expression, evanescent wave absorption can be predicted correctly.

2.4.2 The effective evanescent wave absorption coefficient for bi-tapered sensing regions of multimode optical fibres

In order to increase the sensitivity, modifications of the optical fibre core into bi-tapered geometry sensing regions has been proposed in the design of fibre-optic evanescent wave absorption sensors or spectroscopy [Gupta 1994c and Mignani 1998]. Figure 2-4 shows the geometrical structure of a multimode optical fibre with a bi-tapered sensing region.

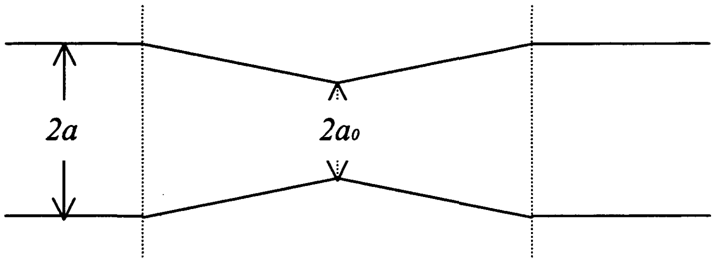

Figure 2-4 Geometry of a tapered sensing region

The effective evanescent wave absorption coefficient for this type considering the effect of the bi-tapered geometry is expressed as:

$$\gamma_{eff}^{bi-tapered} = \frac{\int_{a_o}^{a} \int_{leakily\_skew\_ray} s(\theta_z)\gamma_s(\theta_z, r)d\theta_z dr + \int_{a_o}^{a} \int_{trapped\_ray} s(\theta_z)\gamma_m(\theta_z, r)d\theta_z dr}{(a-a_o)\times \int_{trapped+leakily\_skew\_ray} s(\theta_z)d\theta_z} \tag{2.21}$$

A promising feature offered by bi-tapered sensing region of multimode optical fibre is the improvement of the performance of absorption measurements without any particular illumination masking or modal selection devices. Additionally, the method for fabricating the bi-tapered fibres is simple and is also capable of supplying reproducible tapers at low cost, such as when the unclad fibre is heated and pulled so as to achieve a biconical fibre section.

2.5 Numerical results and discussions

In this section, numerical calculations and discussions are presented to illustrate the theoretical analyses in above section. Trapped and meridional rays have been studied before [Ruddy 1990], this section will be concentrated on the evanescent wave absorption of leaky skew rays.

The parameters used in these numerical calculations are

$n_1 = 1.457, n_2 = 1.335$, $\lambda = 0.6328\mu m$, $d = 100\mu m$, and $\alpha = 100cm^{-1}$.

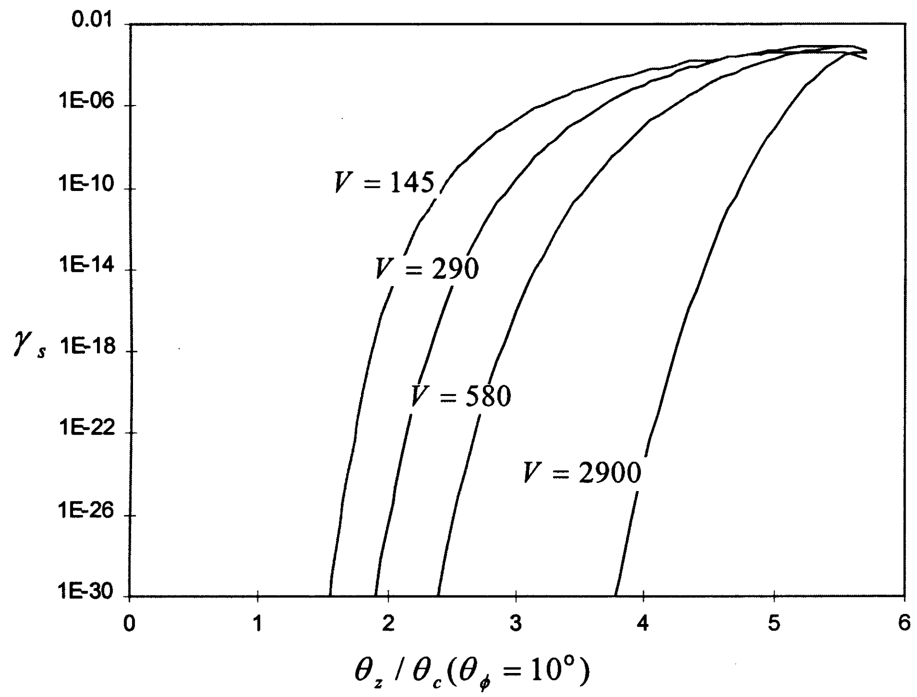

Figure 2-5. Evanescent wave absorption coefficient at $\theta_\phi = 10°$

Figure 2-5 and figure 2-6 show the numerical results of evanescent wave absorption against incident angle θ_z at $\theta_\phi = 10°$ and $\theta_\phi = 30°$, respectively.

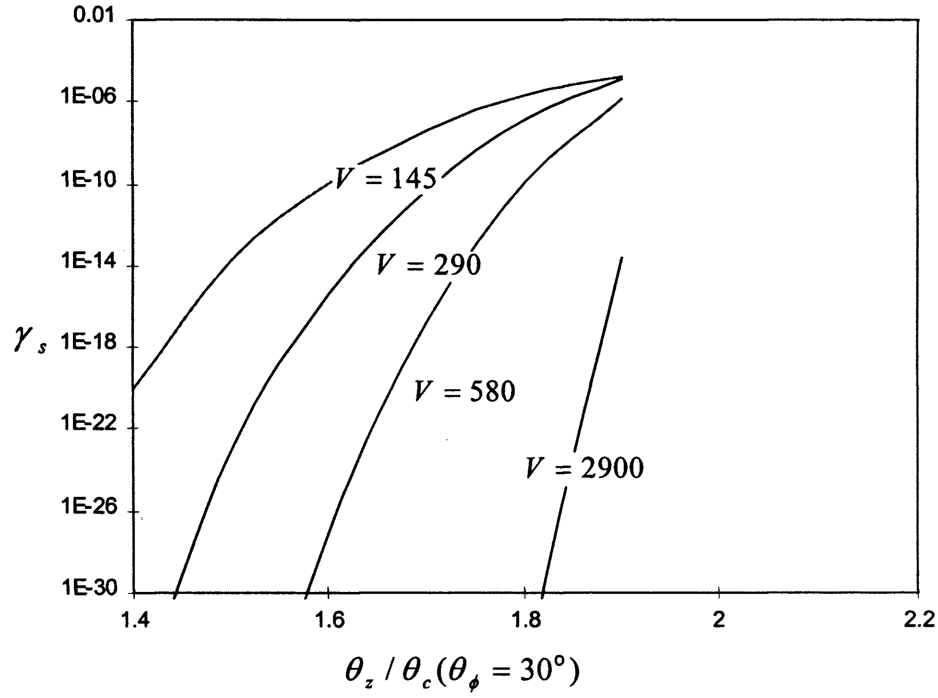

Figure 2-6. Evanescent wave absorption coefficient at $\theta_\phi = 30°$

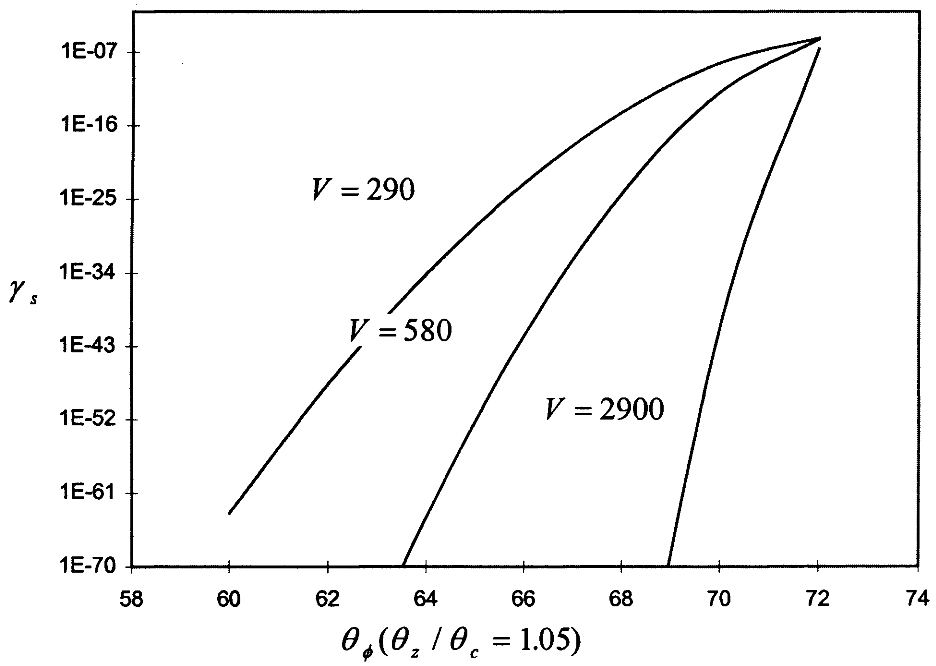

Figure 2-7. Evanescent wave absorption coefficient at $\theta_z / \theta_c = 1.05$

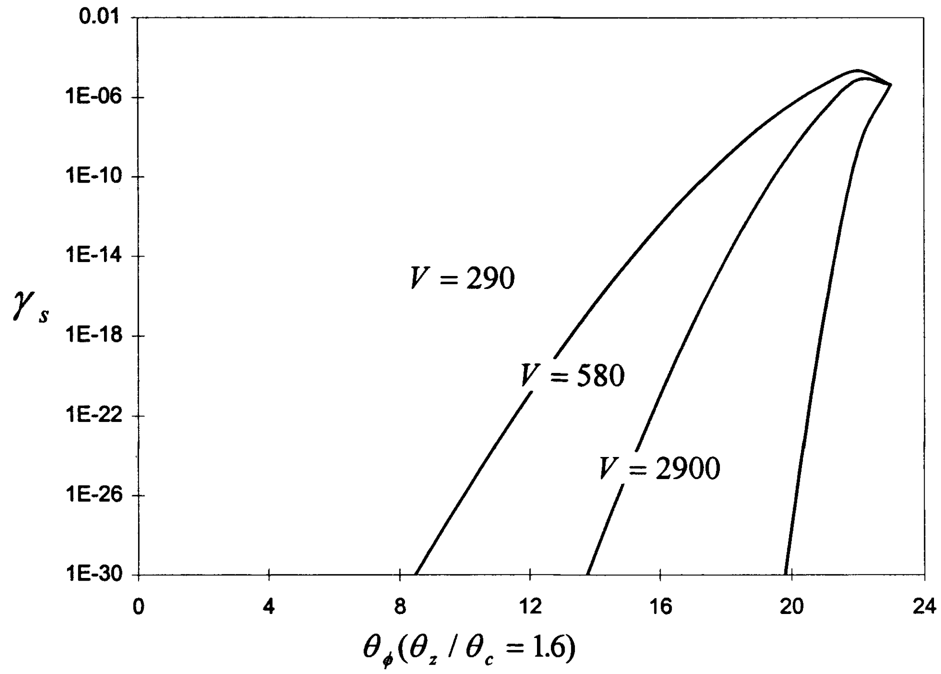

Figure 2-8. Evanescent wave absorption coefficient at $\theta_z / \theta_c = 1.6$

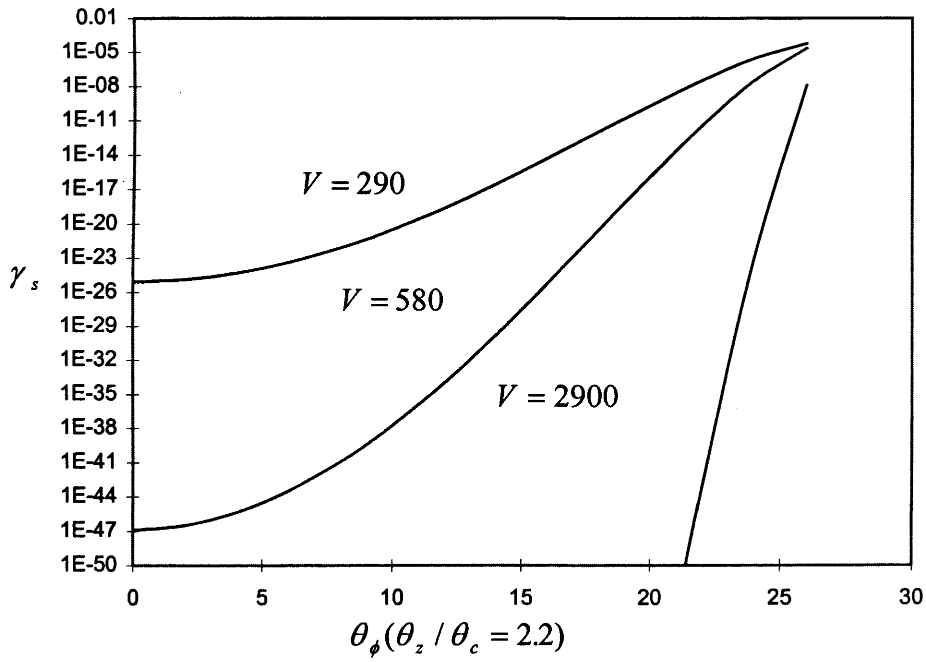

Figure 2-9 Evanescent wave absorption coefficient at $\theta_z / \theta_c = 2.2$

Figure 2-7, figure 2-8 and figure 2-9 show the numerical results of evanescent wave absorption against θ_ϕ at certain incident angles, $\theta_z/\theta_c = 1.05$, $\theta_z/\theta_c = 1.6$ and $\theta_z/\theta_c = 2.2$, respectively.

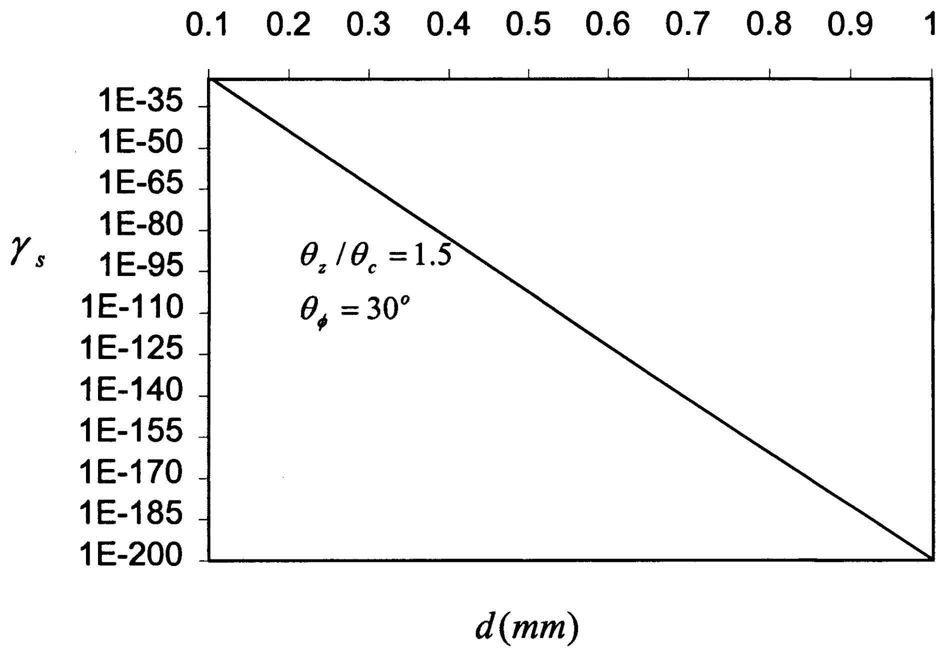

Figure 2-10 Evanescent wave absorption coefficient at $\theta_z/\theta_c = 1.5$ and $\theta_\phi = 30^0$

Figure 2-10 shows the evanescent wave absorption coefficient changes with the core diameter of the optical fibre, when $\theta_z/\theta_c = 1.5$ and $\theta_\phi = 30^0$. The evanescent wave absorption coefficient decreases very significantly with increase of the core diameter.

Figure 2-11 shows the comparison of the evanescent wave coefficient between meridional and leaky skew rays when V=290 and $\theta_\phi = 10°$.

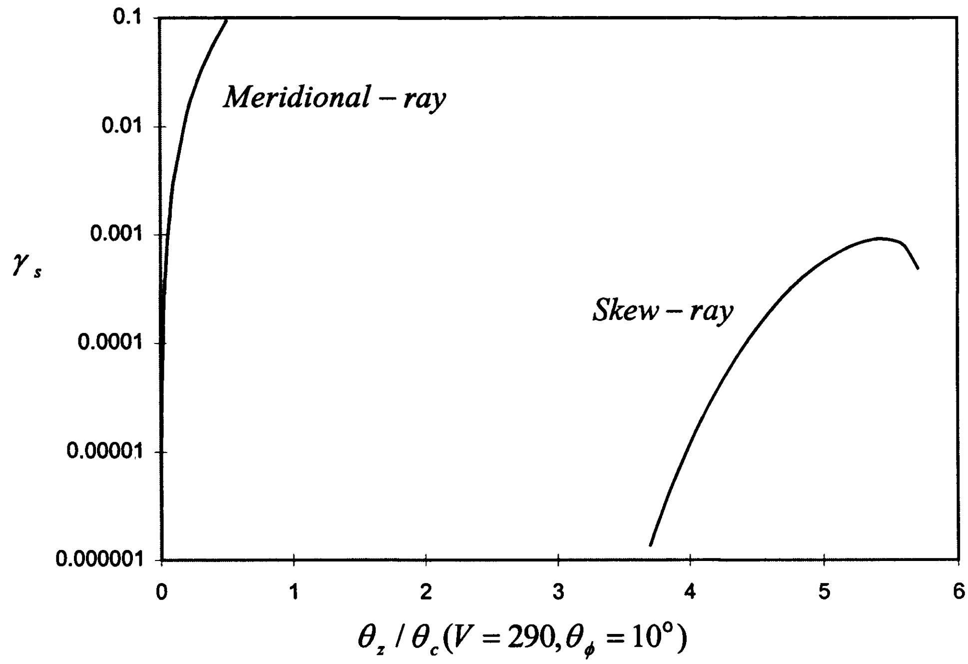

Figure 2-11 Evanescent wave absorption coefficient both meridional and leaky skew rays

From above-mentioned equations, it can be seen that the evanescent wave absorption coefficient changes with the incident angle θ_z, θ_ϕ and V. The critical angle (total reflection angle at the interface) of leaky skew rays is determined by not only n_1 , n_2 (that is θ_c), but also by the skewness of the ray , θ_ϕ, in the formulation of $\theta_z \sin\theta_\phi = \theta_c$.

With increase of V, the absorption decreases significantly (the same as the behaviour of meridional rays). The skewness of leaky skew rays, θ_ϕ, together with θ_z, also plays an important role in evanescent wave absorption.

Stronger evanescent wave absorption for leaky skew rays happens near to the critical angle.

The main difference from trapped and meridional rays is that leaky skew rays are distributed over a wider range, normally a few times θ_c, although they suffer less absorption. Trapped rays are only within the critical angle predicted by Fresnel's law, ie less than θ_c. Under some circumstances and designs these leaky skew rays could carry a large proportion of the transmitted power, and the evanescent wave absorption induced by these leaky skew rays could be important. Figure 6 shows the comparison of evanescent wave absorption between meridional rays and leaky skew rays. Although the evanescent wave absorption coefficients for meridional rays are larger, they are only significant over a relatively smaller range of angles, less than the critical angle θ_c. For leaky skew rays, they are smaller, but their influences cover a larger angle range. That is the reason why in some applications the evanescent wave absorption of leaky skew rays should be involved in the quantitative explanation of the experimental results.

Smaller diameters of optical fibre core increase not only the number of reflections, which will lead to more absorption and higher sensitivity, but will also increase the evanescent wave absorption coefficient. The smaller diameter of optical fibre core is favourable in terms of sensitivity. However, smaller core diameter will cause a larger coupling loss with light sources and detectors, and give a smaller output signal. The selection of optimum diameter has to be a compromise between the sensitivity and the output light power.

It has been confirmed by experiments and theory that the use of a tapered sensing region of multimode optical fibre is an effective approach to increase the sensitivity of evanescent wave absorption sensors and spectroscopy. From the view of manufacture, it is also not difficult to produce the tapered structure in multimode optical fibres. Hence it could become a promising solution to the sensing problem.

2.6 Conclusions

Leaky skew rays have a different behaviour in transmission in optical fibres, and they also show the different characteristics in evanescent wave absorption from trapped and meridional rays. Leaky skew rays can carry a large proportion of the energy in optical fibres. In these cases, without consideration of the contribution from leaky skew rays, the theoretical model of evanescent wave fibre-optic sensors absorption is not accurate enough to allow quantitative evaluation.

The same as trapped or meridional rays, the contribution of the evanescent wave absorption of leaky skew rays changes with the different incident angle θ_z and

V. But the skewness of the leaky skew ray θ_ϕ is another important factor in the absorption of the evanescent wave. A wider angle range (a few times the critical angle θ_c) of leaky skew rays is able to induce evanescent wave absorption.

Based on the analysis, a comprehensive expression of evanescent wave absorption has been worked out, which could be solved easily by numerical calculation. Also evanescent wave absorption fibre-optic sensors with bi-tapered sensing region are examined. This analysis and calculation will allow the optimisation of the design of optical fibre evanescent wave absorption sensors.

Earlier researchers were not so sure what role skew rays play in the theoretical model of evanescent wave absorption in multimode optical fibres and how important skew rays are. They believed the model based on meridional rays only explains the results qualititatively very well [Gupta 1994a].

This work is the first time that the evanescent wave absorption coefficient of skew rays has been theoretically evaluated. Numerical calculations could easily show the amount of the evanescent wave absorption, and the proportion of total light power affected. It also allows researchers to determine the accuracy of the model based on meridional rays only.

Unless there are specially designed light sources to launch all light rays near to the critical angle, which will create much large evanescent wave absorption, the evanescent wave absorption for both meridional and skew rays in optical fibres is too small for industrial applications, compared with bulk optic absorption. It might be a reason why there are no products incorporating fibre-optic evanescent wave absorption sensors in commerical markets today.

But there is no reason to doubt the promising future of fibre-optic evanescent wave chemical and bio-chemical sensors. The unique and distinguishing advantages of fibre-optic evanescent wave are very useful, such as fluorescent excitation and immunoassay techiniques using fibre-optic evanescent wave excitation. That is also a point brought out by this investigation.

Chapter 3

Analytical Estimates of the Characteristics of Surface Plasmon Resonance Fibre-Optic Chemical Sensors

3.1 Introduction

The following chapter is a detailed examination of the characteristics of surface plasmon resonance (SPR) fibre-optic chemical sensors by theoretical analyses and numerical calculations. Using geometrical optics, under the approximation of meridional rays, a mathematical model for light power transmittance has been established, in which Fresnel's equations used for bulk-optics are applied to SPR fibre-optic sensors. These analytical estimations can be applied in SPR fibre-optic chemical sensors both with a transducing layer and without a transducing layer. The results of these numerical calculations agree well with previously published experimental results. This work will aid in the design of SPR fibre-optic chemical sensors in terms of geometrical structure, materials and dynamic range as well as allowing the prediction of performance and of limitations of the design.

3.2 Background of surface plasmon resonance

The electron charges on a metal boundary can perform coherent fluctuations which are called surface plasmon oscillations [Ritchie 1957]. Their existence has been demonstrated in electron energy-loss experiments by Powell [Powell 1960]. The frequency ω of these longitudinal oscillations is tied to its wave vector k_x by dispersion relation $\omega(k_x)$. These charge fluctuations, which can be localised in the z direction within about 1 $\mathring{A}$, are accompanied by a mixed transversal and longitudinal

$$D_0 = \frac{k_{z1}}{\varepsilon_1} + \frac{k_{z2}}{\varepsilon_2} = 0 \tag{3.2}$$

And

$$\varepsilon_i (\frac{\omega}{c})^2 = k_x^2 + k_{zi}^2 \qquad i = 1, 2 \tag{3.3}$$

The wave vector k_x is continuous through the interface. The dispersion relation of Equation (3.2) can be written as:

$$k_x = \frac{\omega}{c}(\frac{\varepsilon_1 \varepsilon_2}{\varepsilon_1 + \varepsilon_2})^{1/2} \tag{3.4}$$

If under the condition of besides a real ω and ε_2 that $\varepsilon_1'' < |\varepsilon_1'|$ ($\varepsilon_1'' > 0$ and $\varepsilon_1' < 0$), a complex $k_x = k_x' + jk_x''$ can be obtained as:

$$k_x' = \frac{\omega}{c}(\frac{\varepsilon_1' \varepsilon_2}{\varepsilon_1' + \varepsilon_2})^{1/2} \tag{3.5}$$

$$k_x'' = \frac{\omega}{c}(\frac{\varepsilon_1' \varepsilon_2}{\varepsilon_1' + \varepsilon_2})^{3/2} \frac{\varepsilon_1''}{2(\varepsilon_1')^2} \tag{3.6}$$

A real value of k_x' can be obtained, if $\varepsilon_1' < 0$ and $|\varepsilon_1'| > \varepsilon_2$, which can be fulfilled in a metal and also a doped semiconductor near the eigen frequency. The parameter k_x' determines the propagating constant of the surface plasmon wave and k_x'' determines the internal absorption in the x direction.

electromagnetic field which disappears at $|z| \to \infty$, shown in Figure 3-1, and has its maximum in the surface $z = 0$, typical for surface waves. This explains their sensitivity to surface properties. The field is described by:

$$E = E_0^{\pm} \exp[+j(k_x x \pm k_z z - \omega t)] \quad (3.1)$$

with + for $z \geq 0$, – for $z \leq 0$, and with imaginary k_z, which causes the exponential decay of the field E_z. The wave vector k_x lies parallel to the x direction; $k_x = 2\pi / \lambda_p$, where λ_p is the wavelength of the plasmon oscillation.

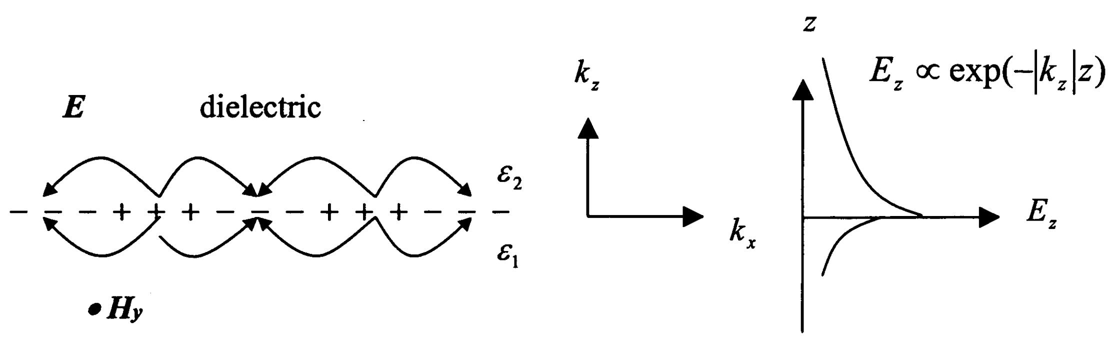

Figure 3-1 The charges and the electromagnetic field of surface plasmon propagating on a surface in the x direction are shown schematically. The exponential dependence of the field E_z is seen on the right. H_Y shows the magnetic field in the y direction of this p-polarised wave

Maxwell's equations yield the dispersion relation for the plane surface of a semi-infinite metal with the dielectric constant ($\varepsilon_1 = \varepsilon_1^{'} + j\varepsilon_1^{''}$), adjacent to a medium of dielectric constant ε_2 such as air or vacuum:

$$D_0 = \frac{k_{z1}}{\varepsilon_1} + \frac{k_{z2}}{\varepsilon_2} = 0 \qquad (3.2)$$

And

$$\varepsilon_i (\frac{\omega}{c})^2 = k_x^2 + k_{zi}^2 \qquad i = 1, 2 \qquad (3.3)$$

The wave vector k_x is continuous through the interface. The dispersion relation of Equation (3.2) can be written as:

$$k_x = \frac{\omega}{c} (\frac{\varepsilon_1 \varepsilon_2}{\varepsilon_1 + \varepsilon_2})^{1/2} \qquad (3.4)$$

If under the condition of besides a real ω and ε_2 that $\varepsilon_1'' < |\varepsilon_1'|$ ($\varepsilon_1'' > 0$ and $\varepsilon_1' < 0$), a complex $k_x = k_x' + jk_x''$ can be obtained as:

$$k_x' = \frac{\omega}{c} (\frac{\varepsilon_1' \varepsilon_2}{\varepsilon_1' + \varepsilon_2})^{1/2} \qquad (3.5)$$

$$k_x'' = \frac{\omega}{c} (\frac{\varepsilon_1' \varepsilon_2}{\varepsilon_1' + \varepsilon_2})^{3/2} \frac{\varepsilon_1''}{2(\varepsilon_1')^2} \qquad (3.6)$$

A real value of k_x' can be obtained, if $\varepsilon_1' < 0$ and $|\varepsilon_1'| > \varepsilon_2$, which can be fulfilled in a metal and also a doped semiconductor near the eigen frequency. The parameter k_x' determines the propagating constant of the surface plasmon wave and k_x'' determines the internal absorption in the x direction.

Figure 3-2 shows the dispersion relation of an example with air or vacuum as the dielectric medium, $\varepsilon_2 = 1$. This dispersion relation changes with the propagation constant k_x, which approaches the light dispersion relation of air or vacuum at small values of (ω/c), but always remains larger than ω/c, so that the surface plasmon wave cannot transform into light, and is therefore a "nonradiative" surface plasmon wave [Raether 1988].

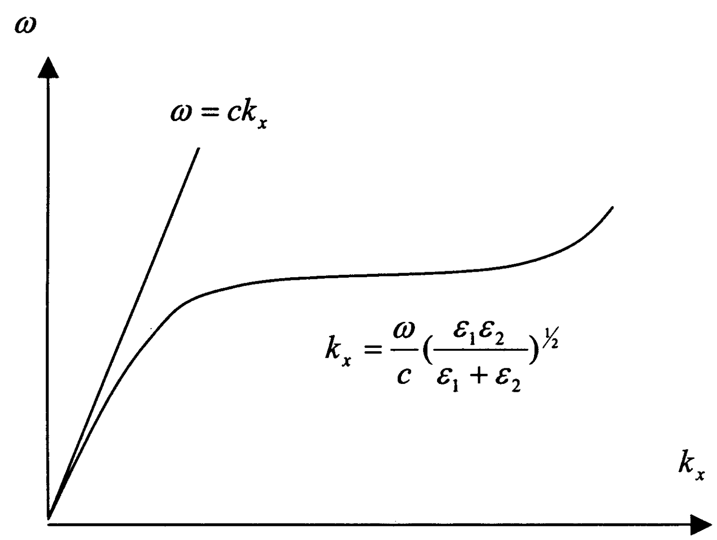

Figure 3-2 The dispersion relation of surface plasmons and the light $\omega = ck_x$

From Equation (3.3), due to the relations $\omega/c < k_x$ and $\varepsilon_1' < 0$, wave vectors k_{z1} and k_{z2} are imaginary, so that, as mentioned above, the field amplitude of the surface plasmon wave decreases exponentially as $\exp(-|k_{zi}||z|)$, normal to the interface. The value of the depth at which the field falls to *1/e*, becomes:

$$z = \frac{1}{|k_{zi}|} \tag{3.7}$$

in the medium with ε_1:

$$z_1 = \frac{\lambda}{2\pi}\left(\frac{\varepsilon_1^{'} + \varepsilon_2}{\varepsilon_1^{'2}}\right)^{1/2} \tag{3.8}$$

in the medium with ε_2:

$$z_2 = \frac{\lambda}{2\pi}\left(\frac{\varepsilon_1^{'} + \varepsilon_2}{\varepsilon_2^{2}}\right)^{1/2} \tag{3.9}$$

If light is reflected at a metal surface (ε_1) covered with a dielectric medium ($\varepsilon_0 > 0$), the projection of the incident light wave vector on the surface, shown in Figure 3-3, is expressed as:

$$k_x^L = \sqrt{\varepsilon_0}\frac{\omega}{c}\sin\theta_0 \tag{3.10}$$

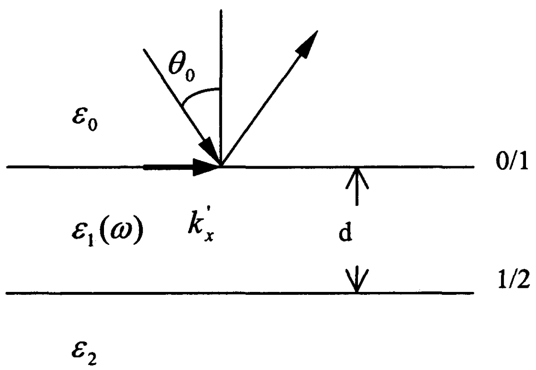

Figure 3-3 Reflection of light at a metal surface, the medium above the metal is dielectric material; below the metal is air or vacuum.

The dispersion relation for a surface plasmon wave on the interface $\varepsilon_2 / \varepsilon_1$ (air/metal) and $\varepsilon_1 / \varepsilon_0$ (metal/dielectric material) can thus be shown in Figure 3-4.

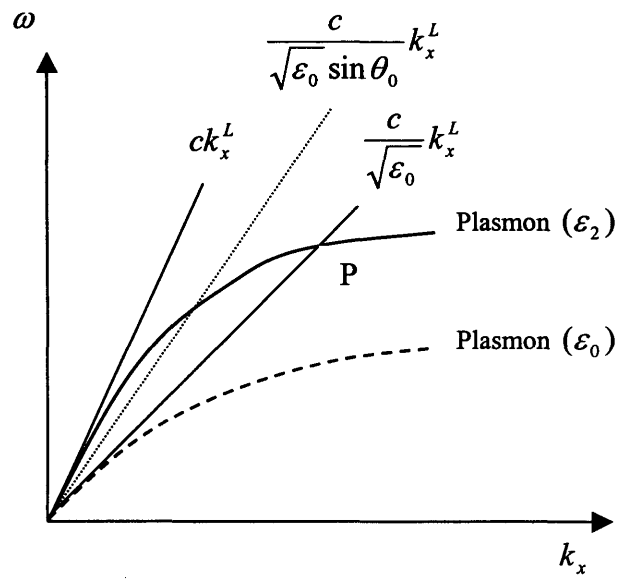

Figure 3-4 Surface plasmon resonance excited by total reflection

Shown in Figure 3-4, the light line in medium ε_0, $(c/\sqrt{\varepsilon_0})k_x^L$, lies to the right of the surface plasmon wave line up to a certain k_x at point P. Light can excite a surface plasmon wave with frequency ω below the crossing point P on the metal/air interface. The surface plasmon wave in the interface metal/dielectric material cannot be excited, since their surface plasmon wave line lies to the right of the light line. The excitation is recognised when there is a minimum in the total reflection. Also the surface plasmon resonance is excited only for *p*-polarised light (TM mode).

The quantitative description of the reflected intensity *R* can be derived from Fresnel's equations. Using a three-layer system as an example, shown in Figure 3-3, ε_0 dielectric material – glass, ε_1 metal film – silver of thickness *d*, ε_2 dielectric material –

air. The reflectance R for p-polarised light, with E_0^p the incident and E_r^p the reflected field, is expressed as:

$$R = \left|\frac{E_r^p}{E_0^p}\right|^2 = \left|\frac{r_{01}^p + r_{12}^p \exp(2jk_{z1}d)}{1 + r_{01}^p r_{12}^p \exp(2jk_{z1}d)}\right|^2 \tag{3.11}$$

with

$$r_{ik}^p = \frac{\dfrac{k_{zi}}{\varepsilon_i} - \dfrac{k_{zk}}{\varepsilon_k}}{\dfrac{k_{zi}}{\varepsilon_i} + \dfrac{k_{zk}}{\varepsilon_k}} \qquad i = 1, 2 \tag{3.12}$$

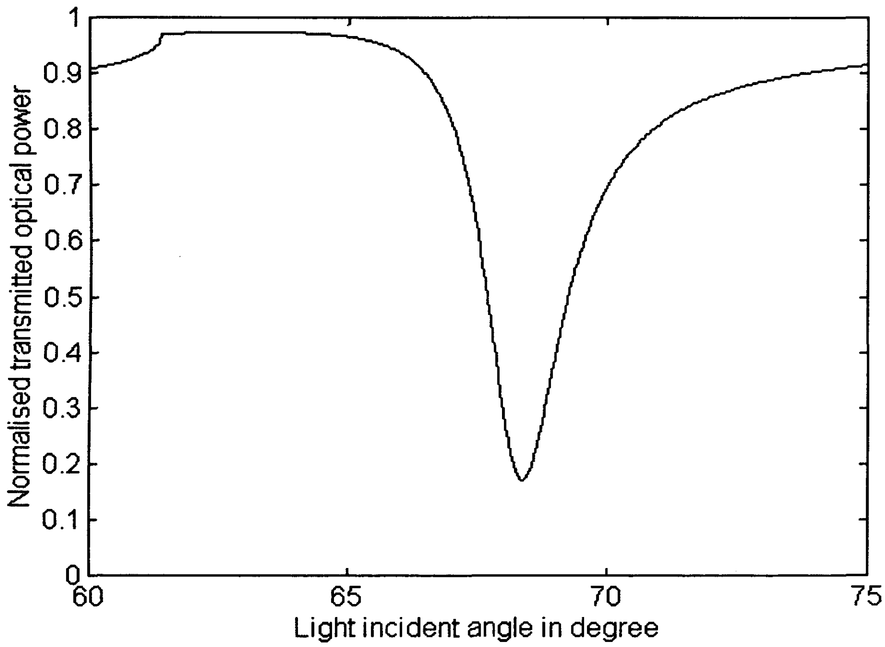

Figure 3.5 Reflectance at silver film of thickness $d = 45.23\text{nm}$, incident light wavelength $\lambda = 632.8\text{nm}$, $n_0 = 1.33$, $n_1 = -16.36 + 0.59j$, $n_2 = 1.515$

When the projection of the incident light wave vector equals the surface plasmon wave vector, *i.e.*, $k_x^L = \sqrt{\varepsilon_0}\,(\omega / c)\sin\theta_{SP} = k_x$, reflectance R is at its minimum value. θ_{SP} is defined as resonance angle. The reflectance of light intensity with surface plasmon resonance excitation changes against incident angle of light as shown in Figure 3-5.

Based on the above-mentioned principle, the study of the surface plasmon excitation technique was started for bulk-optic systems. In 1971, Kretschmann proposed a experimental configuration of surface plasmon resonance excited by the prism shown in Figure 3-6 [Kretschmann 1971].

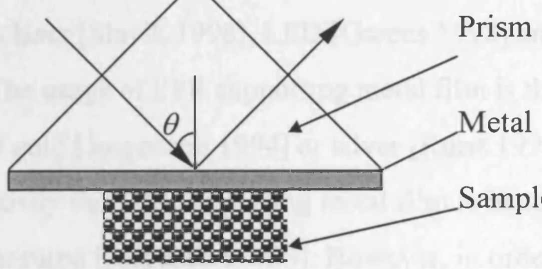

Figure 3-6 Kreschmann's configuration of SPR

Since then, Kretschmann's configuration has been applied in chemical analysis, biosensor, physical constant measurement *etc.*[Chen 1981, Daniels 1988, Lukosz 1991 and Jory 1995]. Today commercial products based on bulk-optic SPR technology have been successfully exploited by Biacore, Quantech and Texas Instruments.

3.3 Surface plasmon resonance fibre-optic sensors

In recent years, with the progress of optical fibre and related techniques, surface plasmon resonance fibre-optic sensors have received a great attention [Kano 1994, Jorgenson 1993, Jorgenson 1994 and Slavik 1998], particularly because of the extra advantages of small size of the fibre-optic probe, immunity of electromagnetic interference, the growing need for remote sensing, *etc.*

In addition, due to the characteristics of the optical fibre, SPR fibre-optic sensors have different features from SPR bulk-optic sensors, such as, no angle scanning is needed and multiple wavelength light sources can be used together with a spectrograph or spectrometer for recording the spectrum.

To date, SPR fibre-optic systems have been developed both for transmission type [Jorgenson 1993] and reflection type [Slavik 1998]. Optical fibres used in these developments included the single-mode optical fibre [Slavik 1998], multi-mode optical fibre [Jorgenson 1993], and even sapphire core optical fibre [Jorgenson 1994] which can increase the upper limit of the refractive index dynamic range. There are also a range of light sources used such as laser [Slavik 1998], LED [Garces 1992] and Tungsten halogen lamp [Jorgenson 1994]. The usage of SPR supporting metal film is the same as in SPR bulk-optic systems, either gold [Jorgenson 1994] or silver [Kunz 1996]. In the structure of the sensing element, mostly the SPR supporting metal film is in contact with the chemical sample to be measured [Jorgenson 1993]. However, in order to increase the dynamic range of the measurement, some designs have included an additional transducing layer deposited upon the metal film and in contact with the chemical sample to be measured [Garces 1992].

3.4 Theoretical model of surface plasmon resonance fibre-optic sensors

Theoretical models for analyses of optical SPR excitation in bulk-optics were well developed by many researchers [Raether 1977, Pockrand 1978, Chen 1980, Reed 1985, Kurosawa 1986, Abeles 1986 and Ctyroky 1997]. These theoretical models have been used to explain experimental results and to design SPR bulk-optic systems. In the multi-mode optical fibre, which is used in many SPR fibre-optic sensors, there are many guided-modes transmitted. Each mode transmits the light ray at one particular angle of internal reflection. Theoretical models for SPR bulk-optic systems can only be applied to the individual ray of each mode in multi-mode optical fibres. For SPR fibre-optic sensors, a comprehensive theoretical analysis, which considers the contributions of all possible transmitted modes, has not been studied systematically. In this section, a theoretical model of the optical power transmittance is derived, then, based on this theoretical model, using numerical calculations, the characteristics of SPR multi-mode fibre-optic sensors are predicted and discussed.

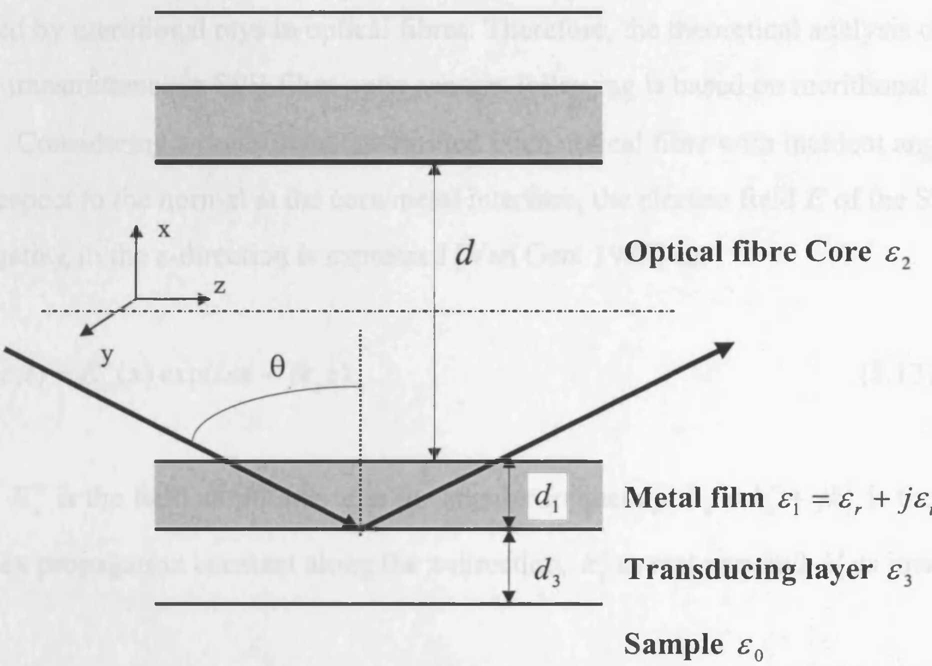

Figure 3-7 The meridional cross-section of the sensing element of the fibre-optic SPR sensor.

Figure 3-7 shows the meridional cross-section of the sensing element of the SPR fibre-optic sensor. A multi-mode optical fibre, with core diameter d and refractive index n_2 (dielectric permittivity ε_2), has the jacket and the cladding removed to expose the core, on which is symmetrically deposited a metal film of thickness d_1 and dielectric permittivity ε_1. In some applications, the metal film is directly in contact with the sample to be measured with dielectric permittivity ε_0, in others, a dielectric isotropic transducing layer with thickness d_3 and dielectric permittivity ε_3 is deposited symmetrically outside the metal film. For generality, in this paper all formulations are derived including this transducing layer. The sensors without transducing layers are considered as special cases by setting $d_3 = 0$.

In multi-mode optical fibre sensors, due to the easiness and effectiveness of describing the behaviour, meridional rays are often used to build up approximate models. Further, in SPR fibre-optic sensors, the theoretical models of SPR for bulk-optics are satisfied by meridional rays in optical fibres. Therefore, the theoretical analysis of optical power transmittance in SPR fibre-optic sensors following is based on meridional rays.

Considering a ray of light transmitted in an optical fibre with incident angle θ with respect to the normal at the core/metal interface, the electric field $\boldsymbol{E}$ of the SPR propagating in the z-direction is expressed [Van Gent 1989] as:

$$E_x(x,z,t) = E_x^0(x)\exp(i\omega t - jk_z z) \tag{3.13}$$

where E_x^0 is the field amplitude, ω is the angular frequency, $k_z = k_z^r + jk_z^i$ is the SPR complex propagation constant along the z-direction, k_z^r as real part and k_z^i as imaginary part.

The resonance condition, under which the propagation constant of the incident light beam in the z-direction is equal to the real part of the SPR propagation constant, is expressed as:

$$k_z^r = k(\varepsilon_2)^{1/2}\sin\theta_{SP} = \frac{2\pi}{\lambda} n_2 \sin\theta_{SP} \tag{3.14}$$

where k is the propagation constant of the incident light beam in vacuum and θ_{SP} is the resonance angle.

Considering the structure of the SPR sensing element in SPR fibre-optic sensors shown in figure 1, the SPR propagation constant is accurately expressed [Raether 1977, Pockrand 1978 and Raether 1988] as:

$$k_z = k^0 + k^R + k^T \tag{3.15}$$

$$k^0 = \left(\frac{\varepsilon_0 \varepsilon_1}{\varepsilon_0 + \varepsilon_1}\right)^{1/2} \times \frac{\omega}{c} \tag{3.16}$$

$$k^R = k^0 \left(\frac{2}{\varepsilon_0 + \varepsilon_1}\right) \times \left(\frac{\varepsilon_0 \varepsilon_1}{\varepsilon_0 + \varepsilon_1}\right)^{3/2} \times \exp\left[j \frac{4\pi d_1}{\lambda} \frac{\varepsilon_1}{(\varepsilon_0 + \varepsilon_1)^{1/2}}\right] \tag{3.17}$$

$$k^T = j\left(\frac{2\pi d_3}{\lambda}\right) \times \left(\frac{\omega}{c}\right) \times \left(\frac{\varepsilon_0 \varepsilon_1}{\varepsilon_0 + \varepsilon_1}\right)^2 \times \frac{1}{(\varepsilon_0 \varepsilon_1)^{1/2} (\varepsilon_0 - \varepsilon_1)} \times \left(\varepsilon_3 + \frac{\varepsilon_0 \varepsilon_1}{\varepsilon_3} - \varepsilon_1 - \varepsilon_0\right) \tag{3.18}$$

k^0 expresses the dispersion relation of SPR at a metal-vacuum interface in a one-sharp-boundary model, k^R expresses the perturbation to k^0 due to the finite physical volume of the optical fibre and k^T expresses the modification to k^0 due to the transducing layer.

It is known that light rays with a range of incident angles are allowed to propagate in the multi-mode optical fibre. The range is determined by the numerical aperture of the fibre, $N.A. = n_2 \cos\theta_c = (n_1^2 - n_2^2)^{1/2}$. Only rays with $\theta > \theta_c$ (critical angle) can be transmitted in the optical fibre. The resonance condition in SPR fibre-optic sensors should involve the contribution from all rays transmitted in optical fibres, which have a range of incident angles (θ_c, 90^0). Therefore, the resonance condition, in SPR fibre-optic sensors, is expressed as:

$$k_z^r = \frac{2\pi n_2}{\lambda_{SP}} \frac{\int_{\theta_c}^{90^0} p(\theta)\sin\theta d\theta}{\int_{\theta_c}^{90^0} p(\theta) d\theta} \tag{3.19}$$

where $p(\theta)$ represents the power distribution of light sources.

This resonance condition determines a resonance wavelength λ_{SP}, which corresponds to the resonance angle θ_{SP} in bulk-optics, and which relies on the power distribution of the light source.

There are two main sorts of essential power distributions of light sources in fibre-optic sensors:

1) diffuse or Lambertian source (such as a LED), which is butted against the optical fibre end face and its surface covers at least some of the core cross section. The power distribution is expressed [Gupta 1994c and Snyder 1983] as:

$$p(\theta) \propto n_2^2 \sin\theta\cos\theta \tag{3.20}$$

2) collimated source (such as a laser) using a microscope objective such that the beam is focused onto the optical fibre end face at the axial point, the power distribution is expressed[Snyder 1983 and Gupta 1993] as:

$$p(\theta) \propto \frac{n_2^2 \sin\theta\cos\theta}{(1 - n_2^2 \cos^2\theta)^2} \tag{3.21}$$

In the following section an important characteristic, the optical power transmittance of SPR fibre-optic sensors, is discussed.

Under the approximation of using meridional rays of the optical fibre, the calculation of intensity reflection coefficient $r(\theta)$ at the interface of metal film and optical fibre core can use the result for SPR bulk-optic systems, which is expressed as [Kretschmann 1971 and Raether 1988]:

$$r(\theta) = |r_{210}|^2 = \left| \frac{r_{21} + r_{130} \exp(2jk_1 d_1)}{1 + r_{21} r_{130} \exp(2jk_1 d_1)} \right|^2 \qquad (3.22)$$

where $r_{21} = \dfrac{z_{21}}{n_{21}}$, $r_{130} = \dfrac{z_{10} - jz_{43} \tan(k_3 d_3)}{n_{10} - jn_{43} \tan(k_3 d_3)}$, $z_{im} = k_i \varepsilon_m - k_m \varepsilon_i$, $n_{im} = k_i \varepsilon_m + k_m \varepsilon_i$,

$k_i = \left[\varepsilon_i (\frac{2\pi}{\lambda})^2 - k^2 \right]^{1/2}$, $k = (\frac{2\pi}{\lambda}) n_2 \sin\theta$, $\varepsilon_4 = \dfrac{\varepsilon_0 \varepsilon_1}{\varepsilon_3}$, $k_4 = \dfrac{k_0 k_1}{k_3}$,

$i, m = 1,2,3,4$

A light ray transmitted in the multi-mode optical fibre with incident angle θ, shown in Figure 3-7, will have N multi-reflections in length L of SPR sensing element. The number N is expressed as:

$$N = \frac{L}{d \tan\theta} \qquad (3.23)$$

Considering the contributions of all rays and multi-reflections, the reflectance R_λ in SPR fibre-optic sensors is expressed as:

$$R_\lambda = \frac{\int_{\theta_c}^{90^0} p(\theta) r^N(\theta) d\theta}{\int_{\theta_c}^{90^0} p(\theta) d\theta} \qquad (3.24)$$

In multi-mode optical fibres, both TE and TM polarised light with respect to the core/metal interface are allowed to propagate. Only half of the transmitted optical power contributes to the SPR excitation, since SPR can only be excited with TM polarised light[Abeles 1986 and Raether 1988].

Thus, the optical power transmittance of SPR fibre-optic sensors is expressed as:

$$T = \frac{I_{TE} + R_{\lambda} \cdot I_{TM}}{I_{TE} + I_{TM}} \tag{3.25}$$

where I_{TE} and I_{TM} represent the transmitted optical power of TE and TM polarised light, respectively.

Under the condition that $I_{TE} = I_{TM}$, the optical power transmittance simplifies to:

$$T = \frac{1 + R_{\lambda}}{2} \tag{3.26}$$

3.5 Illustrative numerical calculations

In SPR fibre-optic sensors, the optical power transmittance is measured via its spectrum which has a resonance at wavelength λ_{SP} where there is minimum transmittance.

In the numerical calculations of this section, the parameters of the optical fibre used in calculations are: $d = 400\mu m$, $n_2 = 1.515$, $N.A. = 0.3$. The power distribution of the light source is a diffuse or Lambertian source, expressed in Equation (3.20).

3.5.1 Numerial calculations about the SPR fibre-optic sensor without a transducing layer ($d_3 = 0$)

In Figure 3-8, + curve represents the case of the refractive index of the sample $n_0 = 1.4$, × curve represents $n_0 = 1.41$ and ° curve represents $n_0 = 1.42$. The continuous curve represents the normalised transmitted optical power of only one light ray with specified angle $\theta = 80°$, suffering only one reflection, $n_0 = 1.4$, which simulates the bulk-optic SPR.

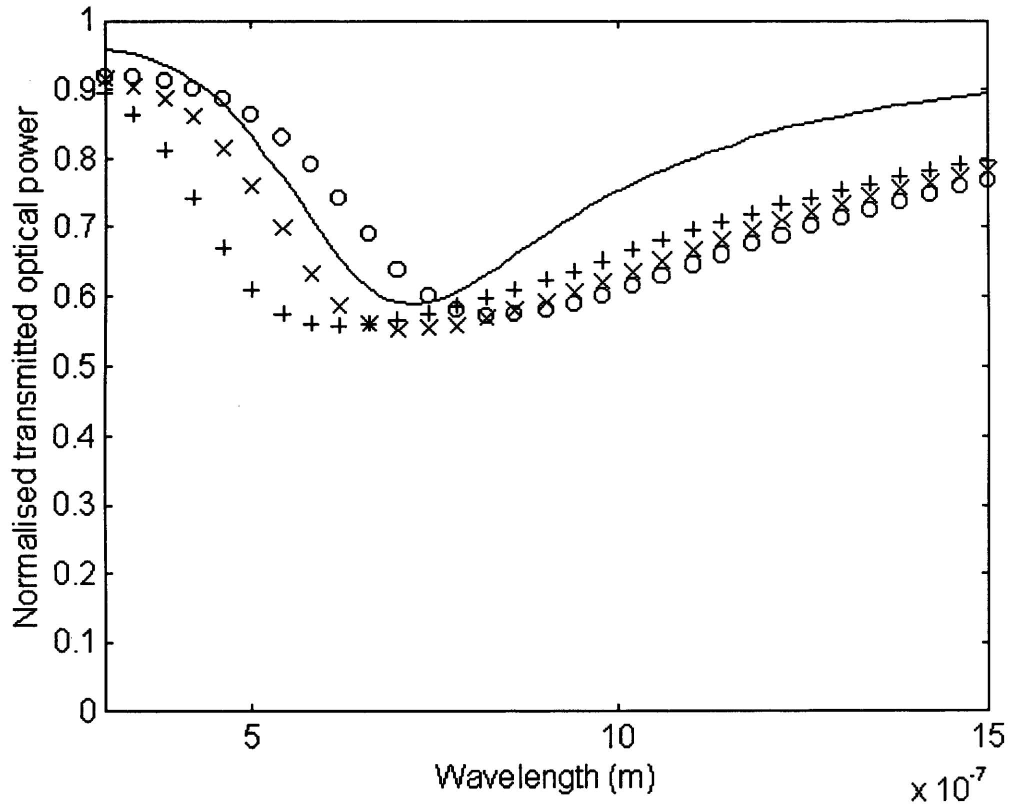

Figure 3-8 Normalised transmitted optical power of the SPR fibre-optic sensor without a transducing layer i.e. $d_3 = 0$, gold as the SPR supporting metal, with $\varepsilon_1 = -13.2 + 1.25j$, length $L = 10mm$ and thickness $d_1 = 40nm$. The refractive index of the sample to be measured changes.

Due to the numerical aperture, there is a range of angle of light rays able to travel in the optical fibre. The contribution of all rays broadens the spectrum of the transmitted optical power in SPR fibre-optic sensors, and, because of multi-reflections inside the optical fibre, which lead to more absorption, the minimum transmittance decreases, compared with that in bulk-optic SPR absorption.

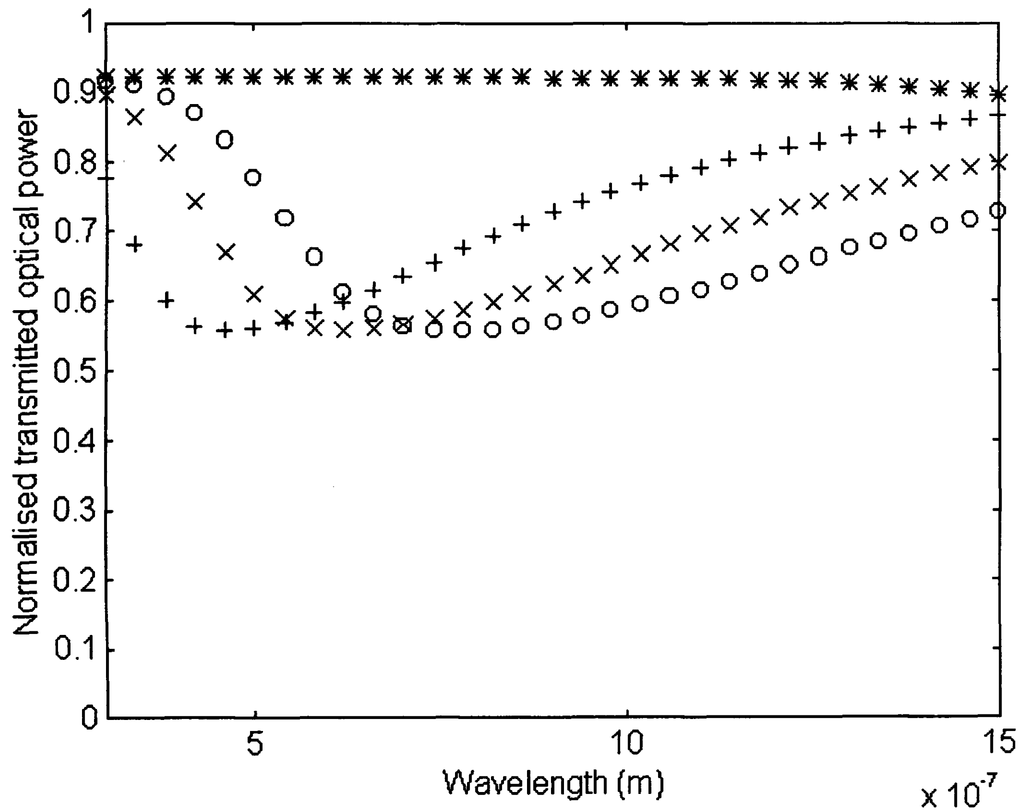

Figure 3-9 Normalised transmitted optical power of the SPR fibre-optic sensor without a transducing layer i.e. $d_3 = 0$, gold as the SPR supporting metal, with $\varepsilon_1 = -13.2 + 1.25j$ and length $L = 10mm$, the refractive index of the sample $n_0 = 1.4$. The thickness of the SPR supporting metal d_1 changes.

In Figure 3-9, + represents the case of the thickness of the SPR supporting metal $d_1 = 30nm$, × represents $d_1 = 40nm$, ° represents $d_1 = 50nm$ and * represents $d_1 = 200nm$.

When the thickness of the SPR supporting metal is large enough, there is no SPR excitation, The optical power of all wavelengths will be reflected almost at the same reflectance, and there is zero sensitivity in this case.

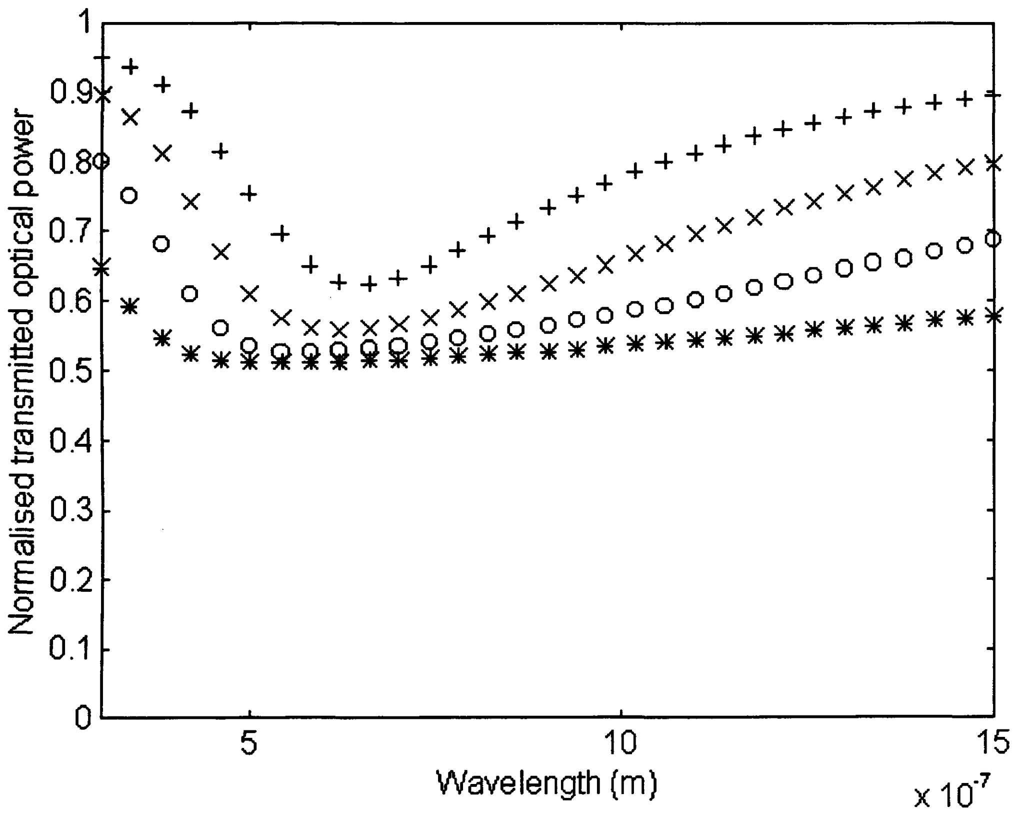

Figure 3-10 Normalised transmitted optical power of the SPR fibre-optic sensor without a transducing layer i.e. $d_3 = 0$, gold as the SPR supporting metal, with $\varepsilon_1 = -13.2 + 1.25j$ and thickness $d_1 = 40nm$, the refractive index of the sample $n_0 = 1.4$. The length of the sensing element L changes.

In Figure 3-10, + represents the case of the length of sensing element $L = 5mm$, × represents, $L = 10mm$, ° represents $L = 20mm$ and * represents $L = 50mm$.

Due to an increased number of reflections, the minimum transmittance decreases with increasing length of sensing element L. When the length is long enough, optical power of all wavelengths will be absorbed, and there is zero sensitivity in this case.

3.5.2 Numerial calculations about the SPR fibre-optic sensor with a transducing layer ($d_3 \neq 0$)

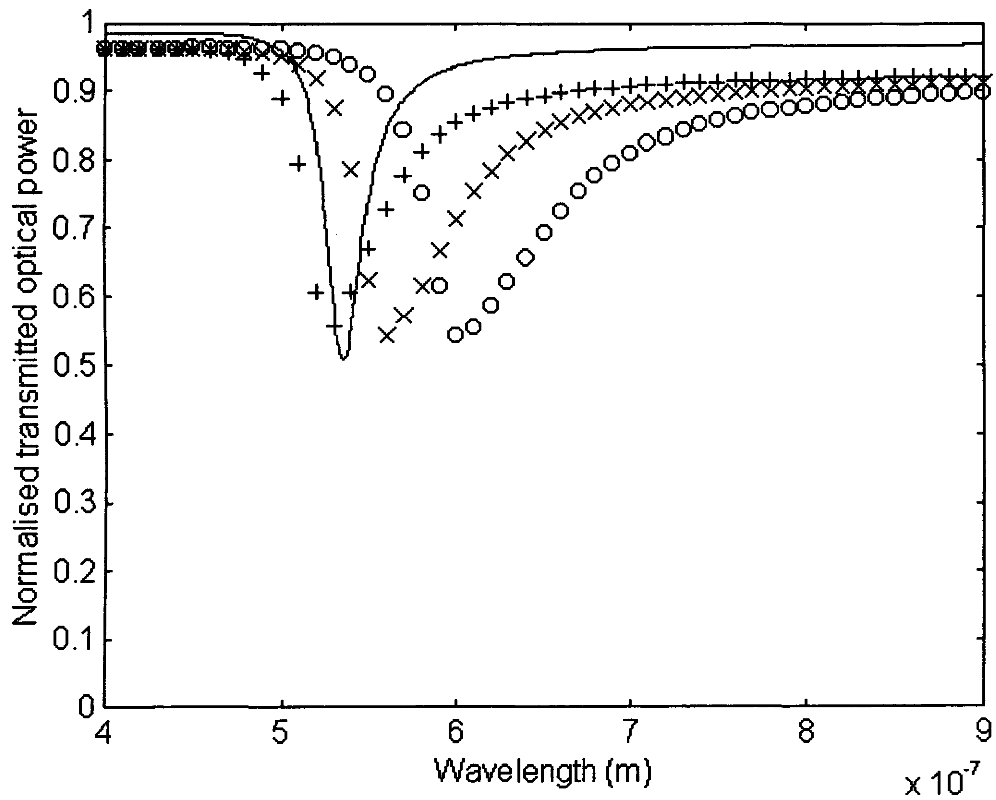

Figure 3-11 Normalised transmitted optical power of the SPR fibre-optic sensor, using zirconium oxide as the transducing layer, with $\varepsilon_3 = n_3^2 = 4.0$, thickness $d_3 = 40nm$, silver as the SPR supporting metal, with $\varepsilon_1 = -17 + 0.6j$, thickness $d_1 = 45nm$ and length $L = 10mm$. The refractive index of the sample to be measured changes.

In Figure 3-11, + curve represents the case of the refractive index of the sample $n_0 = 1.0$, × curve represents $n_0 = 1.05$ and ° curve represents $n_0 = 1.1$. The continuous curve represents the normalised transmitted optical power of only one ray with specified angle $\theta = 80°$, suffering only one reflection, $n_0 = 1.0$, which simulates the bulk-optic SPR.

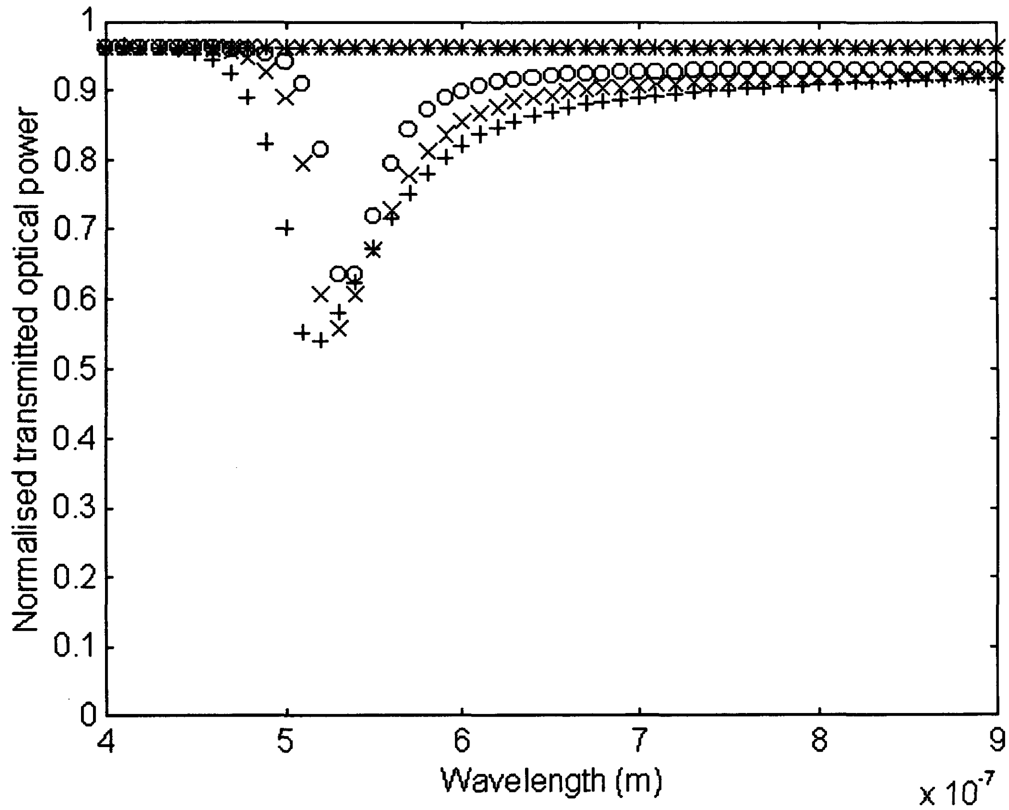

Figure 3-12 Normalised transmitted optical power of the SPR fibre-optic sensor, using zirconium oxide as the transducing layer with $\varepsilon_3 = n_3^2 = 4.0$, thickness $d_3 = 40nm$, silver as the SPR supporting metal, with $\varepsilon_1 = -17 + 0.6j$, and the length of sensing element $L = 10mm$, the refractive index of the sample $n_0 = 1.0$. The thickness of SPR supporting metal changes.

Again because of the numerical aperture, there is a range of angle of light rays which can be transmitted in an optical fibre. The contribution of all such rays broadens the spectrum of the transmitted optical power in SPR fibre-optic sensors, and because of multi-reflections inside the optical fibre which lead to more absorption, the minimum transmittance decreases compared with that of bulk-optic SPR sensors. This behaviour is the same as in SPR fibre-optic sensors without a transducing layer.

In Figure 3-12, + represents in the case of the thickness of the SPR supporting metal $d_1 = 35nm$, × represents $d_1 = 45nm$, ° represents $d_1 = 55nm$ and * represents $d_1 = 200nm$.

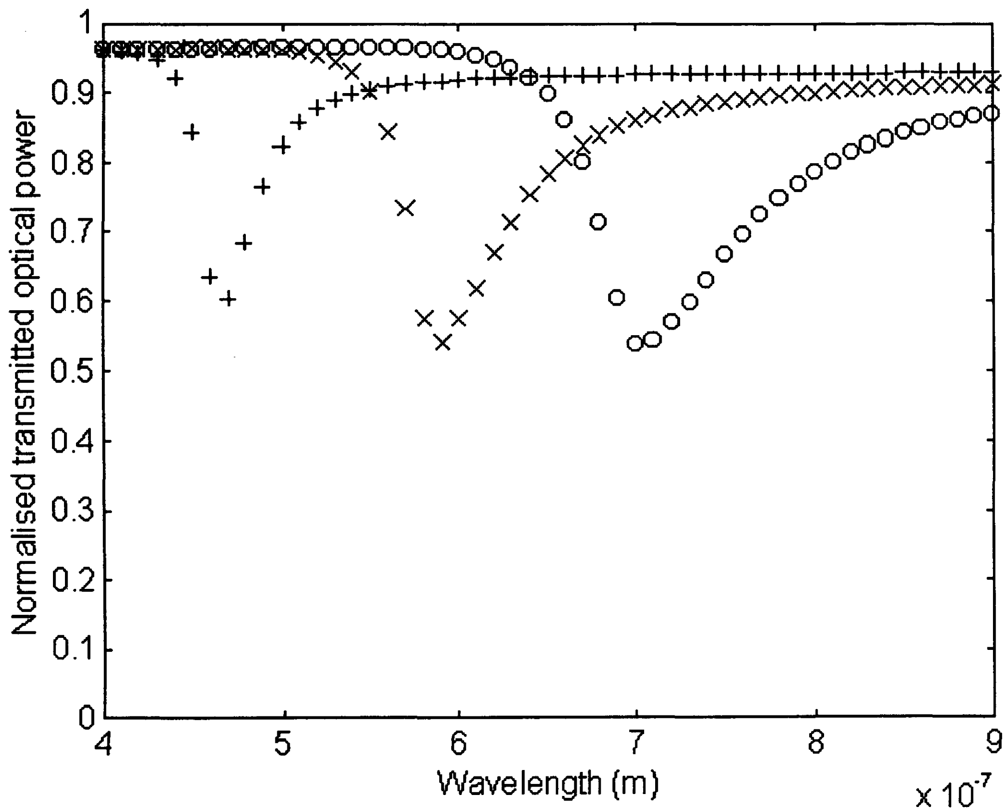

Figure 3-13 Normalised transmitted optical power of the SPR fibre-optic sensor, using zirconium oxide as the transducing layer with $\varepsilon_3 = n_3^2 = 4.0$, silver as the SPR supporting metal, with $\varepsilon_1 = -17 + 0.6j$, with the thickness $d_1 = 45nm$ and the length of the sensing element $L = 10mm$, the refractive index of the sample $n_0 = 1.0$. The thickness of the transducing layer d_3 changes.

When the thickness of SPR supporting metal is large enough, there is no SPR excitation, the optical power of all wavelengths will be reflected at the same reflectance, and there is zero sensitivity in this case as well. This is also the same as that in SPR fibre-optic sensors without the transducing layer.

In Figure 3-13, + represents the case of the thickness of the SPR supporting metal $d_3 = 35nm$, × represents $d_3 = 45nm$ and ° represents $d_3 = 55nm$.

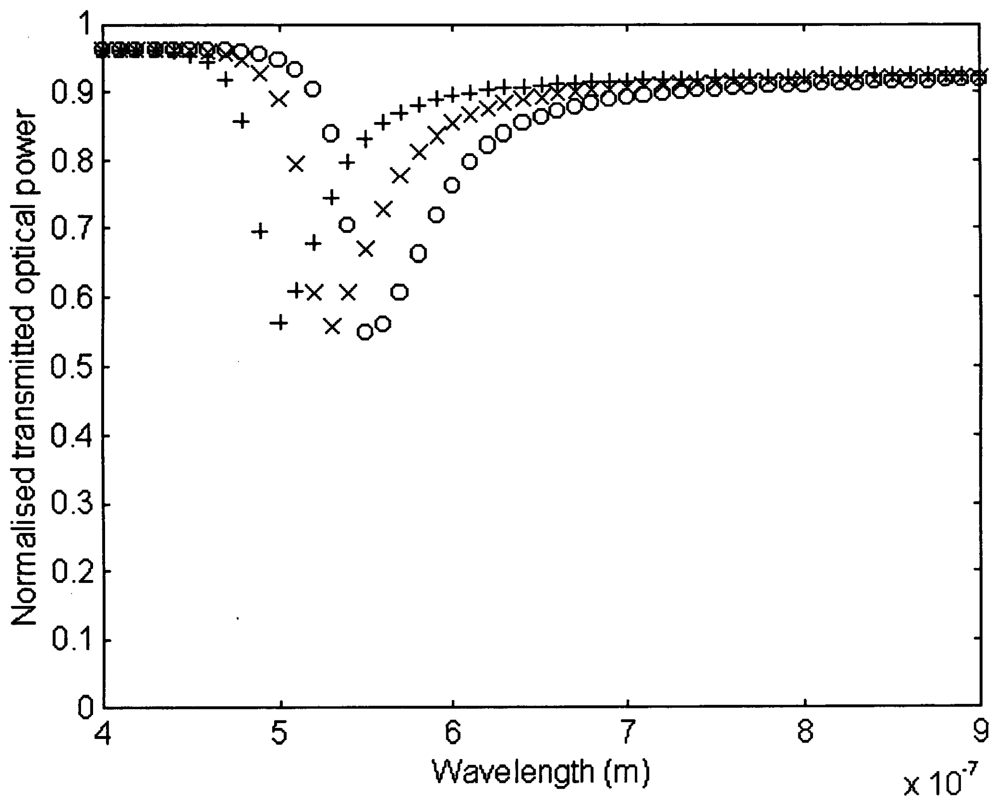

Figure 3-14 Normalised transmitted optical power of the SPR fibre-optic sensor, silver as the SPR supporting metal, with $\varepsilon_1 = -17 + 0.6j$, with the thickness $d_1 = 45nm$ and the length of the sensing element $L = 10mm$, the refractive index of the sample $n_0 = 1.0$. The thickness of the transducing layer $d_3 = 40nm$, but the refractive index of the transducing layer changes.

When the thickness of the transducing layer changes, the SPR resonance wavelength is shifted.

In Figure 3-14, + curve represents the case of the refractive index of the transducing layer $n_3 = 1.95$, × curve represents $n_3 = 2.0$ and ° curve represents $n_3 = 2.05$.

The SPR resonance wavelength is shifted by the change of the refractive index of the transducing layer.

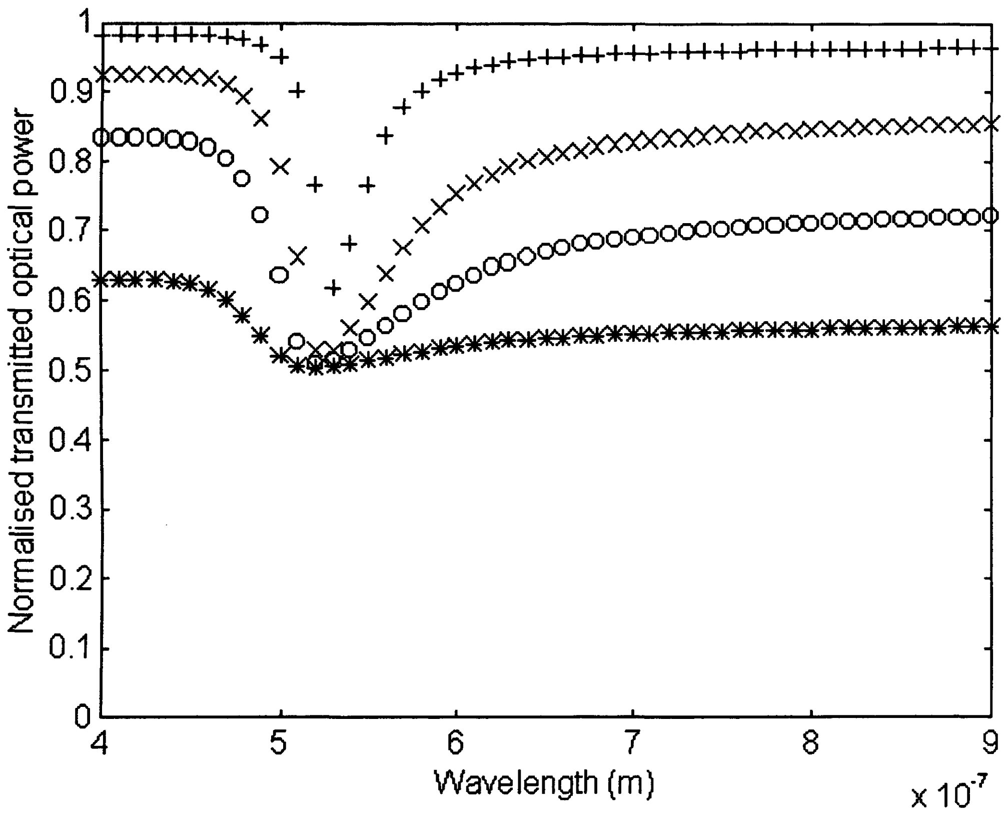

Figure 3-15 Normalised transmitted optical power of the SPR fibre-optic sensor, using zirconium oxide as the transducing layer with $\varepsilon_3 = n_3^2 = 4.0$, thickness $d_3 = 40nm$, silver as the SPR supporting metal, with $\varepsilon_1 = -17 + 0.6j$ and $d_1 = 45nm$, the refractive index of the sample $n_0 = 1.0$. The length of the sensing element L changes.

In Figure 3-15, + represents the case of the length of the sensing element $L = 5mm$, × represents $L = 20mm$, ° represents $L = 50mm$ and * represents $L = 200mm$.

Due to a greater number of reflections, the minimum transmittance decreases with increase of the length of the sensing element L. When the length is long enough, optical power of all wavelengths will be absorbed, again giving zero sensitivity. Compared with SPR fibre-optic sensors without the transducing layer, the length needed for full absorption in all wavelengths is greater, since the transmitted optical power spectrum is narrower.

3.6 Summary and Conclusions

In this chapter, the optical power transmittance, as one of the most important characteristics in SPR fibre-optic sensors both with and without a transducing layer, has been analysed and studied by numerical calculations. The behaviours and characteristics of SPR fibre-optic sensors obtained by numerical calculations agree well with previously published experimental results, such as Jorgenson's work [Jorgenson 1993 and 1994] and Slavik's work [Slavik 1998].

Further, by suitable design of the sensing element in terms of the thickness and the length of the supporting metal, as well as the thickness and refractive index of the transducing layer, the optimal behaviour of the SPR fibre-optic sensor over a wide dynamic range can be achieved.

The optical power spectrum of SPR fibre-optic sensors with a transducing layer is narrower than that of sensors without a transducing layer, This characteristic leads to the SPR fibre-optic sensors with a transducing layer have higher sensitivity. By using a transducing layer, sensing can be achieved by monitoring the change of refractive index in the sample to be measured or in the transducing layer. Thickness change of the transducing layer can be another sensing parameter to design SPR fibre-optic sensors.

Finally, some other issues of the characteristics of SPR fibre-optic sensors, such as sensitivity, dynamic range, the position of minimum reflectance and the dispersion due to the SPR supporting metal, are important and need more detailed discussions.

Chapter 4

An Approximate Theoretical Model of Surface Plasmon Resonance Optical Waveguide and Fibre-Optic Sensors

4.1 Introduction

The following chapter is a detailed description of how to construct an approximate mathematical model for surface plasmon resonance (SPR) optical waveguide and fibre-optic sensors. Optical surface plasmon resonance (SPR) excitation can be theoretically depicted and discussed using Fresnel's equations. However, Fresnel's equations cannot explicitly give expressions to reflect the characteristics of SPR systems, such as the half-width of the reflection curve, and the minimum reflectance. In SPR optical waveguide and fibre-optic sensors this difficulty is even worse. Based on the approximation proposed by Kretschmann in bulk optics, an approximate mathematical model is presented in this chapter to describe the characteristics of SPR large dimension optical waveguide and fibre-optic sensors. This model keeps high accuracy for operation close to the minimum reflection area, at which the resonance condition is achieved. This model can be used to analytically estimate the performance of SPR optical waveguide sensors, and SPR fibre-optic sensors in meridional rays approximation.

4.2 Motivation of the study

As mentioned in Chapter 3, optical surface plasmon resonance (SPR) excitation is a promising technique in the fields of chemical and biochemical sensing, with high sensitivity and fast response as its main features. After study and development over more than two decades, this technique has been applied to the determination of gas concentration [Kalabina 1995, Jory 1995 and Wright 1995], the measurement of optical properties of metals [Fontana 1988, de Bruijn 1990 and Nash 1998], microscopy [Nikitin 1999 and Lahiri 1999] and biosensors [Disley 1998 and Aldinger 1998]. Based on the configuration and the approximate mathematical model proposed by Kretschmann [Kretschmann 1971], there have been successful theoretical and experimental studies of bulk-optic surface plasmon resonance systems [Chen 1981 and Kano 1994]. In recent years, with the progress of optical waveguide and fibres and related techniques, SPR optical waveguide sensors [Harris 1995, Weiss 1996a, Schipper 1996 and Weiss 1996b] and SPR fibre-optic sensors [Garces 1992, Jorgenson 1993, Jorgenson 1994 and Slavik 1998] have attracted much attention. Fresnel's equations are very useful to analyse SPR large dimension optical waveguide and fibre-optic systems. However, parameters which can affect the performance of the sensors are implicit in Fresnel's equations. In order to help the study and design of SPR optical waveguide and fibre-optic sensors, it is necessary to make efforts to construct theoretical models. In Chapter 3, the characteristics of surface plasmon resonance fibre-optic sensors have been analysed numerically [Xu 2000].

Furthermore, the sensing measurement in SPR sensors happens within the area close to the minimum reflection of light power from the interface of the SPR supporting metal film and the dielectric medium (there is a Lorentzian "dip" on the reflection curve around the minimum reflection). Therefore, the characteristics of the reflection curve close to the "dip" are important to the performance of a SPR optical waveguide or fibre-optic sensor. In this chapter, based on the approximation proposed by Kretschmann [Kretschmann 1971] in SPR bulk-optic systems, the explicit approximate expression is derived for SPR large dimension optical waveguide sensors and SPR fibre-optic sensors in meridional rays approximation.

4.3 Approximate mathematical model

4.3.1 Theoretical derivations

An important technique for the study of surface plasmon waves arises by considering bulk optic components particularly the prism. The theoretical derivation in this section is started from Kretschmann's approximate expression in bulk-optics. This approximate expression has been studied and applied by many researchers, such as Kretschmann, Pockrand and Chen.

When light is incident at an angle θ close to the resonance angle θ_{SP}, the TM mode of the incident light is strongly absorbed and the overall reflected light is attenuated very much. With the angle close to θ_{SP}, the reflection coefficient $r(\theta)$ of the TM mode light can be approximately expressed as a function of θ as [Kretschmann 1971 and Chen 1980]:

$$r(\theta) = 1 - \frac{4[\mathrm{Im}(k^0) + \mathrm{Im}(k^T)]\mathrm{Im}(k^R)}{[k_i^z - \mathrm{Re}(k_z)]^2 + \mathrm{Im}(k_z)^2} \tag{4.1}$$

where the definition of variables is the same as in Chapter 3.

Under the condition of $|\mathrm{Im}(k_z)| << |\mathrm{Re}(k_z)|$, the reflectance has a Lorentzian "dip" at θ_{SP} with a half-width (FWHM) W_θ and a minimum reflectance $r_{\min}(\theta)$ given by:

$$W_\theta = \frac{2c\,\mathrm{Im}(k_z)}{n\omega\cos\theta_{SP}} \tag{4.2}$$

$$r_{\min}(\theta) = 1 - \frac{4\eta}{(1+\eta)^2} \tag{4.3}$$

where

$$\eta = \frac{\mathrm{Im}(k^0) + \mathrm{Im}(k^T)}{\mathrm{Im}(k^R)} \tag{4.4}$$

This approximate model for bulk-optic surface plasmon excitation can be used for SPR optical waveguide sensors and SPR fibre-optic sensors in meridional rays approximation.

Because the planar optical waveguide is simply a special case of the optical fibre (with radius = ∞), for generality, the mathematical model in this section is based on the optical fibre. Figure 4-1 shows the meridional cross-section of the sensing element of the SPR fibre-optic sensor.

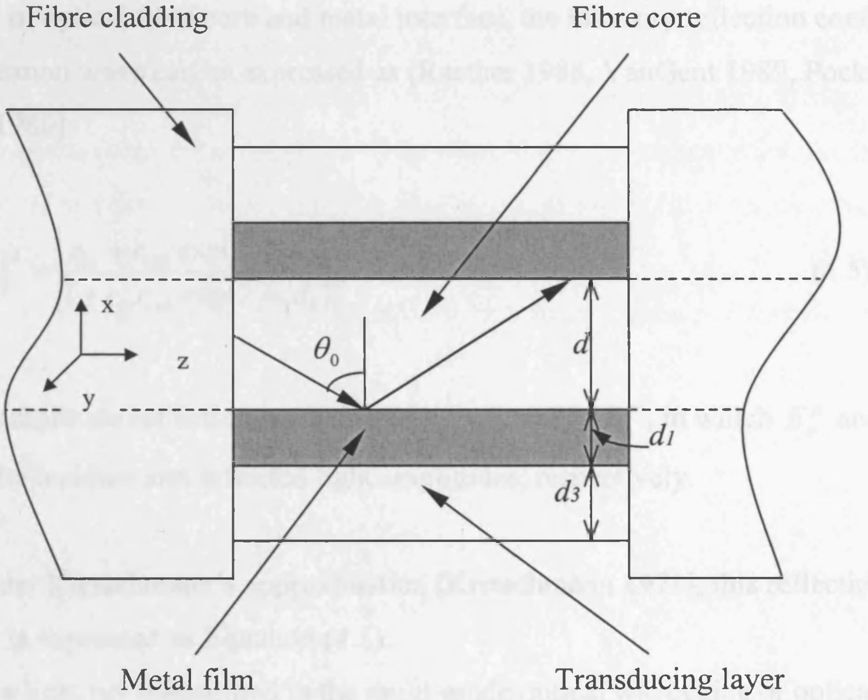

Figure 4-1 Cross-section of the sensing element of the SPR fibre-optic sensor

A multi-mode optical fibre, with core diameter d and refractive index n_2 (dielectric permittivity ε_2), has the jacket and the cladding removed to expose the core, on which is symmetrically deposited a metal film of thickness d_1 and dielectric permittivity ε_1 (refractive index n_1).

In some SPR sensors, the metal film is directly in contact with the sample to be measured with refractive index n_0 (dielectric permittivity ε_0), in others, a dielectric isotropic transducing layer with thickness d_3 and refractive index n_3 (dielectric permittivity ε_3) is deposited symmetrically outside the metal film. In order to obtain a general expression, all formulations are derived in this chapter including this transducing layer. Sensors without transducing layers are considered as a special case by setting $d_3 = 0$.

A ray of light transmitted in an optical fibre with incident angle θ with respect to the normal of optical fibre core and metal interface, the intensity reflection coefficient of surface plasmon wave can be expressed as [Raether 1988, VanGent 1989, Pockrand 1978 and Chen 1980]:

$$r(\theta) = |r_{210}|^2 = \left|\frac{r_{21} + r_{130}\exp(2jk_1d_1)}{1 + r_{21}r_{130}\exp(2jk_1d_1)}\right|^2 \tag{4.5}$$

where the amplitude reflection is calculated by $r_{210} = E_r^p / E_o^p$, in which E_o^p and E_r^p represent the incident and reflected light amplitudes, respectively.

Under Kretschmann's approximation [Kretschmann 1971], this reflection coefficient is expressed as Equation (4.1).

This light ray transmitted in the multi-mode optical waveguide or optical fibre (with incident angle θ, shown in Figure 4-1), will have N reflections in length L of SPR sensing element. Thus, combining the contribution from the N reflections within the SPR sensing element, finally the intensity reflection coefficient is expressed in Equations (4.6) and (4.7):

$$r^N(\theta) = |r_{210}|^{2N} = \left|\frac{r_{21} + r_{130}\exp(2jk_1d_1)}{1 + r_{21}r_{130}\exp(2jk_1d_1)}\right|^{2N} \tag{4.6}$$

$$r^N(\theta) = \left(1 - \frac{4[\mathrm{Im}(k^0) + \mathrm{Im}(k^T)]\mathrm{Im}(k^R)}{[k_i^z - \mathrm{Re}(k)]^2 + \mathrm{Im}(k_z)^2}\right)^N \tag{4.7}$$

In SPR optical waveguide or fibre-optic sensors, the optical power transmittance (the output signal) has to include the contribution from all guided modes, which can be obtained by an integration over all guided modes.

In order to have simple and distinct expressions for further mathematical derivations and analyses of the characteristics of SPR optical waveguide or fibre-optic sensors, some approximate manipulations are taken to Equation (4.7). The ideas of these mathematical manipulations are to approximate the Lorentzian function with the Gaussian function, and approximate the Gaussian function with binomial function, then go from binomial function to exponential function, and finally from exponential function to the final alternative approximation.

All mathematical manipulations following are under the condition of

$[k_i^z - \mathrm{Re}(k_z)]/\mathrm{Im}(k_z) << 1$.

Using Equation (4.7), obtained:

$$r(\theta) = 1 - \frac{4[\mathrm{Im}(k^0) + \mathrm{Im}(k^T)]\mathrm{Im}(k^R)/\mathrm{Im}(k_z)^2}{1 + \left[\frac{k_i^z}{\mathrm{Im}(k_z)} - \frac{\mathrm{Re}(k_z)}{\mathrm{Im}(k_z)}\right]^2} \tag{4.8}$$

$$r(\theta) = 1 - \frac{4[\mathrm{Im}(k^0) + \mathrm{Im}(k^T)]\mathrm{Im}(k^R)}{\mathrm{Im}(k_z)^2}\exp\left[-\left(\frac{k_i^z - \mathrm{Re}(k_z)}{\mathrm{Im}(k_z)}\right)^2 \ln 2\right] \tag{4.9}$$

$$r(\theta) = 1 - \frac{4[\mathrm{Im}(k^0) + \mathrm{Im}(k^T)]\mathrm{Im}(k^R)}{\mathrm{Im}(k_z)^2}\left[1 - \left(\frac{k_i^z - \mathrm{Re}(k_z)}{\mathrm{Im}(k_z)}\right)^2 \ln 2\right] \tag{4.10}$$

$$r(\theta) = 1 - \frac{4[\mathrm{Im}(k^0) + \mathrm{Im}(k^T)]\mathrm{Im}(k^R)}{\mathrm{Im}(k_z)^2} + \frac{4[\mathrm{Im}(k^0) + \mathrm{Im}(k^T)]\mathrm{Im}(k^R)}{\mathrm{Im}(k_z)^2} \times$$

$$\left[\left(\frac{k_i^z - \mathrm{Re}(k_z)}{\mathrm{Im}(k_z)}\right)^2 \ln 2\right] \tag{4.11}$$

$$r(\theta) = \left[1 - \frac{4[\mathrm{Im}(k^0) + \mathrm{Im}(k^T)]\mathrm{Im}(k^R)}{\mathrm{Im}(k_z)^2}\right] \times$$

$$\left\{1 + \frac{\dfrac{4[\mathrm{Im}(k^0) + \mathrm{Im}(k^T)]\mathrm{Im}(k^R)}{\mathrm{Im}(k_z)^2}}{1 - \dfrac{4[\mathrm{Im}(k^0) + \mathrm{Im}(k^T)]\mathrm{Im}(k^R)}{\mathrm{Im}(k_z)^2}} \left[\left(\frac{k_i^z - \mathrm{Re}(k_z)}{\mathrm{Im}(k_z)}\right)^2 \ln 2\right]\right\} \tag{4.12}$$

$$r(\theta) = \left[1 - \frac{4[\mathrm{Im}(k^0) + \mathrm{Im}(k^T)]\mathrm{Im}(k^R)}{\mathrm{Im}(k_z)^2}\right] \times$$

$$\exp\left\{\frac{\dfrac{4[\mathrm{Im}(k^0) + \mathrm{Im}(k^T)]\mathrm{Im}(k^R)}{\mathrm{Im}(k_z)^2}}{1 - \dfrac{4[\mathrm{Im}(k^0) + \mathrm{Im}(k^T)]\mathrm{Im}(k^R)}{\mathrm{Im}(k_z)^2}} \left[\left(\frac{k_i^z - \mathrm{Re}(k_z)}{\mathrm{Im}(k_z)}\right)^2 \ln 2\right]\right\} \tag{4.13}$$

$$r^N(\theta) = \left(1 - \frac{4[\mathrm{Im}(k^0) + \mathrm{Im}(k^T)]\mathrm{Im}(k^R)}{[k_i^z - \mathrm{Re}(k_z)]^2 + \mathrm{Im}(k_z)^2}\right)^N \tag{4.14}$$

$$r^N(\theta) = \left[1 - \frac{4[\mathrm{Im}(k^0) + \mathrm{Im}(k^T)]\mathrm{Im}(k^R)}{\mathrm{Im}(k_z)^2}\right]^N \times$$

$$\exp\left\{N \frac{4[\mathrm{Im}(k^0) + \mathrm{Im}(k^T)]\mathrm{Im}(k^R)}{\mathrm{Im}(k_z)^2 - 4[\mathrm{Im}(k^0) + \mathrm{Im}(k^T)]\mathrm{Im}(k^R)} \left[\left(\frac{k_i^z - \mathrm{Re}(k_z)}{\mathrm{Im}(k_z)}\right)^2 \ln 2\right]\right\}$$

(4.15)

$$r^N(\theta) = \left[1 - \frac{4[\mathrm{Im}(k^0) + \mathrm{Im}(k^T)]\mathrm{Im}(k^R)}{\mathrm{Im}(k_z)^2}\right]^N \times$$

$$\frac{1}{1 - N \frac{4[\mathrm{Im}(k^0) + \mathrm{Im}(k^T)]\mathrm{Im}(k^R)}{\mathrm{Im}(k_z)^2 - 4[\mathrm{Im}(k^0) + \mathrm{Im}(k^T)]\mathrm{Im}(k^R)} \left[\frac{k_i^z - \mathrm{Re}(k_z)}{\mathrm{Im}(k_z)}\right]^2} \qquad (4.16)$$

Both Equation (4.15) and Equation (4.16) are approximate expressions which can be applied to analyse SPR optical waveguide and fibre-optic systems.

4.3.2 Model accuracy

This approximate model is applied to describe the characteristics of the reflection curve close to the resonance angle θ_{SP}, "dip" area. The accuracy of this mathematical model is high in the "dip" area. The farther away from the resonance angle, the worse the accuracy is.

Figure 4-2 shows the reflection coefficient curves calculated by these approximate expressions. The parameters for the calculations are: He-Ne laser, $\lambda = 632.8nm$, core refractive $n_2 = 1.515$, core diameter $d = 600\mu m$, SPR element length $L = 12mm$, light incident angle $\theta = 68^\circ$, silver as SPR supporting metal, and under the assuming: $4[\mathrm{Im}(k^0) + \mathrm{Im}(k^T)]\mathrm{Im}(k^R)/\mathrm{Im}(k_z)^2 = 0.7$.

When $|k_i^z - \mathrm{Re}(k_z)/\mathrm{Im}(k_z)| < 0.14$, the error of the Gaussian approximation is about 9%, the error of the Lorentzian approximation is about 11%.

When $|k_i^z - \mathrm{Re}(k_z)/\mathrm{Im}(k_z)| < 0.1$, the error of the Gaussian approximation is about 5%, the error of the Lorentzian approximation is about 2%.

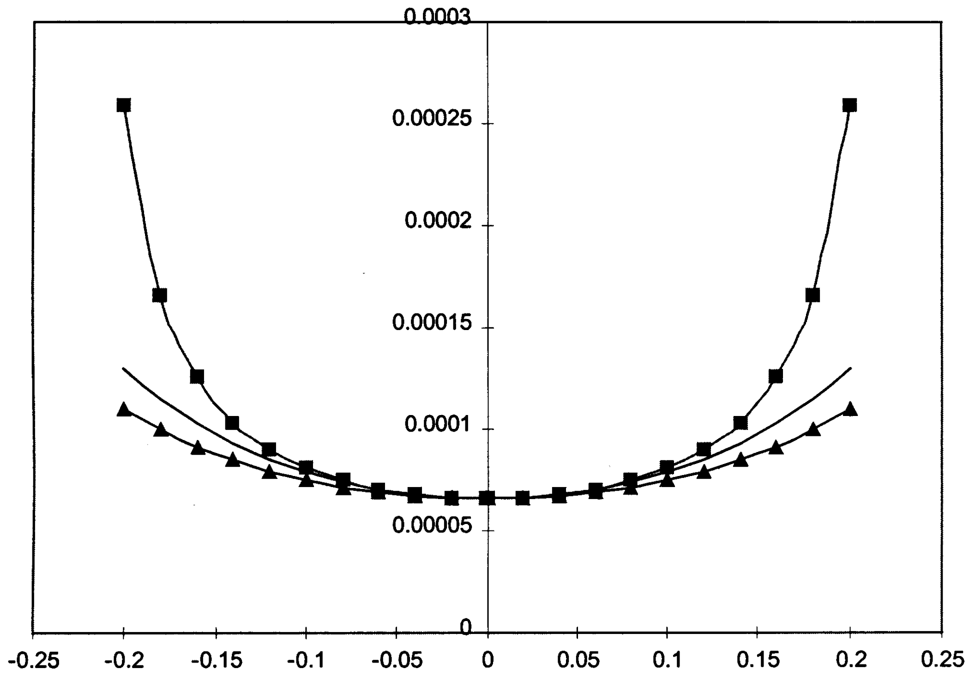

Figure 4-2 The reflection coefficient curves for different approximations, — represents the curve from Equation (4.14), ▲ represents the curve from Equation (4.15) and ■ represents the curve from Equation (4.16)

4.4 Illustrative applications

4.4.1 Characteristic parameters of SPR large dimension optical waveguide sensors

In a SPR large dimension optical waveguide sensor, three parameters, the minimum position θ_{SP} (or k_{SP}^z) where the resonance condition is satisfied, the minimum reflection coefficient $R_{\min}$, and the half-width, FWHM W_θ (or Δk_i^z) are important and closely related to the performance of the sensor. For example, the sensitivity of the sensor is inversely proportional to the half-width FWHM $\Delta\theta$ (or Δk_i^z) [Gent 1990]. Analytical expressions for these three parameters are very useful in estimating the behaviour of the sensor.

Considering an optical waveguide with length L of SPR sensing element, incident TM mode light at angle θ with respect to the normal at the medium/metal interface, the number of reflection at the interface will be $N = L/2d\tan\theta$.

Under condition of $|\mathrm{Im}(k_z)| \ll |\mathrm{Re}(k_z)|$ [Chen 1980 and Chen 1981], using the variable definition in the above section, and using the Equation (4.16), θ_{SP}, $R_{\min}$ and W_θ can be obtained:

When $\mathrm{Re}(k_z) = k(\varepsilon_2)^{1/2}\sin\theta_{SP} = \dfrac{2\pi}{\lambda} n_2 \sin\theta_{SP}$, the minimum position θ_{SP} is achieved.

The minimum reflection coefficient $R_{\min}$ is expressed as:

$$R_{\min} = \sigma^N \tag{4.17}$$

The half-width FWHM of the reflection curve W_θ is expressed as:

$$W_\theta = \frac{2c\,\mathrm{Im}(k_z)}{n\omega\cos\theta_{SP}}\left(\frac{1-\sigma^N}{\upsilon(1+\sigma^N)}\right)^{1/2} \tag{4.18}$$

where $\sigma = 1 - \dfrac{4[\mathrm{Im}(k^0)+\mathrm{Im}(k^T)]\mathrm{Im}(k^R)}{\mathrm{Im}(k_z)^2}$, $\upsilon = N\dfrac{4[\mathrm{Im}(k^0)+\mathrm{Im}(k^T)]\mathrm{Im}(k^R)}{\mathrm{Im}(k_z)^2 - 4[\mathrm{Im}(k^0)+\mathrm{Im}(k^T)]\mathrm{Im}(k^R)}$

4.4.2 Reflectance of SPR fibre-optic sensors

It is known that light rays with a range of incident angles are allowed to propagate in a multi-mode optical fibre. The range is determined by the numerical aperture of the fibre, $N.A.= n_2 \cos\theta_c = (n_1^2 - n_2^2)^{1/2}$. Only rays with $90^0 > \theta > \theta_c$ (critical angle) can be transmitted in the optical fibre. To find the output of the SPR fibre-optic sensor the contribution from all rays transmitted should be considered. Such a consideration depends on the power distribution of the light source. Mathematically, an integration has to be made to combine all these rays' contributions.

For simplicity, if the light power reaching the sensing region is distributed equally among all rays with incident angles in (θ_1, θ_2), the total light power reflectance is expressed [Ruddy 1990]:

$$\gamma_T = \frac{1}{\theta_2 - \theta_1} \int_{\theta_1}^{\theta_2} \gamma(\theta) d\theta \qquad (4.19)$$

where $\gamma(\theta)$ is the reflection coefficient of light ray at angle θ

Then, in fibre-optic sensors, the guided modes within angles of (θ_c, 90^0), the total reflectance of TM mode light is expressed as:

$$R = \frac{1}{90^0 - \theta_c} \int_{\theta_c}^{90^0} r^N(\theta) d\theta = \frac{1}{90^0 - \theta_c} \int_{\theta_c}^{90^0} \frac{\sigma^N}{1 - \upsilon[k_i^z - \mathrm{Re}(k_z)]^2 / \mathrm{Im}(k_z)^2} d\theta$$

(4.20)

Because different ranges of angles suffer different numbers of internal reflections, from 1 to maximum N_m (at θ_c), the total angle range (θ_c, 90^0) can be divided into discrete sub-ranges (θ_m, θ_{m+1}) , $m = 1, \ldots, N_m$, each sub-range suffers the same number of reflections. These angle sub-ranges correspond to propagation constant sub-ranges, (k_m^z, k_{m+1}^z). Therefore, the analytical expression of the reflectance is given by:

$$R = \frac{1}{k_{90^0}^z - k_c^z}\sum_{m=1}^{N_m}\sigma^m \int_{k_m^z}^{k_{m+1}^z} \frac{1}{1-\upsilon[k_i^z - \mathrm{Re}(k_z)]^2/\mathrm{Im}(k_z)^2} dk_i^z$$

$$= \frac{1}{2(k_{90^0}^z - k_c^z)}\sum_{m=1}^{N_m}\sigma^m \left[\log\frac{\mathrm{Im}(k_z)+\sqrt{\upsilon}[k_i^z - \mathrm{Re}(k_z)]}{\mathrm{Im}(k_z)-\sqrt{\upsilon}[k_i^z - \mathrm{Re}(k_z)]}\right]_{k_m^z}^{k_{m+1}^z} \quad (4.21)$$

where $k_{90^0}^z$ and k_c^z represent the propagation constants of guided rays at 90^0 and critical angle θ_c, respectively. The definition of other variables is the same as in earlier equations.

These are illustrative examples to demonstrate the applications of the approximate model. Due to the complication of light power distribution of light sources, the detailed analysis of the reflectance in some cases can only be calculated by numerical methods. In SPR sensors the analysis should also consider that both TE and TM polarised light can propagate in optical waveguides and optical fibres. All the above issues have been studied in Chapter 3 by numerical calculations.

4.5 Conclusions

Theoretical models are important tools in the study and development of surface plasmon resonance (SPR) sensors. However, Fresnel's equations cannot give explicit expressions to reflect the relationship between parameters of the design and the characteristics of the sensor. Furthermore, the performance of SPR optical waveguide and fibre-optic sensors is closely related to the characteristics near the minimum reflection "dip" area in the reflection curve. To construct theoretical models to estimate the characteristics of the curve close to the "dip" is meaningful and very useful. In this chapter, a theoretical model has been presented for SPR large dimension optical waveguide and fibre-optic sensors. This model can be applied to do analytical study as shown in two illustrative examples.

These examples show that the analytical relationship between the characteristic parameters of SPR optical waveguide or fibre-optic sensors (such as those using light reflectance *etc)* can be used to quantitatively estimate the performance in the area close to the minimum "dip". The nearer to the "dip", the higher the accuracy obtained. Theoretically the derived approximation gives no error at the minimum "dip".

Chapter 5

Numerical Error and Limitation Analysis of Two-Wavelength Light Intensity Attenuation-Based Fibre-Optic Chemical Sensors

5.1 Introduction

The following chapter is a detailed evaluation of the errors and limitations of two-wavelength light intensity attenuation-based fibre-optic chemical sensors based on the Beer-Lambert law. A general formulation to express the measurement error and the error induced by the instability of the light power inputted into the absorbing sample to be measured is derived. Using this formulation, two common and important errors in this type of sensor, temperature fluctuation of light sources and bending of optical fibres, are discussed. Numerical calculations are presented to demonstrate the effect of the errors as examples. This approach can be applied not only to the Beer-Lambert law based two-wavelength fibre-optic chemical sensors, but to other types of two-wavelength fibre-optic systems as well.

5.2 Light intensity attenuation-based fibre-optic chemical sensors using the principle of the Beer-Lambert law

Optical bulk-absorption based on the Beer-Lambert law is the most popular and important spectroscopic technique for designing light intensity attenuation-based sensors. Many fibre-optic chemical sensors are developed on this principle, whereby the detected output signal of the sensor is used to determine the concentration of the analyte to be measured.

The basic principle is illustrated schematically in Figure 5-1, which shows an incident light beam of intensity I_0 yielding transmitted I_T or reflected I_R signal, after interaction either directly with the analyte or with an immobilized indicator system.

Although a range of geometrical configurations can be used with optical fibres, the basic principles of interaction remain the same. According to whether transmitted or reflected light is monitored, the sensors can be divided into two classes:

1. transmission-type [Zhou 1988 and Deboux 1995],
2. reflection-type [Peterson 1980 and Landis 1994].

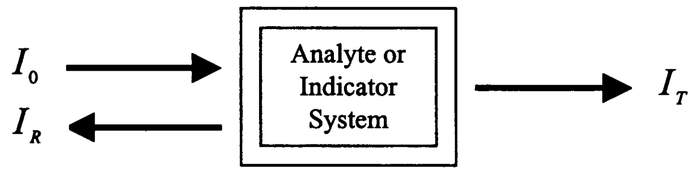

Figure 5-1 Major spectroscopic principles used in fibre-optic chemical sensors

The basic formulation of light intensity attenuation by absorption is characterised by the Beer-Lambert law, expressed in Equations (1.1) and (1.2). These equations can be applied in bulk-absorption and evanescent wave absorption, with the absorption coefficient, α_λ, corresponding to bulk-absorption coefficient or effective evanescent wave coefficient, respectively.

The important practical consequence of the measurement is that when I_0 and I_T are known, the calculated absorptance of $A = \log(I_0 / I_T)$ is directly proportional to the concentration, yielding a linear calibration.

It is important to point out, however, that there are practical limitations to the applicability of the Beer-Lambert law, or, in particular, the linear dependence of absorption on concentration:

(1) The bandwidth $\Delta\lambda$ of the incident light beam should be very narrow, ideally approximating monochromatic radiation. Deviations from perfect Beer-Lambert behaviour increase as $\Delta\lambda$ increases, but are particularly severe when $\Delta\lambda$ is greater than the spectral width of the absorption band of the absorbing species. Such deviations result in a nonlinear calibration in the sensor, which, although

acceptable in some instances, results in a sensitivity that falls off with concentration and a consequent reduction in the useful measurement range.

(2) Deviations from perfect Beer-Lambert behaviour are also observed in highly absorbing or highly scattering media. Both of these effects yield a very limited linear range for the absorbance-concentration relationship. Furthermore, high concentrations of the absorbing species can also result in measurement problems due to reactions taking place. In such circumstances the optical characteristics of the absorbing material will differ significantly from those observed at low concentrations.

5.3 Two-wavelength light intensity attenuation-based (the Beer-Lambert law) fibre-optic chemical sensors

For the purpose of improving accuracy and stability, in the design of light intensity attenuation-based fibre-optic chemical sensors, such as the Beer-Lambert law based sensors, a differential absorption technique is usually used [Dakin 1989]. In this a reference wavelength, different from the measurement beam wavelength, is used. At the measurement wavelength the light will be strongly absorbed by the chemical species to be measured, at the reference wavelength the absorption of light does not happen, or the absorption is small and might be neglected [Chan 1984].

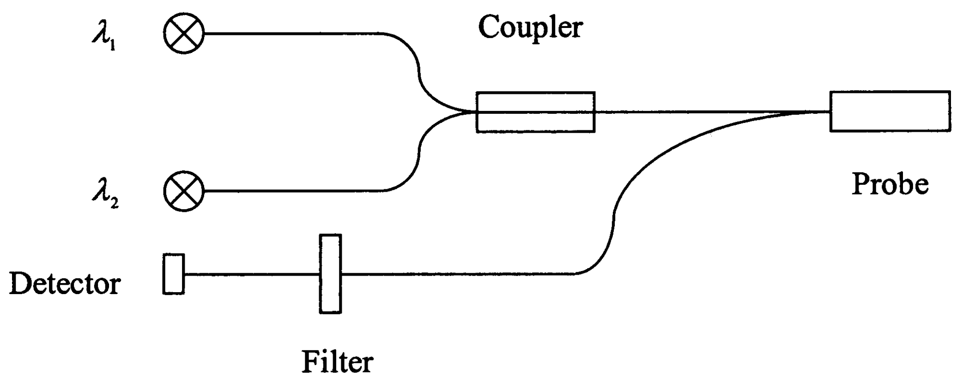

Figure 5-2 Typical example of two-wavelength system

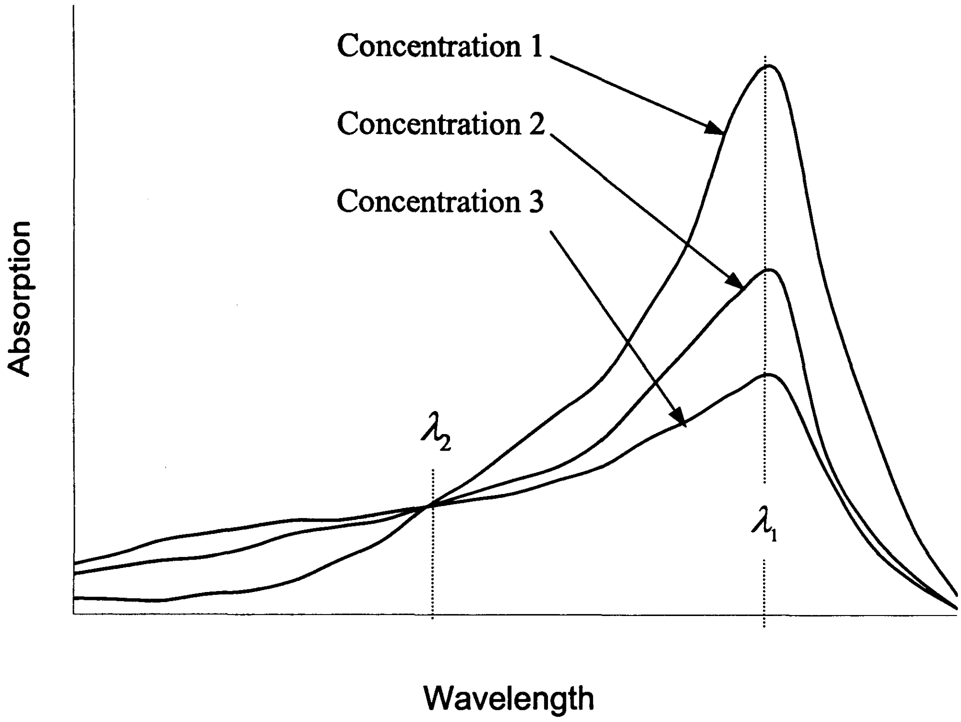

Figure 5-3 Two-wavelength principle: λ_1 signal wavelength, λ_2 reference wavelength, Concentration 1 > Concentration 2 > Concentration 3

Figure 5-2 and Figure 5-3 show the configuration and principle of the two-wavelength system, λ_1 and λ_2 are measurement and reference wavelength, respectively.

Many fibre-optic spectroscopes and sensors have already been developed based on this principle in commercial markets. Much research has been done on these devices as well. The study of error sources and the accuracy limitation of this type of sensor is important. Some authors have reported their work on this topic, such as the analyses of source shot, thermal noises and coherent reflection noise [Jin 1995 and Jin 1997].

In two-wavelength systems, the fluctuation of light output power and power spectra from light sources can be an important error source. And, in fibre-optic sensors, the disturbance of the optical fibre itself is of concern since light power is transmitted by optical fibres. The optical fibre itself is a dispersive component, the attenuation of the transmitted light power induced by disturbing optical fibres such as bending is also due to dispersive processes. The power attenuation is different at different wavelengths, which generates another error source in two-wavelength absorption-based fibre-optic sensors. In this chapter, two common and important issues in the Beer-Lambert law based fibre-optic chemical sensors not well studied considering the operation of two wavelengths before, namely the errors induced by the temperature characteristics of light sources (especially non-coherent broadband light sources) and the effects of bending optical fibres are studied both theoretically and by numerical examples.

5.4 Mathematical model

Light passing through a material can be absorbed by interaction with the molecules and atoms of the host material, or with impurities and defects. At a given wavelength λ, the intensity of the light passing through the material is attenuated as an exponential function of its path length x. This is expressed by the Beer-Lambert law:

$$I_\lambda(x) = I_\lambda(0)\exp(-\alpha_\lambda[M]x) \tag{5.1}$$

where $I_\lambda(x)$ is the light intensity at a distance x, $I_\lambda(0)$ is the incident light intensity at $x = 0$, α_λ is the absorption coefficient and $[M]$ is the concentration of the absorbing material.

As mentioned before, the differential absorption technique, two wavelengths are applied, λ_1 as the measurement wavelength and λ_2 as the reference wavelength. Therefore, the output of sensors can be expressed as:

$$\frac{I_{\lambda 1}(x)}{I_{\lambda 2}(x)} = \frac{I_{\lambda 1}(0)}{I_{\lambda 2}(0)}\exp(-\alpha_{\lambda 1}[M]x + \alpha_{\lambda 2}[M]x) \tag{5.2}$$

where the subscripts represent different wavelengths.

Because the absorption at λ_2 is small, and can be neglected, that is,

$$\alpha_{\lambda 2}[M]x = 0 \tag{5.3}$$

Equation (5.2) can be re-written as:

$$\frac{I_{\lambda 1}(x)}{I_{\lambda 2}(x)} = \frac{I_{\lambda 1}(0)}{I_{\lambda 2}(0)}\exp(-\alpha_{\lambda 1}[M]x) \tag{5.4}$$

Equation (5.4) is the measurement expression of the Beer-Lambert law based two-wavelength fibre-optic chemical sensors. In the measurement, $I_{\lambda 1}(0), I_{\lambda 2}(0)$, $\alpha_{\lambda 1}$ and x are known, the concentration $[M]$ is obtained by measurements of the outputs of the sensor, $I_{\lambda 1}(x)$ and $I_{\lambda 2}(x)$.

The accuracy of the sensor is determined by the errors of the measurement of light intensities outputted from the absorbing sample to be measured, which can be expressed as:

$$\tilde{I}_{\lambda 1}(x) = I_{\lambda 1}(x) + \Delta I_{\lambda 1}(x) \tag{5.5}$$

$$\tilde{I}_{\lambda 2}(x) = I_{\lambda 2}(x) + \Delta I_{\lambda 2}(x) \tag{5.6}$$

and further,

$$\tilde{I}_{\lambda 1}(x) = I_{\lambda 1}(x) \cdot (1 + \delta_{\lambda 1}(x)) \tag{5.7}$$

$$\tilde{I}_{\lambda 2}(x) = I_{\lambda 2}(x) \cdot (1 + \delta_{\lambda 2}(x)) \tag{5.8}$$

where $\Delta I_{\lambda 1}(x)$ and $\Delta I_{\lambda 2}(x)$ represent measurement errors, and $\delta_{\lambda 1}(x) = \Delta I_{\lambda 1}(x) / I_{\lambda 1}(x)$ and $\delta_{\lambda 2}(x) = \Delta I_{\lambda 2}(x) / I_{\lambda 2}(x)$ represent relative measurement errors.

From Equation (5.4), it is known that the accuracy of the sensor is also affected by the stability of the light powers inputted into the absorbing sample, which can be expressed as:

$$\widetilde{I}_{\lambda 1}(0) = I_{\lambda 1}(0) + \Delta I_{\lambda 1}(0) \tag{5.9}$$

$$\widetilde{I}_{\lambda 2}(0) = I_{\lambda 2}(0) + \Delta I_{\lambda 2}(0) \tag{5.10}$$

and further,

$$\widetilde{I}_{\lambda 1}(0) = I_{\lambda 1}(0) \cdot (1 + \delta_{\lambda 1}(0)) \tag{5.11}$$

$$\widetilde{I}_{2}(0) = I_{\lambda 2}(0) \cdot (1 + \delta_{\lambda 2}(0)) \tag{5.12}$$

where $\Delta I_{\lambda 1}(0)$ and $\Delta I_{\lambda 2}(0)$ represent incident light intensity fluctuations, $\delta_{\lambda 1}(0) = \Delta I_{\lambda 1}(0) / I_{\lambda 1}(0)$ and $\delta_{\lambda 2}(0) = \Delta I_{\lambda 2}(0) / I_{\lambda 2}(0)$ represent relative incident light intensity fluctuations.

Here it is assumed that variables α_{λ} and x do not change. Therefore, the concentration measurement formulation of the Beer-Lambert law based two-wavelength fibre-optic fibre-optic chemical sensors can be expressed by Equation (5.13), which includes the above-mentioned errors and fluctuations.

$$\frac{\widetilde{I}_{\lambda 1}(x)}{\widetilde{I}_{\lambda 2}(x)} = \frac{\widetilde{I}_{\lambda 1}(0)}{\widetilde{I}_{\lambda 2}(0)} \exp(-\alpha_{\lambda 1}[M]_m x) \tag{5.13}$$

where $[M]_m$ is the measured concentration value, which would be different from the real value $[M]$.

Substituting the above error expressions into Equation (5.13), and obtaining:

$$\frac{\tilde{I}_{\lambda1}(x)}{\tilde{I}_{\lambda2}(x)} = \frac{I_{\lambda1}(x)\cdot(1+\delta_{\lambda1}(x))}{I_{\lambda2}(x)\cdot(1+\delta_{\lambda2}(x))} \tag{5.14}$$

$$\frac{I_{\lambda1}(x)\cdot(1+\delta_{\lambda1}(x))}{I_{\lambda2}(x)\cdot(1+\delta_{\lambda2}(x))} = \frac{I_{\lambda1}(0)\cdot(1+\delta_{\lambda1}(0))}{I_{\lambda2}(0)\cdot(1+\delta_{\lambda2}(0))}\exp(-\alpha_{\lambda1}[M]_m x) \tag{5.15}$$

The relationship between the real concentration $[M]$ and measured concentration $[M]_m$ is expressed as:

$$\exp[\alpha_{\lambda1}([M]-[M]_m)x] = \frac{(1+\delta_{\lambda1}(x))\cdot(1+\delta_{\lambda2}(0))}{(1+\delta_{\lambda2}(x))\cdot(1+\delta_{\lambda1}(0))} \tag{5.16}$$

Because of the small values of $\delta_{\lambda1}(x)$, $\delta_{\lambda2}(x)$, $\delta_{\lambda1}(0)$ and $\delta_{\lambda2}(0)$, Equation (5.16) can be re-written as:

$$\alpha_{\lambda1}([M]-[M]_m x) = 1+\delta_{\lambda1}(x)-\delta_{\lambda2}(x)-\delta_{\lambda1}(0)+\delta_{\lambda2}(0) \tag{5.17}$$

The measurement errors $\delta_{\lambda1}(x)$ and $\delta_{\lambda2}(x)$ have been studied in Jin's papers [Jin 1995 and Jin 1997]. As illustrative examples, the following numerical calculations are focused on the study of terms $\delta_{\lambda1}(0)$ and $\delta_{\lambda2}(0)$, which are caused by the instability of incident light intensities inputted into the absorbing sample to be measured.

5.5 Illustrative examples of numerical error analyses and discussions

In the Beer-Lambert law based two-wavelength fibre-optic chemical sensors, the reference wavelength λ_2 is used to monitor the background absorption and the fluctuation of output light power from light sources. Ideally $I_{\lambda 1}(0)$ and $I_{\lambda 2}(0)$ do not change during the measurement. In practice, there are many factors which could result in the instability of $I_{\lambda 1}(0)$ and $I_{\lambda 2}(0)$. Among these, the fluctuation of the output light power of light source induced by the temperature change and the physical disturbance of optical fibres are inevitable and significant. In following parts of this section, these are studied as two illustrative examples.

5.5.1 The error due to the temperature fluctuation of light sources

In the Beer-Lambert law based two-wavelength fibre-optic chemical, non-coherent broadband light sources, such as black-body radiators, Lamps and LEDs are usually used. The light output power, even power spectrum, of these light sources could be changed by many factors. For long-term use, the instability of the output power of light sources is extremely important to the performance of the sensor.

The temperature instability of output light power and power spectrum of non-coherent broadband light sources is complicated. It completely depends on the light sources themselves. Different types of light sources have different temperature characteristics. Here the black-body radiator is used as an illustrative example.

The black-body spectral radiation can be analytically expressed as [Chappell 1976]:

$$\tilde{I}_\lambda(0) = \frac{2{c_0}^2 k}{\Omega_0 \lambda^5 \cdot \left(e^{c_0 \cdot h / \lambda \cdot k \cdot T} - 1\right)} \tag{5.18}$$

where $\tilde{I}_\lambda(0)$ is the radiation intensity of the radiator, c_0 is the velocity of light, Ω_0 is the solid angle, k is Boltzmann's constant, h is Planck's constant, T is absolute temperature and λ is the radiation wavelength.

Obviously $\tilde{I}_\lambda(0)$ will be changed by both wavelength and temperature. The accuracy of a Beer-Lambert law based two-wavelength fibre-optic chemical sensor with this type of light source using two-wavelength technique, especially when the difference between the two wavelengths is large, will be apparently affected by the change of temperature.

Fig. 5-4 shows the numerical calculation of errors caused by the temperature variation of the black-body radiator against wavelength.

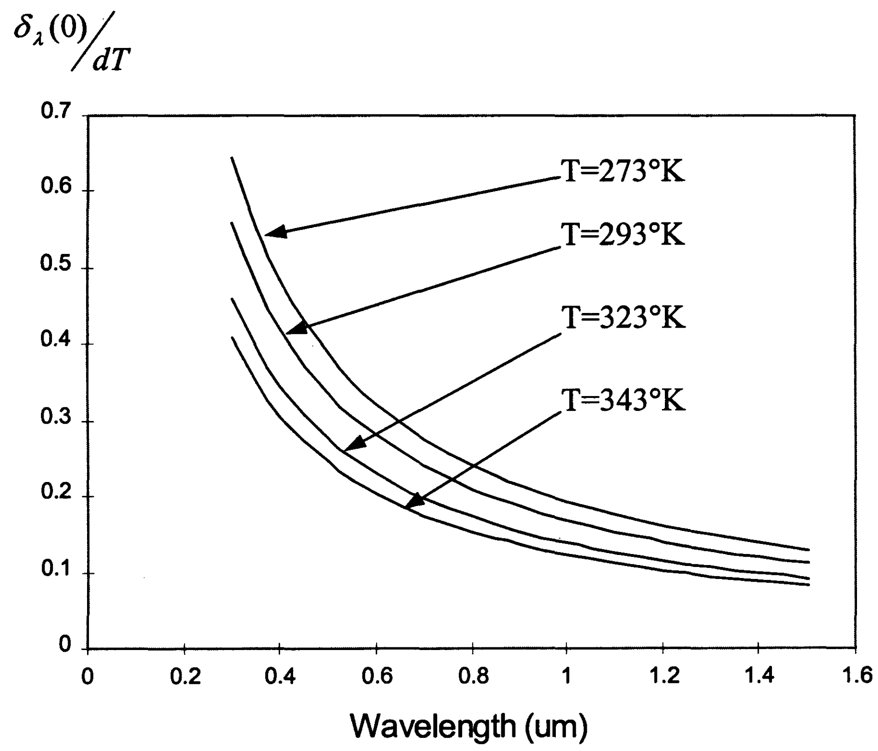

Figure 5-4 The variation of errors at different temperatures against wavelength

At different wavelengths the output power fluctuation caused by temperature change will be different.

For example: assuming $T = 293°K$,

at $\lambda = 1.0\mu m$, $\delta_{\lambda 1}(0) = 0.17dT$ and at $\lambda = 0.5\mu m$, $\delta_{\lambda 2}(0) = 0.34dT$.

In this case, from Equation (5.17), the error of the measured concentration induced by the temperature fluctuation of the output power of the light source is $[M]-[M]_m \mid = 0.17dT/(\alpha_{\lambda 1} \cdot x)$.

The error increases with the increase of temperature. The temperature characteristic of light power spectra of light sources is a critical factor in determining the accuracy of the Beer-Lambert law based two-wavelength fibre-optic chemical sensors. In some applications, in order to obtain high accuracy, temperature controllers or compensators for light sources are needed.

5.5.2 The error due to bending of optical fibres

In practical uses of the Beer-Lambert law based two-wavelength fibre-optic chemical sensors, bending of optical fibres is unavoidable, for example, bending the optical fibre to fit the space restriction. Bending an optical fibre will lead to the attenuation of light power transmitted inside the optical fibre. Especially when the bending curvature is small, this type of loss will increase significantly. Much research has been done in the study of bending optical fibres either by geometric optics [Gloge 1972 and Snyder 1974c] or electromagnetic theory [Marcuse 1976a and Marcuse 1976b]. The influence of bending optical fibres on the accuracy of this two-wavelength fibre-optic systems has not been well studied before. In this section this error is investigated by geometric optics. Multimode optical fibres with large core diameter are often used in this type of sensor and geometric optics is highly effective and useful to analyse the loss in such optical fibres.

Based on the results by Gloge [Gloge 1972], an optical fibre with core diameter *2a*, reflective index n_1, cladding reflective index n_2, the bending loss coefficient α is:

$$\alpha = 2nk(\theta_c^{\ 2} - \theta^2)\exp[-\frac{2}{3}n_1 kR(\theta_c^{\ 2} - \theta^2 - \frac{2a}{R})^{3/2}] \tag{5.19}$$

where k is the free-space propagation constant, R is the curvature radius, θ is angle of the ray (with respect to longitudinal axis of optical fibre) and

$\theta_c = [1-(^{n_c}/_n)^2]^{1/2}$ is the critical angle for total internal reflection.

The mean quantity of bending loss coefficient considering the contributions from all transmitted rays can be calculated by integration. This loss coefficient will vary with the wavelength in detailed analysis.

For simplicity, the following discussion of bending loss coefficient is based on Equation (5.19).

The light power transmission in a bending optical fibre is defined as [Wolf 1979]:

$$P_{out} = P_{in} \cdot e^{-\alpha L/10} \tag{5.20}$$

where P_{out} and P_{in} are the light output and input powers, respectively, L is the bending length of the optical fibre.

In the Beer-Lambert law based two-wavelength fibre-optic chemical sensors, the bending loss of the optical fibre is obviously equivalent to the fluctuations of the light intensities inputted into the absorbing sample, $I_{\lambda 1}(0)$ and $I_{\lambda 2}(0)$. Therefore, the following equations can be obtained:

$$\tilde{I}_\lambda(0) = I_\lambda(0) \cdot e^{-\alpha L/10} \tag{5.21}$$

$$\delta_\lambda(0) = e^{-\alpha L/10} - 1 \tag{5.22}$$

Figure 5-5 shows the numerical calculation of the error induced by the optical fibre bending loss at different bending curvature against wavelength.

From Equation (5.22), it is known that the error depends on both the radius of bending curvature and the light wavelength. Under the same bending, the loss will be different at different wavelengths.

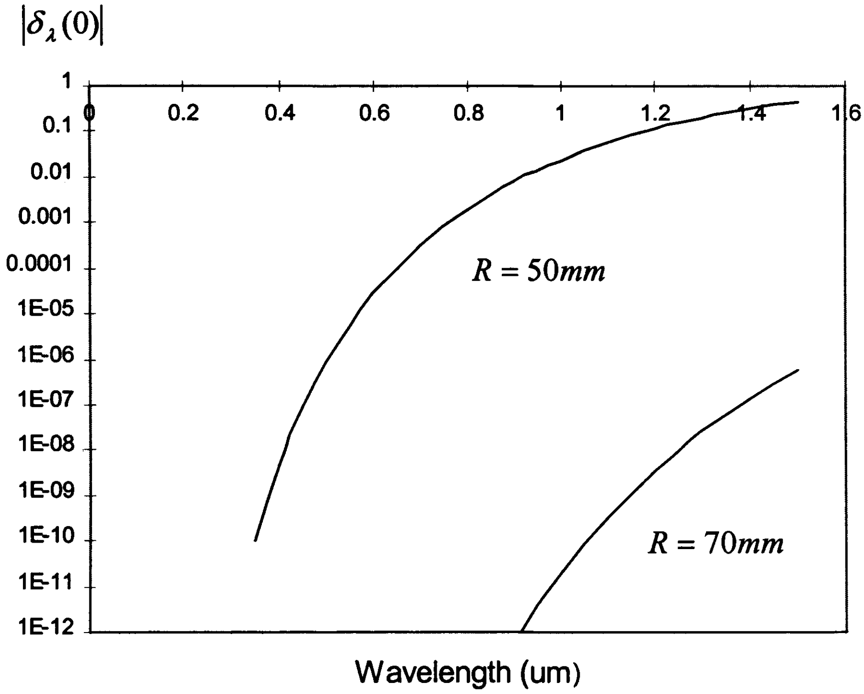

Figure 5-5 The error caused by the fibre bending loss at different curvatures against wavelength

For example: assuming $n_1 = 1.5$, n_2,=1.496, $R = 50$mm, $a = 60\mu$m, $\theta_c = 4.2°, \theta = 2.5°$ and $L=4R$, at $\lambda = 1.5\mu$m, $\delta_{\lambda1}(0) = 0.45$ and at $\lambda = 1.0\mu$m, $\delta_{\lambda2}(0)$ =0.023.

The larger the radius of curvature is, the smaller the loss. The loss difference between the two different wavelengths is also smaller. The loss will increase with the decrease of the radius of bending curvature. A concept of the critical radius (suffering 3-dB loss) is introduced to reflect the relation between light power loss and the bending curvature, which is expressed as [Senior 1985]:

$$R_c = \frac{3n^2\lambda}{4\pi(n^2 - n_c^{\ 2})^{3/2}} \tag{5.23}$$

By Equation (5.23), it is known that when the wavelength is smaller, the critical radius is smaller too and *vice versa*.

For example: using the above optical fibre, at $\lambda = 1.0\mu m$, $R_c = 410\mu m$ and at $\lambda = 0.5\ \mu m$, $R_c = 205\mu m$.

When the radius of bending curvature is between these two critical radii, the loss will be very different at these two wavelengths. Under this circumstance, the use of these two wavelengths as measurement and reference light in a Beer-Lambert based two-wavelength fibre-optic chemical sensor will increase the error induced by bending the optical fibre.

Bending, especially microbending has a significant influence on the accuracy of the Beer-Lambert two-wavelength fibre-optic chemical sensors. Microbending of optical fibres should always be considered carefully.

5.6 Conclusions

In the Beer-Lambert based two-wavelength fibre-optic chemical sensors, the accuracy is affected by many factors such as principle errors, measurement errors and instability of environments. In this chapter, a general formulation has been derived to analyse errors, and using the formulation the error induced by the fluctuation of light power inputted into the absorbing sample is studied. As illustrative examples, the errors induced by temperature instability of light sources and bending optical fibres are numerically analysed since they are not well studied in the Beer-Lambert based two-wavelength fibre-optic chemical sensors.

The environmental physical disturbance (particularly microbending of optical fibres) and temperature fluctuation could be critical to the accuracy of the sensor in some applications. From the design point of view, under such circumstance, in order to achieve high performance of the sensor, temperature controllers or compensators for the light source are needed. Another effective approach to minimise the error is to choose the interval of measurement and reference wavelengths to be as small as possible.

In the design of the light source for the Beer-Lambert based two-wavelength fibre-optic chemical sensors, not only does the stability of output power have to be considered, but the stability of the output power spectra has to be studied carefully as well. Although only the error influence from temperature change of the light source is addressed in this paper, other factors which can change the output light power and power spectrum of light sources such as the driving current of the light sources could be discussed using the same approach.

From Equation (5.17), the effects of different errors in the Beer-Lambert based two-wavelength fibre-optic chemical sensors are not the same, with some of them positive, others negative. In the design, this characteristic could be used to compensate one for another and reduce the overall error of the sensor to the minimum.

The information and consideration drawn from this research can be applied in two-wavelength absorption-based fibre-optic sensors both of the transmission-type and reflection-type.

Part 2: Design Studies

Chapter 6

Design of a "Propofol" Fibre-Optic Sensor

6.1 Introduction

This chapter details the design of a "propofol" fibre-optic sensor as an example design study of the extrinsic type of light intensity attenuation-based fibre-optic chemical sensor. A "Propofol" fibre-optic sensor is developed to measure the concentration of an anaesthetic, **Propofol**, in infusion. As mentioned before, the design of extrinsic fibre-optic sensors is mainly focused on the probe and on overall system optimisation with regard to the proper selection of light source, detector, *etc.* The objective of this chapter is to summarise the considerations during the design process and give the reasoning behind the decisions regarding every key element of the sensor, such as the design of the probe structure and materials. A full system including mechanical structures and electronic circuits has been suggested for further development. This system has been constructed and tested.

6.2 Optical anaesthetics sensors

6.2.1 Concentration measurement of anaesthetics

Since the first use of ether and chloroform in the 1840s, anaesthetics have been applied to clinical effect. It is important to be able to measure the concentration so that the rate can be controlled at optimal levels for each stage of the procedure. Good control will allow appropriate depth of anaesthesia to be maintained at all times and provide good patient recovery characteristics. The common techniques available today for measuring the concentration of anaesthetics include high-performance liquid chromatography (HPLC) [Plummer 1987], mass spectroscopy, Raman spectroscopy [Westenskow 1989a, 1989b and Gregonis 1990], infrared absorption [Guyton 1990], and piezoelectric sorption detection [Cooper 1981, Westenskow 1991 and Schmautz 1992]. However these techniques are either too fragile or complex and expensive [Cooper 1981], and usually require special reagents and solutions with appropriate dilutions, which determine these methods are *in vitro* and need to be supported by a biomedical laboratory.

To date there is no rapid direct method for monitoring general anaesthetics (volatile and infusible) in blood or tissue [Cooper 1981 and MacDonald 1994]. The routine clinical measurement of anaesthetics has been a difficult target for researchers. Some approaches have been proposed [Lowe 1971, Cooper 1981 and Gregonis 1990]. Optical detection is a promising technique among these approaches. Particularly, in recent years, with the progress of the optical fibre and its related technology, fibre-optic sensors have exhibited great potential for concentration measurement of anaesthetics *in vivo* monitoring, with unmatched advantages in clinical applications such as very low toxicity, minimal tissue damage, fast response and high accuracy.

6.2.2 Optical principles for the fibre-optic anaesthetic sensors

Commonly used optical principles in the design of fibre-optic anaesthetic sensors are light bulk absorption (the Beer-Lambert law) [Junger 1996 and Wu 1996], fluorescence excitation [Merlo 1990 and Yager 1992] and Raman scattering [Parnell 1995 and Parnell 1996]. Each principle has its own features. Following is a brief evaluation of these principles in the context of anaesthetic concentration measurement in clinics.

a. light bulk absorption

Light bulk absorption is possibly the simplest principle suitable for use in measurement of the concentration of anaesthetics. Light intensity is attenuated by the accumulation of the absorbing species (anaesthetic molecules) in the light path. This attenuation is related to the concentration of the absorbing species via the Beer-Lambert law.

A suitable wavelength of light, which is strongly absorbed by the anaesthetic to be measured, has to be selected to achieve high sensitivity. The light can be ultraviolet, visible or infrared. The medium for absorbing the anaesthetic in the light path usually must be optically transparent to the selected light wavelength. The difficulty of this method is the interference by other compounds or species which can also cause strong absorption at the same wavelength. In order to overcome this difficulty and discriminate the anaesthetic to be measured from other compounds, sometimes multiple wavelengths may be needed.

b. fluorescence

Fluorescence is the radiative deexcitation of a molecule flowing absorption of a photon. In general, the emitted photon is of lower energy than the absorbed photon. Consequently, the fluorescence emission peak of a species is at a longer wavelength than the absorption peak. Its superiority over absorption are:

1. Fluorescence yields a signal that usually increases with the anaesthetic concentration and is measured against a zero background light level (ideally). In contrast, absorption is based on measurement of a signal that decreases with increasing concentration and is measured with respect to a high background. Intrinsically, therefore, the fluorescence approach will yield higher signal-to-noise ratios than absorption does.
2. In the case of fluorescence, one measures light that has been emitted by anaesthetic molecules. Consequently, it contains much useful information about these molecules. For example, one can measure fluorescence intensity, decay time and polarisation anisotropy and can also detect the phenomenon of energy transfer. Absorption, on the other hand, is based on the measurement of residual transmitted light, which contains little information about the absorption molecule.

However, the difficulty of fluorescence detection of anaesthetics is that some anaesthetics may not have strong enough fluorescent excitation to be measured.

c. Raman scattering

Raman scattering involves vibrational interaction with the electron transition causes a frequency shift of the incident light and can also alter the polarisation.

If absorption occurs at the same time as the scattering, part of the energy of the incident light induces vibrations and/or rotations in the molecules and hence produces a change in the energy states of the molecule. This is Raman scattering. When the molecule returns to its equilibrium ground state, energy can be emitted as radiation. The emission lines occur at lower energies or longer wavelengths than the unscattered radiation, called Stokes lines. Emissions can also occur at higher energies than the unscattered light, called anti-Stokes lines.

Raman scattering may be used to yield "fingerprint" vibrational spectra of anaesthetics. It can be used for both quantificational and compositional identifications.

Basic problems in Raman scattering aproach are:

1. The poor efficiency of the Raman scattering process, high power light sources, and sensitive detectors.
2. The high amount of interference from the unwanted fluorescence and Raman scattering generated within the transmitting optical fibre in fibre-optic systems.

6.3 About "Propofol"

Propofol (Diprivan) is a short-acting, rapidly metabolised popular intravenous agent for inducing anaesthesia. The investigation into its anaesthetic activity was started in the late of 1970's. Since then clinical trials and effects have been studied intensively.

Propofol is used as a general anaesthetic as well as an agent for sedation during regional anaesthesia or for ICU sedation. One key property of propofol is its ability to induce "sleep" rapidly and reversibly.

The research work on determination of propofol level or concentration has been done by many researchers, mainly these were focused on the conventional methods applied in clinics such as high-performance liquid chromatographic (HPLC), in which the plasma was used as the testing sample. Up till now there is no research reported in use of fibre-optic sensors to measure the concentration of propofol *in vivo* in clinics successfully.

In chemistry, propofol is an alkylphenol compound, its chemical definition is "2,6-di-isopropylphenol". Chemical expression is shown in Figure 6-1.

Propofol has a pKa of 11. And its molecular weight is 178. When placed in an environment pH of 11, the propofol is 50% dissociated.

Propofol is highly fat soluble and dissolves poorly in water.

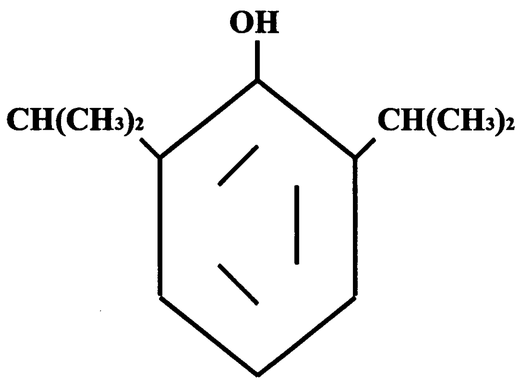

Figure 6-1 Chemical structure of "Propofol"

Propofol is light yellow liquid. In visible light range it has a weak absorption at the wavelength of 425nm, which was probably not strong enough to use in a sensor, shown in Figure 6-2a. It has a strong absorption to ultraviolet light around 270nm. Figure 6-2b shows the light absorption spectrum in ultraviolet light. These curves in the figures are measured by a ***SP8-100UV-VIS Spectrophotometer***, with a light absorption path of 10mm, and the absorption is calculated by $\log(I_{in} / I_{out})$, where I_{in} and I_{out} represent the input and output light powers, respectively. The propofol was dissolved in mineral oil obtained from Sigma Chemical Co. (Product No: M3516)

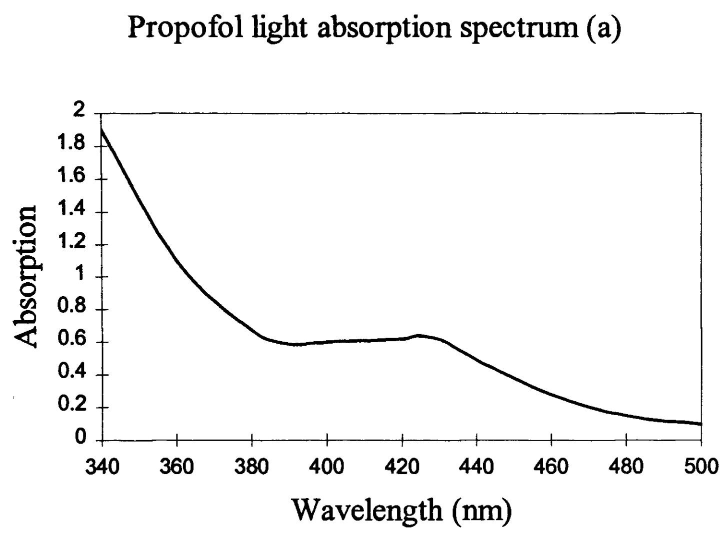

Figure 6-2a The light absorption spectrum of propofol in visible light

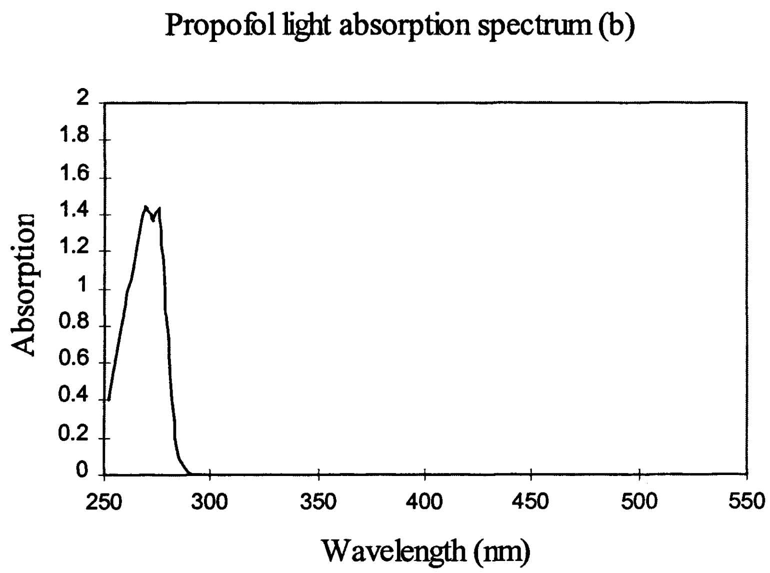

Figure 6-2b The light absorption spectrum of propofol in ultraviolet light, with 0.01% propofol concentration by volume

6.4 Conceptual design of a "propofol" fibre-optic sensor

6.4.1 Design criteria

The "Propofol" fibre-optic sensor is to be designed for real-time monitoring of the propofol concentration in blood during operations, to aid the control of optimal delivery of propofol. The following basic requirements are proposed in the design:

1. The minimum amount of propofol to be discriminated in clincs is 4 ~ 8 *μg/ml.*
2. The response time of the measurement is ≤ 30 seconds.
3. The outside diameter of the probe of the sensor is ≤ 3mm.
4. Real-time monitoring
5. All materials in the probe should be non-toxic.

6.4.2 Determinations of propofol fibre-optic sensor in optics

1. Light absorption principle (the Beer-Lambert law)

By comparing different measurement principles in optics, the light absorption principle based on the Beer-Lambert law was chosen to design the sensor. The reasons behind this decision are:

- Simple in principle leading to a simple system: the optical system is simple, so not many optical components are required.
- Low in cost: there are no especially expensive optical components needed, such as gratings, or high quality laser as in Raman spectroscopy.
- Short development period: due to the simplicity of the system, the developing time is short for a prototype sensor.
- Easy in manufacture: there are no complicated optics to be adjusted in the sensor, it is easy to be manufactured in industry.

2. Ultraviolet light as the measurement light

By examining the light absorption spectrum of propofol, it can be seen that there is an absorption peak at 270nm wavelength which is the strongest absorption. Using the data and information in Figure 6-2, the light absorption at 270nm wavelength for a 0.01% concentration propofol solution is about 96.2% with a 10mm light path length. Ultraviolet light at 270nm wavelength is chosen as the measurement wavelength to achieve the highest absorption sensitivity.

3. Fibre-optic system

Considering the physical constraint of the sensor in clinics, the fibre-optic system is the best choice. Using the ultraviolet transmission optical fibre, the attenuation of the light transmitted in the optical fibre at 270nm wavelength is acceptable for the measurement.

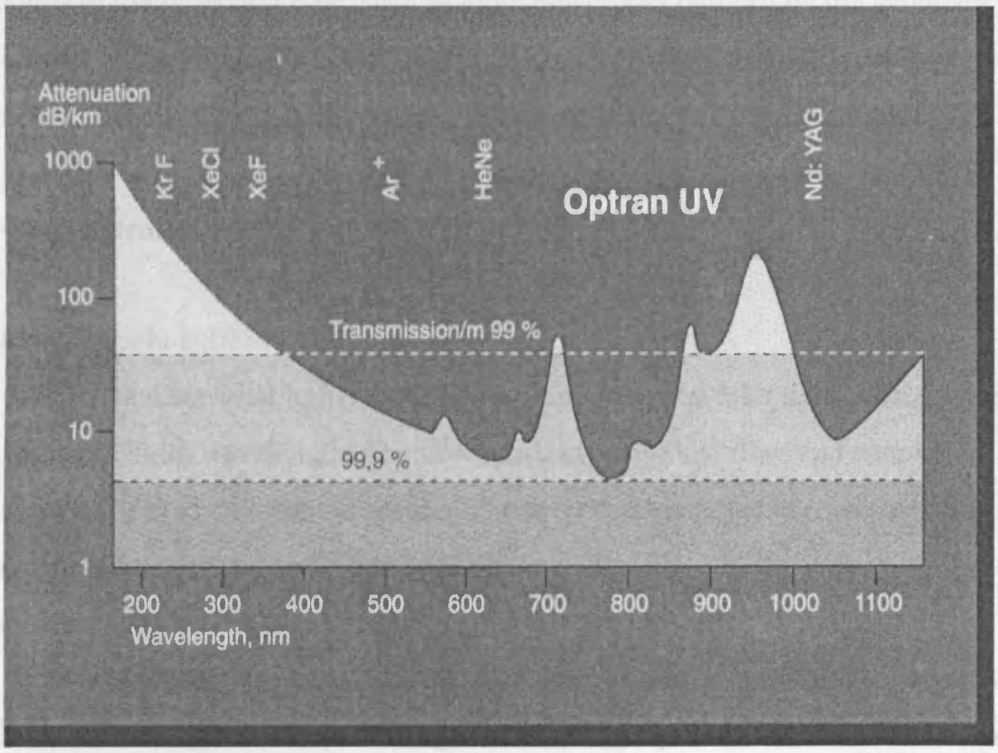

Figure 6-3 The transmission spectrum of CeramOptec's ultraviolet optical fibre

Figure 6-3 shows the light power transmission spectrum of ultraviolet optical fibre made by CeramOptec (Bonn, Germany). The attenuation at 270nm wavelength is about 200dB/km, therefore the attenuation at a few meters of optical fibre is small (for 10m length, the power loss is about 18%).

In addition, besides small size, there are some extra advantages from the use of a optical fibre. The components introduced into the body are:

- Disposable
- Non-toxic

4. Reflection type fibre-optic sensor

There are two types of the Beer-Lambert law based light absorption fibre-optic sensors, transmission type and reflection type. Considering the physical constrain, the reflection type is the only solution for propofol fibre-optic sensor, although, there are weak points of the reflection type, such as more power loss induced by the geometrical configuration of the probe, the complication of the probe structure and the difficulty of adjustment.

6.4.3 Considerations of the system

1. Ultraviolet light system

This is an ultraviolet light fibre-optic system. An ultraviolet light source is used to obtain light at 270nm wavelength. The UV-transmitting optical fibre and coupler are used to transmit the light to and from the probe. The detection system also consists of an UV-sensitive photodetector and low-noise preamplifer.

2. Stability

A two-wavelength system is constructed, one wavelength at 270nm is used as the measurement channel, the other wavelength at 310nm is chosen as the reference channel. Because propofol does not absorb light at 310nm wavelength, the reference channel can be used to stabilise the system, to compensate the influence from sources other than propofol concentration. As an example, one design of the two-wavelength technique is achieved by using two narrowband filters centred at 270nm and 310nm, respectively, located on a rotating filter wheel.

3. Probe geometrical arrangement

The substantial advantage of fibre-optic sensors over conventional optical sensors is the ease of miniaturisation of the probe. The possibilities for size reduction depend on the probe geometry. The Beer-Lambert law based fibre-optic sensors may be simply classified into two categories, according to the probe geometry: the two-fibre type shown in Figure 6-4a and the single-fibre Y-coupler type shown in Figure 6-4b.

• Two-fibre type

In this case, each separate fibre acts merely as a lightguide, one carrying the light from the light source to the probe tip, the other bringing the light back to a detector from the tip containing the chemical species to be measured.

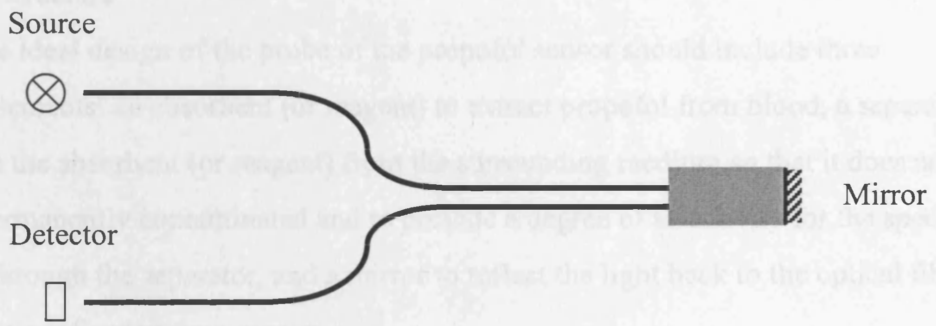

Figure 6-4a Two-fibre type probe

• Single-fibre Y-coupler type

This type uses a single fibre between the measurement probe and the instrumentation unit, with a directional Y-coupler to isolate the incident light from the detector unit. The light power is transmitted to the probe tip by one branch of the Y-coupler, and received by the other.

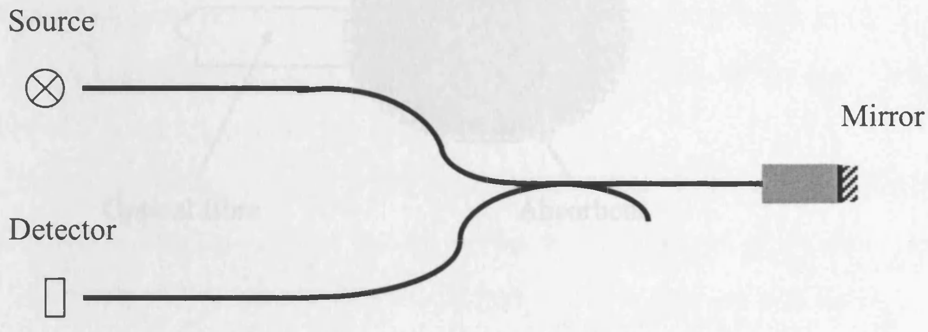

Figure 6-4b Single-fibre Y-coupler type

4. Probe structure

The ideal design of the probe of the propofol sensor should include three essential elements: an absorbent (or reagent) to extract propofol from blood, a separator to separate the absorbent (or reagent) from the surrounding medium so that it does not become permanently contaminated and to provide a degree of selectivity for the species diffusing through the separator, and a mirror to reflect the light back to the optical fibres to construct a reflection type sensor.

There are three types of probe structures which can achieve these elements: membrane structure shown in Figure 6-5a, fibre structure shown in Figure 6-5b and waveguide structure shown in Figure 6-5c.

• Membrane structure

This structure uses an ion-permeable membrane on the end of the optical fibre(s) to enclose and protect the absorbent (or reagent) which could be liquid, gel or solid state. A mirror should be located inside the membrane.

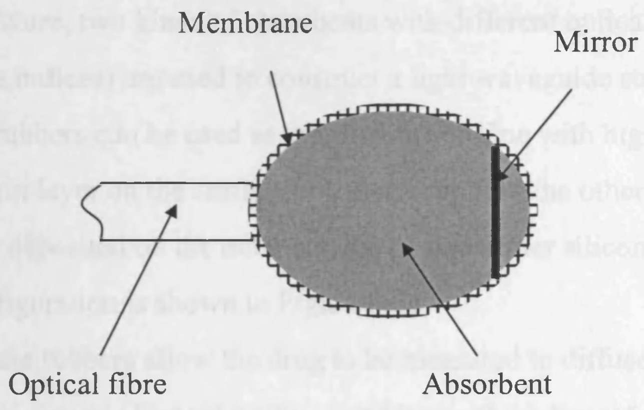

Figure 6-5a Membrane structure

• Fibre structure

Fibre structure uses the commercial product: porous wall hollow fibres. The optical fibre(s) is inserted into one end of the hollow fibre, the other is mounted with a mirror, and the absorbent is enclosed inside of the hollow fibre.

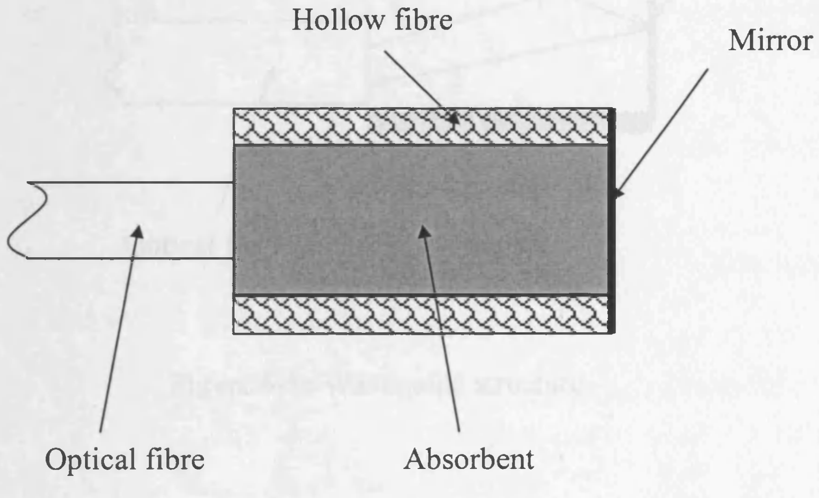

Figure 6-5b Fibre structure

• Waveguide structure

In this structure, two kinds of absorbents with different optical properties (such as different refractive indices) are used to construct a light waveguide structure. Two different silicone rubbers can be used as the absorbents. One with higher refractive index is modelled in a thin layer on the surface of a metal support, the other with lower refractive index is deposited on the outer surface of the former silicone rubber. The cross-section of the configuration is shown in Figure 6-5c.

Both silicone rubbers allow the drug to be measured to diffuse through. The measurement light is coupled into the silicone rubber with higher refractive index, and trapped by this waveguide structure. The advantages of this design are less light transmission loss and interference from the outside environment. A mirror is needed for the reflection-type sensor.

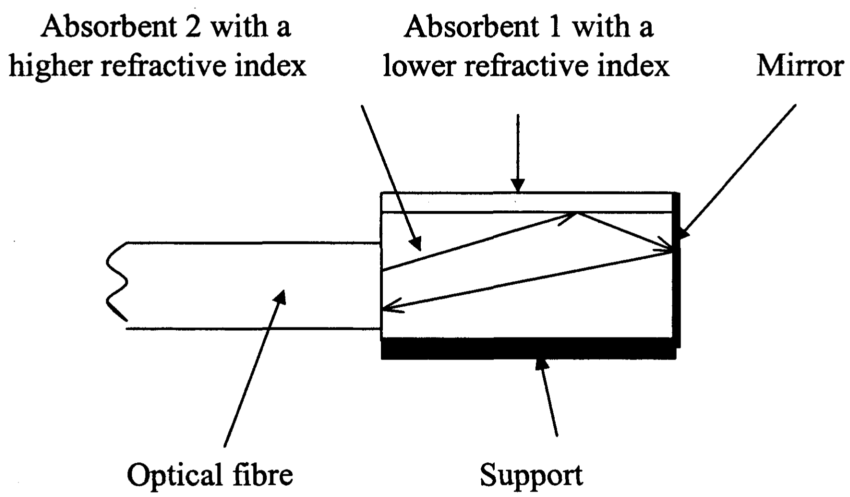

Figure 6-5c Waveguide structure

6.5 Absorbent material investigation

Potential materials which can dissolve propofol are fat, paraffin type of oils, alcohol and silicone rubbers. The basic requirements for the absorbent of the propofol fibre-optic sensor are that it should be:

1. Non-toxic
2. Propofol soluble
3. Transparent to UV-light at 270nm
4. Immobilised

Table 6-1 shows the summary of these four materials in these requirements. ✓ represents that the material satisfies the requirement, ✗ represents that the material does not satisfy the requirement.

Table 6-1

	NON-TOXIC	SOLUBLE	TRANSPARENT	IMMOBILISED
FAT	✓	✓	✗	✓
PARAFFIN	✗	✓	✗	✗
ALCOHOL	✓	✓	✓	✗
SILICONE	✓	✓	✓	✓

Based on the evaluation of these four basic requirements, silicone rubber is the best substance available at present to be the absorbent.

DOW CORNING (Midland, MI, USA) product, **Sylgard 527 – silicone dielectric gel**, has been tested as the absorbent.

Sylgard 527 is a two-part, low viscosity liquid encapsulant, which has been used as the absorbent to develop the fibre-optic sensor for general anaesthetics based on Raman spectroscopy before [Macdonald 1994].

During the test, Sylgard 527 base (part A) was mixed with the curing agent (part B) at different, relatively low, ratios. The low ratio of mixture was employed to keep the degree of crosslinking low enough to allow substantial absorption of propofol.

Figure 6-6a and Figure 6-6b show the light absorption spectra of Sylgard 527, the measurements were taken using a ***SP8-100UV-VIS Spectrophotometer***, with a light absorption path length of 10mm.

The definition of the absorption is $\log(I_{in} / I_{out})$, where I_{in} and I_{out} represent input and output light powers, respectively.

In Figure 6-6a, the Sylgard 527 sample was made by mixing two parts (part A and part B) of Sylgard 527 in a ratio of 1:1 in weight at room temperature, then curing the mixture at 65°C for four hours. The sample is in the state of a gel.

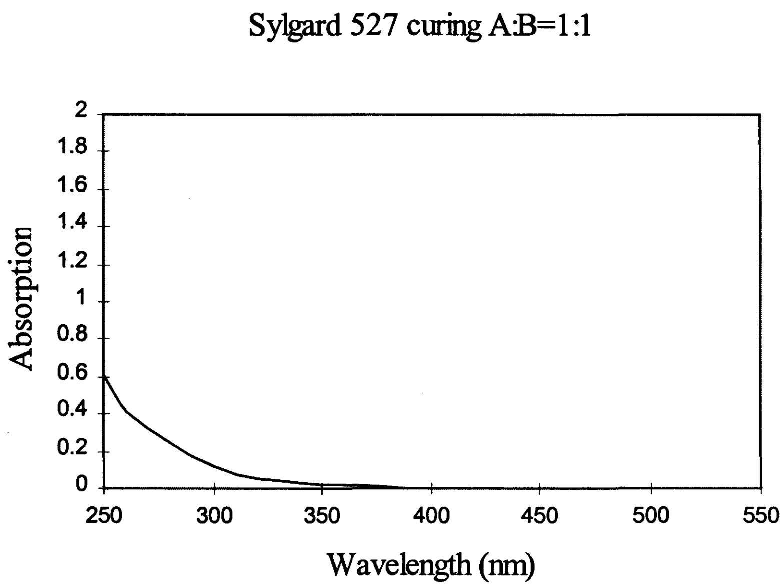

Figure 6-6a Sylgard 527 light absorption spectrum

In Figure 6-6b, a Sylgard 527 sample was made by mixing two parts (part A and part B) of Sylgard 527 at ratio of 1:3 in weight at room temperature, then curing the mixture at 65°C for four hours. The sample is in the "rubber" state.

From the absorption curves, about 30%~50% input light is absorbed by the Sylgard 527.

Figure 6-7 shows the qualitative absorption tests of Sylgard 527 to propofol, in which two Sylgard 527 samples (the ratio of part A and part B is 1:2) were made by the same procedures as in Figure 6-6. One sample was dipped into 0.01% propofol solution for 2 minutes, the other was dipped into 0.1% propofol solution for 2 minutes. Both were taken out and washed with water to remove remaining solution from the surfaces. Using a ***SP8-100UV-VIS Spectrophotometer*** to measure the light absorption spectra, the lower curve at 275nm in Figure 6-7 was obtained from the sample dipped into 0.01% solution, the upper curve was obtained from the sample dipped into 0.1% solution.

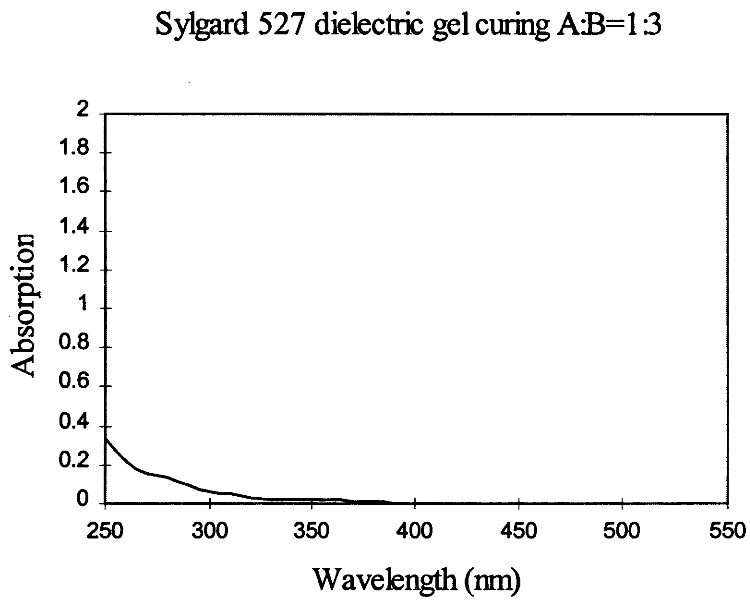

Figure 6-6b Sylgard 527 light absorption spectrum

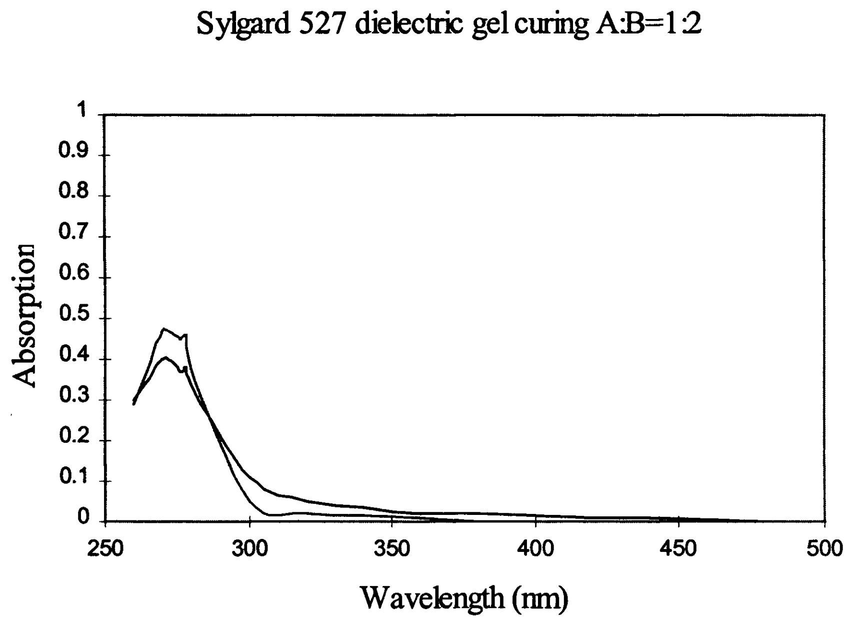

Figure 6-7 Sylgard 527 light absorption spectrum after dipping into propofol solutions for 2 minutes

Two basic results are obtained from the tests:

1. Sylgard 527 – silicone dielectric gel absorbs the ultraviolet light, however its absorption is much weaker than that of propofol.
2. Sylgard 527 – silicone dielectric gel can be used as the absorbent to absorb propofol.

Although, these tests are more or less qualitative, the results have shown that Sylgard 527 – silicone dielectric gel is highly promising as the absorbent. It is worth constructing a prototype sensor using it.

6.6 Considerations of the system design

6.6.1 Mechanical design (Probe design)

The probe together with the optical fibre pigtail is changeable. The configuration of the design is shown in Figure 6-8:

Figure 6-8 Probe configuration of propofol fibre-optic sensor:
(a) two-fibre type, (b) single-fibre Y coupler type

The optical fibre pigtail is used to connect the probe to the main body of the sensor using commercial optical fibre connectors. The 3-D maximum dimension of the probe is shown in Figure 6-9 (not to scale).

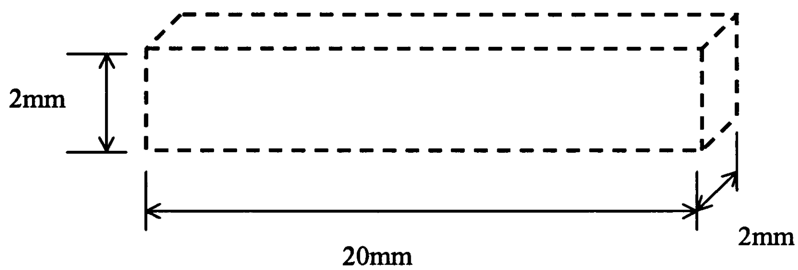

Figure 6-9 3-D maximum dimension of the probe

Under the constraint of maximum dimensions, there are two designs, one uses a porous wall hollow fibre to contain the absorbent, silicone rubber, the other uses an U-shape metal channel to contain the absorbent. In both designs, a metal mirror has to be mounted on the one end of the container (of the absorbent) to reflect the light back to the receiving optical fibre.

The advantages of the design of the changeable probe include:

- Economic: to reduce the cost of the sensor, expensive devices such as optical components, light source, detector, electronics and processing unit are permanently used, only the probe needs to be changed at every measurement.
- Safety: to prevent the contamination of the sensor, during the measurement, the probe is the only component which contacts with the blood, other components are not contaminated.
- Initialisation: after the measurement, some remaining propofol will be left in the absorbent even after it is removed from the blood. This may give a false reading initially when the probe is reused.

6.6.2 Optics

The sensor is designed as an ultraviolet light system, with a pulsed ultraviolet light source (Xe strobe), an ultraviolet sensitive photodetector, an interference bandpass filter and ultraviolet optical fibres. All light paths are in optical fibres connected to each other by optical fibre connectors. The benefits from such design are:

- Easy adjustment: after the connection of all parts, there is no optical component needing to be adjusted during the measurement.
- Safe in use: ultraviolet light is trapped inside optical fibres, and enclosed inside devices. There is less ultraviolet radiation to harm operators.
- Less in power loss: avoiding ultraviolet light travelling in air or other media which will increase the attenuation of light power.
- Minimising in the sensor system: making the sensor compacted in volume, and light in weight, flexible in application.
- Immune to the disturbance from free air environments.

6.6.3 Electronic circuits design

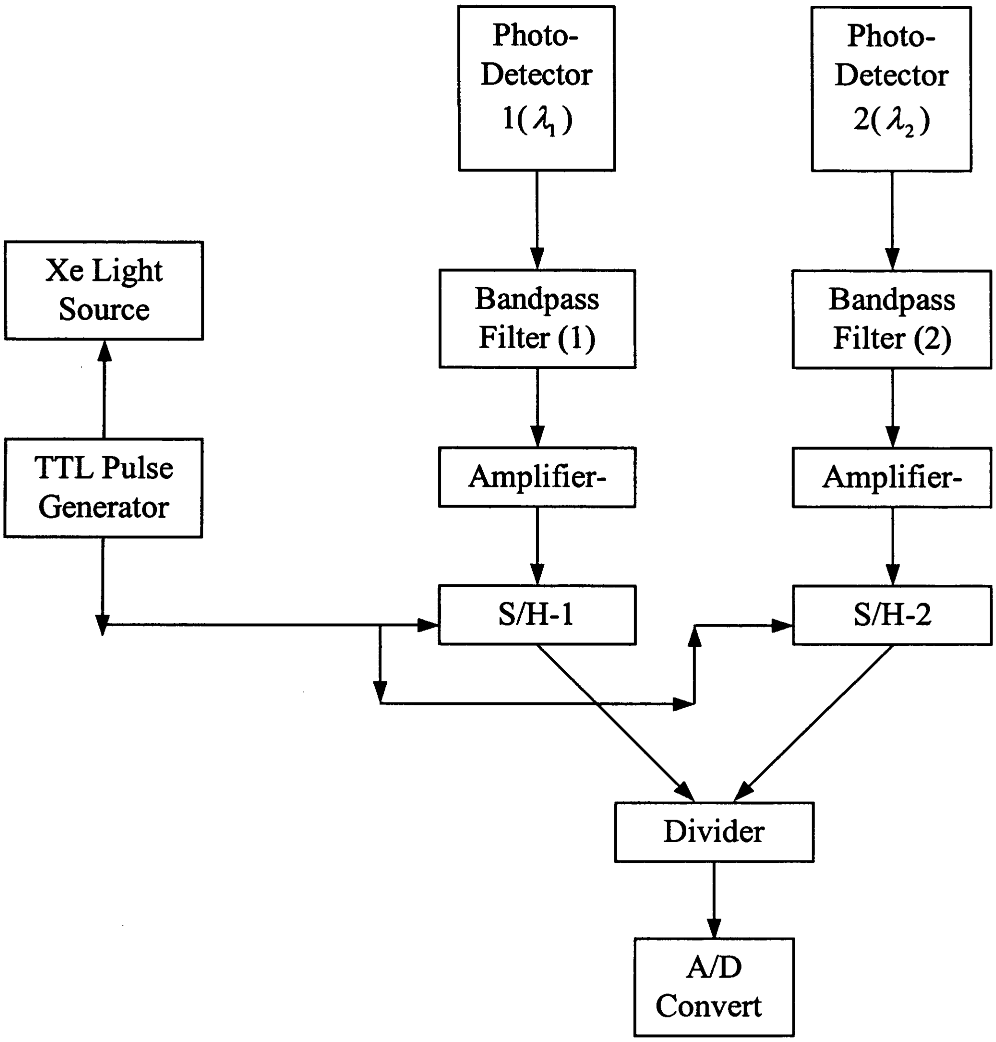

Figure 6-10 The principle of circuits in propofol sensor

In order to realise the concentration measurement of propofol, electronic circuits are designed.

The principle of these circuits are:

A pulse generator is used to generate a TTL pulse train to control the Xe light source working in pulsed mode. Meanwhile, this pulse train is used to synchronise the state of Sample and Hold (S/H) circuits, which is a common technique to pick up the signal from the background. Amplifier stage is constructed to amplify the signal from "Current to Voltage" after the photodetector. Two similar sets of circuits are used to obtain outputs at wavelengths λ_1 and λ_2, respectively, so as to build a two-wavelength system to improve the performance of the sensor. An analogue divider is used to divide the signals from these two wavelengths. The block diagram of these circuits is shown in Figure 6-10.

Figure 6-11 shows the schematic drawing of the circuit. These circuits are analysed as following:

1. Pulse generator.

The 555 timer is used to construct a pulse generator. Diode D1 is used so as to get a small duty cycle (less than 50%).

The pulse frequency is decided by Equation (6.1).

$$f = \frac{1.44}{(R10 + 2R11) \cdot C4} \tag{6.1}$$

The duty cycle is given by Equation (6.2)

$$\text{Duty cycle} = \frac{t_H}{T} = \frac{R10}{R10 + R11} \tag{6.2}$$

2. Bandpass filter.

A multiple-feedback bandpass filter is constructed. R5 and C1 provide the low pass response, R2 and C2 provide the high pass response.

Making C1 = C2 = C, the central frequency is expressed as:

$$f_0 = \frac{1}{2\pi C}\sqrt{\frac{R5 + R8}{R2 \cdot R5 \cdot R8}} \tag{6.3}$$

Q-factor can be expressed as:

$$Q = \pi f_0 CR2 \qquad (6.4)$$

3. Amplifier

A simple amplifier stage is used to increase the signal, its amplification is expressed as:

$$Gain = -\frac{R3}{R7} \qquad (6.5)$$

4. Sample-and-Hold (S/H)

A field effect transistor (FET) and a capacitor are used to construct a simple Sample-and-Hold (S/H). During the pulse, the signal passes the FET Q1 to charge the capacitor C3, then held until next pulse.

5. Divider

The linear multiplier MC1595 is used to construct a divider to divide the two amplified signals from the two detectors.

The circuits design in this section is preliminary, and is mainly used to examine the feasibility of whole system. It has been proved by the experiments using these circuits that the system design and the selections of optical components are appropriate. In the final design alternative circuits might be used to improve the performance of the sensor, for example, the A/D converter can be used to convert the analog signals into digital signals, and further micro-processor can be used to process these digital signals and execute calculations, such as division.

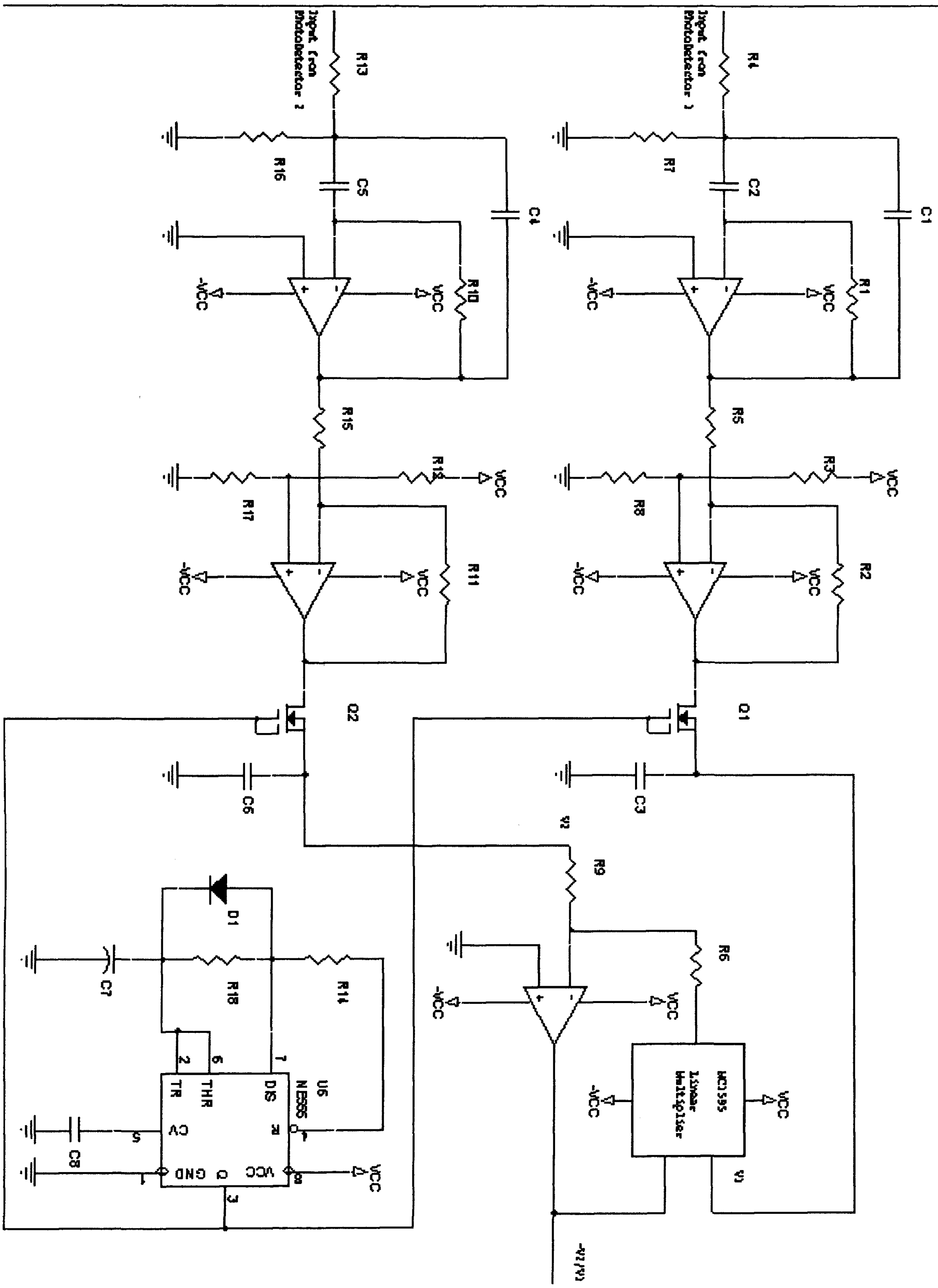

Figure 6-11 Schematic drawing of circuit

6.6.4 Overall system arrangement

The overall system of the propofol fibre-optic sensor is shown in Figure 6-12.

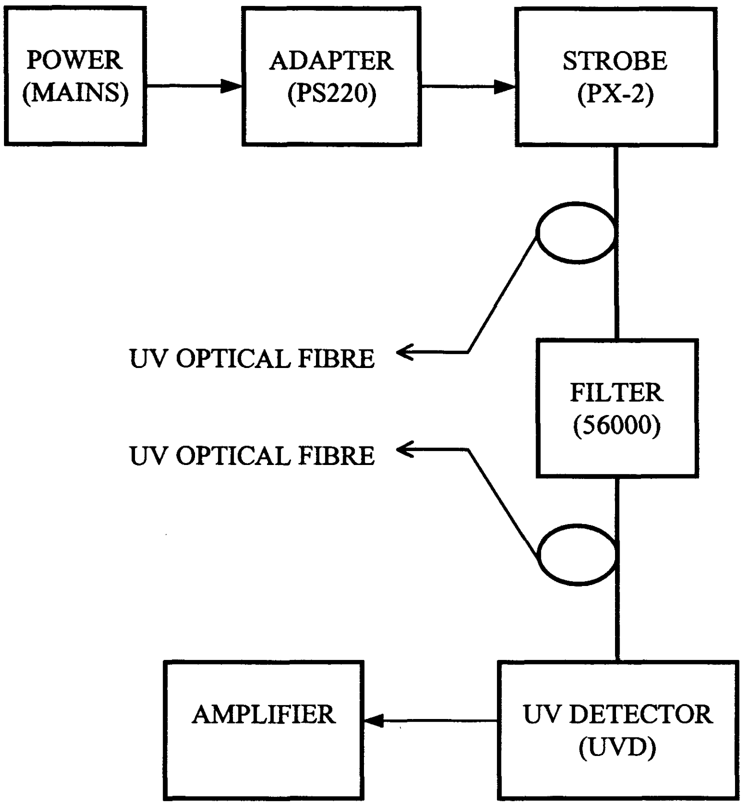

Figure 6-12 System arrangement of propofol sensor

This is an all optical fibre ultraviolet system. Some components are available in commercial markets.

6.6.5 Key components choice and specification

1. Xe light source

Figure 6-13 shows the picture of the PX-2 Xe ultraviolet light source, the product of Ocean Inc. (Dunedin, FL, USA).

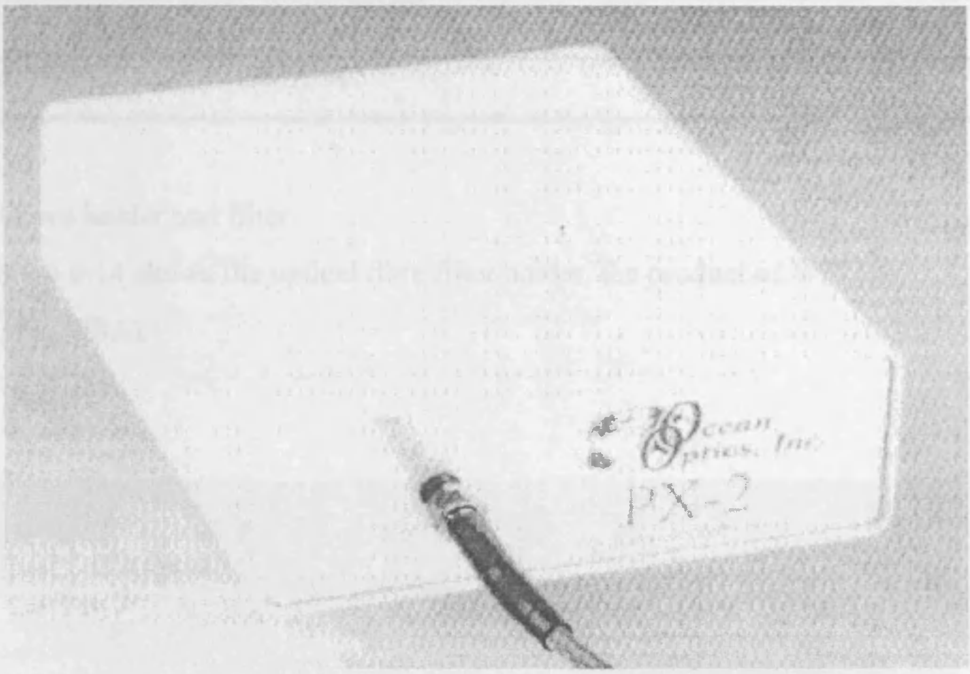

Figure 6-13 PX-2 Xe light source

The main specifications:

SPECTRAL RANGE:	220 – 750NM
Approximate dimensions:	14cm × 10.5cm × 4 cm (LWH)
Power input:	1.3A@11V@220Hz, 100mA@12V@10Hz
Trigger input:	External TTL positive pulse via 15-pin connector
Output:	45millijoules per pulse maximum 9.9 watts average power 220 Hz pulse rate maximum
Pulse duration:	5 microsecconds (at 1/3 height of pulse)

Lifetime:	10^9 pulses (estimated 230 days continuous operation at 50Hz pulse rate)
Aperture:	3 mm
Connector:	SMA 905

2. Optical fibre holder and filter

Figure 6-14 shows the optical fibre filter holder, the product of WPI Inc. (Sarasota, FL, USA).

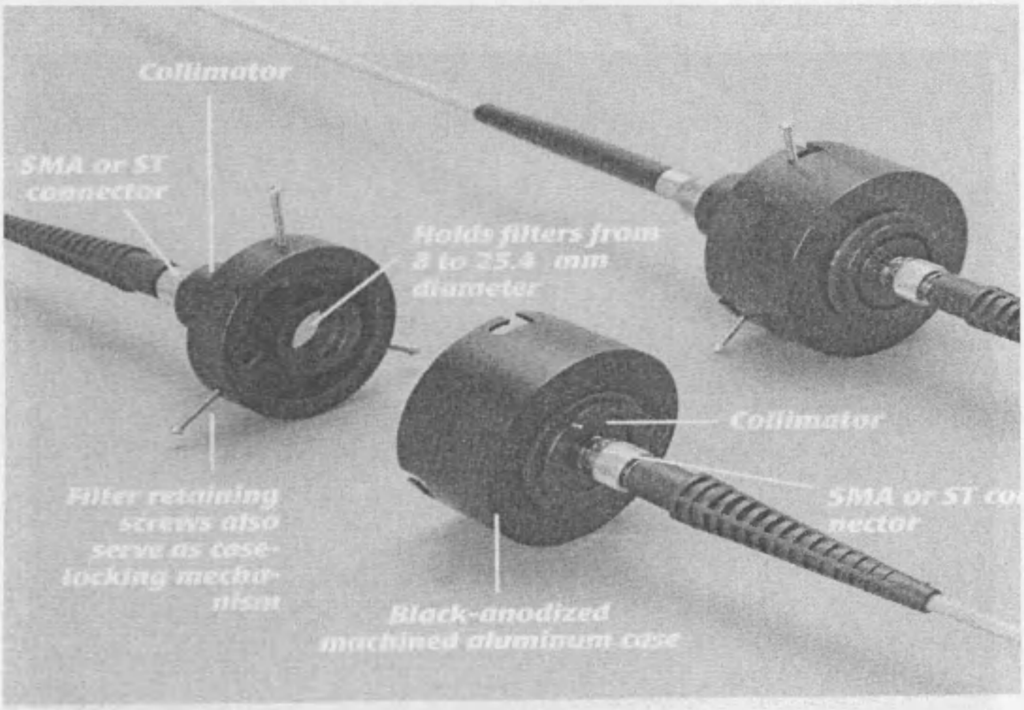

Figure 6-14 The optical fibre filter holder

A bandpass interference filter, the product of Corion (Franklin, MA, USA) is mounted inside the holder. The specification of this filter are:

Centre wavelength (nm)	270±2 nm
Bandwidth FWHM (nm)	12±2 nm
Minimum peak transmittance	12%

3. Ultraviolet light photodetector

Figure 6-15 shows the ultraviolet light photodetector, the product of WPI Inc. (Sarasota, FL, USA). Figure 6-16 shows the spectral response graph.

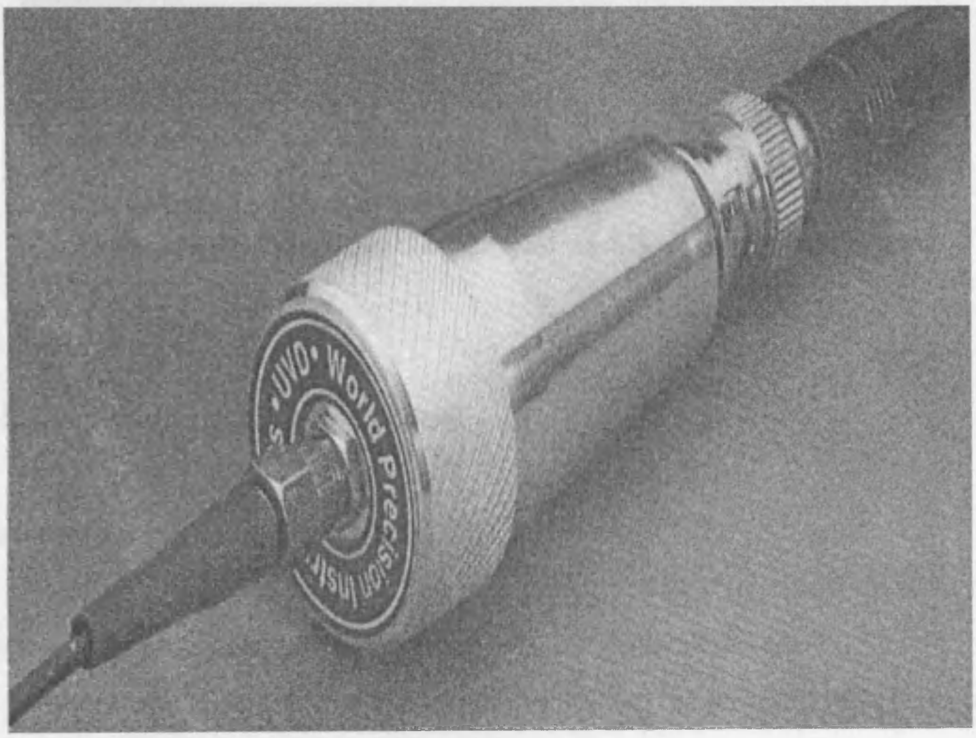

Figure 6-15 UV-light photodetector

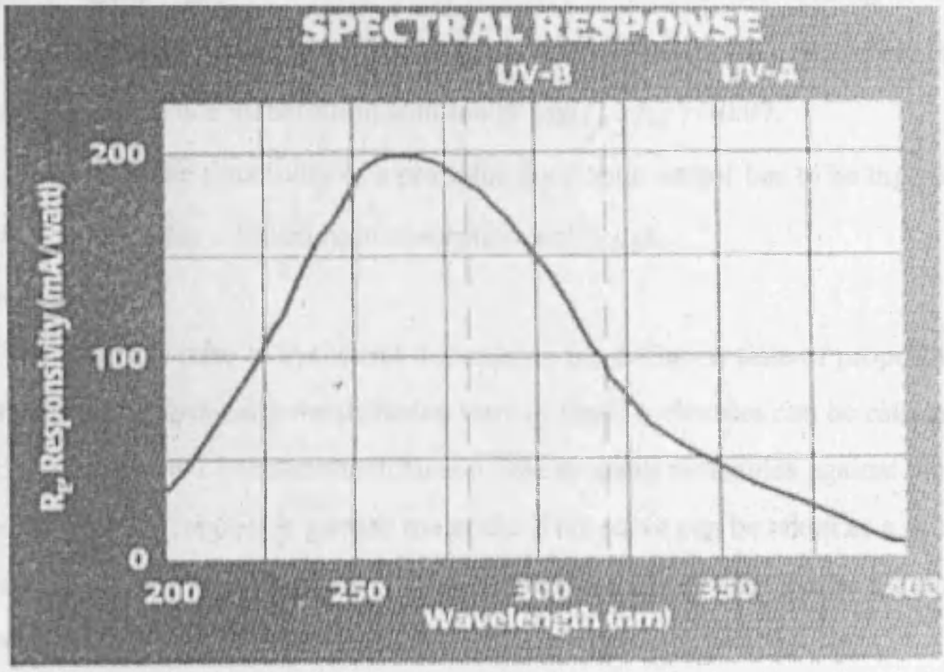

Figure 6-16 The spectral response of the UV light photodetector

6.6.6 Sensitivity and response time

1. Sensitivity

Sensitivity is one of the most important characteristics of a sensor. Based on the basic tests of propofol, the sensitivity of this design is estimated.

The clinical requirement of the minimum delivery of propofol during operations is $4 \sim 8\ \mu g/ml$.

Because the molecular weight of propofol is 178, 1 Mol propofol = 178 $\mu g/ml$.

Thus, 8 $\mu g/ml \approx 45\ \mu$ Mol ≈ 0.0008% concentration of solution.

From Figure 6-2, the light absorption of propofol at wavelength 270nm ultraviolet light equals $\log(I_{in} / I_{out}) = 1.4$ for 0.01% concentration solution. According to the Beer-Lambert law, the light absorption is proportional to the concentration, therefore the light absorption of 0.0005% concentration solution is $\log(I_{in} / I_{out}) = 0.07$.

As a result, the sensitivity of a propofol fibre-optic sensor has to be higher than $\log(I_{in} / I_{out}) = 0.07$ for a 10mm light absorption path length.

2. Response time

The response time of the sensor depends on the diffusion time of propofol into silicone rubber. Theoretically the diffusion time of small molecules can be estimated [Bray 1992]. Figure 6-17 shows the diffusion time of small molecules against the thickness of water. Propofol is a small molecule. This curve can be taken as a reference to estimate the diffusion time. But silicone rubber is denser than water, hence the diffusion in silicone rubber is slower than in water.

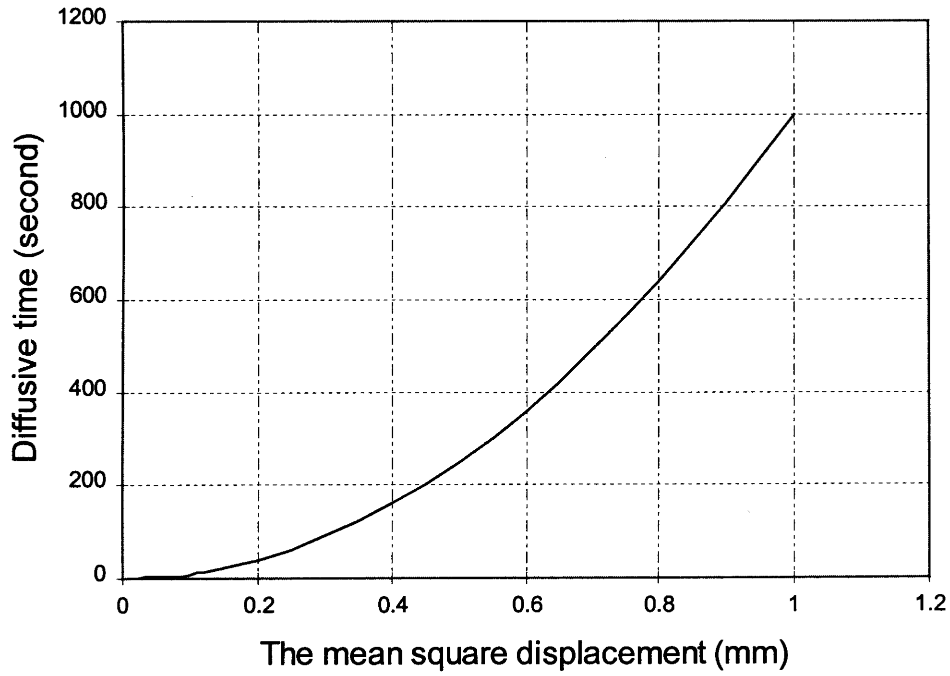

Figure 6-17 Small molecule diffusion time in water

From the curve, when the water thickness is 0.5mm, the diffusion time is about 4 minutes, when the water thickness is 1.0mm, the diffusion time is about 16.7 minutes.

In order to obtain a fast response for the propofol fibre-optic sensor, the absorbent – silicone rubber has to be as thin as possible, however, it is difficult to produce a very thin absorbent for this type of probe.

From the design point of view, a potential scheme to reduce the response time is to consider the absorption behaviour of the absorbent. Because propofol continuously diffuses into silicone rubber, the propofol concentration in the silicone rubber rises gradually, therefore light absorption induced by propofol increases gradually to maximum point. Following is a brief explanation.

The movement of a substance from an area of higher concentration to lower concentration is expressed as the Fick's second law [Kotyk 1988]:

$$\frac{\partial c_i}{\partial t} = D\frac{\partial^2 c_i}{\partial^2 t} \tag{6.6}$$

where D is the diffusion coefficient, c_i is the concentration of the substance at time t, at x distance from the interface between two different concentration areas.

Under the initial condition: $t = 0,\ x > 0:\ c_i = 0$

and the boundary conditions: $t > 0,\ x = 0:\ c_i = c_0,\ t > 0,\ x \to \infty:\ c_i = 0$

The solution of Equation (6.6) is :

$$c_i = c_0[1 - erf(\frac{x}{2\sqrt{Dt}})] \tag{6.7}$$

where erf is the error function.

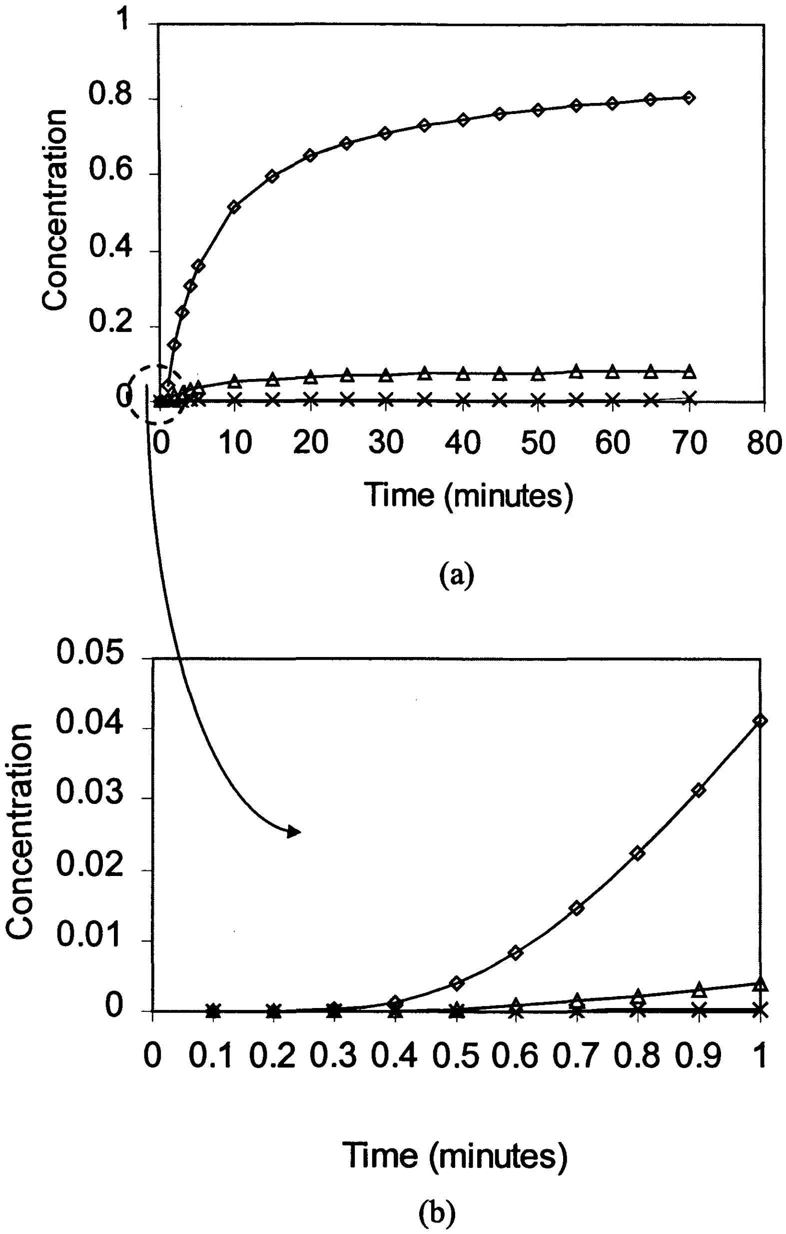

Figure 6-18 The theoretical estimation of the concentration change in the probe against time, ◊ with $c_0 = 1.0\mu g/ml$, Δ with $c_0 = 0.1\mu g/ml$ and × with $c_0 = 0.01\mu g/ml$ concentration.
(a) representing long term change, (b) representing short time period change

Equation (6.7) can be used to approximate the propofol absorption in the probe, where c_0 is the propofol concentration in blood and c_i is the concentration in the absorbent of the probe. The change of the concentration in the probe leads to the change of the light absorption. Figure 6-18 shows the curves of the concentration change against the diffusion time in different solutions, assuming $x = 0.05cm$, $D = 5 \times 10^{-6} cm^2 / \sec$ (for small molecules) and the assumed length of the absorption path is 1 *cm*.

The output light absorption is proportional to the concentration. By monitoring the change of the output light, it is possible to find within a short time period which curve the absorption follows by using signal processing techniques and so the concentration can be determined quickly.

Figure 6-19 shows a qualitative measurement of the behaviour of light absorption of the silicone rubber changing vs time when placed in different concentrations of solutions. The propofol solution represented by ◊ has higher concentration compared with the solution represented by Δ, the solution represented by × has no propofol diffused.

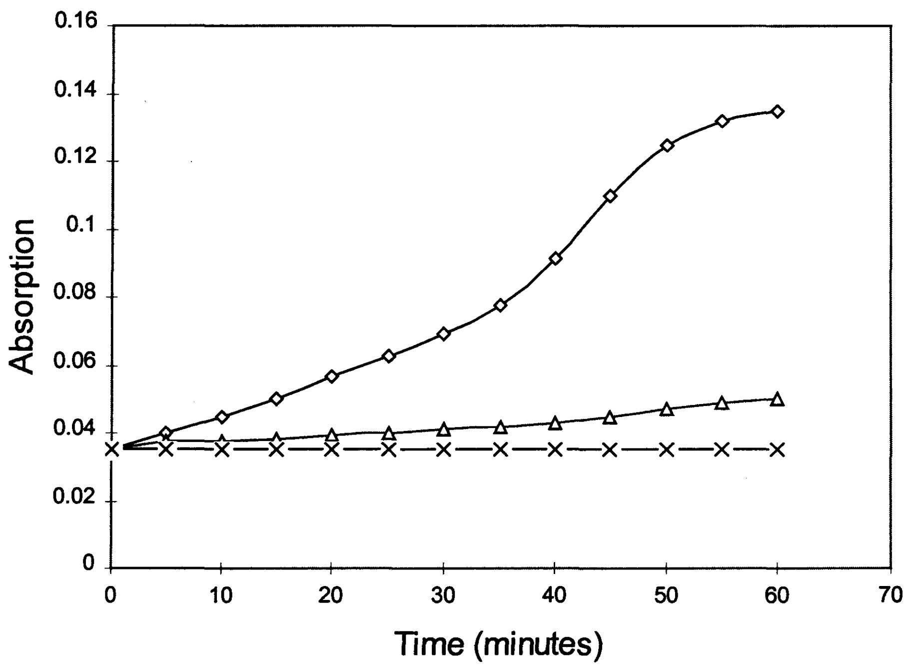

Figure 6-19 Silicone rubber absorption of propofol against time

The experimentally derived curves in Figure 6-19 are reasonably consistent with the theoretical estimates in Figure 6-18. In this way, the method of improving the response time of the sensor is possible.

It is noted however that when practical implementation is considered, the accuracy of the early data needs to be such that the track of the curves can be properly estimated.

6.7 Conclusions and further work

To date, there is no rapid, direct method for monitoring the concentration of general anaesthetics in blood. The potential application and market value of a "propofol fibre-optic sensor" is high. The design studies in this chapter show that:

- A new design for a propofol fibre-optic sensor is possible,
- It is possible to develop a propofol fibre-optic sensor for potential use *in vivo,*
- The proposed sensor is simple in principle, and of low cost.

However, further work has to be done in following aspects:

- Investigations of alternative silicone materials,
- Quantitative measurement of response time and sensitivity,
- Circuit design optimisation,
- Prototype sensor production and tests of repeatability, stability etc.

Chapter 7

Surface Plasmon Resonance Fibre-Optic Chemical Sensors

7.1 Introduction

Chapter 6 considered the extrinsic approach to sensor design. The intrinsic approach is the other division of fibre-optic sensing techniques, in which the optical fibre works as the probe and the light signal interacts with the optical fibre in response to the measurand. This chapter details the design of surface plasmon resonance (SPR) fibre-optic chemical sensors as an example of design studies of intrinsic light intensity attenuation-based fibre-optic chemical sensors. Using the principle of optical surface plasmon excitation and the characteristics discussed in Chapter 3 and Chapter 4, novel types of high performance SPR fibre-optic chemical sensors are proposed. Patents are under consideration for the schemes proposed. The aim of this chapter is to explore further the abilities and potential of surface plasmon excitation in fibre-optic chemical sensing techniques.

7.2 Surface plasmon resonance fibre-optic sensors in concentration measurements

Optical surface plasmon excitation has been acclaimed as a very good technique to design fibre-optic sensors for concentration measurement of chemical substances in chemical and biochemical applications. Surface plasmon resonance (SPR) fibre-optic chemical sensors work in two implementations. One implementation can be referred to as bulk chemical sensing in which the refractive index of a chemical sample is measured.

The refractive index changes in accordance with the change of the concentration of the chemical substance [Jorgenson 1994 and Kunz 1996]. The other implementation uses a so-called "chemical transducing layer" at the interface of the sensor/chemical sample (between the surface plasmon supporting metal layer and the chemical sample) to achieve the concentration measurement. The concentration is determined by measuring the refractive index change or physical thickness change of the chemical transducing layer, which is induced by the diffusion of the chemical substance, and is in accordance with the change of the concentration [Garces 1992 and Slavik 1998].

Based on these two implementations, SPR fibre-optic chemical sensors have been developed for concentration determination of chemical substances in a chemical sample to be measured. Figure 7-1 shows a typical configuration of a SPR fibre-optic sensor. The light source can be a multi-wavelength lamp (Tungsten light source) or a laser, the detector can be either a spectrometer (spectrograph, CCD linear array detector) to receive the light power spectrum from the multi-wavelength light source, or a photomultiplier to receive the light power from laser light source.

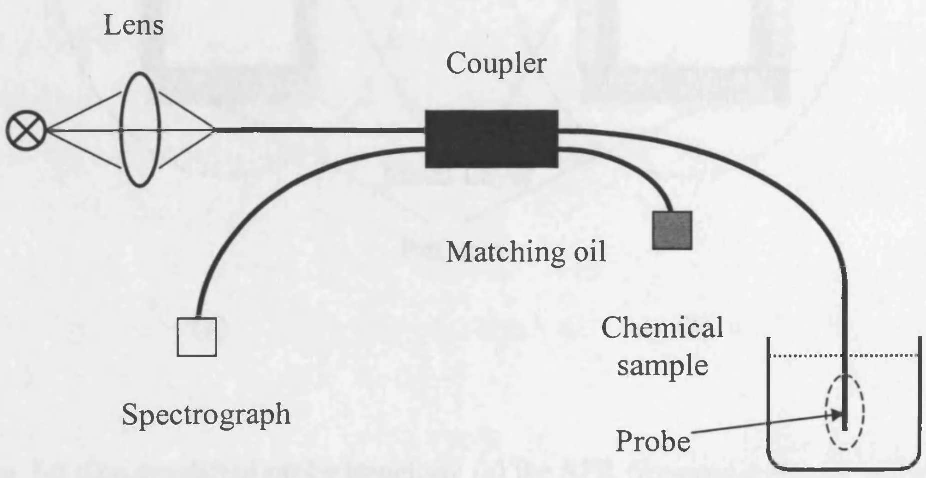

Figure 7-1 Typical system of SPR fibre-optic chemical sensors

Figure 7-2 shows the detailed structure of the probe. The SPR supporting metal is gold or silver at a thickness of a few tens of nanometers. If the thickness is too large, there will be no SPR excitation. On the end surface of the optical fibre, a metal mirror is deposited to reflect the light back to receiver, which can be aluminium or silver at an appropriate thickness (a few hundreds of nanometers).

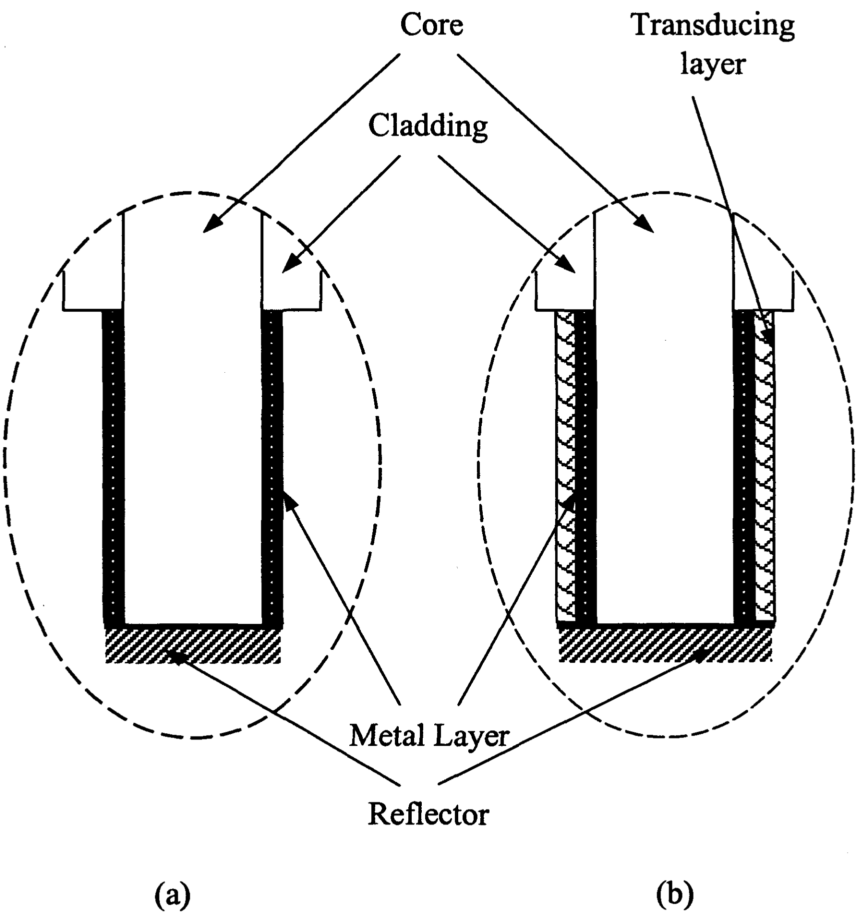

Figure 7-2 The amplified probe structure: (a) the SPR fibre-optic sensor without a transducing layer, (b) the SPR fibre-optic sensor with a transducing layer

The chemical sample to be measured at the structure shown in Figure 7-2(a) is aqueous with refractive index about 1.33. In order to increase the dynamic range of the sensor, a transducing layer, which is a dielectric material, of a few tens of nanometers thickness, shown in Figure 7-2(b), can be coated symmetrically outside the metal layer, for example, a tantalum pentoxide layer [Slavik 1998].

Mostly multimode plastic clad silica (PCS) optical fibres are used to construct the sensor, since the plastic cladding is easy to remove by chemical methods. A few applications proposed use monomode optical fibres, in which the cladding is polished to let the evanescent field contact the SPR supporting metal coated on the top of the polished surface.

7.3 Surface plasmon resonance fibre-optic chemical sensors using a swellable transducing layer

Those SPR fibre-optic sensors which have been studied to date use the change of refractive index (either the chemical sample or the transducing layer) to sense the concentration variation. These designs require the refractive index of the chemical sample to be measured is able to change with the variation of concentration. If the refractive index does not change with the concentration, these sensors will not work.

From theoretical analyses in Chapter 3, it is known that the thickness of the transducing layer can be another parameter to design SPR sensors giving very high sensitivity. The output signal (reflectance) from SPR sensors changes significantly with the thickness of the transducing layer.

Based on this design idea, a SPR fibre-optic chemical sensor using a swellable transducing layer is proposed. The sensor comprises a single or multi mode optical fibre with a core, a cladding and a jacket, wherein the optical fibre has a sensing section with a swellable layer as the transducing element coated symmetrically outside the SPR supporting metal layer. The thickness of the swellable transducing layer changes due to diffusion of the chemical substance into it or reaction of chemical substance with it. The thickness change of the swellable transducing layer is in accordance with the concentration of the chemical substance in the chemical sample. The SPR excitation responds strongly to the physical thickness of the swellable transducing layer. By monitoring the output light power spectrum of the sensor, the concentration of the chemical substance can be determined.

In fact, swellable materials have been studied to design optical and fibre-optic sensors in chemical applications before [Shakhsher 1994, Michie 1995 and Suzuki 1996]. These have been mentioned as giving a new direction for fibre-optic chemical sensor design [Seitz 1993].

The design of SPR sensor using swellable transducing layer has been proposed in bulk optics [Roth 1997 and Liu 1999]. By combining the swellable material and the fibre-optic surface plasmon resonance principle, as proposed here, a sensor can be designed with many advantages such as: miniaturisation, high sensitivity, fast response time and cheaper.

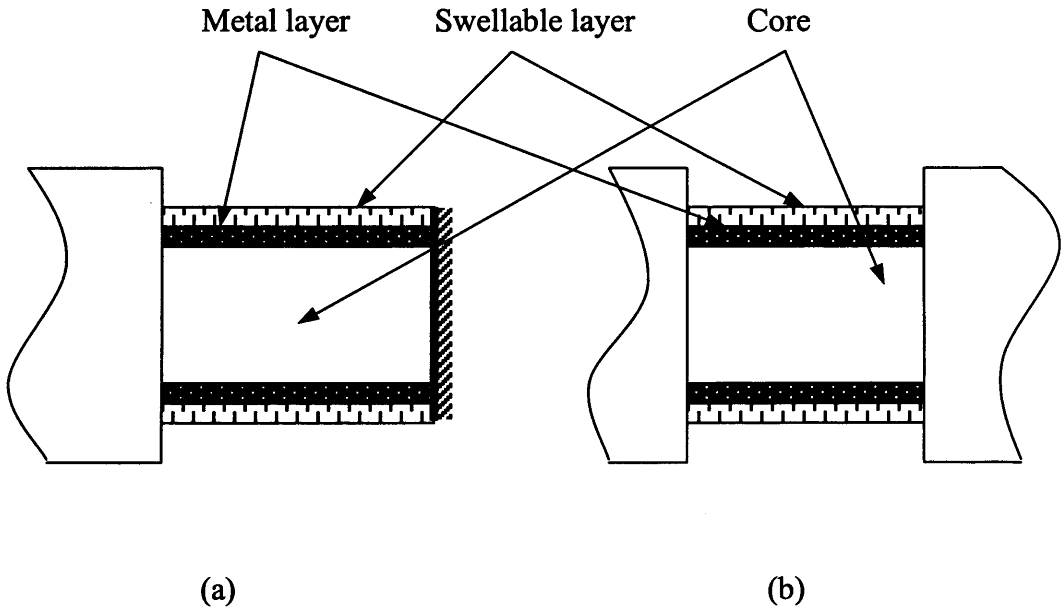

Figure 7-3 The structure of the sensing element using the swellable layer: (a) reflection type, (b) transmission type

Figure 7-3 shows the geometrical structure of a sensing element with a swellable transducing layer. Other parts of the sensor are the same as normal SPR fibre-optic sensors. The sensitivity of the sensor relies strongly on the characteristics of the swellable material used.

7.4 Distributed surface plasmon resonance (SPR) fibre-optic chemical sensors

7.4.1 Distributed fibre-optic sensors

Distributed fibre-optic sensors are defined as whose which operate over a length of fibre, yet are capable of determining the variations of a parameter along the length of the fibre at a series of specified locations. Fibre-optic sensors have been developed as distributed systems to monitor the magnitude of the physical and chemical parameter along the length of an optical fibre before [Lieberman 1993, Englund 1997, Potyrailo 1998 and Urbanczyk 1999]. Optical fibres provide a powerful and economical means of covering a large number of locations within a significant area.

A typical and successful technique for distributed fibre-optic sensors is optical time-domain reflectometer (OTDR). This technique utilizes an optical radar concept to examine the continuity and attenuation of optical fibres from a measurement of the backscattering versus time characteristics when a short pulse of light is launched into an optical fibre.

Another popular approach for distributed fibre-optic sensors is optical frequency-domain reflectometry (OFDR), which is a fibre-optic interferometric technique. For example, if an OFDR system is operated in backscattering mode in a continuous monomode optical fibre, the beat signal produced at the detector increases in frequency in direct proportion to the distance from which the light is retroscattered. If the detected beat signal is displayed on a conventional electronic spectrum analyzer, the power in each frequency increment represents the level of scattered light received from a short section of fibre situated at a distance corresponding to the frequency offset observed.

Theoretically OFDR technique has a far superior distance resolution capability than OTDR method.

7.4.2 Distributed surface plasmon resonance fibre-optic chemical sensors

Using optical surface plasmon excitation in the design of distributed fibre-optic sensors is a challenge. The distributed SPR fibre-optic sensor is used for the measurement of chemical information, with following advantages:

1. This distributed system uses a sequence of sensing elements, each of which is a point sensor. By using commercially available optical fibre connectors such as SMA connectors, sensing elements can be connected together to construct a distributed system.
2. Because multi-wavelength light sources are needed, there is no coherent noise generated by the coherent light source, which is major difficulty of OFDR distributed sensors.
3. The light signal detecting system is a spectrograph, which is much cheaper than those requires for OTDR or OFDR systems.
4. The wavelength resource of multi-wavelength light source is fully used.

A particular point SPR fibre-optic chemical sensor operates at one resonance wavelength λ_{SP}, which is determined by the structure and materials of the sensing element. The measurement of concentration operates close to this resonance wavelength. Consequently, the sensing element can be specified by the resonance wavelength.

The idea of designing distributed SPR fibre-optic chemical sensors is to multiplex some sensing elements (at least two, connected to each other by optical fibre connectors) along an optical fibre, each sensing element with a different resonance wavelength from the others.

Each sensing element is associated with a specified resonance wavelength. By monitoring the light intensity change at these resonance wavelengths, the concentrations of the chemical substances in the chemical samples located around sensing elements are determined, respectively. The different resonance wavelength in each sensing element is designed in terms of thickness of the metal layer and the transducing layer, as well as the material of metal and transducing layers.

Using a broadband light source, the received output light power spectrum should have peaks, each corresponding to a specified resonance wavelength and a sensing element, shown in Figure 7-4.

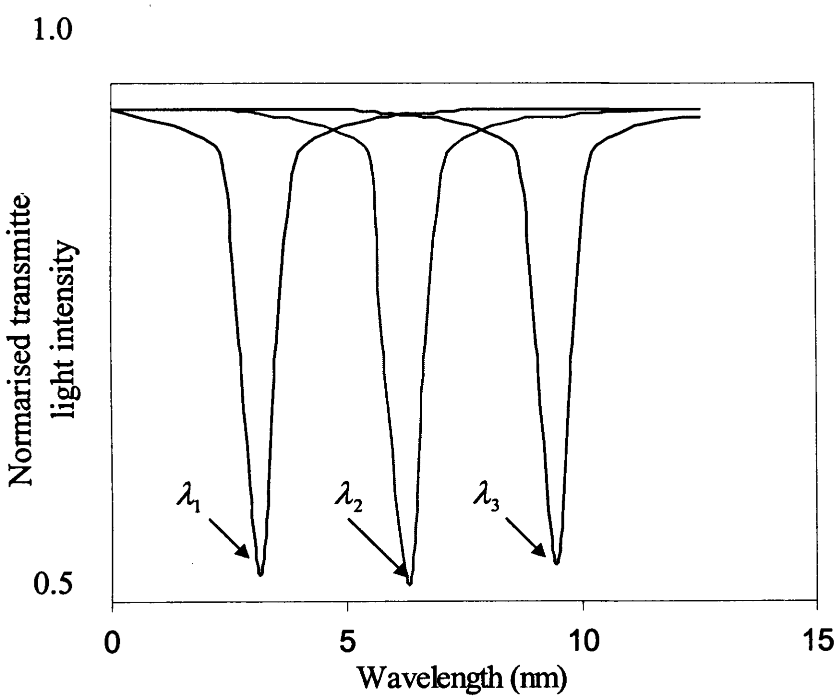

Figure 7-4 The principle of distributed SPR fibre-optic sensors

Regarding the light source for a distributed SPR fibre-optic sensor, the output power spectra of the light source should include all designed resonance wavelengths, and have powerful enough output at these wavelengths. Therefore, broadband lamp is a good choice, and a combination light sources is another possible choice. Figure 7-5 shows a combined light source with three discrete light sources and associated optical components as an example.

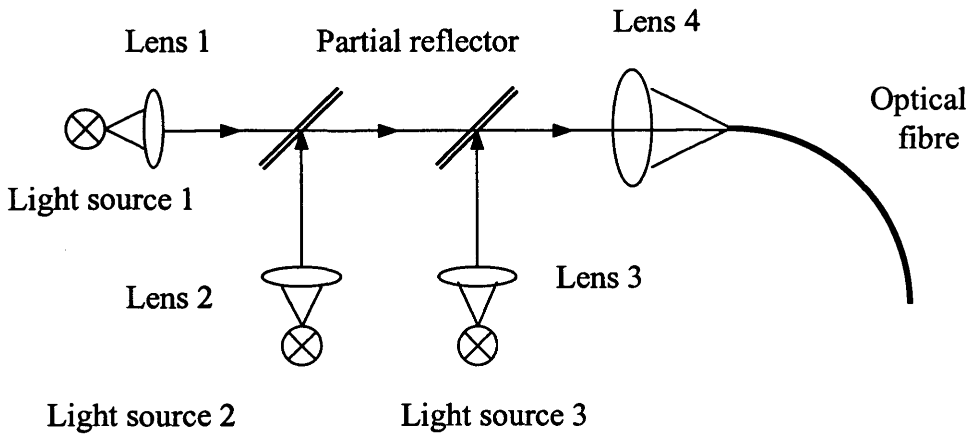

Figure 7-5 Combined light sources

Figure 7-6 shows the arrangement of a distributed SPR fibre-optic sensor. The sensor is constructed by serially connecting some sensing elements. Each sensing element operates at a specified resonance wavelength, which is different and independent from the others.

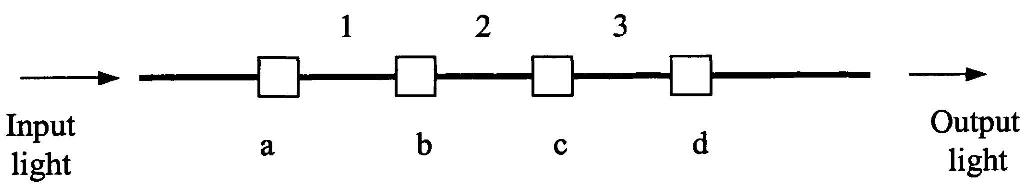

Figure 7-6 Configuration of distributed SPR fibre-optic sensors, 1, 2 and 3 represent three sensing elements, a, b, c, and d represent four optical fibre connectors

Regarding the SPR supporting metals, the dielectric constant ($\varepsilon_2 = \varepsilon_r + i\varepsilon_i$) of metals which can be used to support the surface plasmon resonance excitation are listed in Table 7-1. For ultraviolet light, aluminium can be used, for visible light, gold or silver can be used, for infrared light, copper, gold and silver can be used.

Table 7-1 [Palik 1985]

	λ	η	κ		ε_r	ε_i
Aluminium	300	0.25	3.33		-11.026	1.665
	492	0.64	5.5		-29.840	7.040
	700	1.55	7		-46.598	21.700
	900	1.96	7.7		-55.448	30.184
Cadmium	280	0.41	2		-3.832	1.640
Copper	450	0.87	2.2		-4.083	3.828
	600	0.186	2.98		-8.846	1.109
	750	0.157	4.46		-19.867	1.400
	900	0.19	5.57		-30.989	2.117
	1350	0.45	7.81		-60.794	7.029
Gold	600	0.2	2.9		-8.370	1.160
	750	0.14	4.27		-18.213	1.196
	900	0.166	5.34		-28.488	1.773
	1000	0.179	6.04		-36.450	2.162
Indium	420	0.65	1.84		-2.963	2.392
	600	1.29	2.59		-5.044	6.682
	710	1.38	6.24		-37.033	17.222
	1050	1.83	7.94		-59.695	29.060
	1560	2.31	11.3		-122.354	52.206
Silver	500	0.05	2.87		-8.234	0.287
	700	0.075	4.62		-21.339	0.693
	900	0.105	6.22		-38.677	1.306
	1250	0.37	7.7		-59.153	5.698
	1500	0.45	9		-80.798	8.100

There are two principles to design such distributed SPR sensor to determine the concentration of the chemical sample to be measured. One uses the information of the refractive index change of the chemical sample or the transducing layer, the other uses a swellable layer the thickness of which varies with the concentration.

Because each sensing element is in accordance with a specified resonance wavelength, by monitoring the output power at each resonance wavelength, the location and concentration of the change can be determined.

7.5 Conclusions

Optical surface plasmon excitation has been studied in the applications of chemical sensing. The design studies in this chapter are focused on two aspects: one is the point-type sensor using a swellable transducing layer to determine concentration, which gives high sensitivity, fast response time, the other is distributed-type sensors for distributed measurement of concentration. Both design ideas are novel and can be used for the measurement of gaseous and liquid solutions.

The structure of distributed-type sensors is flexible and it is easy to combine different numbers of sensing elements. Each sensing element can use the principle of sensing refractive index change or thickness change of the transducing layer or both refractive index and thickness changes. The distinguishing features of the distributed design include, high sensitivity, fast response, low price and flexibility.

The interference (crosstalk) between two adjacent resonance wavelengths is a major potential difficulty which can limit the maximum number of sensing elements and the accuracy of the sensor. A signal processing technique has to be used to obtain high performance of distributed systems.

Although this design is for concentration measurement, it can be used for other chemical applications such as monitoring chemical reaction.

Chapter 8

Conclusions and Further Work

8.1 Introduction

The research discussed in this thesis is the investigations of light intensity attenuation-based fibre-optic chemical sensors. In order to obtain an extensive scale of studies, the investigations have involved both intrinsic and extrinsic types of systems in two aspects: theoretical analyses and design studies. To this end, four piecess of work were presented as shown in Table 8-1.

Table 8-1 Overall view of the research

	THEORETICAL ANALYSES	DESIGN STUDIES
INTRINSIC Type	✓	✓
EXTRINSIC Type	✓	✓

1. Novel surface plasmon resonance fibre-optic sensors

1. Evanescent wave absorption fibre-optic sensors
2. Surface plasmon resonance fibre-optic sensors

1. Two-wavelength light intensity attenuation-based fibre-optic sensors

1. "Propofol" fibre-optic sensor

The theoretical side of the research is focused on the construction of theoretical models and the discussion of the performance of the sensors. The design side of the research is concentrated on the design studies of novel sensors to aid commercial developments.

8.2 Summary of theoretical analyses and implications for intrinsic type sensors

The theoretical analysis of the intrinsic type of light intensity attenuation-based fibre-optic chemical sensors is always an attractive topic, because new intrinsic sensing principles or measurement approaches keep occurring. Each new principle or measurement approach has to be modelled by theoretical expressions.

As the first part of this research, fibre-optic evanescent wave absorption sensors and surface plasmon resonance (SPR) sensors are studied theoretically (Chapter 2 to Chapter 4).

The first step in these studies is the construction of mathematical models. Then based on the mathematical models, either numerical calculations or analytical derivations can be applied for further estimations of the characteristics of the sensors.

Following this procedure, in the research of fibre-optic evanescent wave absorption sensors, leaky skew rays were discussed since the evanescent wave absorption of leaky skew rays has not been evaluated before. The model using meridional rays can only give an approximate expression and leaky skew rays often transmit a non-negligible light power in optical fibres. The contribution of leaky skew rays to the evanescent wave absorption has not previously been determined. That is the importance and meaning of this research. Numerical calculations are used to discuss the evanescent wave absorption quantitatively. Finally a comprehensive expression of evanescent wave absorption including both meridional and leaky skew rays for evanescent wave absorption fibre-optic sensors and spectroscopy is presented.

In the theoretical research on SPR fibre-optic sensors, Fresnel's equations are the basic expressions to describe the characteristics of the sensors. However, the previous models are suitable for SPR bulk-optic sensors, in which only one light beam with a specified incident angle is involved.

A multi-wavelength light source is used in the SPR fibre-optic sensor, the output light signal has to consider the contribution from all guided modes (a range of angles) and multi-wavelength (a range of wavelengths) during the use of Fresnel's equations. Theoretical models were derived for further analytical derivations and numerical calculations.

An important consideration in the theoretical analyses is light sources. The light power distribution of light source could be one of crucial factors for increasing the sensitivity of the sensor. It is also helpful for estimating the characteristics of the sensors in the design.

8.3 Summary of theoretical analyses and implications for extrinsic type sensors

Two-wavelength fibre-optic chemical sensors based on the Beer-Lambert law are very popular. They can usually use successfully techniques and even devices developed for bulk-optic systems. The accuracy of sensor is determined by the noise level of the components composing the sensor.

Dispersion is one of the major characteristics of multi-wavelength fibre-optic systems. In two-wavelength fibre-optic sensors, the light power loss induced by microbending optical fibres is dispersive and different wavelengths suffer different loss. In the design of such systems, the error influence from microbending the optical fibre should be considered carefully, because in some applications, microbending is unavoidable.

Temperature fluctuation is a common problem for all kinds of sensors (which can cause the output power fluctuations of light sources both in amplitude and phase). Special efforts have to be made in the design of highly accurate optical devices, such as the use of cooling systems and compensating approaches. In two-wavelength light intensity attenuation-based fibre-optic sensors, this temperature disturbance manifests itself as the fluctuation of the output power spectrum of light sources. At different temperatures, two wavelengths (measurement and reference wavelengths) have different output power ratio.

The error influences from microbending and temperature fluctuation have been numerically studied in the research. One useful message drawn from the research is that the effect of different errors can be very different, and even in opposite directions. Some errors have positive effects, others have negative contributions. It is possible to compensate these errors against each other to realise the optimisation of the system.

The best measurement principle, the optimal technique approach and high quality of hardware components are always the most important design consideration for the development of highly accurate sensors.

8.4 Summary of design studies and implications for intrinsic type sensors

Previously published results and experiments in the development of surface plasmon resonance fibre-optic sensors by other researchers are very useful in the design studies in this thesis. The work in this part of the research is mainly focused on the design studies of novel types of sensors.

The novel distinguished feature of SPR fibre-optic sensors with a swellable tansducing layer is that the thickness change of the transducing layer is used to sense the concentration of the chemical sample. The swellable materials are key elements to realise the design. Therefore the material has to have a good swellable characteristic, and this swellable characteristic has to be stable and repeatable. Ideally this material has to be ion-selectable as well.

The novel distinguished feature of distributed SPR fibre-optic sensors is that the information on resonance wavelength is used to specify the location of the sensing element. The interference (crosstalk) between channels, particularly between two adjacent channels, could be a serious factor in the performance of the sensor. Signal processing techniques have to be considered for such systems.

SPR fibre-optic sensors are highly promising techniques in chemical sensing applications. The sensors are high sensitivity, have high response speed and small size compared with conventional sensors.

The selection of SPR supporting metals is an important issue, especially when the resonance wavelength is in the ultraviolet or infrared regions. Unfortunately, at present, there are not many choices (usually noble metals are used as the SPR supporting metals). Explorations of new SPR supporting materials are needed for new future developments. Semiconductors are potential materials for this purpose since some semiconductors have similar characteristics of dielectric constants to metals.

Another problem faced in the development of SPR fibre-optic sensors is in manufacturing. It is difficult to coat perfect thin multi-layers symmetrically on the surface of the optical fibre core. And it is also difficult to make these multi-layers strong enough.

8.5 Summary of design studies and implications for extrinsic type sensors

The optical measurement principle for designing the "propofol" fibre-optic sensor is not new. The main difficulties encountered during the design study are related with how to optimise the sensor and to achieve the best performance.

There are two types of probe design: one uses porous hollow fibres, the other uses metal U-shape channel. The 3-D dimensions of the probe are critical parameters to make the sensor applicable in clinics. However, from the manufacturing point of view, if the size of the probe is too small, this will increase the difficulty and cost in production; if porous hollow fibres are used, the strength of the probe could be another serious issue with small size probe. These issues should be carefully considered in prototype construction.

The material of absorbent is silicone, which is a two-part gel. Different types of silicone can display different performance in terms of diffusion speed, hardness, curing temperature, *etc*.. The diffusion speed is concerned with the response time of the sensor, which is a vital characteristic for in-*vivo* measurements. Hardness of silicone material is able to affect the diffusion speed. Hardness can be controlled by the ratio of the two parts. The harder the silicone, the slower the diffusion speed is.

The stability of the sensor, influenced by the output power fluctuation of the Xe light source, is addressed in the design study. The output power of the Xe light source should be monitored during the measurement with high accuracy. For this purpose, several approaches can be used, for example, the two-wavelength technique discussed in Chapter 5.

Before using the sensor to do the concentration measurement of propofol, the sensor has to be calibrated. One of the possible calibration methods could be to deposit the probe into blood without the anaesthetic, propofol, to initialise the output of the sensor.

After use, the probe is disconnected from the rest of the system, and thrown away. Therefore there is less problem with sterilisation.

One important consideration during the design study is the cost of the sensor. Low cost is always the requirement of commercial markets. In the design and selection of hardware, the compromise between cost and performance has to be dealt with.

8.6 Further work

Light intensity attenuation-based fibre-optic chemical sensors are very extensively used in chemistry. The research in this area is worthy of further exploration. Following on from the achievements of this thesis both further theoretical and design study explorations are proposed.

8.6.1 Theoretical

1. Fibre-optic evanescent wave absorption

In this issue, the evanescent wave absorption coefficient of leaky skew rays in optical fibres has been formulated. This formulation, together with the expression for the evanescent wave absorption of meridional rays, makes quantitative calculations of the evanescent wave absorption fibre-optic sensor possible. Combining this with the study of the light power distribution of the light source, comprehensively numerical calculations of evanescent wave absorption in optical fibres will be possible which will help in the design of evanescent wave absorption fibre-optic sensors and fibre-optic immunoassay. Although it is time-consuming work, to write a software package to calculate the evanescent wave absorption in optical fibre systems, it is worth the effort in order to optimise fibre-optic evanescent wave absorption systems.

2. Fibre-optic surface plasmon resonance (SPR) excitation

Recently fibre-optic surface plasmon resonance (SPR) sensors have been developed intensively. In the research of the thesis the theoretical models so far constructed are based on the approximation of meridional rays. An accurate model should consider the contribution from leaky skew rays. Further theoretical work in SPR fibre-optic sensors can be the theoretical analysis of the SPR excitation by leaky skew rays in optical fibres, which is also a requirement of the design in high performance of SPR fibre-optic sensors. Theoretical analysis of multi-layer structure SPR fibre-optic sensors requires further work too.

8.6.2 Design studies

1. "Propofol" fibre-optic sensors

The concentration measurement of "Propofol" has potential commercial value. The design studies in the thesis is a feasibility study for the development in the near future of such a device. The next step for this work is related to making a prototype sensor. By using the prototype sensor, sensitivity and response time of the sensor will be estimated. Optimal structure for the probe will be determined. Some compensation approaches will be considered to reduce the noise and disturbance from the environment. Towards the in-*vivo* monitoring, the experiments in blood environments have to be done.

2. SPR fibre-optic chemical sensors

Prototype sensors should be made for preliminary experiments and tests of SPR fibre-optic chemical sensors using swellable materials and distributed systems. Materials, including the swellable layer and the SPR supporting layer in ultraviolet and infrared light, have to be studied. Signal process techniques should be considered to reduce the interference among channels in distributed systems.

References

[Abeles 1986] Abeles, F., in Wallis, R.F., and Stegemann, G.I., (Eds.), 1986, Electromagnetic Surface Excitations, Berlin: Springer-Verlag

[Aldinger 1998] Aldinger, U., Pfeifer, P., Schwotzer, G., and Steinruecke, P., 1998, Comparative study of spectral and angle-dependent SPR devices in biological applications, Sensors and Actuators B, 51, 298-304

[Boisde 1996] Boisde, G., and Harmer, A., 1996, Chemical and biochemical sensing with optical fibers and waveguides, Boston: Artech House

[Bray 1992] Bray, D., 1992, Cell Movements, Graland Publishing Inc., New York & London

[Chan 1984] Chan, K., Ito, H., and Inaba, H., 1984, Remote sensing system for near-infrared differential absorption of CH4 gas using low-loss optical fibre link, Appl. Opt., 23, 3415-3420

[Chappell 1976] Chappell, A., 1976, Optoelectronics theory and practice, Bedford: Texas Instrument Ltd.

[Chen 1980] Chen, W.P., and Chen, J.M., 1980, Surface plasma wave study of submonolayer Cs and CsO covered Ag surface, Surface Sci., 91, 601-617

[Chen 1981] Chen, W.P., and Chen, J.M., 1981, Use of surface plasma wave for determination of the thickness and optical constants of thin metalic films, J. Opt. Soc. Am., 71, 189-191

[Cooper 1981] Cooper, J.B., Edmondson, J.H., Joseph, D.M., and Newbower, R.S., 1981, Piezoelectric sorption anaesthetic sensors, IEEE Trans. Biomedical Eng., 28, 459-466

[Ctyroky 1997] Ctyroky, J., Homola, J., and Skalsky, M., 1997, Modelling of surface plasmon resonance waveguide sensor by complex mode expansion and propagation method, Opt. Quantum Electron., 29, 301-311

[Daniels 1988] Daniels, P.B., Deacon, J.K., Eddowes, M.J., Pedley, D.G., 1988, Surface plasmon resonance applied to immunosensing, Sensors and Actuators, 15, 11-18

[Dakin 1989] Dakin, John and Culshaw, Brian, 1989, Optical fiber sensors, Artech House, Inc. London

[Deboux 1995] Deboux, B.J.C., Lewis, E., Scully, P.J., and Edwards, R.J., 1995, A novel technique for optical-fiber pH sensing based on methylene-blue absorption, J. Lightwave Technol., 13, 1407-1414

[de Bruijn 1990] de Bruijn, H.E.D., Kooyman, R.P.H., and Gerve, J., 1990, Determination of dielectric permittivity and thickness of a metal layer from a surface plasmon resonance experiment, Appl. Opt., 29, 1974-1978

[Degrandpre 1988] DeGrandpre, M.D., and Burgess, L.W., 1988, Long path fibre-optic-sensor for evanescent field absorbance measurements, Anal. Chem., 60, 2582-2586

[Diamond 1998] Diamond, D., 1998, Principles of Chemical and Biological Sensors, John Wiley & Sons, Inc., New York

[Disley 1998] Disley, D.M., Cullen, D.C., You, H.X., and Lowe, C.R., 1998, Covalent coupling of immunolobulin G to self-assembled monolayers as a method for immobilizing the interfacial-recognition layer of a surface plasmon resonance immunosensor, Biosensor & Bioelectronics, 13, 1213-1225

[Englund 1997] Englund, M., Ipatti, A., and Karioja, P., 1997, fiber-optic security monitoring sensor, Proc. of SPIE, 3099, 284-299

[Enson 1962] Enson, Y., Briscoe, W.A., Polanyi, M.L., and Gournand, A., 1962, In vivo studies with an intravascular and intracardiac oximeter, J. Appl. Physiol., 17, 552-558

[Feinstein 1991] Feinstein-Jaffe, I., Borenstein, A., and Katz, M., 1991, Fiber optic attenuated reflection spectroscopy (FO-ATR) for investigation of organoetallic ploymeric films, J. Am. Chem.Soc., 113, 7042-7044

[Fontana 1988] Fontana, E., Pantell, R.H., and Moslehi, M., 1988, Characterization of dieelctric-coated, metal mirrors using surface-plasmon spectroscopy, Appl. Opt., 27, 3334-3340

[Frant 1994] Frant, M.S., 1994, History of the early commercialization of ion-selective electrodes, Analyst, 119, 2293-2301

[Garces 1992] Garces, I., Aldea, C., and Mateo, J., 1992, Four-layer chemical fiber optic plasmon-based sensor, Sensors and Actuators B, 7, 771-774

[Gloge 1972] Gloge, D., 1972, Bending loss in multimode fibers with graded and ungraded core index, Appl. Opt., 11, 2506-2513

[Giuliani 1983] Giuliani, J.F., Wohltjen, H., and Jarvis, N.L., 1983, Reversible optical waveguide sensor for ammonia vapors, Opt. Lett., 8, 54-56

[Gregonis 1990] Gregonis, D., Wagenen, Coleman, D., and Mitchell, J., 1990, A commercial anesthetic-respiratory gas monitor utilizing Raman spectroscopy, SPIE Reman and Luminescence Spectroscopies in Tech. II, 1336, 247-255

[Gupta 1993] Gupta, B.D., Sharma, A., and Singh, C.D., 1993, Evanescent wave absorption sensors based on uniform and tapered fibers: a comparative study of their sensitivities, Internat. J. Optoelectro., 8, 409-418

[Gupta 1994a] Gupta, B.D., and Singh, C.D., 1994, Fiber-optic evanescent wave absorption sensor: a theoretical evaluation, Fiber and Integrated Opt., 13, 433-443

[Gupta 1994b] Gupta, B.D., Singh, C.D., and Sharma, A., 1994, Fiber optic evanescent wave absorption sensor: effect of launching condition and the geometry of the sensing region, Optical Eng., 33, 1864-1868

[Gupta 1994c] Gupta, B.D., and Singh, C.D., 1994, Evanescent absorption coefficient for diffuse source ilumination: uniform and tapered fiber sensors, Appl. Opt., 33, 2737-2742

[Guyton 1990] Guyton, D.C., Gravenstein, N., 1990, Infrared analysis of volatile anesthetics: impact of monitor agent setting, volatile mixtures, and alcohol, J. Clin.Monit., 6, 203-206

[Harrick 1967] Harrick, N.J., 1967, Internal Reflection Spectroscopy, Wiley , New York

[Harris 1995] Harris, R.D., and Wilkinson, J.S., 1995, Waveguide surface plasmon resonance sensors, Sensors and Actuators B, 29, 261-267

[Hulanicki 1991] Hulanicki, A., Glab, S., and Ingman, F., 1991, Chemical sensors definitions and classification, Pure & Appl. Chem, 63, 1247- 1250

[Iwamoto 1984] Iwamoto, R., and Ohta, K., 1984, Quantitative surface analysis by Fourier transform attenuated total reflection infrared spectroscopy, Appl. Spectrosc., 38, 359-365

[Jackson 1986] D.A.Jackson and J.D.C.Jones, 1986, Extrinsic fibre-optic sensors for remote measurement: part one , Optics and Laser Technol., 18, 243-252

[Jakusch 1997] Jakusch, M., Mizaikoff, B., Kellner, R., and Katzir, A., 1997, Towards a remote IR fiber-optic sensor system for the determination of chlorinated hydrocarbons in water, Sensors and Actuators B, 38, 83-87

[Jin 1995] Jin, W., Stewart, G., and Culshaw, B., 1995, Source noise limitation in an optical methane detection system using a broadband source, Appl. Opt., 34, 2345-2349

[Jin 1997] Jin, W., Stewart, G., Philp, W., Culshaw, B., and Demokan, M.S., 1997, Limitation of absorption-based fibre optic gas sensors by coherent reflections, Appl. Opt., 36, 6251-6255

[Jorgenson 1993] Jorgenson, R.C., and Yee, S.S., 1993, A fiber-optic chemical sensor based on surface plasmon resonance, Sensors and Actuators B, 12, 213-220

[Jorgenson 1994] Jorgenson, R.C., and Yee, S.S., 1994, Control of the dynamic range and sensitivity of a surface plasmon resonance based fiber optic sensor, Sensors and Actuators A, 43, 44-48

[Jory 1995] Jory, M.J., Bradberry, G.W., Cann, P.S., and Sambles, J.R., 1995, Surface plasmon based optical sensor using acousto optics, Measurement Sci. & Tech., 6, 1193-1200

[Junger 1996] Junger, S., Lutter, N., Schwider, J., Goettler, D., Weber, N., Burte, E., 1996, Mainstream sensor unit for closed-circle anesthetic gas monitoring, Proc. of SPIE, 2676, 190-197

[Kalabina 1995] Kalabina, N.A., Ksenevich, T.I., Beloglazov, A.A., and Nikitin, P.I., 1995, Pesticide sensing by surface-plasmon resonance, Proc. of SPIE, 2367, 126-132

[Kano 1994] Kano, H., and Kawata, S., 1994, Surface-plasmon sensor for absorption-sensitivity enhancement, Appl. Opt., 33, 5166-5170

[Kapany 1964] Kapany, N.S., and Silbertrust, N., 1964, Fibre optics Spectrophotometer for in vivo Oximeter, Nature, 204, 138-142

[Kapany 1967] Kapany, N.S., 1967, Fiber Optics, New York: Academic

[Kotyk 1988] Kotyk, A., Janacek, K., and Koryta, J.,1988, Biophysical Chemistry of Membrane Functions, New York: John Wiley & Sons

[Kretschmann 1971] Kretschmann, E., 1971, Die bestimmung optischer konstanten von metallen durch anregung von oberflaechenplasmaschwingungen, Z. Phys., Vol.241, 1971, pp.313-324

[Krska 1992] Krska, R., Rosenberg, E., Taga, K., Kellner, R., Messica, A., and Katzir, A., 1992, Polymer coated silver halide infrared fibers as sensing devices for chorinated hydrocarbons in water, Appl. Phys. Lett., 61, 1778-1780

[Kunz 1996] Kunz, U., Katerkamp, A., Renneberg, R., Spener, F., and Cammann, K., Sensing fatty acid binding protein with planar and fiber-optical surface plasmon resonance spectroscopy devices, Sensors and Actuators B, 32, 149-155, 1996

[Kurosawa 1986] Kurosawa, K., Pierce, R.M., Ushioda, S., and Hemminger, J.C., 1986, Raman scattering and attenuated-total-reflection studies of surface plasmon polaritions, Phys. Rev., B, 33, 789-798

[Landis 1994] Landis, D.A., Seliskar, C.J., and Heineman, W.R., 1994, Fiber-optic-graded-index-lens absorption sensor with wavelength-scanning capability, Appl.Opt., 33, 3432-3439

[Laniri 1999] Lahiri, J., Ostuni, E., and Whitesides, G.M., 1999, Patterning ligands on reactive SAMs by microcontat printing, Langmuir, 15, 2055-2060

[Leidberg 1983] Leigberg, B., Nylander, C. and Lundstrom, I., 1983, Surface plasmon resonance for gas detection and biosensing, Sensors and Actuators, 4, 299-304

[Lieberman 1993] Lieberman, R.A., 1993, Recent progress in intrinsic fiber-optic chemical sensing II, Sensors and Actuators B, 11, 43-55

[Liu 1999] Liu;Y., et al , 1999, US patent No.5,858,799

[Lorrain 1988] Lorrain, P., Corson, D.P., and Lorrain, F., 1988, Electromagnetic fields and Waves, New York: Freeman

[Lowe 1971] Lowe, H.J., and Hagler, K., Clinical and laboratory evaluation of an expred anesthetic gas monitor (Narko-Test), 1971, Anesthesiology, 34, pp.378-382

[Lukosz 1991] Lukosz, W., 199, Principles and sensitivities of integrated optical and surface plasmon sensors for direct affinity sensing and immunisensing, Biosensors and Bioelectronics, 6, 215-225

[MacDonald 1994] Macdonald, H.L., Liu, H., and Yager, P., 1994, Fiber optic sensor for general anesthetics based on Raman spectroscopy, Proc. SPIE, 2131, 514-523

[Marcuse 1976a] Marcuse, D., 1976, Curvature loss formula for optical fibers, J. Opt. Soc. Am., 66, 216-220.

[Marcuse 1976b] Marcuse, D., 1976, Field deformation and loss caused by curvature of optical fibers, J. Opt. Soc. Am., 66, 313-319.

[Margalit 1989] Margalit, E., Dodiuk, H., Kosower, E.M., and Katzir, A., 1989, Infrared fiber evanescent wave spectroscopy for in-situ monitoring of chemical processes, in Infrared fiber Optics, Harrington, J.A., and Katzir, A.,eds., SPIE Proc., 2048, 145-152

[Mendelson 1988] Mendelson, Y., Lin,, B.Y., Peura, R.A., and Clermont, A.C., 1988, Carbon dioxide laser based multipie ATR technique for measuring glucose in aqueous solutions, Appl. Opt., 27, 5077-5080

[Merlo 1990] Merlo, S., Yager, P., Burgess, L. W., 1990, Optical method for detecting anesthetics and other lipid-soluble compounds, Sensors and Actuators A, 23, 1150-1154

[Merschman 1998] Merschman, S.A., and Tilotta, D.C., 1998, Fiber-optic sensor for aromatic compounds in water based on solid-phase microectraction and ultraviolet evanescent wave absorption spectroscopy Appl. Spectrosc, 52, 106-111

[Messica 1992] Messica, A., Katzir, A., Schiessl, U., and Tacke, M., 1992, Liquid and gas fiber optic evanescent-wave spectroscopy by tunable lasers, Proc. of SPIE, 1591, 192-200

[Messica 1994] Messica, A., Greenstein, A., and Katzir, A., 1994, Fiber-optic evanescent wave sensor for gas detection, Opt. Lett., 19, 1167-1169

[Messica 1996] Messica, A., Dreenstein, A., and Katzir, A., 1996, Theory of fiber-optic, evanescent-wave spectroscopy and sensors, Appl. Opt., 35, 2274-2284

[Michie 1995] Michie, W.C., Culshaw, B., Konstantaki, M., McKenzie, I., Kelly, S., Graham, N.B., and Moran, C., 1995, Distributed pH and water detection using fiber-optic sensors and hydrogels, 13, 1415-1419

[Mignani 1998] Mignani, A.G., Falciai, R., and Ciaccheri, L., 1998, Evanescent wave absorption spectroscopy by means of bi-tapered multimode optical fibers, Appl. Spectrosc.,52,546-551

[Montgomery 1981] Montgomery, J.D., and Dixon F.W., 1981, Fibre optics in process control, Proc. ISA/IMC Conf. Promecon' 81, London: 81-90

[Nash 1998] Nash, D.J., and Sambles, J.R., 1998, Surface plasmon-polariton study of the optical dielectric function of zinc, J. of Mod. Optics, 45, 2585-2569

[Nikitin 1999] Nikitin, P., 1999, Phase jump under surface plasmon resonance and its using for biosensing and microscopy, Proc. of SPIE, 3749, 464-465

[Palik 1985] Palik, E.D., 1985, Handbook of optical constants of solid, London: Academic Press Inc.

[Parnell 1995] Parnell, J.R., and Yager, P., 1995, Application of multiplicative signal correction (MSC) to Raman spectra for use in an anesthetic sensor, Proc. of SPIE, 2388, 481-492

[Parnell 1996] Parnell, J.R., and Yager, P., 1996, Potential for a silicone probe in a Raman spectroscopic general-anesthetic sensor, Proc. of SPIE, 2676, 205-215

[Paul 1987] Paul, P. H., and Kychakoff, G., 1987, Fiber-optic evanescent wave absorption sensor, Appl. Phys. Lett., 51, 12-14

[Peterson 1980] Peterson, J.I., Goldstein, S.R., and Fitzgerald, R.V., 1980, Fiber optic pH probe for physiological use", Anal. Chem., 52, 864-869

[Piraud 1992] Piraud, C., Mwarania, E.K., Yao, J., O'Dwyer, K., Schiffrin, D.J., and Wilkinson, J.S., 1992, Optoelectrochemical transaction on planar optical waveguides, J. Lightwave Technol., 10, 693-699

[Ploanyi 1962] Polanyi, M.L., and Hehir, R.M., 1962, Invivo oximeter with fast dynamic response, Rev. Sci. Instrum., 33,1050-1054

[Plummer 1987] Plummer, G.F., Improved method for the determination of propofol in blood by high-performance liquid chromatography with fluorescence detection, 1978, J. of Chromatogr., 421, 171-176

[Pockrand 1978] Pockrand, I., 1978, Surface plasma oscillations at silversurface with thin transparent and absorbing coatings, Surface Sci., 72, 577-588

[Potter 1961] Potter, R.J., 1961, Transmission properties of optical fibers, J.Opt. Soc. Am., 51, 1079-1089

[Potyrailo 1998]	Potyrailo, R.A., and Hieftje, G.M., 1998, Distributed fiber-optic chemical sensor with chemically modified plastic cladding, Appl. Spectro. 52, 1092-1095
[Potyrailo 1998]	Potyrailo, R.A., Hobbs, S.E., and Hieftje, G.M., 1998, Near-ultraviolet evanescent-wave absorption sensor based on a multimode optical fiber, Anal. Chem., 70, 1639-1645
[Powell 1960]	Powell, C.J., and Swan, J.B., 1960, Effect oxidation on the characteristic loss spectra of aluminum and magnesium, Phys. Rev., 118, 640-649
[Qing 1996]	Qing, D.K., Chen, X.M., Itoh, K., and Murabayashi, M., 1996, A theoretical evaluation of the absorption coefficient of the optical waveguide chemical or biological sensors by group index method", J. Lightwave Technol., 14, 1907-1917
[Raether 1977]	Raether, H., in Hass, G., Francombe, M.H., and Hoffman, R.W., (Eds.), 1977, Physica of Thin Films, Vol.9, New York: Academic
[Raether 1988]	Raether, H., 1988, Surface Plasmons on Smooth and Rough Surfaces and on Gratings, Vol.111of Springer Tracts in Modern Physics, Heidelberg: Springer-Verlag
[Reed 1985]	Reed, C.E., Giergiel, J., Ushioda, S., and Hemminger, J.C., 1985, Effects of annealing on the attenuated-total-reflection spectra of cold-evaporated silver films, Phys. Rev., B, 31, 1873-1880
[Regan 1997]	Regan, F., MacCraith, B.D., Walsh, J.E., Odwyer, K., Vos, J.G., and Meaney M., 1997, Novel Tefol-coate optical fibres for TCE determination using FTIR spectroscopy, Vibrational Spectroscopy, 14, 239-246
[Reick 1965]	Reick, F.G., 1965, The optical whispering mode of polished cylinders and its implications in laser technology, Appl. Opt., 4, 1395-1399
[Ritchie 1957]	Ritchie, R.H., 1957, Plasma losses by fast electrons in thin films, Phys. Rev., 106, 874-881
[Roth 1997]	Roth; C., et al , 1997, US patent No.5,640,234

[Ruddy 1990] Ruddy, V., 1990, An effective attenuation coefficient for evanescent wave spectroscopy using multimode fiber, Fiber Integrated Opt., 9, 142-150

[Schipper 1996] Schipper, E.F., Kooyman, R.P.H., Borreman, A., and Greve, J., 1996, Critical sensor: a new type of evanescent wave innunosensor, Biosensors and Bioelectronics, 11, 295-304

[Schmautz 1992] Schmautz, A., 1992, Application-specific design of a piezoelectric chemosensor array, Sensors and Actuators B, 6, 38-44

[Schnitzer 1990] Schnitzer, I., and Katzir, A., 1990, Evanescent field IR spectroscopy using optical fibres and tunable diode lasers, Materials Sci and Eng., B5, 333-337

[Schwotzer 1997] Schwotzer, G., Latka, I., Lehmann, H., and Willsch, R., 1997, Optical sensing of hydrocarbons in air or in water using UV absorption in the evanescent field of fibers, Sensors and Actuators B, 38-39, 150-153

[Seitz 1993] Seitz, W.R., 1993, New directions of fiber optic chemical sensors: sensors based on polymer swelling, J. of Molecular Structure, 292, 105-114

[Senior 1985] Senior, J.M., 1985, Optical fiber communications principles and practice, London: Prentice Hall

[Shakhsher 1994] Shakhsher, Z, and Seitz, W.R., 1994, Single fiber-optic pH sensor based on changes in reflection accompanying polymer swelling, Anal. Chem., 66, 1731-1735

[Simhony 1988] Simhony, S., Schnitzer, I., Katzir, A., and Kosower, E.M., 1988, Evanescent wave infrared spectroscopy of liquids using silver halide optical fibers , J. Appl. Phys., 64, 3732-3734

[Slavik 1998] Slavik, R., Homola, J., and Ctyroky, J., 1998, Miniaturization of fiber optic surface plasmon resonance sensor, Sensors and Actuators B, 51, 311-315

[Snyder 1974a] Snyder, A.W., and Mitchell, D.J., 1974, Leaky rays on circular optical fibers, J. Opt. Soc. Am., 64, 599-607

[Snyder 1974b] Snyder, A.W., Mitchell, D.J., and Pask, C., 1974, Failure of geometric optics for analysis of circular optical fibers, J. Opt. Soc. Am., 64, 608-614

[Snyder 1974c] Snyder, A.W., and Mitchell, D.J., 1974, Bending losses of multimode optical fibres, Electron Lett., 10, 11-12

[Snyder 1983] Snyder, A.W., and Love, J.D., 1983, Optical Waveguide Theory, London: Chapman and Hall

[Stewart 1990] Stewart, G., Clark, D.F., Culshaw, B., and Andonovic, I., 1990, Referencing systems for evanescent wave sensors, SPIE Proc., 1314, 262-269

[Suzuki 1996] Suzuki, A., Ishii, T., and Maruyama, Y., 1996, Optical switching in polymer gels, J. Appl. Phys., 80, 131-136

[Tracy 1991] Tracy, P.M., 1991, Intrinsic fibre-optic sensors, IEEE Trans on Indust. Appl., 27, 96-98

[Urbanczyk 1999] Urbanczyk, W., 1999, selected applications of fiber-optic sensors, Proc. of SPIE, 3824, 221-234

[Ursula 1998] Ursula E. S. K., 1998, Chemical Sensors and Biosensors for Medical and Biological Applications, Wiley-VHC, Weinheim

[VanGent 1989] VanGent, J., Lambeck, P., Kreuwel, H., Gerritsma, G., Sudholter, E., Reinhoudt, D., and Popma, J., 1989, Chromoionophores in optical ion sensors, Sensors and Actuators, 17, 297-305

[VanGent 1990] VanGent, J., Lambeck, P.V., Kreuwel, H.J.M., Gerritsma, G.J., Sudholter, E.J.. Reinhoudt, D.N., and Popma, T.J.A., 1990, Optimization of a chenooptical surface plasmon resonance based sensor, Appl. Opts., 29, 2843-2849

[Vo-Dinh 1987] Vo-Dinh, T., Tromberg, B.J., Grifffin, G.D., Ambrose, K.R., Sepaniak, M.J., and Gardenhire, E.M., 1987, Antibody-based fiber-optics biosensor for the carcinogen benzo(a)pyrene, Appl. Spectrosc., 41, 735-738

[Walczak 1992] Walczak, I.M., Love, W.F., Cook, T.A., and Slovacek, R.E., 1992, Application of evanescent wave sensing to a high-sensitivity fluoroimmunoassay, Biosensors Bioelectron. 7, 39-48

[Weiss 1996a] Weiss, M.N., Srivastava, R., and Groger, H., 1996, Experimental investigation of a surface plasmon resonance-based integrated-optic humidity sensor, Electronics Letts, 32, 842-843

[Weiss 1996b] Weiss, M.N., Srivastava, R., Groger, H.P., 1996, Theoretical and experimental investigations of surface plasmon waveguide structures for sensing applications, Proc. of SPIE, 2695, 195-201

[Westenskow 1989a] Westenskow, D.R., Smith, K.W., Coleman, D.L., Gregonis, D.E., and Wagenen, R.A.V., 1989, Clinical evaluation of a Raman scattering multiple gas analyzer for the operating room, Anesthesiology, 70, 350-355

[Westenskow 1989b] Westenskow, D.R., Smith, K.W., Coleman, D.L., Gregonis, D.E., and Wagenen, R.A.V., 1989, First clinical evaluation of a Raman scattering gas analyzer, Annu. Meeting of the Am. Soc. Anesthesiology, 67-73

[Westenskow 1991] Westenskow, D.R., Silva, F.H., 1991, Laboratory evaluation of the vital signs (ICOR) piezoelectric anesthetic agent analyzer, J. Clin.Monit., 6,52-58

[Wolf 1979] Wolf, H.F., 1979, Handbook of fiber optics: theory and applications, New York: Garland STPM Press

[Wright 1989] Wright, N.A., Curbelo, R., Compton, D.A.C., and Hill, S.L., 1989, The use of mid-infrared optical fibers for analytical applications, in Infrared fiber Optics, Harrington, J.A., and Katzir, A.,eds., SPIE Proc., 2048, 153-161

[Wright 1995] Wright, J.D., Cado, A., Peacock, S.J., Rivalle, V., and Smith, A.M., 1995, Effects of nitrogen dioxide on surface plasmon resonance of substituted phthalocyanine films, Sensors and Actuators B, 29, 108-114

[Wu 1996] Wu, N., Song, H., Ceng, Y., Shan, J., and Zheng, X., 1996, Development of infrared monitor for anesthetic agent and carbon dioxide concentrations, Chinese J. of Biomedical Eng., 15, 81-85

[Xu 2000] Xu, Y., Jones, N.B., Fothergill, J.C., and Hanning, C.D., 2000, Analytical estimates of the characteristics of surface plasmon resonance fibre-optic sensors, J. of Mod. Optics, 47, 1099-1110

[Yager 1992] Yager, P. and Abrams, S. B., 1992, detection of volatile and soluble general anesthetics using a fluorescence-based fiber optic sensor: recent progress in chemical sensitivity and noise sources, Proc. of SPIE, 1648, 51-62

[Zhou 1988] Zhou, Q., Shahriari, M.R., Kritz, D., and Sigel, Jr. G.H., 1988, Porous fiber-optic sensor for high-sensitivity humidity Measurements, Anal. Chem., 60, 2317-2320

Poor quality text due to the nature of the material.

Image quality is best available.

Appendix 1

Yu Xu, N. Barrie Jones, John C. Fothergill and Chris D. Hanning, 1999, Theoretical analysis of the evanescent wave absorption coefficient for multimode fibre-optic evanescent wave absorption sensors, Journal of Modern Optics, Vol.46, No.14, pp.2007-2014

JOURNAL OF MODERN OPTICS, 1999, VOL. 46, NO. 14, 2007–2014

Theoretical analysis of the evanescent wave absorption coefficient for multimode fibre-optic evanescent wave absorption sensors

YU XU, N. BARRIE JONES, JOHN C. FOTHERGILL

Engineering Department, University of Leicester, Engineering Department, University of Leicester, University Road, Leicester LE1 7RH, UK. Tel: 0116-2522673, Fax: 0116-252619, Email: yx2@leicester.ac.uk

and CHRIS D. HANNING

Department of Anaesthesia, Leicester General Hospital, Leicester LES 4PW

(*Received 15 June 1999*)

Abstract. In an optical fibre of circular cross section, leaky skew rays transmit power in a different way from trapped and meridional rays. In this paper, a theoretical analysis of the evanescent wave absorption coefficient for leaky skew rays in multimode optical fibre evanescent wave absorption sensors is presented. Further, a comprehensive expression for the effective evanescent wave absorption coefficient is obtained. Some numerical results are given to illustrate this theoretical analysis. This work could be applied to optimize the design of fibre-optic evanescent wave absorption sensors.

1. Introduction

Fibre-optic evanescent wave absorption sensors, which use attenuated total internal reflection (ATIR) [1], have been studied in many applications over past decade [2–5]. The light wavelength employed has extended from the infrared [6, 7] and visible [8, 9] to near-ultraviolet [10, 11]. Theoretical evaluation of evanescent wave absorption has been attempted since the appearance of the sensor. Both electromagnetic field theory [12, 13] and geometric optics [14–16] have been used to build theoretical models for the explanation of experimental results. Because of its simplicity and effectiveness, geometric optics is playing an important role in the development of theoretical models. In the derivation of these models using geometric optics, Fresnel's law is applied, and only meridional or trapped rays have so far been considered. There is a class of weakly attenuated rays, so-called leaky rays, in an optical fibre of circular cross section. The behaviour of these leaky rays is incorrectly predicted by Fresnel's law [17, 18]. Many skew rays or tunnelling rays within a circular optical fibre, which geometric optics predicts are trapped by total internal reflection, are in fact leaky. These leaky skew rays which carry a significant proportion of the power have different transmission characteristics. When there is absorbing cladding, leaky skew rays contribute to

Journal of Modern Optics ISSN 0950–0340 print ISSN 1362–3044 online
http://www.tandf.co.uk/JNLS/mop.htm
http://www.taylorandfrancis.com/JNLS/mop.htm

evanescent wave absorption in a different way from that of other rays. In order to build an accurate theoretical model for evanescent wave absorption in fibre-optic sensors, it is necessary to analyse the transmission of these leaky skew rays in the optical fibre. In the following sections, we present a theoretical analysis of evanescent wave absorption of leaky skew rays under the weakly guided approximation.

2. The evanescent wave absorption coefficient

A random ray of wavelength λ incident at P on the interface of a multimode step-profile fibre of core diameter d, with n_1 and n_2 the refractive indices of the core and the cladding, respectively, is shown in figure 1. Relative to the normal PO, the angle of incidence or reflection is α. Both incident and reflected rays make angles θ_z with the axial direction PZ, and θ_Φ in the cross-section between the tangent PQ and the path projection, i.e. PR for the reflected ray.

The V value of the optical fibre is:

$$V = \frac{\pi d}{\lambda}(n_1^2 - n_2^2)^{1/2}. \tag{1}$$

Under the condition of a large core diameter optical fibre ($V \gg 1$), geometric optics is highly effective and useful, and is therefore used to analyse the evanescent wave absorption coefficient of both trapped and leaky skew rays.

In a circular optical fibre, due to the curvature of the fibre surface, there are three classes of ray, differentiated by the critical angle, $\theta_c(\cos\theta_c = n_2/n_1)$ [17, 18]:

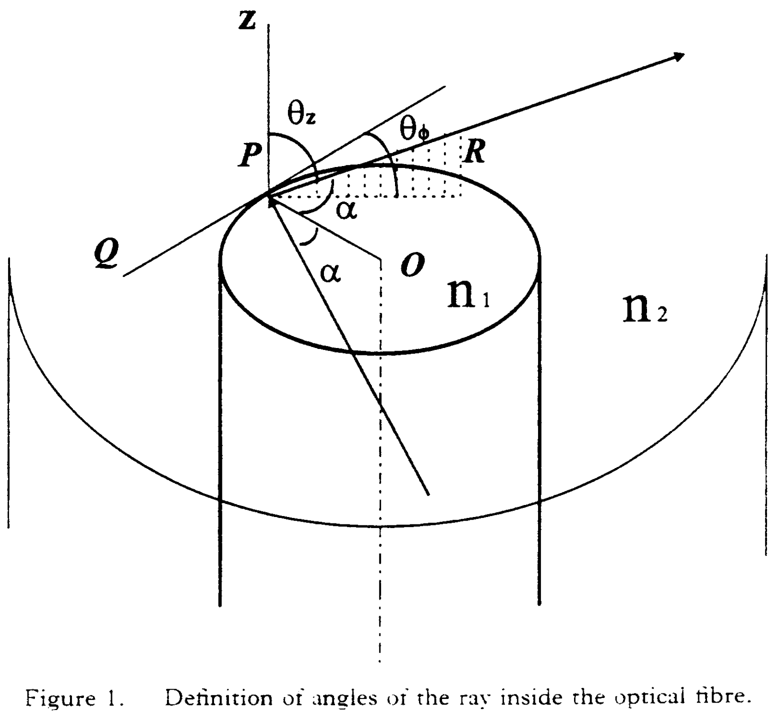

Figure 1. Definition of angles of the ray inside the optical fibre.

(i) trapped rays: $0 \leqslant \theta_z < \theta_c$;
(ii) refracted rays: $\alpha < (\pi/2 - \theta_c)$;
(iii) leaky skew rays: $\pi/2 \geqslant \theta_z > \theta_c$ and $\pi/2 \geqslant \alpha > (\pi/2 - \theta_c)$.

It is known that evanescent wave absorption is induced by the absorption of both trapped and leaky skew rays in the cladding medium. Evanescent wave absorption of trapped rays can be explained by the attenuated total internal reflection described by Fresnel's law. However, leaky skew rays are reflected in a different way.

If P_0 is the power transmitted by the optical fibre in the absence of an absorbing cladding, then the transmitted power in the presence of an absorbing medium is given by:

$$P(z) = P_0 \exp(-\gamma L) \tag{2}$$

where L is the length of the cladding absorbing medium and γ is an evanescent wave absorption coefficient.

2.1. *The evanescent wave absorption coefficient for trapped and meridional rays [14]*

We now proceed on the basis of Fresnel's law, and consider a multimode optical fibre with core diameter d. When the cladding has been replaced locally by an absorbing medium, the refractive index can be expressed as $n_2 = n_{cl} - in_2'$, and the bulk absorption coefficient of the absorption cladding medium at the employed wavelength is: $\alpha = 4\pi n_2'/\lambda$.

Under the condition of weak absorption ($n_{cl} \gg n_2'$), the evanescent wave absorption coefficient is given by Ruddy [14],

$$\gamma_m(\theta_z) = \frac{\alpha \lambda n_2 \sin^2 \theta_z}{\pi d \cos \theta_z [\cos^2 \theta_z - (n_2/n_1)^2]^{1/2} (n_1^2 - n_2^2)}. \tag{3}$$

2.2. *The evanescent wave absorption coefficient for leaky skew rays*

It is known by theory and experiment that the transmission behaviour of leaky skew rays is quite different from that of trapped rays [18]. Fresnel's law cannot predict the transmission of leaky skew rays correctly. For a weakly guided, large diameter optical fibre ($V \gg 1$), the power attenuation of leaky skew rays is expressed by equation (4) [17, 18].

$$\begin{aligned}
\gamma_s(\theta_z) &= \frac{4\theta_c}{d}\left(\frac{\theta_z}{\theta_c}\right)^2 \left[1 - \left(\frac{\theta_z}{\theta_c}\right)^2 \sin^2 \theta_\phi\right]^{1/2} \times \exp\left\{(-\tfrac{4}{3}\Gamma)\frac{[1 - (\theta_z/\theta_c)^2 \sin^2 \theta_\phi]^{3/2}}{(\theta_z/\theta_c)^2 - 1}\right\} \\
&= \left[\frac{n_1^2 - n_{cl}^2 - n_2'^2}{n_1(n_1^2 - n_2^2)^{1/2}} + i\frac{2n_{cl}n_2'}{n_1(n_1^2 - n_2^2)^{1/2}}\right] \times \frac{4}{d}\left(\frac{\theta_z}{\theta_c}\right)^2 \left[1 - \left(\frac{\theta_z}{\theta_c}\right)^2 \sin^2 \theta_\phi\right]^{1/2} \\
&\quad \times \exp\left\{(-\tfrac{4}{3}\Gamma)\frac{[1 - (\theta_z/\theta_c)^2 \sin^2 \theta_\phi]^{3/2}}{(\theta_z/\theta_c)^2 - 1}\right\}
\end{aligned} \tag{4}$$

where the definition of variables is as given in the previous sections.

In most applications of optical fibre sensors, where the transmission distance is short, this attenuation can be neglected. However, in the application of evanescent wave absorption sensors, when the cladding has mostly become an absorbing medium, this attenuation cannot be negligible. Such influence has been found and mentioned by many researchers [9, 19, 20].

Under the condition of weak absorption, from equation (4), the evanescent wave absorption coefficient, for leaky skew rays, induced by the absorbing cladding is obtained as:

$$\gamma_s(\theta_z) = \left[\frac{n_2'^2}{n_1(n_1^2 - n_2^2)^{1/2}}\right] \times \frac{4}{d}\left(\frac{\theta_z}{\theta_c}\right)^2\left[1 - \left(\frac{\theta_z}{\theta_c}\right)^2 \sin^2\theta_\phi\right]^{1/2}$$
$$\times \exp\left\{(-\tfrac{2}{3}V)\frac{[1-(\theta_z/\theta_c)^2\sin^2\theta_\phi]^{3/2}}{(\theta_z/\theta_c)^2 - 1}\right\}$$
$$= \left[\frac{\alpha^2\lambda^2}{4\pi^2 d n_1(n_1^2 - n_2^2)^{1/2}}\right] \times \left(\frac{\theta_z}{\theta_c}\right)^2\left[1 - \left(\frac{\theta_z}{\theta_c}\right)^2 \sin^2\theta_\phi\right]^{1/2}$$
$$\times \exp\left\{(-\tfrac{2}{3}V)\frac{[1-(\theta_z/\theta_c)^2\sin^2\theta_\phi]^{3/2}}{(\theta_z/\theta_c)^2 - 1}\right\}. \quad (5)$$

3. The effective evanescent wave absorption coefficient

In order to build a comprehensive theoretical model of evanescent wave absorption in fibre-optic sensors, both trapped and leaky skew rays have to be considered carefully, because leaky skew rays transmit a non-negligible proportion of power in the optical fibre. Under the weakly guided approximation, this proportion has been studied by Snyder [18], and is expressed as:

$$p = \frac{P_S}{P_S + P_T} = 1 - \frac{\sin^2\theta_c}{1 - \frac{2}{\pi}[(\delta - \delta^2)^{1/2} + (1 - 2\delta)\cos^{-1}\sqrt{\delta}]} \quad (6)$$

where $\delta = 1 - (n_2/n_1)^2$, p is the proportion of the power transmitted by leaky skew rays and P_S and P_T are powers transmitted by leaky skew rays and trapped rays, respectively. Under such consideration, the effective evanescent wave absorption coefficient γ_{eff} is given by:

$$\gamma_{eff} = \frac{\int_{\text{leaky skew ray}} s(\theta_z)\gamma_s(\theta_z)\,d\theta_z + \int_{\text{trapped ray}} s(\theta_z)\gamma_m(\theta_z)\,d\theta_z}{\int_{\text{trapped-leak skew ray}} s(\theta_z)\,d\theta_z} \quad (7)$$

where $s(\theta_z)$ represents the power distribution of the rays and integrations are performed according to different classes of rays.

Equation (7) is an accurate expression for the effective evanescent wave absorption coefficient, and can be used to predict evanescent wave absorption correctly. On the other hand, leaky skew ray illumination conditions can be constructed easily [21].

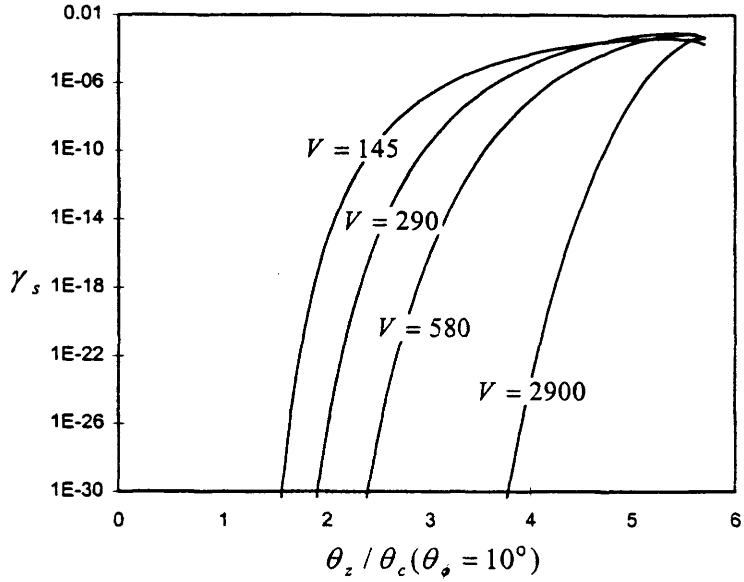

Figure 2. Evanescent wave absorption coefficinet at $\theta_\phi = 10°$.

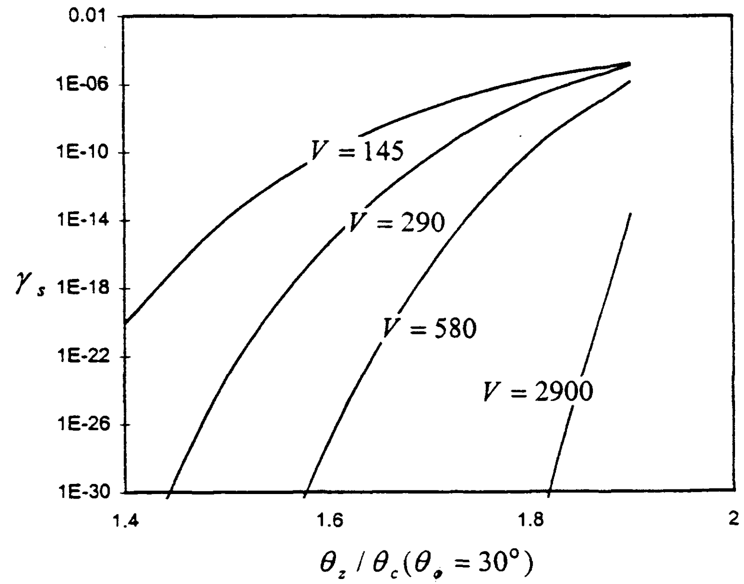

Figure 3. Evanescent wave absorption coefficient at $\theta_\phi = 30°$.

4. Numerical results and discussions

Trapped and meridional rays have been studied before [14]. In this section, our numerical calculations and discussions will be concentrated on the evanescent wave absorption of leaky skew rays. The parameters used in these numerical calculations are $n_1 = 1.457$, $n_2 = 1.335$, $\lambda = 0.6328\,\mu m$, $d = 100\,\mu m$, and $\alpha = 100\,cm^{-1}$.

Figures 2 and 3 show the numerical results of evanescent wave absorption against incident angle θ_z at $\theta_\phi = 10°$ and $\theta_\phi = 30°$, respectively.

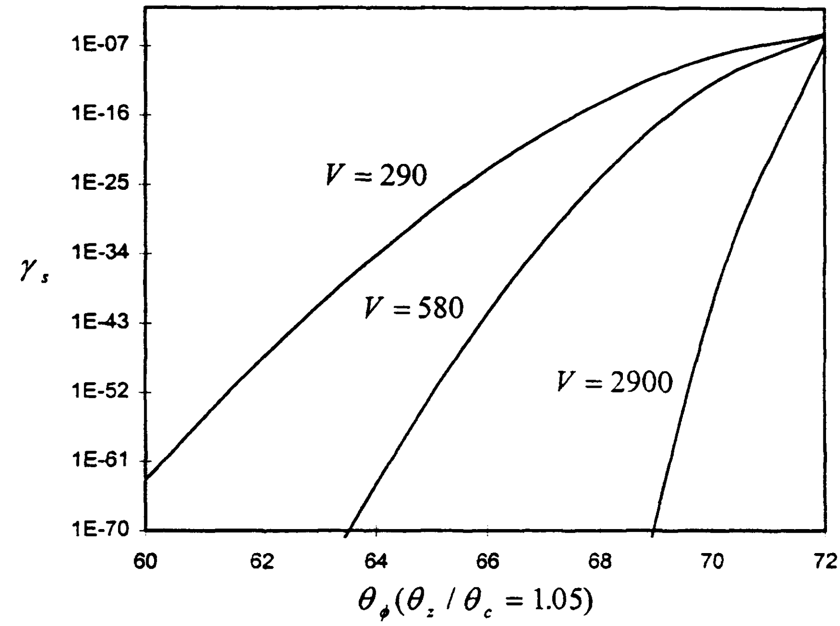

Figure 4. Evanescent wave absorption coefficient at $\theta_z/\theta_c = 1.05$.

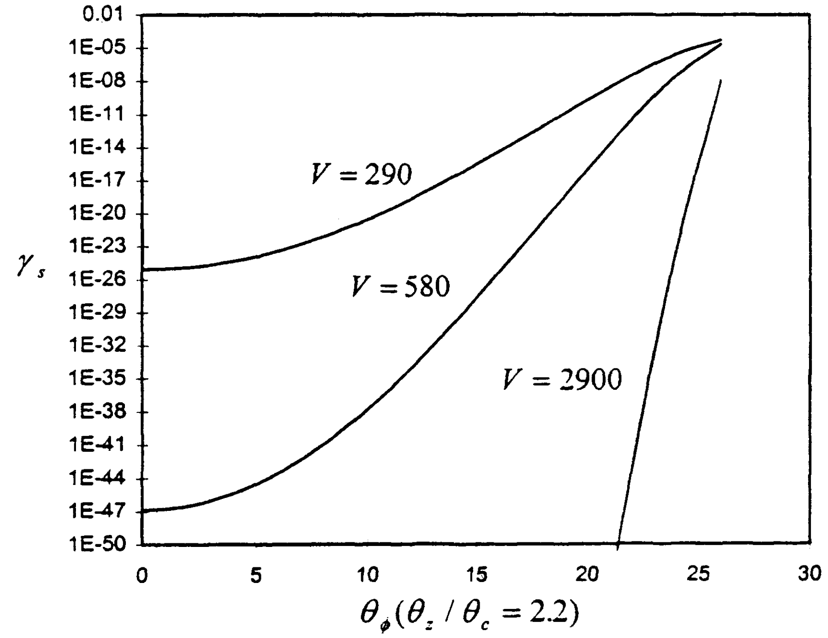

Figure 5. Evanescent wave absorption coefficinet at $\theta_z/\theta_c = 2.2$.

Figures 4 and 5 show the numerical results of evanescent wave absorption against θ_ϕ at certain incident angles $\theta_z/\theta_c = 1.05$ and $\theta_z/\theta_c = 2.2$, respectively.

Figure 6 shows the comparison of the evanescent wave coefficient between meridional and leaky skew rays when $V = 290$ and $\theta_z = 10°$.

From the above-mentioned equations, it can be seen that the evanescent wave absorption coefficient changes with the incident angle θ_z, θ_ϕ and V. The critical

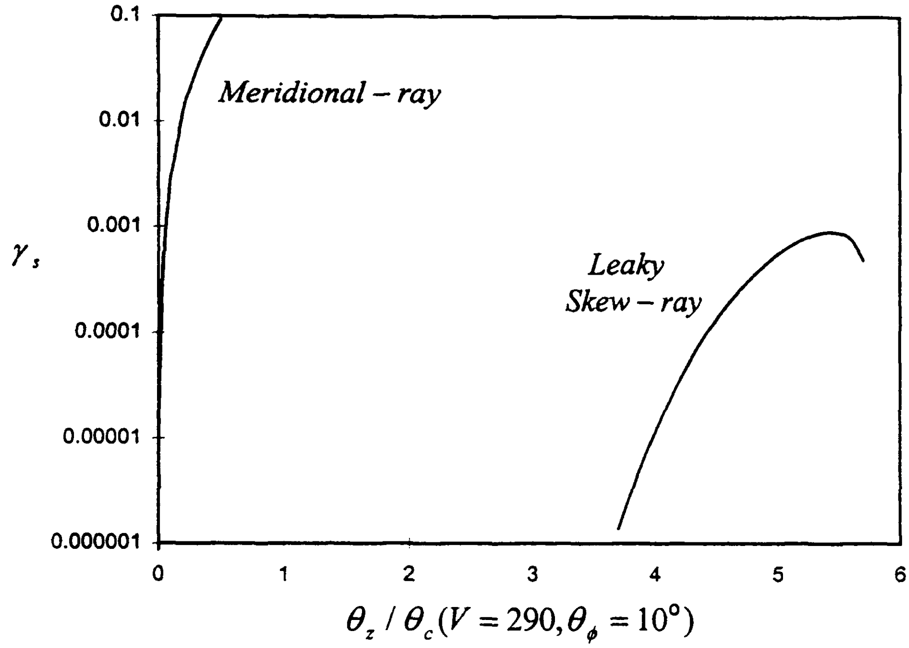

Figure 6. Evanescent wave absorption coefficient for meridional and leaky skew rays.

angle (total reflection angle) of leaky skew rays is determined not only by n_1, n_2 (that is θ_c), but also by the skewness of the ray, θ_ϕ, in the formulation of $\theta_z \sin\theta_\phi = \theta_c$. With increase of V, the absorption decreases significantly (the same as the behaviour of meridional rays). The skewness of leaky skew rays, θ_ϕ, together with θ_z, also plays an important role in evanescent wave absorption.

Stronger evanescent wave absorption for leaky skew rays occurs near to the critical angle. The main difference between trapped and meridional rays is that leaky skew rays are distributed over a wider range, normally a few times θ_c, although they have less absorption. Trapped rays occur only within the critical angle predicted by Fresnel's law, i.e. less than θ_c. Under some circumstances and designs these leaky skew rays could carry a large proportion of the transmitted power, and the evanescent wave absorption induced by the leaky skew rays could be important. Figure 6 shows the comparison of evanescent wave absorption between meridional rays and leaky skew rays. Although the evanescent wave absorption coefficients for meridional rays are larger, they are only significant over a relatively smaller range of angles—less than the critical angle θ_c. For leaky skew rays, they are smaller, but their influence covers a larger angle range. That is the reason why in some applications the evanescent wave absorption of leaky skew rays should be involved in the quantitative explanation of the experimental results.

5. Conclusions

Leaky skew rays have a unique behaviour in transmission and evanescent wave absorption in optical fibres. As with trapped or meridional rays, the contribution to the evanescent wave absorption of leaky skew rays changes with variation in the incident angle θ_z and V. But the skewness of the leaky skew ray θ_ϕ is another important factor for evanescent wave absorption. A wider angle range (a few times the critical angle θ_c) of leaky skew rays can induce evanescent wave absorption. Based on our analysis, a comprehensive expression for evanescent wave absorption has been derived which can be solved easily by numerical calculation. This analysis and calculation will allow optimization of the design of optical fibre evanescent wave absorption sensors.

Acknowledgments

This work is supported in part by CVCP Overseas Research Scholarship Scheme and Astra-Zeneca Limited.

References

[1] Harrick, N. J., 1967, *Internal Reflection Spectroscopy* (New York: Wiley).
[2] Messica, A., Greenstein, A., and Katzir, A., 1994, *Appl. Opt.* **19,** 1167.
[3] Schwotzer, G., Latka, I., Lehmann, H., and Willsch, R., 1997, *Sensors and Actuators*, **B38-39,** 150.
[4] Paul, P. H., and Kychakoff, G., 1987, *Appl. Phys. Lett.*, **51,** 12.
[5] Simhony, S., Schnitzer, I., Katzir, A., and Kosower, E. M., 1988, *J. appl. Phys.*, **64,** 3732.
[6] Jakusch, M., Mizaikoff, B., Kellner, R., and Katzir, A., 1997, *Sensors and Actuators*, **B38,** 83.
[7] Regan, F., MacCraith, B. D., Walsh, J. E., Odwyer, K., Vos, J. G., and Meaney, M., 1997, *Vib. Spectrosc.*, **14,** 239.
[8] DeGrandpre, M. D., and Burgess, L. W., 1988, *Anal. Chem.*, **60,** 2582.
[9] Deboux, B. J. C., Lewis, E., Scully, P. J., and Edwards, R. J., 1995, *J. Lightwave Technol.*, **13,** 1407.
[10] Potyrailo, R. A., Hobbs, S. E., and Hieftje, G. M., 1998, *Anal. Chem.*, **70,** 1639.
[11] Merschman, S. A., and Tilotta, D. C., 1998, *Appl. Spectrosc.*, **52,** 106.
[12] Piraud, C., Mwarania, E. K., Yao, J., O'Dwyer, K., Schiffrin, D. J., and Wilkinson, J. S., 1992, *J. Lightwave Technol.*, **10,** 693.
[13] Qing, D. K., Chen, X. M., Itoh, K., and Murabayashi, M., 1996, *J. Lightwave Technol.*, **14,** 1907.
[14] Ruddy, V., 1990, *Fiber Integrated Opt.*, **9,** 142.
[15] Schnitzer, I., and Katzir, A., 1990, *Mater. Sci. Eng.*, **B5,** 333.
[16] Gupta, B. D., and Singh, C. D., 1994, *Fiber Integrated Opt.*, **13,** 433.
[17] Snyder, A. W., and Mitchell, D. J., 1974, *J. opt. Soc. Am.*, **64,** 599.
[18] Snyder, A. W., Mitchell, D. J., and Pask, C., 1974, *J. opt. Soc. Am.*, **64,** 608.
[19] Messica, A., Greenstein, A., and Katzir, A., 1996, *Appl. Opt.*, **13,** 2274.
[20] Gupta, B. D., Singh, C. D., and Sharma, A., 1994, *Opt. Eng.*, **33,** 1864.
[21] Reick, F. G., 1965, *Appl. Opt.*, **4,** 1395.

Appendix 2

Yu Xu, N. Barrie Jones, John C. Fothergill and Chris D. Hanning, 2000, Analytical estimates of the characteristics of surface plasmon resonance fibre-optic sensors, Journal of Modern Optics, Vol.47, No.6, pp.1099-1110

JOURNAL OF MODERN OPTICS, 2000, VOL. 47, NO. 6, 1099–1110

Analytical estimates of the characteristics of surface plasmon resonance fibre-optic sensors

YU XU†, N. BARRIE JONES†, JOHN C. FOTHERGILL† and CHRIS D. HANNING‡

† Engineering Department, University of Leicester, Leicester LE1 7RH, UK

‡ Department of Anaesthesia, Leicester General Hospital, Leicester LE5 4PW, UK

(*Received 6 September 1999; revision received 12 November 1999*)

Abstract. In surface plasmon resonance (SPR) fibre-optic sensors, the optical power transmittance is important in determining behaviour. In this paper numerical calculations are used to estimate the optical power transmittance of SPR fibre-optic sensors. These analytical estimations can be applied in SPR fibre-optic sensors both with a transducing layer and without a transducing layer. The results of these numerical calculations agree well with previously published experimental results. This work will aid in the design of SPR fibre-optic sensors in terms of geometrical structure, materials and dynamic range as well as allowing the prediction of performance and of limitations of the design.

1. Introduction

Light surface plasmon resonance (SPR) excitation, as a useful and sensitive method, has been studied in chemical and biochemical sensing applications [1–3] for more than two decades. Commercial products based on bulk-optic SPR technology have been successfully exploited by Biacore, Quantech and Texas Instruments. With the development of fibre-optic sensing technology, SPR fibre-optic sensors have received a great deal of attention by researchers in recent years [4–7], particularly because of the extra advantages of small size of the fibre-optic probe and the growing need for remote sensing. In addition, due to the characteristics of the optical fibre, SPR fibre-optic sensors have different characteristics from SPR bulk-optic sensors, such as, no angle scanning is needed and multiple wavelength light sources can be used together with a spectrometer for recording the spectrum.

Theoretical models for the analysis of light SPR excitation in bulk optics have been well developed by many researchers [8–14]. These theoretical models have been used to explain experimental results and to design SPR bulk-optic systems. In the multi-mode optical fibre which is used in many SPR fibre-optic sensors, there are many guided modes transmitted—each mode transmits the light ray at one particular angle of internal reflection. Theoretical models for SPR bulk-optic systems can only be applied to the individual ray of each mode in multi-mode optical fibres. For SPR fibre-optic sensors, a comprehensively theoretical analysis,

Journal of Modern Optics ISSN 0950–0340 print ISSN 1362–3044 online © 2000 Taylor & Francis Ltd
http://www.tandf.co.uk/journals/tf/09500340.html

which considers the contributions of all possible transmitted modes, has not been studied systematically. In this paper, based on the theoretical analysis of the optical power transmittance using numerical calculations, the characteristics of SPR multi-mode fibre-optic sensors are predicted and discussed.

2. Basic theory

Figure 1 shows the meridional cross-section of the sensing element of the SPR fibre-optic sensor. A multi-mode optical fibre, with core diameter d and refractive index n_2 (dielectric permittivity ε_2), has the jacket and the cladding removed to expose the core, on which is symmetrically deposited a metal film of thickness d_1 and dielectric permittivity ε_1. In some applications, the metal film is directly in contact with the sample to be measured with dielectric permittivity ε_0, in others, a dielectric isotropic transducing layer with thickness d_3 and dielectric permittivity ε_3 is deposited symmetrically outside the metal film. For generality, in this paper all formulations are derived including this transducing layer. The sensors without transducing layers are considered as a special case by setting $d_3 = 0$.

In multi-mode optical fibre sensors, due to the easiness and effectiveness of describing the behaviour, meridional rays are often used to build up approximate models. Further, in SPR fibre-optic sensors, the theoretical models of SPR for bulk optics are satisfied by meridional rays in optical fibres. Therefore, the theoretical analysis of optical power transmittance in SPR fibre-optic sensors in the following is based on meridional rays.

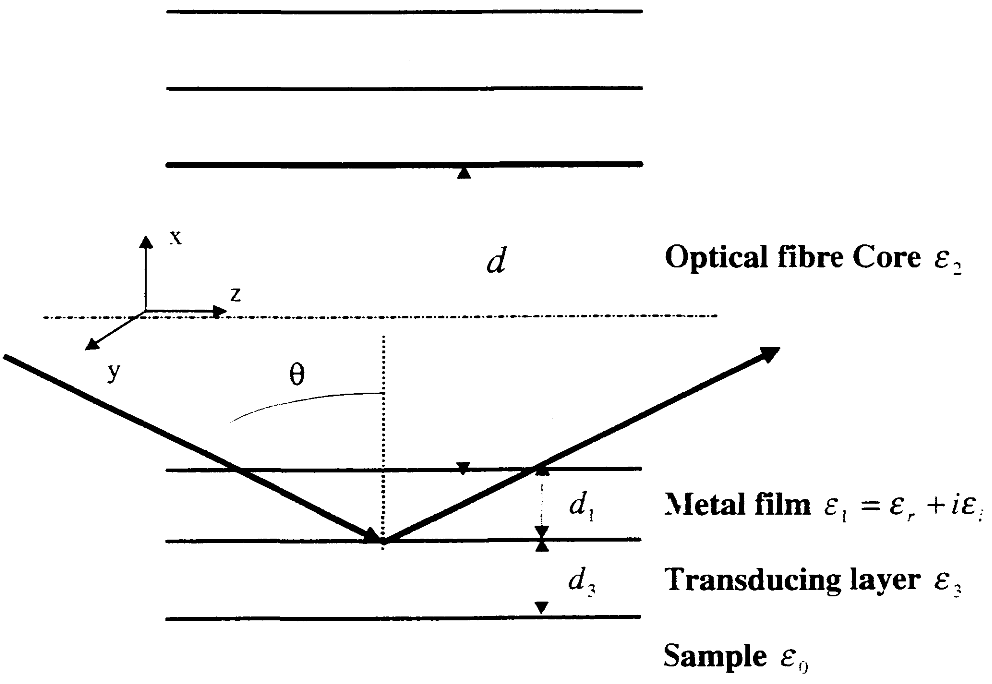

Figure 1. The meridonial cross-section of the sensing element of the fibre-optic SPR sensor.

Considering a ray of light transmitted in an optical fibre with incident angle θ with respect to the normal of a core–metal interface, the electric field **E** of the SPR propagating in the z direction is expressed [15] as:

$$E_x(x, z, t) = E_x^0(x) \exp(\mathrm{i}\omega t - \mathrm{i}k_z z). \tag{1}$$

where E_x^0 is the field amplitude, ω is the angular frequency, $k_z = k_z^r + \mathrm{i}k_z^i$ is the SPR complex propagation constant along the z direction, with k_z^r as the real part and k_z^i as the imaginary part.

The resonance condition, under which the propagation constant of the incident light beam in the z direction is equal to the real part of the SPR propagation constant, is expressed as:

$$k_z^r = k(\varepsilon_2)^{1/2} \sin\theta_{\mathrm{SP}} = \frac{2\pi}{\lambda} n_2 \sin\theta_{\mathrm{SP}}. \tag{2}$$

where k is the propagation constant of the incident light beam and θ_{SP} is the resonance angle.

Considering the structure of the SPR sensing element in SPR fibre-optic sensors shown in figure 1, the SPR propagation constant is accurately expressed [9, 10, 16] as:

$$k_z = k^0 + k^{\mathrm{R}} + k^{\mathrm{T}}. \tag{3}$$

$$k^0 = \left(\frac{\varepsilon_0\varepsilon_1}{\varepsilon_0 - \varepsilon_1}\right)^{1/2} \frac{\omega}{c}. \tag{4}$$

$$k^{\mathrm{R}} = k^0 \left(\frac{2}{\varepsilon_0 - \varepsilon_1}\right)\left(\frac{\varepsilon_0\varepsilon_1}{\varepsilon_0 - \varepsilon_1}\right)^{3/2} \exp\left[\mathrm{i}\frac{4\pi d_1}{\lambda}\frac{\varepsilon_1}{(\varepsilon_0 - \varepsilon_1)^{1/2}}\right]. \tag{5}$$

$$k^{\mathrm{T}} = \mathrm{i}\left(\frac{2\pi d_3}{\lambda}\right)\left(\frac{\omega}{c}\right)\left(\frac{\varepsilon_0\varepsilon_1}{\varepsilon_0 - \varepsilon_1}\right)^2 \frac{1}{(\varepsilon_0\varepsilon_1)^{1/2}(\varepsilon_0 - \varepsilon_1)}\left(\varepsilon_3 - \frac{\varepsilon_0\varepsilon_1}{\varepsilon_3} - \varepsilon_1 - \varepsilon_0\right). \tag{6}$$

k^0 expresses the dispersion relation of SPR of a metal–vacuum interface in a one-sharp-boundary model, k^{R} expresses the perturbation to k^0 due to the finite physical volume of the optical fibre and k^{T} expresses the modification to k^0 due to the transducing layer.

It is known that light rays with a range of incident angles are allowed to propagate in the multi-mode optical fibre. The range is determined by the numerical aperture of the fibre, $NA = n_2 \cos\theta_c = (n_2^2 - n_3^2)^{1/2}$. Only rays with $\theta > \theta_c$ (critical angle) can be transmitted in the optical fibre. The resonance condition in SPR fibre-optic sensors should involve the contribution from all rays transmitted in optical fibres, which have a range of incident angles $(\theta_c, 90^\circ)$. Hence the resonance condition, in SPR fibre-optic sensors, is expressed as:

$$k_z^r = \frac{2\pi n_2}{\lambda_{\mathrm{SP}}} \frac{\int_{\theta_c}^{90^\circ} p(\theta) sin\theta \, \mathrm{d}\theta}{\int_{\theta_c}^{90^\circ} p(\theta) \, \mathrm{d}\theta}. \tag{7}$$

where $p(\theta)$ represents the power distribution of light sources.

This resonance condition decides a resonance wavelength λ_{SP}, which corresponds to the resonance angle θ_{SP} in bulk optics.

There are two main sorts of essential power distributions of light sources in fibre-optic sensors.

(1) Diffuse or Lambertian source (such as a LED), which is butted against the optical fibre end face and its surface covers at least some of the core cross-section. The power distribution is expressed [17, 18] as:

$$p(\theta) \propto n_2^2 \sin\theta \cos\theta. \tag{8}$$

(2) Collimated source (such as a laser) using a microscope objective such that the beam is focused onto the optical fibre end face at the axial point, the power distribution is expressed [18, 19] as:

$$p(\theta) \propto \frac{n_2^2 \sin\theta \cos\theta}{(1 - n_2^2 \cos^2\theta)^2}. \tag{9}$$

In this paper a very important characteristic, the optical power transmittance of SPR fibre-optic sensors, is discussed. Other characteristics, such as the influence of k^R and k^T terms, especially in the sensitivity of SPR fibre-optic sensors will be discussed in another paper.

Under the approximation of using meridional rays of the optical fibre, intensity reflection coefficient $r(\theta)$ at the interface of the metal film and the optical fibre core can use the result for the SPR bulk-optic system, which is expressed as [1, 16]:

$$r(\theta) = |r_{210}|^2 = \left|\frac{r_{21} + r_{130}\exp(2ik_1 d_1)}{1 + r_{21} r_{130}\exp(2ik_1 d_1)}\right|^2. \tag{10}$$

where

$$r_{21} = \frac{z_{21}}{n_{21}},$$

$$r_{130} = \frac{z_{10} - iz_{43}\tan(k_3 d_3)}{n_{10} - in_{43}\tan(k_3 d_3)},$$

$$z_{ij} = k_i\varepsilon_j - k_j\varepsilon_i,$$

$$n_{ij} = k_i\varepsilon_j + k_j\varepsilon_i,$$

$$k_i = \left[\varepsilon_i\left(\frac{2\pi}{\lambda}\right)^2 - k^2\right]^{1/2},$$

$$k = \left(\frac{2\pi}{\lambda}\right) n_2 \sin\theta,$$

$$\varepsilon_4 = \frac{\varepsilon_0\varepsilon_1}{\varepsilon_3},$$

$$k_4 = \frac{k_0 k_1}{k_3}, \quad i, j = 1, 2, 3, 4.$$

A light ray transmitted in the multi-mode optical fibre, with incident angle θ (shown in figure 1), will have N multi-reflections in length L of the SPR sensing element. The number N is expressed as:

$$N = \frac{L}{d \tan \theta}. \tag{11}$$

Considering the contributions of all rays and multi-reflections, the reflectance R_λ in SPR fibre-optic sensors is expressed as:

$$R_\lambda = \frac{\int_{\theta_c}^{90^\circ} p(\theta) r^N(\theta)\, d\theta}{\int_{\theta_c}^{90^\circ} p(\theta)\, d\theta}. \tag{12}$$

In multi-mode optical fibres, both TE (transverse electric) and TM (transverse magnetic) polarized light with respect to the core–metal interface are allowed to propagate. Only half of the transmitted optical power contributes to the SPR excitation, since SPR can only be excited with TM polarized light [13, 17].

Thus, the optical power transmittance of SPR fibre-optic sensors is expressed as:

$$T = \frac{I_{TE} + R_\lambda I_{TM}}{I_{TE} + I_{TM}}. \tag{13}$$

where I_{TE} and I_{TM} represent the transmitted optical power of TE and TM polarized light, respectively. Under the condition that $I_{TE} = I_{TM}$, the optical power transmittance simplifies to:

$$T = \frac{1 - R_\lambda}{2}. \tag{14}$$

3. Illustrative numerical calculations

In SPR fibre-optic sensors, the optical power transmittance is measured via its spectrum which has a resonance at wavelength λ_{SP} where there is minimum transmittance.

In the numerical calculations of this section, the parameters of the optical fibre used in calculations are: $d = 400\,\mu m$, $n_2 = 1.515$ and $NA = 0.3$. The power distribution of the light source is diffuse or Lambertian source, expressed in equation (8).

In figure 2, the + curve represents the case of the refractive index of the sample $n_0 = 1.4$, the × curve represents $n_0 = 1.41$ and the ○ curve represents $n_0 = 1.42$. The continuous curve represents the normalized transmitted optical power of only one light ray with specified angle $\theta = 80^\circ$, suffering only one reflection, $n_0 = 1.4$, which simulates the bulk-optic SPR. Due to the numerical aperture, there is a range of angle of light rays able to travel in the optical fibre. The contribution of all rays broadens the spectrum of the transmitted optical power in SPR fibre-optic sensors, and, because of multi-reflections inside the optical fibre, which lead to more absorption, the minimum transmittance decreases, compared with that in bulk-optic SPR absorption.

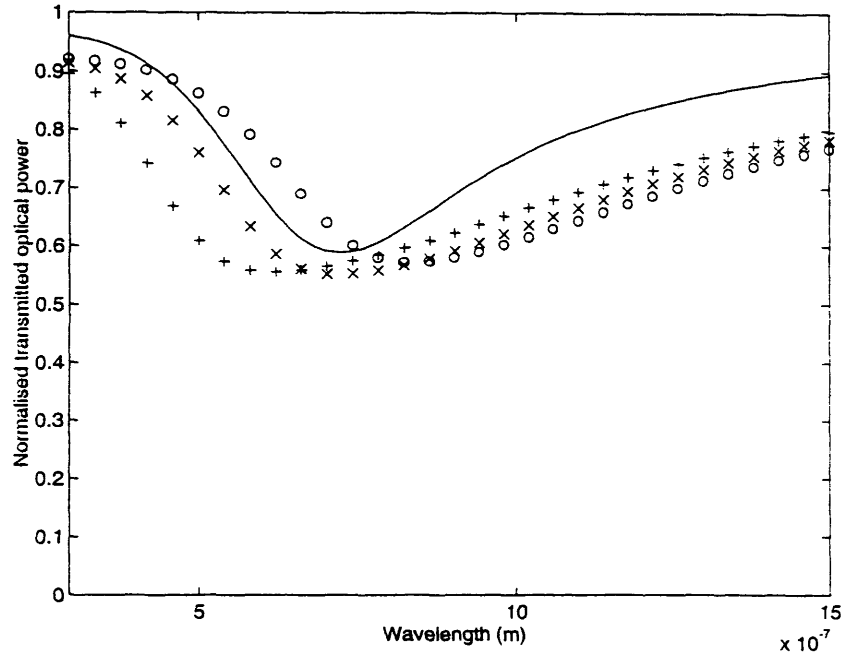

Figure 2. Normalized transmitted optical power of the SPR fibre-optic sensor without a transducing layer, i.e. $d_3 = 0$, gold as the SPR supporting metal, with $\varepsilon_1 = -13.2 - 1.25i$, length $L = 10$ mm and thickness $d_1 = 40$ nm. The refractive index of the sample to be measured changes.

In figure 3, + represents the case of the thickness of the SPR supporting metal $d_1 = 30$ nm, × represents $d_1 = 40$ nm, o represents $d_1 = 50$ nm and * represents $d_1 = 200$ nm. When the thickness of the SPR supporting metal is large enough, there is no SPR excitation, the optical power of all wavelengths will be reflected almost at the same reflectance, and there is zero sensitivity in this case.

In figure 4, + represents the case of the length of sensing element $L = 5$ mm, × represents $L = 10$ mm, o represents $L = 20$ mm and * represents $L = 50$ mm. Due to an increased number of reflections, the minimum transmittance decreases with increasing length of sensing element L. When the length is long enough, optical power of all wavelengths will be absorbed, and there is zero sensitivity in this case.

In figure 5, the – curve represents the case of the refractive index of the sample $n_0 = 1.0$, the × curve represents $n_0 = 1.05$ and the o curve represents $n_0 = 1.1$. The continuous curve represents the normalized transmitted optical power of only one ray with specified angle $\theta = 80°$, suffering only one reflection, $n_0 = 1.0$, which simulates the bulk-optic SPR. Again because of the numerical aperture, there is a range of angle of light rays which can be transmitted in an optical fibre. The contribution of all such rays broadens the spectrum of the transmitted optical power in SPR fibre-optic sensors, and because of multi-reflections inside the optical fibre which lead to more absorption, the minimum transmittance decreases, compared with that of bulk-optic SPR sensors. This behaviour is the same as in SPR fibre-optic sensors without a transducing layer.

In figure 6, + represents the case of the thickness of the SPR supporting metal $d_1 = 35$ nm, × represents $d_1 = 45$ nm, o represents $d_1 = 55$ nm and * represents $d_1 = 200$ nm. When the thickness of the SPR supporting metal is large enough,

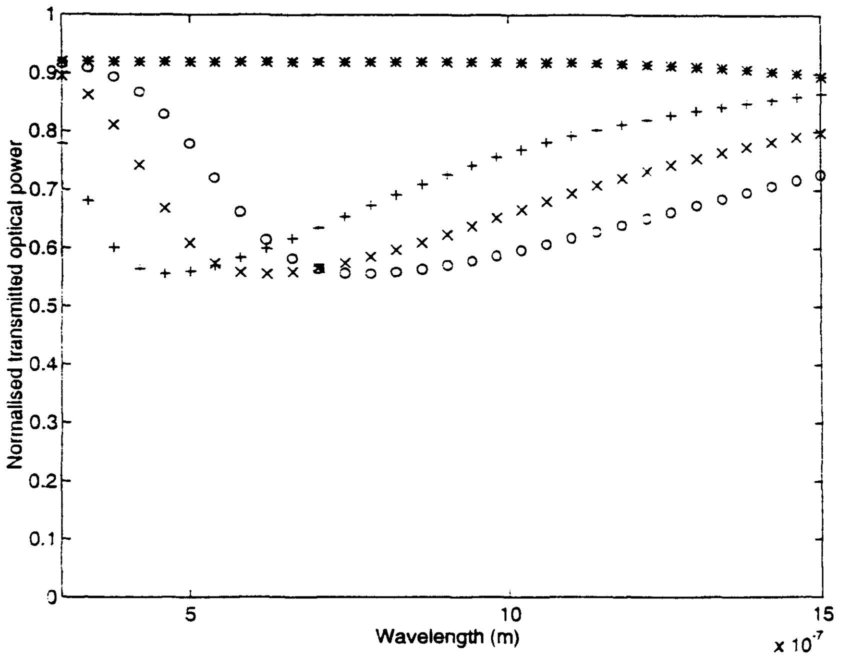

Figure 3. Normalized transmitted optical power of the SPR fibre-optic sensor without a transducing layer, i.e. $d_3 = 0$, gold as the SPR supporting metal, with $\varepsilon_1 = -13.2 + 1.25i$ and length $L = 10\,\text{mm}$. The refractive index of the sample $n_0 = 1.4$. The thickness of the SPR supporting metal d_1 changes.

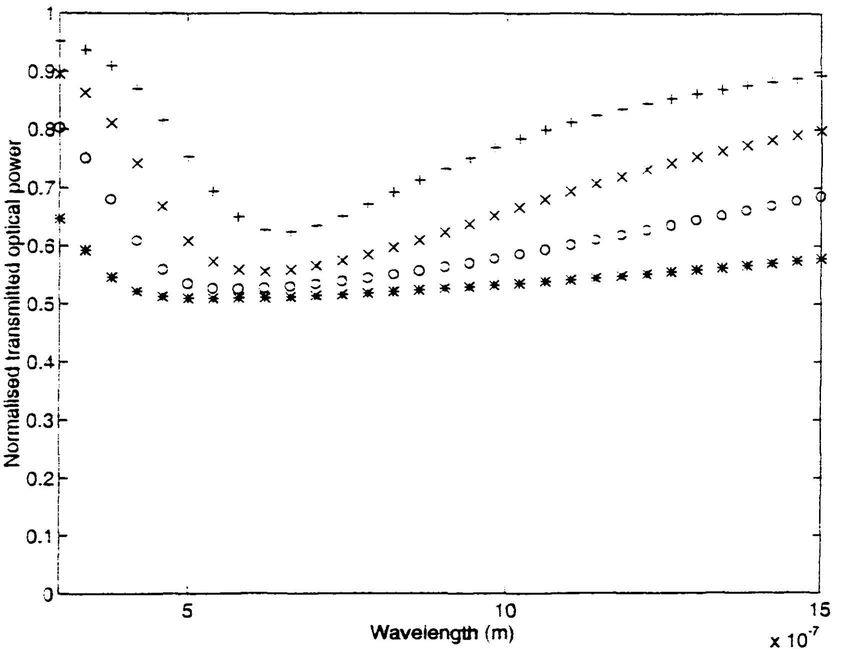

Figure 4. Normalized transmitted optical power of the SPR fibre-optic sensor without a transducing layer, i.e. $d_3 = 0$, gold as the SPR supporting metal, with $\varepsilon_1 = -13.2 - 1.25i$ and thickness $d_1 = 40\,\text{nm}$. The refractive index of the sample $n_0 = 1.4$. The length of the sensing element L changes.

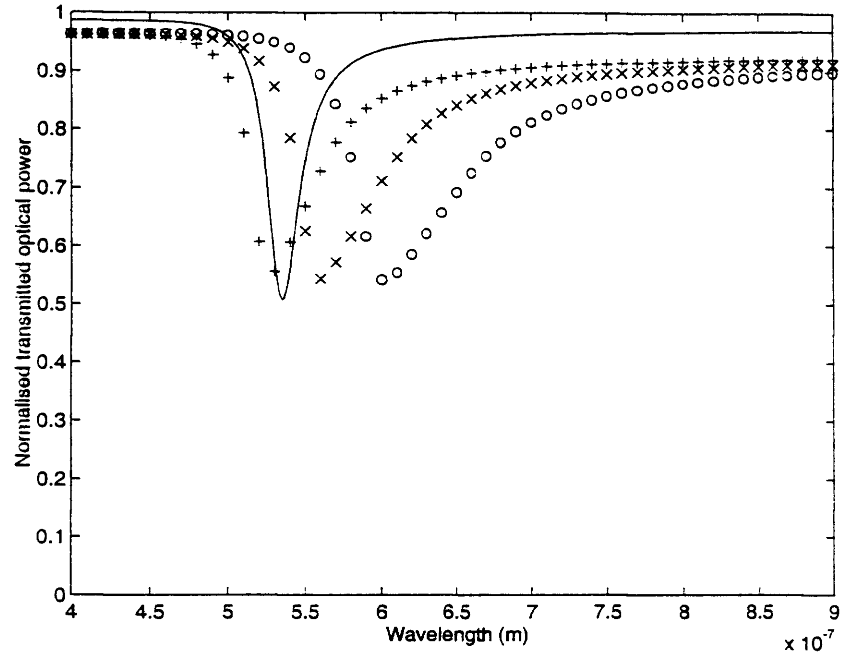

Figure 5. Normalized transmitted optical power of the SPR fibre-optic sensor, using zirconium oxide as the transducing layer, with $\varepsilon_3 = n_3^2 = 4.0$, thickness $d_3 = 40$ nm, silver as the SPR supporting metal, with $\varepsilon_1 = -17 - 0.6i$, thickness $d_2 = 45$ nm and length $L = 10$ mm. The refractive index of the sample to be measured changes.

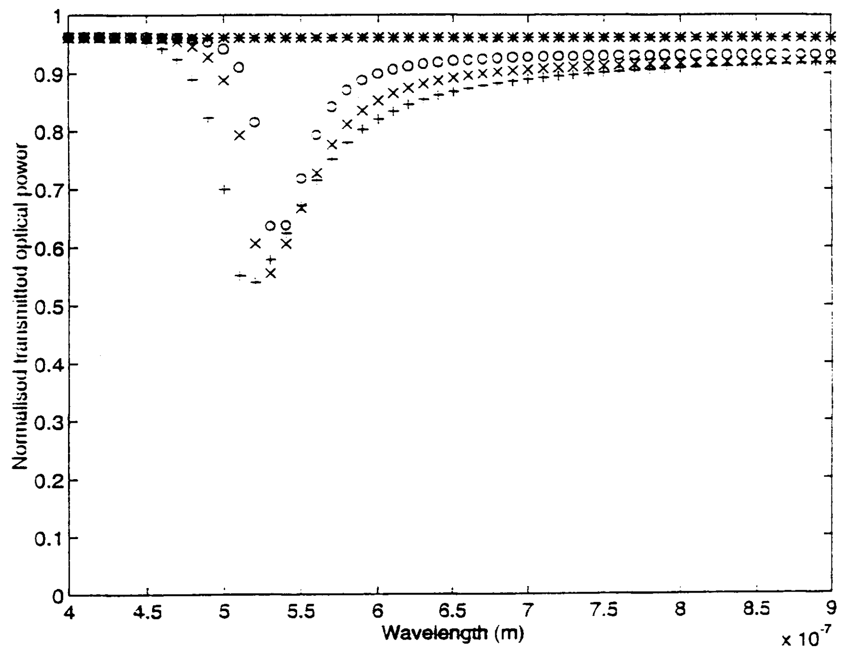

Figure 6. Normalized transmitted optical power of the SPR fibre-optic sensor, using zirconium oxide as the transducing layer with $\varepsilon_3 = n_3^2 = 4.0$, thickness $d_3 = 40$ nm, silver as the SPR supporting metal, with $\varepsilon_1 = -17 - 0.6i$, and the length of sensing element $L = 10$ mm. The refractive index of the sample $n_0 = 1.0$. The thickness of SPR supporting metal changes.

there is no SPR excitation, the optical power of all wavelengths will be reflected at the same reflectance, and there is zero sensitivity in this case as well. This is also the same as that in SPR fibre-optic sensors without the transducing layer.

In figure 7, + represents the case of the thickness of the SPR supporting metal $d_3 = 35$ nm, × represents $d_3 = 45$ nm and ○ represents $d_3 = 55$ nm. When the thickness of the transducing layer changes, the SPR resonance wavelength is shifted.

In figure 8, the + curve represents the case of the refractive index of the transducing layer $n_3 = 1.95$, the × curve represents $n_3 = 2.0$ and the ○ curve represents $n_3 = 2.05$. The SPR resonance wavelength is shifted by the change of the refractive index of the transducing layer.

In figure 9, + represents the case of the length of the sensing element $L = 5$ mm, × represents $L = 20$ mm, ○ represents $L = 50$ mm and * represents $L = 200$ mm. Due to a greater number of reflections, the minimum transmittance decreases with increase of the length of the sensing element L. When the length is long enough, optical power of all wavelengths will be absorbed, giving zero sensitivity in this case. Compared with SPR fibre-optic sensors without the transducing layer, the length needed for full absorption in all wavelengths is greater, since the transmitted optical power spectrum is narrower.

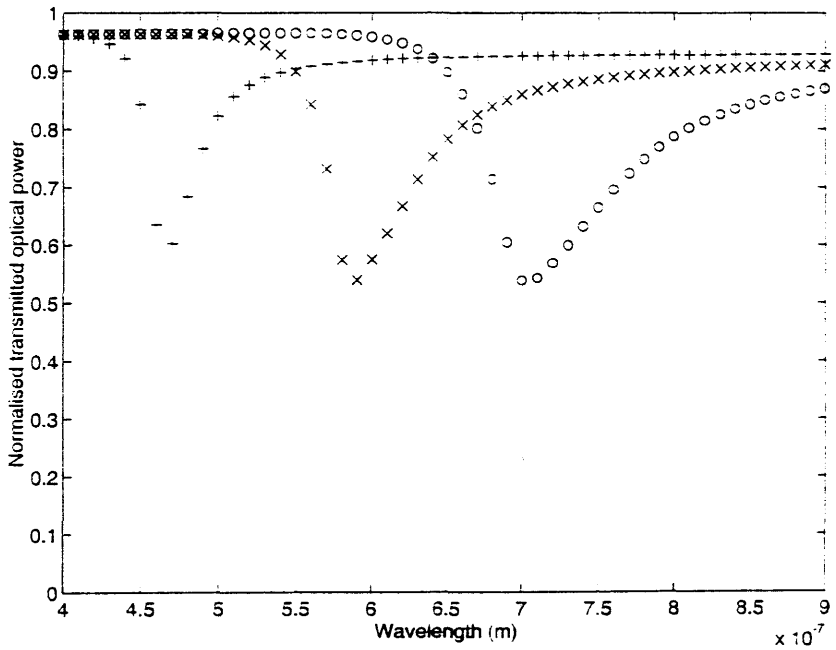

Figure 7. Normalized transmitted optical power of the SPR fibre-optic sensor, using zirconium oxide as the transducing layer with $\varepsilon_3 = n_3^2 = 4.0$, silver as the SPR supporting metal, with $\varepsilon_2 = -17 + 0.6i$, with the thickness $d_1 = 45$ nm and the length of the sensing element $L = 10$ mm. The refractive index of the sample $n_0 = 1.0$. The thickness of the transducing layer d_3 changes.

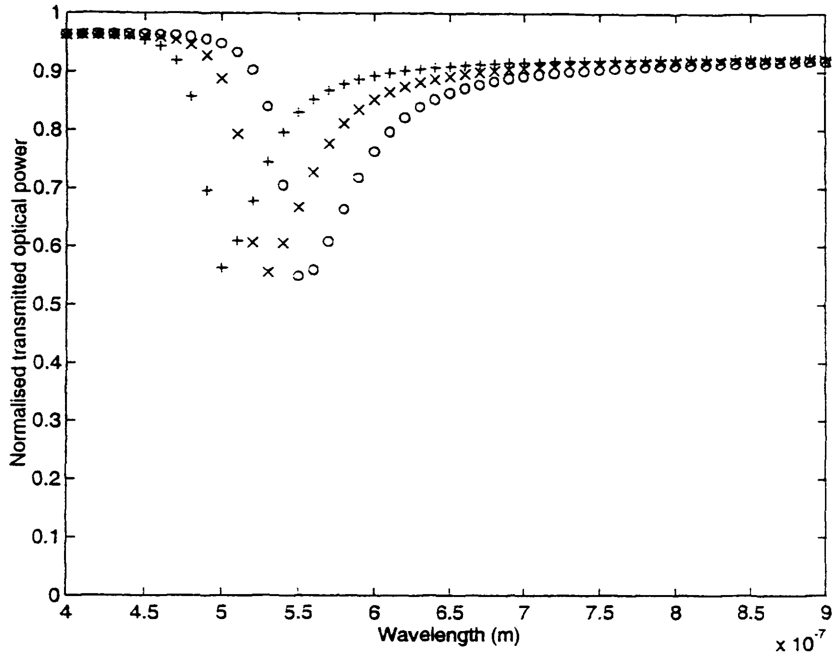

Figure 8. Normalized transmitted optical power of the SPR fibre-optic sensor, silver as the SPR supporting metal, with $\varepsilon_1 = -17 + 0.6i$, with the thickness $d_1 = 45$ nm and the length of the sensing element $L = 10$ mm. The refractive index of the sample $n_0 = 1.0$. The thickness of the transducing layer $d_3 = 40$ nm, but the refractive index of the transducing layer changes.

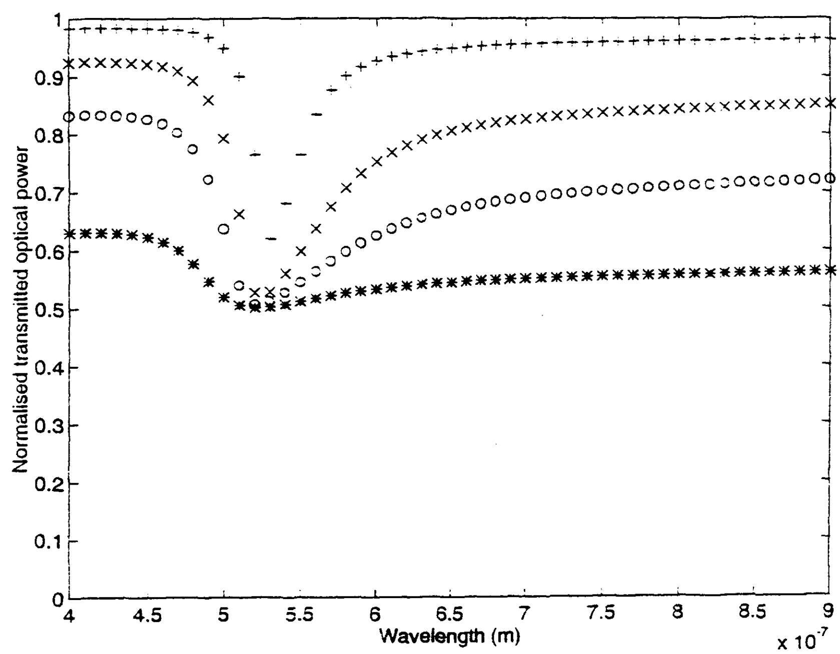

Figure 9. Normalized transmitted optical power of the SPR fibre-optic sensor, using zirconium oxide as the transducing layer with $\varepsilon_3 = n_3^2 = 4.0$, thickness $d_3 = 40$ nm, silver as the SPR supporting metal, with $\varepsilon_1 = -17 - 0.6i$ and $d_1 = 45$ nm. The refractive index of the sample $n_0 = 1.0$. The length of the sensing element L changes.

4. Summary and conclusions

In this paper, the optical power transmittance, as one of most important characteristics in SPR fibre-optic sensors both with and without a transducing layer, has been analysed and studied by numerical calculations. The behaviours and characteristics of SPR fibre-optic sensors obtained by numerical calculations agree well with previously published experimental results, such as Jorgenson and Yee's work [5, 6] and Slavik *et al.*'s work [7].

Further, by the suitable design of the sensing element in terms of the thickness and the length of the supporting metal, as well as the thickness and refractive index of the transducing layer, the optimal behaviour of the SPR fibre-optic sensor over a wide dynamic range can be achieved.

The optical power spectrum of SPR fibre-optic sensors with a transducing layer is narrower than that of sensors without a transducing layer. This characteristic leads to the SPR fibre-optic sensors with a transducing layer of higher sensitivity.

By using a transducing layer, sensing can be achieved by monitoring the change of refractive index in the sample to be measured or in the transducing layer. Thickness change of the transducing layer can be another sensing parameter in designing SPR fibre-optic sensors.

Finally, some other issues relating to the characteristics of SPR fibre-optic sensors, such as sensitivity, dynamic range, the position of minimum reflectance and the dielectric constant dispersion of the SPR supporting metal, are important and need more detailed discussions. These will be presented in another paper.

Acknowledgments

This work is supported in part by the CVCP Overseas Research Scholarship Scheme and by Astra-Zeneca Limited.

References

[1] Kretschmann, E., 1971, *Z. Phys.*, **241**, 313.
[2] Chen, W. P., and Chen, J. M., 1981, *J. opt. Soc. Am.*, **71**, 189.
[3] Kano, H., and Kawata, S., 1994, *Appl. Optics*, **33**, 5166.
[4] Garces, I., Aldea, C., and Mateo, J., 1992, *Sens. Actuators B*, **7**, 771.
[5] Jorgenson, R. C., and Yee, S. S., 1993, *Sens. Actuators B*, **12**, 213.
[6] Jorgenson, R. C., and Yee, S. S., 1994, *Sens. Actuators A*, **43**, 44.
[7] Slavik, R., Homola, J., and Ctyroky, J., 1998, *Sens. Actuators B*, **51**, 311.
[8] Raether, H., 1977, *Physica of Thin Films*, Vol. 9, edited by G. Hass, M. H. Francombe and R. W. Hoffman (New York: Academic).
[9] Pockrand, I., 1978, *Surf. Sci.*, **72**, 577.
[10] Chen, W. P., and Chen, J. M., 1980, *Surf. Sci.*, **91**, 601.
[11] Reed, C. E., Giergiel, J., Ushioda, S., and Hemminger, J. C., 1985, *Phys. Rev. B*, **31**, 1873.
[12] Kurosawa, K., Pierce, R. M., Ushioda, S., and Hemminger, J. C., 1986, *Phys. Rev. B*, **33**, 789.
[13] Abeles, F., 1986, *Electromagnetic Surface Excitations*, edited by R. F. Wallis and G. I. Stegemann (Berlin: Springer-Verlag).
[14] Ctyroky, J., Homola, J., and Skalsky, M., 1997, *Opt. quantum Electron.*, **29**, 301.
[15] Vangent, J., Lambeck, P., Kreuwel, H., Gerritsma, G., Sudholter, E., Reinhoudt, D., and Popma, J., 1989, *Sens. Actuators*, **17**, 297.

[16] Raether, H., 1988, *Surface Plasmons on Smooth and Rough Surfaces and on Gratings*, Vol. 111, *Springer Tracts in Modern Physics* (Heidelberg: Springer-Verlag).
[17] Gupta, B. D., and Singh, C. D., 1994, *Appl. Optics,* **33,** 2737.
[18] Snyder, A. W., and Love, J. D., 1983, *Optical Waveguide Theory* (London: Chapman and Hall).
[19] Gupta, B. D., Sharma, A., and Singh, C. D., 1993, *Int. J. Optoelectron.*, **8,** 409.

Appendix 3

Yu Xu, N. Barrie Jones, John C. Fothergill and Chris D. Hanning, 2000, Numerical Error Analysis of Two-Wavelength Absorption-Based Fibre-Optic Sensors, Optics & Laser Technology, Under revision for publication

Numerical Error Analysis of Two-Wavelength Absorption-Based Fibre-Optic Sensors

Yu Xu, N. Barrie Jones, John C. Fothergill, and Chris D. Hanning*

Engineering Department, University of Leicester
Engineering Department, University of Leicester, Leicester LE1 7RH, UK
Telephone: 0116-2522673, Fax: 0116-2522619

*Department of Anaesthesia, Leicester General Hospital, Leicester LE5 4PW, UK

Abstract

A numerical error analysis of two-wavelength absorption-based fibre-optic sensors is presented in this paper. A general formulation to express the measurement error and the error induced by the instability of the light power inputted into the absorbing sample to be measured is derived. And, using this formulation, two common and important errors in this type of sensor, temperature fluctuation of light sources and bending of optical fibres, are discussed. The analyses and results can be applied in both transmission-type and reflection-type absorption-based fibre-optic sensors.

Keywords: Fibre-optic, Absorption, Error

1. Introduction

By using different principles and technologies, fibre-optic sensors have been designed for measurements in chemistry and biochemistry, and have been applied successfully to detect pH, pO_2, pCO_2, methane, ozone and ammonia, etc.[1][2]. Among these, fibre-optic sensors based on the light absorption, which can be deduced from the Beer-Lambert law, are important, and possibly simplest. They can be divided into two classes: 1. transmission-type absorption-based fibre-optic sensors[3][4], 2. reflection-type absorption-based fibre-optic sensors [5][6]. Much research has been done on these devices. The study of error sources and the accuracy limitation of absorption-based fibre-optic sensors is important. Some authors have reported their work on this topic[7][8]. Because measurement by this type of sensor is achieved by comparing the light power outputted from the absorbing sample with the initial light power inputted into the sample, the stability of light power inputted to the absorbing sample is critical to the accuracy of the sensor. A two-wavelength technique is a commonly used approach to improve the performance of the sensors. In this a reference wavelength, different from the measurement beam wavelength, is used. In two-wavelength systems, the fluctuation of light output power and power spectra from light sources can be an important error source. And, in fibre-optic sensors, the disturbance of the optical fibre itself is of concern since light power is transmitted by optical fibres. The optical fibre itself is a dispersive component, the attenuation of the transmitted light power induced by disturbing optical fibres such as bending is also due to a dispersive process. The power attenuation is different at different wavelengths, which generates another error source in two-wavelength absorption-based fibre-optic sensors. In this paper, two common and important issues in absorption-based fibre-optic sensors not well studied in two-wavelength systems before, namely the errors induced by the temperature characteristics of light sources (especially non-coherent broadband light sources) and the effects of bending optical fibres are studied both theoretically and by numerical examples.

2. Basic theory

Light passing through a material can be absorbed by interaction with the molecules and atoms of the host material, or with impurities and defects. At a given wavelength λ, the intensity of the light passing through the material is attenuated as an exponential function of its path length x. This is expressed by the Beer-Lambert law:

$$I_\lambda(x) = I_\lambda(0)\exp(-\alpha_\lambda[M]x) \quad (1)$$

where $I_\lambda(x)$ is the light intensity at a distance x, $I_\lambda(0)$ is the incident light intensity at $x = 0$, α_λ is the absorption coefficient and [M] is the concentration of the absorbing material.
Absorption-based fibre-optic sensors work on this principle. In two-wavelength absorption-based fibre-optic sensors, two wavelengths are used, one as the measurement wavelength λ_1, another as the reference wavelength λ_2. At the measurement wavelength the light will be absorbed strongly by the material, at the reference wavelength the absorption of light does not happen, or the absorption is small and might be neglected. Therefore, the output of sensors can be expressed as:

$$\frac{I_{\lambda 1}(x)}{I_{\lambda 2}(x)} = \frac{I_{\lambda 1}(0)}{I_{\lambda 2}(0)}\exp(-\alpha_{\lambda 1}[M]x + \alpha_{\lambda 2}[M]x) \quad (2)$$

where the subscripts represent the two different wavelengths.

Because the absorption at λ_2 is small, and can be neglected, equation (2) can be re-written as:

$$\frac{I_{\lambda 1}(x)}{I_{\lambda 2}(x)} = \frac{I_{\lambda 1}(0)}{I_{\lambda 2}(0)}\exp(-\alpha_{\lambda 1}[M]x) \quad (3)$$

Equation (3) is the measurement formulation of two-wavelength absorption-based fibre-optic sensors. In the measurement, $I_{\lambda 1}(0)$, $I_{\lambda 2}(0)$, α_λ and x are known, the concentration [M] is obtained by measurements of the outputs of the sensor, $I_{\lambda 1}(x)$ and $I_{\lambda 2}(x)$.
The accuracy of the sensor is determined by the errors in the measurement of the light powers outputted from the absorbing sample to be measured, which could be expressed as:
$\tilde{I}_{\lambda 1}(x) = I_{\lambda 1}(x) + \Delta I_{\lambda 1}(x)$ and $\tilde{I}_{\lambda 2}(x) = I_{\lambda 2}(x) + \Delta I_{\lambda 2}(x)$,
and further, $\tilde{I}_{\lambda 1}(x) = I_{\lambda 1}(x)\cdot(1 + \delta_{\lambda 1}(x))$ and $\tilde{I}_{\lambda 2}(x) = I_{\lambda 2}(x)\cdot(1 + \delta_{\lambda 2}(x))$,
where $\Delta I_{\lambda 1}(x)$ and $\Delta I_{\lambda 2}(x)$ represent measurement errors, $\delta_{\lambda 1}(x) = \Delta I_{\lambda 1}(x) / I_{\lambda 1}(x)$ and $\delta_{\lambda 2}(x) = \Delta I_{\lambda 2}(x) / I_{\lambda 2}(x)$ represent relative measurement errors.
The accuracy of the sensor is also affected by the stability of the light powers inputted into the absorbing sample, which can be expressed as:
$\tilde{I}_{\lambda 1}(0) = I_{\lambda 1}(0) + \Delta I_{\lambda 1}(0)$ and $\tilde{I}_{\lambda 2}(0) = I_{\lambda 2}(0) + \Delta I_{\lambda 2}(0)$,
and further, $\tilde{I}_{\lambda 1}(0) = I_{\lambda 1}(0)\cdot(1 + \delta_{\lambda 1}(0))$ and $\tilde{I}_2(0) = I_{\lambda 2}(0)\cdot(1 + \delta_{\lambda 2}(0))$,
where $\Delta I_{\lambda 1}(0)$ and $\Delta I_{\lambda 2}(0)$ represent intensity fluctuations, $\delta_{\lambda 1}(0) = \Delta I_{\lambda 1}(0) / I_{\lambda 1}(0)$ and $\delta_{\lambda 2}(0) = \Delta I_{\lambda 2}(0) / I_{\lambda 2}(0)$ represent relative intensity fluctuations.
Here it is assumed that variables α_λ and x do not change.
Therefore, the concentration measurement formulation of two-wavelength absorption-based fibre-optic sensors can be expressed by equation (4), which includes the above-mentioned errors and fluctuations.

$$\frac{\tilde{I}_{\lambda 1}(x)}{\tilde{I}_{\lambda 2}(x)} = \frac{\tilde{I}_{\lambda 1}(0)}{\tilde{I}_{\lambda 2}(0)}\exp(-\alpha_{\lambda 1}[M]_m x) \quad (4)$$

where $[M]_m$ is the measured concentration value, which would be different from the real value [M].
Substituting the above error expressions into equation (4), and obtaining:

$$\frac{I_{\lambda1}(x)\cdot(1+\delta_{\lambda1}(x))}{I_{\lambda2}(x)\cdot(1+\delta_{\lambda2}(x))}=\frac{I_{\lambda1}(0)\cdot(1+\delta_{\lambda1}(0))}{I_{\lambda2}(0)\cdot(1+\delta_{\lambda2}(0))}\exp(-\alpha_{\lambda1}[M]_m x) \tag{5}$$

The relationship between the real concentration $[M]$ and measured concentration $[M]_m$ is expressed as:

$$\exp[\alpha_{\lambda1}([M]-[M]_m)x]=\frac{(1+\delta_{\lambda1}(x))\cdot(1+\delta_{\lambda2}(0))}{(1+\delta_{\lambda2}(x))\cdot(1+\delta_{\lambda1}(0))} \tag{6}$$

Because of the small values of $\delta_{\lambda1}(x)$, $\delta_{\lambda2}(x)$, $\delta_{\lambda1}(0)$ and $\delta_{\lambda2}(0)$, the concentration error can be re-written as:

$$\alpha_{\lambda1}([M]-[M]_m x)=1+\delta_{\lambda1}(x)-\delta_{\lambda2}(x)-\delta_{\lambda1}(0)+\delta_{\lambda2}(0) \tag{7}$$

The measurement errors $\delta_{\lambda1}(x)$ and $\delta_{\lambda2}(x)$ have been studied by Jin[7][8]. As illustrative examples, the following numerical calculations are focused on the study of terms $\delta_{\lambda1}(0)$ and $\delta_{\lambda2}(0)$, which are caused by the instability of the light powers inputted into the absorbing sample.

3. Illustrative examples of numerical error analyses and discussions

In two-wavelength absorption-based fibre-optic sensors, the reference wavelength λ_2 is used to monitor the background absorption and the fluctuation of output light power from light sources. Ideally $I_{\lambda1}(0)$ and $I_{\lambda2}(0)$ do not change during the measurement. In practice, there are many factors which could result in the instability of $I_{\lambda1}(0)$ and $I_{\lambda2}(0)$. Among these, the fluctuation of the output light power of light source induced by the temperature change and the physical disturbance of optical fibres are inevitable and significant. In following parts of this section, these are studied as two illustrative examples.

a. The error due to the temperature fluctuation of light sources

In two-wavelength absorption-based fibre-optic sensors, non-coherent broadband light sources, such as black-body radiators, Lamps, LEDs, are usually used. The output light power, even power spectrum, of these light sources could be changed by many factors. For long-term use, the instability of the output light power is extremely important to the performance of the sensor.

The temperature instability of output light power and power spectrum of non-coherent broadband light sources is complicated. It completely depends on the light sources themselves. Different types of light sources have different temperature characteristics. Here the black-body radiator is used as an illustrative example.

The black-body spectral radiation can be analytically expressed as [9]:

$$\widetilde{I}_\lambda(0)=\frac{2{c_0}^2k}{\Omega_0\lambda^5\cdot(e^{c_0\cdot h/\lambda\cdot k\cdot T}-1)} \tag{8}$$

where $\widetilde{I}_\lambda(0)$ is the radiation intensity of the radiator, c_0 is the velocity of light, Ω_0 is the solid angle, k is Boltzmann's constant, h is Planck's constant, T is absolute temperature and λ is the radiation wavelength.

$\widetilde{I}_{\lambda}(0)$ can be changed by both wavelength and temperature. The accuracy of an absorption-based fibre-optic sensor with this type of light source using the two-wavelength technique, especially when the difference between the two different wavelengths is large, will be apparently affected by the change of temperature.
Figure 1 shows the numerical calculation of errors caused by the temperature variation of the black-body radiator against wavelength.

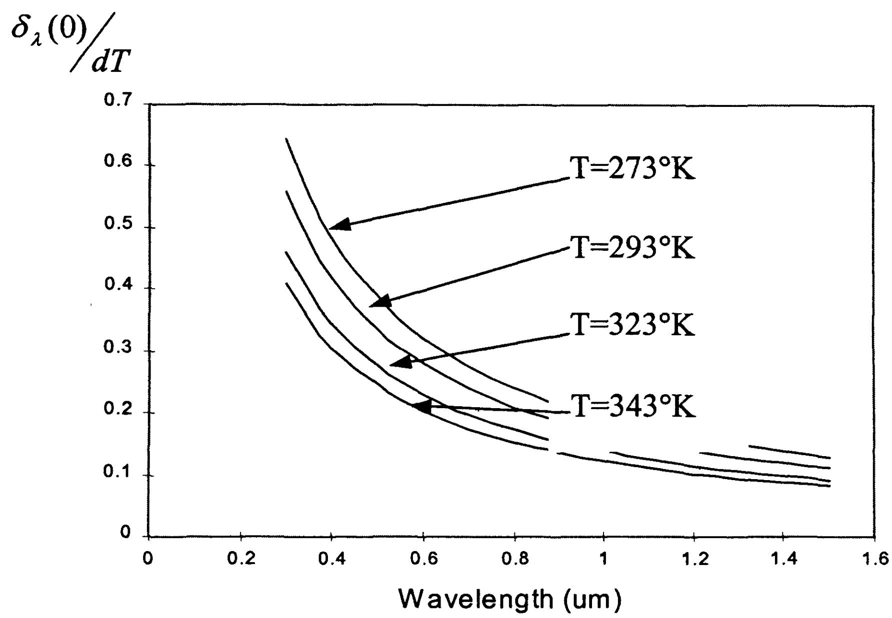

Figure 1 The variation of errors at different temperatures against wavelength

At different wavelengths the output power fluctuation caused by temperature change will be different.
For example: assuming $T = 293°K$,
at $\lambda = 1.0\mu m$, $\delta_{\lambda 1}(0) = 0.17dT$ and at $\lambda = 0.5\mu m$, $\delta_{\lambda 2}(0) = 0.34dT$.
In this case, from equation (7), the error of the measured concentration induced by the temperature fluctuation of the output power of the light source is: $|[M]-[M]_m| = 0.17dT/(\alpha_{\lambda 1}\cdot x)$.
The error increases with the increase of temperature. The temperature characteristics of light power spectra of light sources is a critical factor to determine the accuracy of two-wavelength absorption-based fibre-optic sensors. In some applications, in order to obtain high accuracy, temperature controllers or compensators for light sources are needed.

b. The error due to bending optical fibres

In practical uses of two-wavelength absorption-based fibre-optic sensors, bending of optical fibres is unavoidable, for example, bending the optical fibre to fit the space restriction. Bending an optical fibre will lead to the attenuation of light power transmitted inside the optical fibre. Especially when the bending curvature is small, this type of loss will increase significantly. Much research has been done in the study of bending optical fibres either by the light ray method[10][11] or via the electromagnetic field[12][13]. The influence of bending optical fibres on the accuracy of two-wavelength absorption-based fibre-optic sensors has not been well studied before. In this section this error is investigated by geometric optics. Multimode optical fibres with large core diameter are often used in this type of sensor and geometric optics is highly effective and useful to analyse the loss in such optical fibres.
Based on the results by Gloge[10], an optical fibre with core reflective index n, cladding reflective index n_c, the bending loss coefficient α is:

$$\alpha = 2nk(\theta_c^{\ 2} - \theta^2)\exp[-\frac{2}{3}nkR(\theta_c^{\ 2} - \theta^2 - \frac{2a}{R})^{3/2}] \qquad (9)$$

where k is the free-space propagation constant, a is radius of optical fibre core, R is the curvature radius, θ is angle of the ray and $\theta_c = [1 - (n_c/n)^2]^{1/2}$ is the critical angle for total internal reflection.

The mean quantity of bending loss coefficient considering the contributions from all transmitted rays can be calculated by integration. This loss coefficient will vary with the wavelength in detailed analysis. For simplicity, the following discussion of bending loss coefficient is based on equation (9).
The light power transmission in a bending optical fibre is defined as [14]:

$$P_{out} = P_{in} \cdot e^{-\alpha L/10} \qquad (10)$$

where P_{out} and P_{in} are the light output and input powers, respectively, L is the bending length of the optical fibre.

In two-wavelength absorption-based fibre-optic sensors, the bending loss of the optical fibre is obviously equivalent to the fluctuation of the light power inputted into the absorbing sample, therefore the following equations can be obtained:

$$\tilde{I}_\lambda(0) = I_\lambda(0) \cdot e^{-\alpha L/10} \qquad (11)$$

$$\delta_\lambda(0) = e^{-\alpha L/10} - 1 \qquad (12)$$

Figure 2 shows the numerical calculation of the error induced by the optical fibre bending loss at different bending curvature against wavelength.

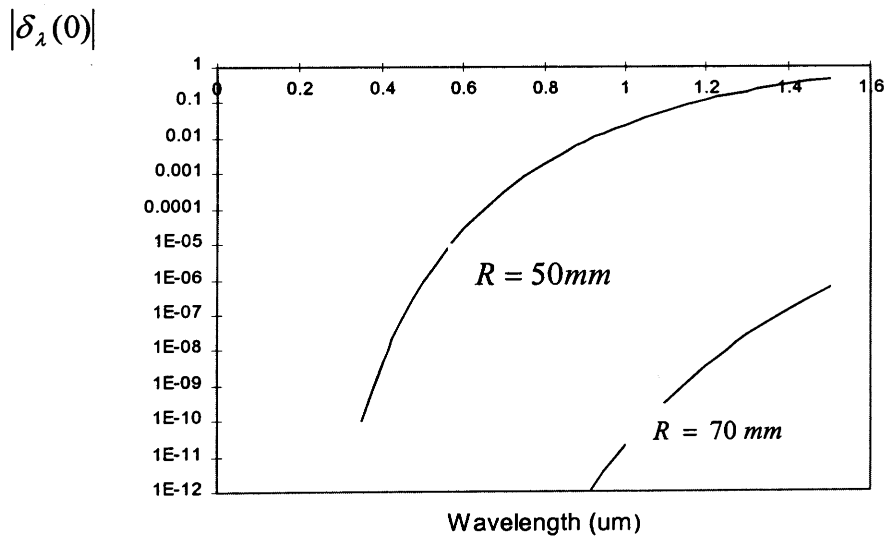

Figure 2 The error caused by the fibre bending loss at different curvatures against wavelength

From equation (12), it is known that the error depends on both the radius of bending curvature and the light wavelength. Under the same bending, the loss will be different at different wavelengths.

For example: assuming $n = 1.5$, n_c,=1.496, $R = 50$mm, $a = 60\mu$m, $\theta_c = 4.2°$, $\theta = 2.5°$ and $L=4R$,

at $\lambda = 1.5\mu$m, $\delta_{\lambda 1}(0) = 0.45$ and at $\lambda = 1.0\mu$m, $\delta_{\lambda 2}(0) = 0.023$.

The larger the radius of curvature is, the smaller the loss. The loss difference between the two different wavelengths is also smaller. The loss will increase with the decrease of the radius of bending curvature. A concept of the critical radius (suffering 3-dB loss) is introduced to reflect the relation between light power loss and the bending curvature, which is expressed as [15]:

$$R_c = \frac{3n^2\lambda}{4\pi(n^2 - n_c^{\,2})^{3/2}} \qquad (13)$$

For example: using the above optical fibre, at $\lambda = 1.0\mu$m, $R_c = 410\mu$m and at $\lambda = 0.5\mu$m, $R_c = 205\mu$m.

When the radius of bending curvature is between these two critical radii, the loss will be very different at these two wavelengths. Under this circumstance, the use of these two wavelengths as measurement and reference light in a two-wavelength absorption-based fibre-optic sensor will increase the error induced by bending the optical fibre.

Bending, especially microbending has a significant influence on the accuracy of two-wavelength absorption-based fibre-optic sensors. Microbending of optical fibres should always be considered carefully.

4. Conclusion

In two-wavelength absorption-based fibre-optic sensors, the accuracy is affected by many factors such as errors due to the method itself, measurement errors and instability of the environment. In this paper, a general formulation has been derived to analyse errors, and using this formulation the error induced by the fluctuation of light power inputted into the absorbing sample is studied. As illustrative examples, the errors induced by temperature instability of light sources and the bending of optical fibres are numerically analysed since they are not previously well studied in two-wavelength absorption-based fibre-optic sensors. The environmental physical disturbance (particularly microbending of optical fibres) and temperature fluctuation could be critical to the accuracy of the sensor in some applications. From the design point of view, under such circumstance, in order to achieve high performance of the sensor, temperature controllers or compensators for the light source are needed. Another effective approach to minimise the error is to choose the difference between the measurement and reference wavelengths to be as small as possible.

In the design of the light source for two-wavelength absorption-based fibre-optic sensors, not only does the stability of output power have to be considered, but the stability of the output power spectrum has to be studied carefully as well. Although only the error arising from temperature change of the light source is addressed in this paper, other factors which can change the output light power and power spectrum of light sources such as the driving current could be discussed using the same approach.

From equation (7), the effects of different errors in two-wavelength absorption-based fibre-optic sensors are not the same, with some of them positive, others negative. In the design, this characteristic could be used to compensate one against the other and reduce the overall error of the sensor to the minimum.

The information and conclusions drawn from this research can be applied in two-wavelength absorption-based fibre-optic sensors both of the transmission-type and reflection-type.

Acknowledgements

This work is supported in part by the CVCP Overseas Research Scholarship Scheme and by Astra-Zeneca Limited.

References

1. Montgomery JD and Dixon FW. Fibre optics in process control. Proc. ISA/IMC Conf. Promecon' 81, London: 81-90.
2. Boisde G and Harmer A. Chemical and biochemical sensing with optical fibers and waveguides. Boston: Artech House, 1996.
3. Deboux BJC, Lewis E, Schlly PJ, and Edwards R. A novel technique for optical fiber pH sensing based on Methylene blue adsorption. J. Ligthwave Technol. 1995; 13(7): 1407-1414.
4. Zhou Q, Shahriari MR, Kritz D, and Sigel Jr GH. Porous fiber-optic sensor for high-sensitivity humidity measurements. Anal. Chem. 1988; 60(20): 2317-2320.
5. Peterson JI, Goldstein SR, and Fitzgerald RV. Fiber optic pH probe for physiological use. Anal. Chem. 1980; 52(6): 864-869.
6. Landis DA, Seliskar CJ, and Heineman WR. Fiber-optic-graded-index-lens absorption sensor with wavelength-scanning capability. Appl.Opt. 1994; 33(15): 3432-3439.
7. Jin W, Stewart G, and Culshaw B. Source noise limitation in an optical methane detection system using a broadband source. Appl. Opt. 1995; 34(13): 2345-2349.
8. Jin W, Stewart G, Philp W, Culshaw B, and Demokan MS. Limitation of absorption-based fibre optic gas sensors by coherent reflections. Appl. Opt. 1997; 36(25): 6251-6255.
9. Chappell A. Optoelectronics theory and practice. Bedford: Texas Instrument Ltd., 1976
10. Gloge D. Bending loss in multimode fibers with graded and ungraded core index. Appl. Opt. 1972; 11(11): 2506-2513.
11. Snyder AW, and Mitchell DJ. Bending losses of multimode optical fibres. Electron Lett. 1974; 10(1): 11-12.
12. Marcuse D. Curvature loss formula for optical fibers. J. Opt. Soc. Am. 1976; 66(3): 216-220.
13. Marcuse D. Field deformation and loss caused by curvature of optical fibers. J. Opt. Soc. Am. 1976; 66(4): 31-319.
14. Wolf HF. Handbook of fiber optics: theoty and applications. New York: Garland STPM Press, 1979.
15. Senior JM. Optical fiber communications principles and practice. London: Prentice Hall, 1985.

Appendix 4

Yu Xu, N. Barrie Jones, John C. Fothergill and Chris D. Hanning, 2000, An Approximate Theoretical Model of Surface Plasmon Resonance Optical Waveguide and Fibre-Optic Sensors, IEEE J-LT, Submitted publication

An Approximate Theoretical Model of Surface Plasmon Resonance Optical Waveguide and Fibre-Optic Sensors

Yu Xu, N. Barrie Jones, John C. Fothergill, and Chris D. Hanning*

Engineering Department, University of Leicester
Engineering Department, University of Leicester, Leicester LE1 7RH, UK

*Department of Anaesthesia, Leicester General Hospital, Leicester LE5 4PW, UK

Abstract

Optical surface plasmon resonance (SPR) excitation can be theoretically depicted and discussed using Fresnel's equations. However, Fresnel's equations cannot explicitly give expressions to reflect the characteristics of SPR systems, especially in SPR optical waveguide and fibre-optic sensors. In this paper an approximate mathematical model based on the approximation proposed by Kretschmann in bulk optics is presented to describe the characteristics of SPR large dimension optical waveguide and fibre-optic sensors. This model keeps high accuracy for operation close to the minimum reflection area, at which the resonance condition is achieved. This model can be used to analytically estimate the performance of SPR optical waveguide sensors, and SPR fibre-optic sensors in meridional rays approximation.

Indexing terms: surface plasmon resonance (SPR), optical waveguide, fibre-optic sensors,

1. Introduction

Optical surface plasmon resonance (SPR) excitation is a promising technique in the fields of chemical and biochemical sensing, with high sensitivity as its main feature. After study and development over more than two decades, this technique has been applied to the determination of gas concentration [1-3], the measurement of optical properties of metals [4-5], microscopy [6-7] and biosensors [8-9]. Based on the configuration and the approximate mathematical model proposed by Kretschmann [10], there have been successful theoretical and experimental studies of bulk-optic surface plasmon resonance systems [11-12]. In recent years, with the progress of optical waveguides and fibres and related techniques, SPR optical waveguide sensors [13-16] and SPR fibre-optic sensors [17-20] have attracted much attention. Fresnel's equations are very useful to analyse SPR large dimension optical waveguide and fibre-optic systems. However, parameters which can affect the performance of SPR sensors are implicit in Fresnel's equations. In order to help the study and design of SPR optical waveguide and SPR fibre-optic sensors, it is necessary to make efforts to construct theoretical models. It was with this in mind that the characteristics of SPR fibre-optic sensors were analysed numerically in our previous paper[21].

Furthermore, the sensing measurement in SPR sensors happens within the area close to the minimum reflection of light power from the interface of the SPR supporting metal film and the dielectric medium (there is a Lorentizan "dip" on the reflection curve around the minimum reflection). Therefore, the characteristics of the reflection curve close to the "dip" is important to the performance of a SPR optical waveguide or fibre-optic sensor. In this paper, based on the approximation proposed by Kretschmann [10] in SPR bulk-optic systems, an explicit, approximate expression is derived for large dimension optical waveguide sensors and fibre-optic sensors in the approximation of meridional rays. This model keeps high accuracy in the area close to the reflection "dip".

2. Mathematical Model

Because the planar optical waveguide is simply a special case of the optical fibre (with radius = ∞), for generality, the mathematical model in this section is based on the optical fibre. Figure 1 shows the meridional cross-section of the sensing element of the SPR fibre-optic sensor.

A multi-mode optical fibre, with core diameter d and refractive index n_2 (dielectric permittivity ε_2), has the jacket and the cladding removed to expose the core, on which is symmetrically deposited a metal film of thickness d_1 and dielectric permittivity ε_1 (refractive index n_1).

In some SPR sensors, the metal film is directly in contact with the sample to be measured with dielectric permittivity ε_0 (refractive index n_0), in others, a dielectric isotropic transducing layer with thickness d_3 and dielectric permittivity ε_3 (refractive index n_3) is deposited symmetrically outside the metal film. For generality, in this paper all formulations are derived including this transducing layer. Sensors without transducing layers are considered as a special case by setting $d_3 = 0$.

[Insert figure 1 about here]

In multi-mode optical fibre sensors, due to the easiness and effectiveness of describing the behaviour, meridional rays are often used to construct approximate models. Further, the theoretical models of SPR for bulk-optics are satisfied by meridional rays in optical fibres. Therefore the following theoretical analysis of light power reflection in the interface of the SPR supporting metal film and the dielectric medium in SPR fibre-optic sensors is based on meridional rays.

Considering a ray of light transmitted in an optical fibre with incident angle θ with respect to the normal to core/metal interface, the expressions related to the surface plasmon wave are summarised as [21-25]:

The propagation constant of the incident light in z direction is:

$$k_i^z = \frac{2\pi}{\lambda} n_2 \sin\theta \qquad (1)$$

The electric field E of the SPR propagating in the z-direction is expressed as:

$$E_z(x,z,t) = E_z^0(x)\exp(i\omega t - ik_z z) \qquad (2)$$

where E_z^0 is the field amplitude, ω is the angular frequency, k_z is the SPR complex propagation constant in the z-direction.

The resonance condition, under which the propagation constant of the incident light beam in the z-direction is equal to the real part of the SPR propagation constant, is expressed as:

$$\mathrm{Re}(k_z) = k(\varepsilon_2)^{1/2} \sin\theta_{SP} = \frac{2\pi}{\lambda} n_2 \sin\theta_{SP} \qquad (3)$$

where k is the propagation constant of the incident light beam in vacuum and θ_{SP} is the resonance angle. The SPR propagation constant is accurately given by:

$$k_z = k^0 + k^R + k^T \qquad (4)$$

$$k^0 = \left(\frac{\varepsilon_0\varepsilon_1}{\varepsilon_0 + \varepsilon_1}\right)^{1/2} \times \frac{\omega}{c} \qquad (5)$$

$$k^R = k^0\left(\frac{2}{\varepsilon_0 + \varepsilon_1}\right)\times\left(\frac{\varepsilon_0\varepsilon_1}{\varepsilon_0 + \varepsilon_1}\right)^{3/2} \times \exp\left[-i\frac{4\pi d_1}{\lambda}\frac{\varepsilon_1}{(\varepsilon_0 + \varepsilon_1)^{1/2}}\right] \tag{6}$$

$$k^T = i\left(\frac{2\pi d_3}{\lambda}\right)\times\left(\frac{\omega}{c}\right)\times\left(\frac{\varepsilon_0\varepsilon_1}{\varepsilon_0 + \varepsilon_1}\right)^2 \times \frac{1}{(\varepsilon_0\varepsilon_1)^{1/2}(\varepsilon_0 - \varepsilon_1)} \times\left(\varepsilon_3 + \frac{\varepsilon_0\varepsilon_1}{\varepsilon_3} - \varepsilon_1 - \varepsilon_0\right) \tag{7}$$

k^0 expresses the dispersion relation of SPR of a metal-vacuum interface in a one-sharp-boundary model, k^R expresses the perturbation to k^0 due to the finite physical volume of the optical fibre and k^T expresses the modification to k^0 due to the transducing layer.
Intensity reflection coefficient $r(\theta)$ in the interface of metal film and optical fibre core can use the result for SPR bulk-optic system, which is obtained as:

$$r(\theta) = |r_{210}|^2 = \left|\frac{r_{21} + r_{130}\exp(2ik_1d_1)}{1 + r_{21}r_{130}\exp(2ik_1d_1)}\right|^2 \tag{8}$$

where $r_{21} = \dfrac{z_{21}}{n_{21}}$, $r_{130} = \dfrac{z_{10} - iz_{43}\tan(k_3d_3)}{n_{10} - in_{43}\tan(k_3d_3)}$, $z_{ij} = k_i\varepsilon_j - k_j\varepsilon_i$, $n_{ij} = k_i\varepsilon_j + k_j\varepsilon_i$,

$$k_i = \left[\varepsilon_i\left(\frac{2\pi}{\lambda}\right)^2 - (k_i^z)^2\right]^{1/2},\quad k_i^z = \left(\frac{2\pi}{\lambda}\right)n_2\sin\theta,\quad \varepsilon_4 = \frac{\varepsilon_0\varepsilon_1}{\varepsilon_3},\quad k_4 = \frac{k_0k_1}{k_3},$$

$$i, j = 1,2,3,4$$

When light is incident at an angle close to θ_{SP} , the resonance angle, the TM mode of the incident light is strongly absorbed and the overall reflected light is attenuated very much. At resonance angle θ_{SP} the strongest absorption happens, therefore creating a "dip", the minimum reflection.
With the angle close to θ_{SP}, the reflection coefficient $r(\theta)$ of the TM light can be approximately expressed as a function of θ as [10][22]:

$$r(\theta) = 1 - \frac{4[\mathrm{Im}(k^0) + \mathrm{Im}(k^T)]\,\mathrm{Im}(k^R)}{[k_i^z - \mathrm{Re}(k_z)]^2 + \mathrm{Im}(k_z)^2} \tag{9}$$

This function has a Lorentzian dip at θ_{SP}.
This light ray transmitted in the multi-mode optical fibre (with incident angle θ, shown in figure 1), will have N reflections in length L of SPR sensing element. The number N is expressed as:

$$N = \frac{L}{d\tan\theta} \tag{10}$$

3. Illustrative Applications

3.1 Characteristic parameters of SPR optical waveguide sensors

In a SPR large dimension optical waveguide sensor, three parameters, the minimum position θ_{SP} (or k_{SP}^z) where the resonance condition is achieved, the minimum reflection coefficient $R_{\min}$, and the half-width, FWHM W_θ (or Δk_i^z) are important and closely related to the performance of the sensor. For example, the sensitivity of the sensor is inversely proportional to the half-width FWHM $\Delta\theta$ (or Δk_i^z) [26].
Considering an optical waveguide with length L of SPR sensing element, incident TM mode light at angle θ with respect to the normal at the medium/metal interface, the number of reflections at the interface will be $N = L/2d\tan\theta$.
Under condition of $|\mathrm{Im}(k_z)| \ll |\mathrm{Re}(k_z)|$ [11][25], using the variable definition in above section, and using the equation (14), θ_{SP}, $R_{\min}$ and W_θ can be obtained:

When $\mathrm{Re}(k_z) = k(\varepsilon_2)^{1/2}\sin\theta_{SP} = \dfrac{2\pi}{\lambda}n_2\sin\theta_{SP}$, the minimum position θ_{SP} is achieved.

The minimum reflection coefficient $R_{\min}$ is expressed as:

$$R_{\min} = \sigma^N \tag{15}$$

The half-width FWHM of the reflection curve W_θ is expressed as:

$$W_\theta = \frac{2c\,\mathrm{Im}(k_z)}{n\omega\cos\theta_{SP}}\left(\frac{1-\sigma^N}{\upsilon(1+\sigma^N)}\right)^{1/2} \tag{16}$$

where $\sigma = 1 - \dfrac{4[\mathrm{Im}(k^0)+\mathrm{Im}(k^T)]\,\mathrm{Im}(k^R)}{\mathrm{Im}(k_z)^2}$, $\upsilon = N\dfrac{4[\mathrm{Im}(k^0)+\mathrm{Im}(k^T)]\,\mathrm{Im}(k^R)}{\mathrm{Im}(k_z)^2 - 4[\mathrm{Im}(k^0)+\mathrm{Im}(k^T)]\,\mathrm{Im}(k^R)}$

3.2 Reflectance of SPR fibre-optic sensors

It is known that light rays with a range of incident angles are allowed to propagate in a multi-mode optical fibre. The range is determined by the numerical aperture of the fibre, $N.A. = n_2\cos\theta_c = (n_1^2 - n_2^2)^{1/2}$.
Only rays with $90^0 > \theta > \theta_c$ (critical angle) can be transmitted in the optical fibre. To find the output of the SPR fibre-optic sensor the contribution from all of rays transmitted should be considered. Such a consideration depends on the power distribution of the light source. Mathematically an integration has to be made to combine all these rays' contributions.
For simplicity, if the light power reaching the sensing region is distributed equally among all rays with incident angles in (θ_1, θ_2), the total light power reflectance is expressed [27]:

$$\gamma_T = \frac{1}{\theta_2-\theta_1}\int_{\theta_1}^{\theta_2}\gamma(\theta)d\theta \tag{17}$$

where $\gamma(\theta)$ is the reflection coefficient of light ray at angle θ.

Then, in fibre-optic sensors, the guided modes within angles of (θ_c, 90^0), the total reflectance of TM mode light is expressed as:

$$R = \frac{1}{90^0 - \theta_c} \int_{\theta_c}^{90^0} r^N(\theta) d\theta = \frac{1}{90^0 - \theta_c} \int_{\theta_c}^{90^0} \frac{\sigma^N}{1 - \upsilon[k_i^z - \mathrm{Re}(k_z)]^2 / \mathrm{Im}(k_z)^2} d\theta$$

(18)

Because different ranges of angles suffer different number of internal reflections, from 1 to maximum N_m (at θ_c), the total angle range (θ_c, 90^0) can be divided into discrete sub-ranges (θ_j, θ_{j+1}) , j = 1,... , N_m, each sub-range suffers the same number of reflections. These angle sub-ranges correspond to propagation constant sub-ranges, (k_j^z , k_{j+1}^z) . Therefore, the analytical expression for the reflectance is given by:

$$R = \frac{1}{k_{90^0}^z - k_c^z} \sum_{j=1}^{N_m} \sigma^j \int_{k_j^z}^{k_{j+1}^z} \frac{1}{1 - \upsilon[k_i^z - \mathrm{Re}(k_z)]^2 / \mathrm{Im}(k_z)^2} dk_i^z$$

$$= \frac{1}{2(k_{90^0}^z - k_c^z)} \sum_{j=1}^{N_m} \sigma^N \left[\log \frac{\mathrm{Im}(k_z) + \sqrt{\upsilon}[k_i^z - \mathrm{Re}(k_z)]}{\mathrm{Im}(k_z) - \sqrt{\upsilon}[k_i^z - \mathrm{Re}(k_z)]} \right]_{k_j^z}^{k_{j+1}^z} \qquad (19)$$

where $k_{90^0}^z$ and k_c^z represent the propagation constants of guided rays at 90^0 and critical angle θ_c, respectively, and the definition of other variables is the same as in earlier equations.

These are illustrative examples to demonstrate the application of the approximate model. Due to the complication of light power distribution of light sources, the detailed analysis of the reflectance in some cases can only be calculated by numerical methods, and, in SPR sensors, the analysis should also consider that both TE and TM polarised light are possibly allowed to propagate in optical waveguides or optical fibres. All these have been studied in our previous paper [21].

4. Conclusions

Theoretical models are important tools in the study and development of surface plasmon resonance (SPR) sensors. However, Fresnel's equations cannot give explicit expressions to reflect the relationship between parameters of the design and the characteristics of the sensor. Furthermore, the performance of SPR optical waveguides and fibre-optic sensors is closely related to the characteristics near the minimum reflection "dip" area in the reflection curve. To construct theoretical models to estimate the characteristics of the curve close to the "dip" is meaningful and very useful. In this paper, a theoretical model has been presented for SPR optical waveguide and fibre-optic sensors. This model can be applied to analytical study as shown in two illustrative examples.

These examples show that the analytical relationship between the characteristic parameters of SPR large dimension optical waveguide or fibre-optic sensors (such as those using light reflectance etc.) can be used to quantitatively estimate the performance in the area close to the minimum "dip". The nearer to the "dip", the higher the accuracy obtained. Theoretically the derived approximation gives no error at the minimum "dip".

Appendix A

All mathematical manipulations in this appendix are under the condition of $\frac{k_i^z - \mathrm{Re}(k_z)}{\mathrm{Im}(k_z)} << 1$

$$r(\theta) = 1 - \frac{4[\mathrm{Im}(k^0) + \mathrm{Im}(k^T)]\mathrm{Im}(k^R)}{[k_i^z - \mathrm{Re}(k_z)]^2 + \mathrm{Im}(k_z)^2} \tag{A1}$$

$$r(\theta) = 1 - \frac{4[\mathrm{Im}(k^0) + \mathrm{Im}(k^T)]\mathrm{Im}(k^R)/\mathrm{Im}(k_z)^2}{1 + \left[\frac{k_i^z}{\mathrm{Im}(k_z)} - \frac{\mathrm{Re}(k_z)}{\mathrm{Im}(k_z)}\right]^2} \tag{A2}$$

$$r(\theta) = 1 - \frac{4[\mathrm{Im}(k^0) + \mathrm{Im}(k^T)]\mathrm{Im}(k^R)}{\mathrm{Im}(k_z)^2} \exp\left[-\left(\frac{k_i^z - \mathrm{Re}(k_z)}{\mathrm{Im}(k_z)}\right)^2 \ln 2\right] \tag{A3}$$

$$r(\theta) = 1 - \frac{4[\mathrm{Im}(k^0) + \mathrm{Im}(k^T)]\mathrm{Im}(k^R)}{\mathrm{Im}(k_z)^2} \left[1 - \left(\frac{k_i^z - \mathrm{Re}(k_z)}{\mathrm{Im}(k_z)}\right)^2 \ln 2\right] \tag{A4}$$

$$r(\theta) = 1 - \frac{4[\mathrm{Im}(k^0) + \mathrm{Im}(k^T)]\mathrm{Im}(k^R)}{\mathrm{Im}(k_z)^2} + \frac{4[\mathrm{Im}(k^0) + \mathrm{Im}(k^T)]\mathrm{Im}(k^R)}{\mathrm{Im}(k_z)^2} \times$$

$$\left[\left(\frac{k_i^z - \mathrm{Re}(k_z)}{\mathrm{Im}(k_z)}\right)^2 \ln 2\right] \tag{A5}$$

$$r(\theta) = \left[1 - \frac{4[\mathrm{Im}(k^0) + \mathrm{Im}(k^T)]\mathrm{Im}(k^R)}{\mathrm{Im}(k_z)^2}\right] \times$$

$$\left\{1 + \frac{\frac{4[\mathrm{Im}(k^0) + \mathrm{Im}(k^T)]\mathrm{Im}(k^R)}{\mathrm{Im}(k_z)^2}}{1 - \frac{4[\mathrm{Im}(k^0) + \mathrm{Im}(k^T)]\mathrm{Im}(k^R)}{\mathrm{Im}(k_z)^2}} \left[\left(\frac{k_i^z - \mathrm{Re}(k_z)}{\mathrm{Im}(k_z)}\right)^2 \ln 2\right]\right\} \tag{A6}$$

$$r(\theta) = \left[1 - \frac{4[\mathrm{Im}(k^0) + \mathrm{Im}(k^T)]\mathrm{Im}(k^R)}{\mathrm{Im}(k_z)^2}\right] \times$$

$$\exp\left\{\frac{\frac{4[\mathrm{Im}(k^0) + \mathrm{Im}(k^T)]\mathrm{Im}(k^R)}{\mathrm{Im}(k_z)^2}}{1 - \frac{4[\mathrm{Im}(k^0) + \mathrm{Im}(k^T)]\mathrm{Im}(k^R)}{\mathrm{Im}(k_z)^2}}\left[\left(\frac{k_i^z - \mathrm{Re}(k_z)}{\mathrm{Im}(k_z)}\right)^2 \ln 2\right]\right\} \tag{A7}$$

$$r^N(\theta) = \left(1 - \frac{4[\mathrm{Im}(k^0) + \mathrm{Im}(k^T)]\mathrm{Im}(k^R)}{[k_i^z - \mathrm{Re}(k_z)]^2 + \mathrm{Im}(k_z)^2}\right)^N \tag{A8}$$

$$r^N(\theta) = \left[1 - \frac{4[\mathrm{Im}(k^0) + \mathrm{Im}(k^T)]\mathrm{Im}(k^R)}{\mathrm{Im}(k_z)^2}\right]^N \times$$

$$\exp\left\{N\frac{4[\mathrm{Im}(k^0) + \mathrm{Im}(k^T)]\mathrm{Im}(k^R)}{\mathrm{Im}(k_z)^2 - 4[\mathrm{Im}(k^0) + \mathrm{Im}(k^T)]\mathrm{Im}(k^R)}\left[\left(\frac{k_i^z - \mathrm{Re}(k_z)}{\mathrm{Im}(k_z)}\right)^2 \ln 2\right]\right\} \tag{A9}$$

$$r^N(\theta) = \left[1 - \frac{4[\mathrm{Im}(k^0) + \mathrm{Im}(k^T)]\mathrm{Im}(k^R)}{\mathrm{Im}(k_z)^2}\right]^N \times$$

$$\frac{1}{1 - N\frac{4[\mathrm{Im}(k^0) + \mathrm{Im}(k^T)]\mathrm{Im}(k^R)}{\mathrm{Im}(k_z)^2 - 4[\mathrm{Im}(k^0) + \mathrm{Im}(k^T)]\mathrm{Im}(k^R)}\left[\frac{k_i^z - \mathrm{Re}(k_z)}{\mathrm{Im}(k_z)}\right]^2} \tag{A10}$$

Appendix B

Figure B1 shows the reflection coefficient curves calculated from the approximate expressions derived in Appendix A. The parameters for the calculations are: He-Ne laser, $\lambda = 632.8nm$, core refractive $n_2 = 1.515$, core diameter $d = 600\mu m$, SPR element length $L = 12mm$, light incident angle $\theta = 68^\circ$, and SPR metal silver. Assuming: $4[\mathrm{Im}(k^0) + \mathrm{Im}(k^T)]\mathrm{Im}(k^R) / \mathrm{Im}(k_z)^2 = 0.7$.

[Insert figure B1 about here]

When $\left|k_i^z - \mathrm{Re}(k_z)/\mathrm{Im}(k_z)\right| < 0.14$, the error of the Gaussian approximation is about 9%, the error of the Lorentzian approximation is about 11%, when $\left|k_i^z - \mathrm{Re}(k_z)/\mathrm{Im}(k_z)\right| < 0.1$ the error of the Gaussian approximation is about 5%, the error of the Lorentzian approximation is about 2%.

Acknowledgements

This work is supported in part by the CVCP Overseas Research Scholarship Scheme of UK and by Astra-Zeneca Limited in UK.

References

1. N. A. Kalabina, T. I. Ksenevich, A. A. Beloglazov and P. I. Nikitin, "Pesticide sensing by surface-plasmon resonance" Proc. of SPIE, vol.2367, pp.126-132, 1995
2. M. J. Jory, G. W. Bradberr, P. S. Cann and J. R. Sambles, "Surface plasmon based optical sensor using acousto optics" Measurement Sci. & Tech., vol.6, pp.1193-1200, 1995
3. J. D. Wright, A. Cado, S. J. Peacock, V. Rivalle and A. M. Smith "Effects of nitrogen dioxide on surface plasmon resonance of substituted phthalocyanine films" Sensors and Actuators B, vol.29, pp.108-114, 1995
4. H. E. D. de Bruijn, R. P.H. Kooyman and J. Gerve "Determination of dielectric permittivity and thickness of a metal layer from a surface plasmon resonance experiment" Appl. Opt., vol.29, pp.1974-1978. 1990
5. E. Fontana, R. H. Pantell and M. Moslehi "Characterization of dieelctric-coated, metal mirrors using surface-plasmon spectroscopy" Appl. Opt., vol.27, pp.3334-3340, 1988
6. P. Nikitin"Phase jump under surface plasmon resonance and its using for biosensing and microscopy" Proc. of SPIE, vol.3749, pp.464-465, 1999
7. J. Lahiri, E. Ostuni and G. M. Whitesides "Patterning ligands on reactive SAMs by microcontat printing" Langmuir, vol.15, pp.2055-2060, 1999
8. D. M. Disley, D. C. Cullen, H. X. You and C. R. Lowe "Covalent coupling of immunolobulin G to self-assembled monolayers as a method for immobilizing the interfacial-recognition layer of a surface plasmon resonance immunosensor" Biosensor & Bioelectronics, vol.13, pp.1213-1225, 1998
9. U. Aldinger, P. Pfeifer, G. Schwotzer and P. Steinruecke "Comparative study of spectral and angle-dependent SPR devices in biological applications" Sensors and Actuators B, vol.51, pp.298-304, 1998
10. E. Kretschmann "Die bestimmung optischer konstanten von metallen durch anregung von Oberflaechenplasmaschwingungen" Z. Phys., vol.241, pp.313-324, 1971
11. W. P. Chen and J. M. Chen "Use of surface plasma wave for determination of the thickness and optical constants of thin metalic films" J. Opt. Soc. Am., vol.71, pp.189-191, 1981
12. H. Kano and S. Kawata "Surface-plasmon sensor for absorption-sensitivity enhancement" Appl. Opt., vol.33, pp.5166-5170, 1994
13. R. D. Harris and J. S. Wilkinson "Waveguide surface plasmon resonance sensors" Sensors and Actuators B, vol.29, pp.261-267, 1995
14. M. N. Weiss, R. Srivastave, and H. Groger "Experimental investigation of a surface plasmon resonance-based integrated-optic humidity sensor" Electronics Letts, vol.32, pp.842-843, 1996
15. E. F. Schipper, R. P. H. Kooyman, A. Borreman and J. Greve "Critical sensor: a new type of evanescent wave innunosensor" Biosensors and Bioelectronics, vol.11, pp.295-304, 1996
16. M. N. Weiss, R. Srivastave and H. Groger "Theoretical and experimental investigations of surface plasmon waveguide structures for sensing applications" Proc. of SPIE, vol.2695, pp.195-201, 1996
17. I. Garces, C. Aldea and J. Mateo "Four-layer chemical fiber optic plasmon-based sensor" Sensors and Actuators B, vol.7, pp.771-774, 1992
18. R. C. Jorgenson,and S. S. Yee "A fiber-optic chemical sensor based on surface plasmon resonance"

Sensors and Actuators B, vol.12, pp.213-220, 1993
19. R. C. Jorgenson and S. S. Yee "Control of the dynamic range and sensitivity of a surface plasmon resonance based fiber optic sensor" Sensors and Actuators A, vol.43, pp.44-48, 1994
20. R. Slavik, J. Homola and J. Ctyroky "Miniaturization of fiber optic surface plasmon resonance sensor" Sensors and Actuators B, vol.51, pp.311-315, 1998
21. Y. Xu, N. B. Jones, J. C. Fothergill and C. D. Hanning "Analytical estimates of the characteristics of surface plasmon resonance fibre-optic sensors" accepted by J. of Mod. Optics
22. H.Raether. Surface Plasmons on Smooth and Rough Surfaces and on Gratings, Vol.111of Springer Tracts in Modern Physics, Heidelberg: Springer-Verlag, 1988
23 J. VanGent, P. Lambeck, H. Kreuwel, G. Gerritsma, E. Sudholter, D. Reinhoudt and J. Popma "Chromoionophores in optical ion sensors" Sensors and Actuators, vol.17, pp.297-305,1989
24. I. Pockrand, "Surface plasma oscillations at silver surface with thin transparent and absorbing coatings" Surface Sci., vol.72, pp.577-588, 1978
25. W. P. Chen and J. M. Chen "Surface plasma wave study of submonolayer Cs and CsO covered Ag surface" Surface Sci., vol.91, pp.601-617, 1980
26. J. VanGent, P. V. Lambeck, H. J. M. Kreuwel, G. J. Gerritsma, E. J. Sudholter, D. N. Reinhoudt and T. J. A. Popma "Optimization of a chenooptical surface plasmon resonance based sensor" Appl. Opts., vol.29, pp.2843-2849, 1990
27. V. Ruddy "An effective attenuation coefficient for evanescent wave spectroscopy using multimode fiber" Fiber and Integrated Opt., vol.9, pp.142-150, 1990

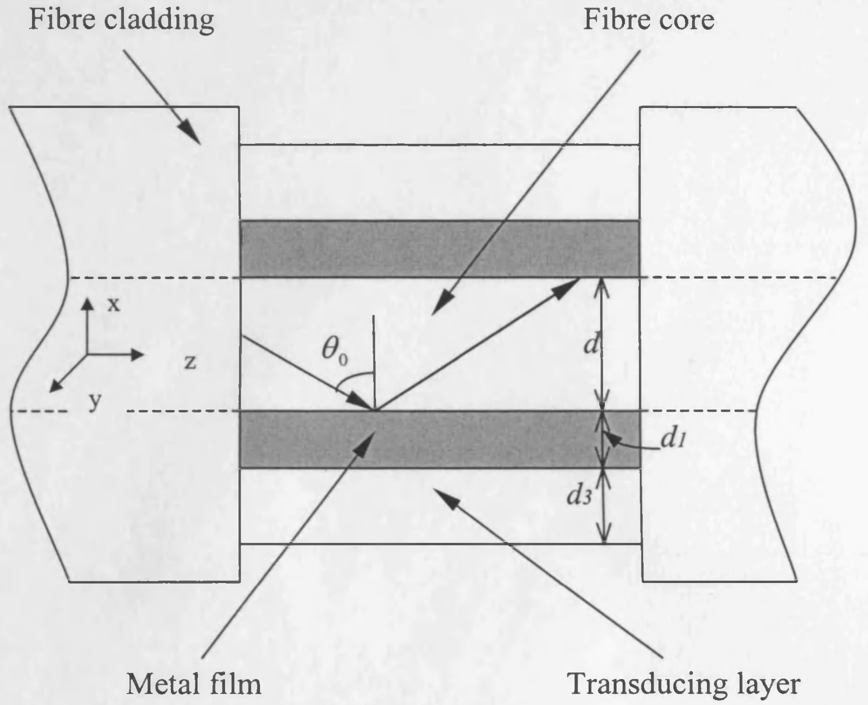

Figure 1. The meridional cross-section of the sensing element of the optical waveguide or fibre-optic SPR sensor.

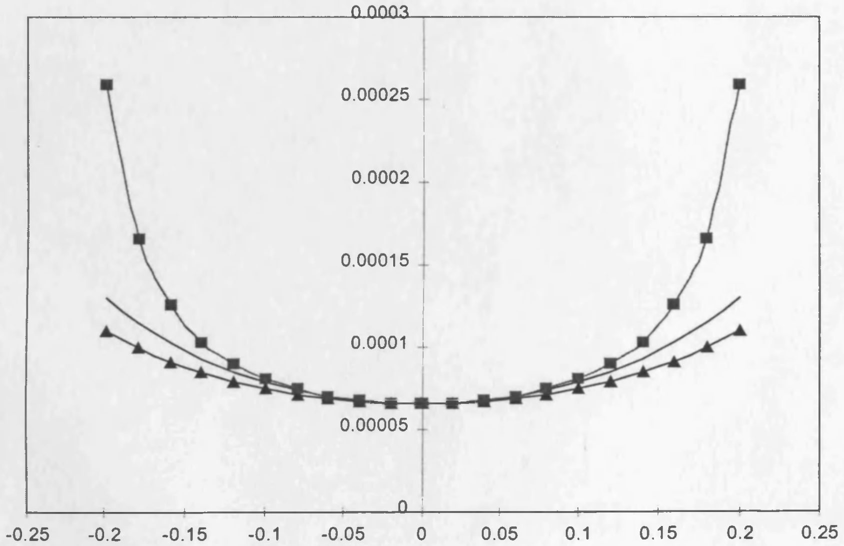

Figure B1. The reflection coefficient curves for different approximations, — represents the curve from equation (A8), ▲ represents the curve from equation (A9) and ■ represents the curve from (A10).